THEORETICAL AND EXPERIMENTAL STUDY OF THE ABSORPTION PROCESS OF AMMONIA IN IONIC LIQUIDS FOR ABSORPTION REFRIGERATION SYSTEMS

Ronny Rives Sanz

UNIVERSITAT ROVIRA i VIRGILI

THEORETICAL AND EXPERIMENTAL STUDY OF THE ABSORPTION PROCESS OF AMMONIA IN IONIC LIQUIDS FOR ABSORPTION REFRIGERATION SYSTEMS

RONNY RIVES SANZ

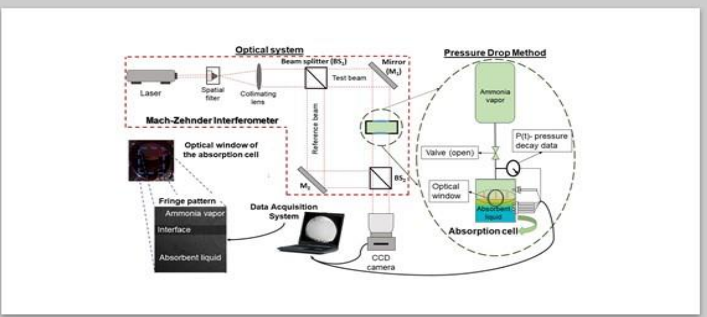

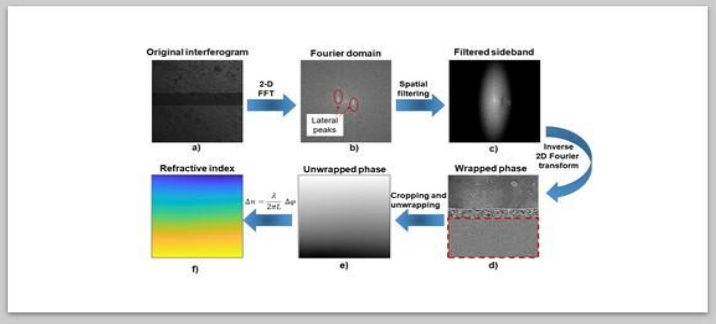

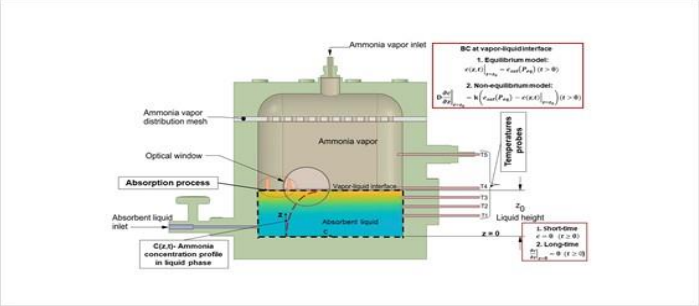

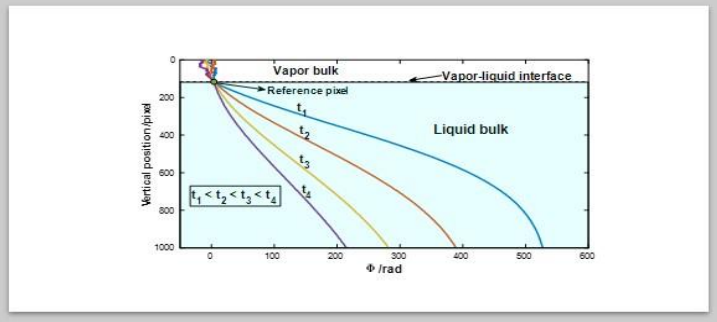

DOCTORAL THESIS
2020

UNIVERSITAT ROVIRA I VIRGILI
THEORETICAL AND EXPERIMENTAL STUDY OF THE ABSORPTION PROCESS OF AMMONIA IN IONIC LIQUIDS FOR ABSORPTION REFRIGERATION SYSTEMS
Ronny Rives Sanz

UNIVERSITAT ROVIRA I VIRGILI
THEORETICAL AND EXPERIMENTAL STUDY OF THE ABSORPTION PROCESS OF AMMONIA IN IONIC LIQUIDS FOR ABSORPTION REFRIGERATION SYSTEMS
Ronny Rives Sanz

UNIVERSITAT ROVIRA I VIRGILI
THEORETICAL AND EXPERIMENTAL STUDY OF THE ABSORPTION PROCESS OF AMMONIA IN IONIC LIQUIDS FOR ABSORPTION REFRIGERATION SYSTEMS
Ronny Rives Sanz

Ronny Rives Sanz

Theoretical and Experimental Study of the Absorption Process of Ammonia in Ionic Liquids for Absorption Refrigeration Systems

DOCTORAL THESIS

Supervised by
Prof. Alberto Coronas

Department of Mechanical Engineering
CREVER - Group of Applied Thermal Engineering

UNIVERSITAT ROVIRA I VIRGILI

Tarragona, 2020

UNIVERSITAT
ROVIRA i VIRGILI
DEPARTAMENT D'ENGINYERIA MECÀNICA
Escola Tècnica Superior d'Enginyeria Química (ETSEQ).
Avgda Paisos Catalans, 26 ; 43007 Tarragona (Spain)

Declaration

I STATE that the present thesis, entitled "**Theoretical and experimental study of the absorption process of ammonia in ionic liquids for absorption refrigeration systems**", presented by **Ronny Rives Sanz** for the degree of Doctor, has been carried out under my supervision at CREVER Research Group in the Department of Mechanical Engineering of Rovira i Virgili University, and that it fulfils all the requirements to be eligible for the International Doctorate Award.

Tarragona, 23 November 2020

Prof. Alberto Coronas

Dedication

To my mother, Emelina, for her unconditional support,
To my future wife, Suly, for her infinite love,
To my family, for being my inspiration.

Acknowledgements

I would like to express my deep gratitude and sincere appreciation to my supervisor Prof. Alberto Coronas for giving me this great opportunity for my academic training and personal development, for his time and consideration, for his invaluable assistance and oversight of my research, for always being aware of our well-being not only at the university but also in all aspects of the daily life of an international student, and for everything that I learned from him.

I would also like to show gratitude to Prof. María Soledad Larrechi for her thoughtful comments on some papers and chapters of this thesis and for always fostering a passion for chemistry in my engineering thinking. I would like to thank Prof. Juan Campos of the Universitat Autònoma de Barcelona, for his help, assistance and discussion of various issues especially related to the implementation of the Mach-Zehnder interferometer. My sincere thanks to Dr Dereje S. Ayou for his contributions in reviewing the writing of the thesis and some related papers.

I would like to express my deep gratitude to Prof. Valentina Shevtsova (currently at Mondragon University), Dr Aliaksandr Mialdun and Dr Viktar Yasnou of the Universitè Libre de Bruxelles, for their invaluable advice, support and supervision during my research stay in Belgium. I am very grateful to them for giving me the opportunity to be one more member of their excellent research group, their kindness, and their helpful recommendations for my professional development.

I would like to thank Dr Daniel Salavera for his help in the experimental part of this thesis, especially in the implementation of the experimental setup. I would also like to thank Dr Hebert Pérez Rosés from the Rovira i Virgili University for his help in the mathematical processing of the experimental data and the programming in Matlab.

My sincere acknowledgement to the Universitat Rovira i Virgili for the opportunity to accomplish my doctoral studies. This research was supported by the Ministry of Economy and Competitiveness and the European Regional Development Fund, FEDER, (ref. DPI2015-71306-R).

I would like to thank all academic and technical staff of the CREVER Group for supporting and facilitating my research and providing a quality graduate education. In particular, I would like to thank Dr Juan Prieto for his help in the implementation of the Data Acquisition System of the experimental setup.

A special thanks and affection to my family, my father Miguel, my cousin Jorge, my aunt Bárbara, my in-laws Sulema and Diosfreni, my brothers and sisters, my stepfather Oramas, my uncles Miguel, Antonio, Koki, and to my entire family for their unconditional support and motivation during these years.

Thanks to my friends Ernesto, María Paula, Gisselle, Alejandro, for always being up to date on the development of this thesis and to all those friends that despite the distance I have always been in their good thoughts.

A big thank you to all my colleagues at Lab 113 for the moments we have shared over the years, providing a friendly atmosphere in our lab and helpful discussions.

Thanks to all the primary, secondary and pre-university teachers who in one way or another have contributed to my academic training.

Thanks to my undergraduate professors, who later became my companions for two years, for all the knowledge transmitted and for always being aware of my academic training.

Of course, this thesis could not be completed without the participation and assistance of so many colleagues, friends and well-wishers whose names may not contain all the enumerated. Their contributions are sincerely appreciated and gratefully acknowledged.

Abstract

Ionic liquids (ILs) have recently been proposed as alternative, tunable absorbents for natural refrigerants in absorption refrigeration systems. However, the high viscosity, low mass diffusivity, and the lack of reliable information on the thermophysical properties of their mixtures with these refrigerants are important limitations for effective implementation.

The main objective of this thesis is to study the absorption process of ammonia in ionic liquids and determine the experimental time evolution of the absorption rate and the concentration profiles in the absorbent fluid. These experimental data are useful for developing and validating heat and mass transfer models for describing the absorption process of natural refrigerants in ionic liquids.

The ionic liquids (ILs) studied are: ethylammonium nitrate (EAN); 1-ethyl-3-methylimidazolium-tetrafluoroborate ([emim][BF_4]); and 1-butyl-3-methyl-imidazolium-tetrafluoroborate ([bmim][BF_4]). They all have different ammonia (NH_3) solubilities and viscosities.

The Pressure Drop Method was implemented to determine the time evolution of the absorption rate of ammonia in the ILs selected throughout the absorption process. Absorption experiments lasting 15 hours were performed at infinite dilution of ammonia, at temperatures of 293.15 K and 303.15 K. The absorption rate of ammonia in the ILs was more than 20 times lower than in the conventional absorbent (water).

The relevance of mass diffusivity in the absorption process prompted a review of the literature on the methods for measuring and modeling this property. Compared to other natural refrigerant/IL mixtures, the experimental data on diffusivity for NH_3/IL mixtures is limited. The mass diffusivity of refrigerant vapors in ionic liquids is most commonly determined by the gravimetric method. The results obtained with this method are generally expressed in terms of an average diffusivity, which can lead to erroneous conclusions in the screening of ionic liquids as absorbents if the concentration of refrigerant in the refrigerant/IL solution is not explicitly considered. Furthermore, unlike optical interferometry methods, conventional methods such as the gravimetric method do not provide

information on refrigeration concentration profiles in the absorbent during the absorption process.

Thus, to obtain the time evolution of the concentration profiles in the absorbent, an Optical Digital Interferometry (ODI) method was used. To understand and develop the ODI method, we first determined mass diffusivity in a binary liquid mixture of the natural refrigerant, water, and the ionic liquid 1-(2-hydroxyethyl)-3-methylimidazolium tetrafluoroborate ([EtOHmim][BF_4]). Mass diffusivity measurements were performed throughout the range of the ionic liquid mass fraction and at temperatures ranging from 298.15 K to 313.15 K.

It was found that the mass diffusivity of the binary mixture H_2O/[EtOHmim][BF_4] decreases as the IL mass fraction increases, although the rate of the decrease is significant only in regions that are IL-poor or IL-rich. The results showed an almost linear increase in the mass diffusivity value with temperature. The ability of four models to describe the experimental mass diffusivity values was also assessed. The Modified Group Contribution model provides the best estimates of mass diffusivity, a relative deviation from experimental data of 7.9% and 2.1% using binary interaction parameters regressed from vapour-liquid equilibria and diffusion data, respectively. The experience we acquired from studying the mass diffusivity in this binary mixture enabled us to modify and adapt the ODI method to investigate the absorption process of ammonia in the ionic liquids selected.

Then, the time evolution of the ammonia concentration profiles in the absorbent during the absorption process was visualized using the ODI method. Two mass diffusion models based on a one-dimensional unsteady-state diffusion equation were used to describe the ammonia mass diffusion in the ionic liquids during the absorption process. The two mass diffusion models – namely, the equilibrium and non-equilibrium models – are dissimilar in the key assumptions and boundary conditions they use.

The use of the ODI method for investigating the absorption process was validated using the conventional working pair Ammonia/Water as the reference fluid mixture. It was found that the two mass diffusion models used can successfully reproduce the experimental profiles of the ammonia concentration in the absorbent depending on the time analyzed during the absorption process. The

relative deviations obtained during the validation were around 20% and 5%, for the equilibrium and non-equilibrium mass diffusion models, respectively.

The mass diffusivity of ammonia in the ionic liquids obtained using the equilibrium model ranges from 2.49×10^{-10} m^2/s to 9.01×10^{-10} m^2/s. We also observed that the accuracy of the equilibrium model improves with time after the start of the absorption process.

In the case of the non-equilibrium model, ammonia diffusivity ranges from 1.18×10^{-10} m^2/s to 5.71×10^{-10} m^2/s. The non-equilibrium model shows better agreement with the literature than the equilibrium model, but can only be applied for short times during the absorption process in which the diffusion front does not reach the bottom of the field of view.

In all cases, the determined mass diffusivity of ammonia in the ionic liquids studied, using both mass diffusion models, increased with temperature and follows the order: [EAN] > [emim][BF_4] > [bmim][BF_4]. Moreover, the diffusivity values of ammonia in the ionic liquids studied are more than ten times lower than those for water, conventional absorbent of ammonia.

The ability of various models and correlations to estimate experimental values of the mass diffusivity of ammonia in ionic liquids was evaluated. From the correlations in the literature, we obtained a modified correlation that provides the best estimates of the mass diffusivity of ammonia in ionic liquids with a relative deviation of 28% from experimental data.

Finally, we investigated how the solubility and mass diffusivity of ammonia in selected ionic liquids affected the performance of the absorption process. For the analysis, a model based on the mass balances in the components of a single-stage absorption cycle was used. When the degree of saturation during the absorption process is considered, the results reveal a comparable solution circulation ratio for NH_3/[emim][BF_4] and NH_3/[bmim][BF4], despite the higher solubility of ammonia in [bmim][BF_4]. Thus, the results highlight the importance of considering favourable mass diffusivity in addition to good solubility characteristics when screening ILs as absorbents.

This thesis provides new experimental absorption data on the mass diffusivity of natural refrigerants in ILs, information which is essential if the heat and mass

transfer performance of these working pairs is to be studied in detail so that the IL-based absorption system can be properly designed.

Resumen

Recientemente, se han propuesto líquidos iónicos como absorbentes ajustables alternativos para refrigerantes naturales en sistemas de refrigeración por absorción. Sin embargo, la alta viscosidad, la baja difusividad de masa y la falta de información confiable sobre las propiedades termofísicas de sus mezclas con estos refrigerantes son limitaciones importantes para su implementación efectiva.

El objetivo principal de esta tesis es estudiar el proceso de absorción del amoniaco en líquidos iónicos para determinar la evolución temporal de la tasa de absorción y los perfiles de concentración en el absorbente. Estos datos experimentales son útiles para el desarrollo y validación de modelos de transferencia de calor y masa utilizados en la descripción del proceso de absorción de refrigerantes naturales en líquidos iónicos.

Los líquidos iónicos (ILs) estudiados son: nitrato de etilamonio (EAN); 1-etil-3-metilimidazolio tetrafluoroborato ([emim][BF_4]); y 1-butil-3-metil-imidazolio tetrafluoroborato ([bmim][BF_4]), que exhiben diferentes viscosidades y solubilidades de amoniaco (NH_3).

Se implementó el método de caída de presión para determinar la evolución temporal de la tasa de absorción de amoníaco en los IL seleccionados, en el proceso de absorción. Los experimentos de absorción del amoniaco se realizaron a dilución infinita a las temperaturas de 293,15 K y 303,15 K, durante periodos de unas 15 horas. Los valores de la tasa de absorción del amoníaco en los liquidos ionicos estudiados fueron de más de 20 veces menores que en el agua.

La revisión bibliográfica realizada reveló que la interferometría óptica brinda una excelente oportunidad para obtener conocimientos más profundos sobre el proceso de absorción mediante la visualización directa. Además, los datos experimentales de difusividad másica para mezclas de NH_3/IL son muy escasos en comparación con los datos disponibles para otras mezclas de refrigerantes naturales/ILs.

Así, para obtener la evolución temporal de los perfiles de concentración en el absorbente, se implementó un método de Interferometría Óptica Digital (ODI). Primero, para entender bien y desarrollar la metodología del método ODI, hemos determinado la difusividad de masa en una mezcla líquida binaria que involucra el refrigerante natural, agua y el líquido iónico, de 1-(2-hidroxietil)-3-metilimidazolio tetrafluoroborato ([EtOHmim][BF_4]). Las mediciones de la difusividad de masa se realizaron en todo el rango de fracción de masa del líquido iónico y a temperaturas que oscilan entre 298,15 K y 313,15 K.

Se encontró que la difusividad de masa de la mezcla binaria H_2O/[EtOHmim][BF_4] disminuye al aumentar la fracción de masa de líquido iónico, aunque la tasa de disminución es esencial solo en regiones que son pobres o ricas en líquido iónico. Los resultados mostraron un aumento casi lineal en el valor de difusividad de masa con la temperatura. También se evaluó la capacidad de cuatro modelos para describir los valores experimentales de la difusividad de masa. El modelo de Contribución de Grupo Modificado proporciona las mejores estimaciones de la difusividad de masa: una desviación relativa de los datos experimentales del 7,9% y el 2,1% utilizando parámetros de interacción binaria regresados de los equilibrios vapor-líquido y de los datos de difusión, respectivamente. La experiencia adquirida en el estudio de la difusividad de masa en esta mezcla binaria nos permitió modificar y adaptar el método ODI para la investigación del proceso de absorción de amoniaco en los líquidos iónicos seleccionados.

Luego, se visualizó el tiempo de evolución de los perfiles de concentración de amoniaco en el absorbente durante el proceso de absorción utilizando el método ODI. Se utilizaron dos modelos de difusión de masa basados en una ecuación de difusión de unidimensional para describir la difusión de masa de amoníaco en los líquidos iónicos durante el proceso de absorción. Los dos modelos de difusión de masa, denominados, modelo de equilibrio y modelo de no equilibrio, son diferentes en los supuestos clave y las condiciones de contorno utilizadas.

El uso del método ODI para la investigación del proceso de absorción se validó utilizando el par de trabajo convencional Amoníaco/Agua como mezcla de fluido de referencia. Se encontró que los dos modelos de difusión de masa utilizados pueden reproducir con éxito los perfiles experimentales de la concentración de

amoníaco en el absorbente en función del período de tiempo analizado durante el proceso de absorción. Las desviaciones relativas obtenidas durante la validación rondaron el 20% y el 5%, para los modelos de difusión de masa en equilibrio y no equilibrio, respectivamente.

La difusividad de masa del amoniaco en los líquidos iónicos estudiados obtenidos utilizando el modelo de equilibrio varía de 2.49×10^{-10} m^2/s a 9.01×10^{-10} m^2/s. Además, observamos que la precisión del modelo de equilibrio mejora a medida que pasa más tiempo después del inicio del proceso de absorción.

En el caso del modelo de no equilibrio, la difusividad del amoníaco varía entre 1.18×10^{-10} m^2/s to 5.71×10^{-10} m^2/s. El modelo de no equilibrio muestra una mejor concordancia con la literatura que el modelo de equilibrio, pero la aplicación del modelo de no equilibrio se restringe a tiempos cortos del proceso de absorción en los que el frente de difusión no llega al fondo del campo de visión.

En todos los casos, la difusividad de masa determinada del amoníaco en los líquidos iónicos estudiados, utilizando ambos modelos de difusión de masa, aumentó con la temperatura y sigue el orden: [EAN]> [emim][BF_4]> [bmim][BF_4]. Además, los valores de difusividad del amoniaco en los líquidos iónicos estudiados son más de diez veces inferiores a los del agua, absorbente convencional de amoniaco.

Se evaluó la capacidad de estimación de varios modelos y correlaciones para describir valores experimentales de difusividad de masa de amoníaco en líquidos iónicos. Con base en las correlaciones de la literatura, obtuvimos una correlación modificada que proporciona las mejores estimaciones de la difusividad de masa del amoníaco en líquidos iónicos con una desviación relativa del 28% de los datos experimentales.

Finalmente, hemos investigado la relevancia para el desempeño del proceso de absorción de la solubilidad y la difusividad de masa de amoníaco en líquidos iónicos seleccionados. En aras del análisis, se utilizó un modelo basado en los balances de masa en los componentes de un ciclo de absorción de una sola etapa. Cuando se considera el grado de saturación alcanzado durante el proceso de absorción, los resultados revelan una relación de circulación de la solución

comparable para NH_3/[emim][BF_4] y NH_3/[bmim][BF_4], a pesar de la mayor solubilidad del amoníaco en [bmim][BF_4]. Por lo tanto, los resultados resaltan la importancia de considerar una difusividad de masa favorable además de buenas características de solubilidad cuando se seleccionan las IL como absorbentes.

Esta tesis aporta nuevos datos experimentales de absorción sobre la difusividad de masa de refrigerantes naturales en líquidos iónicos, información esencial para proceder al estudio detallado del rendimiento de transferencia de calor y masa de estos pares de trabajo y, por tanto, para el diseño adecuado de un sistema de absorción basado en líquidos iónicos.

Contents

List of Tables

List of Figures

Chapter I
Introduction, justification and objectives

This chapter is dedicated to the background, justification, and objectives of this thesis. It discusses the absorption refrigeration systems, the conventional working pairs, their limitations, and the potential use of ILs as absorbent liquids. It also reveals the need for an experimental investigation of the absorption process and further highlights the importance of the mass diffusivity of natural refrigerants in ionic liquids. It then goes on to give a brief description of some experimental studies on the absorption process of ammonia in absorbents. Of the methods presented, Optical Digital Interferometry and the Pressure Drop Method stand out. Finally, the objectives and structure of this thesis are presented.

I.1 Introduction

Heating and cooling in buildings and industries were recently reported to account for half of the energy consumed in the European Union (EU) [1]. The current demand for heating in buildings and industry exceeds the demand for cooling. However, the latter is increasing faster, mainly due to the growing demand for air conditioning and the refrigeration of food and medical supplies [2]. Moreover, the growth in demand for cooling is expected to skyrocket as the global population increases, ambient temperatures rise, and incomes and living standards improve, especially in developing countries with warmer climates, as illustrated in Figure I-1.

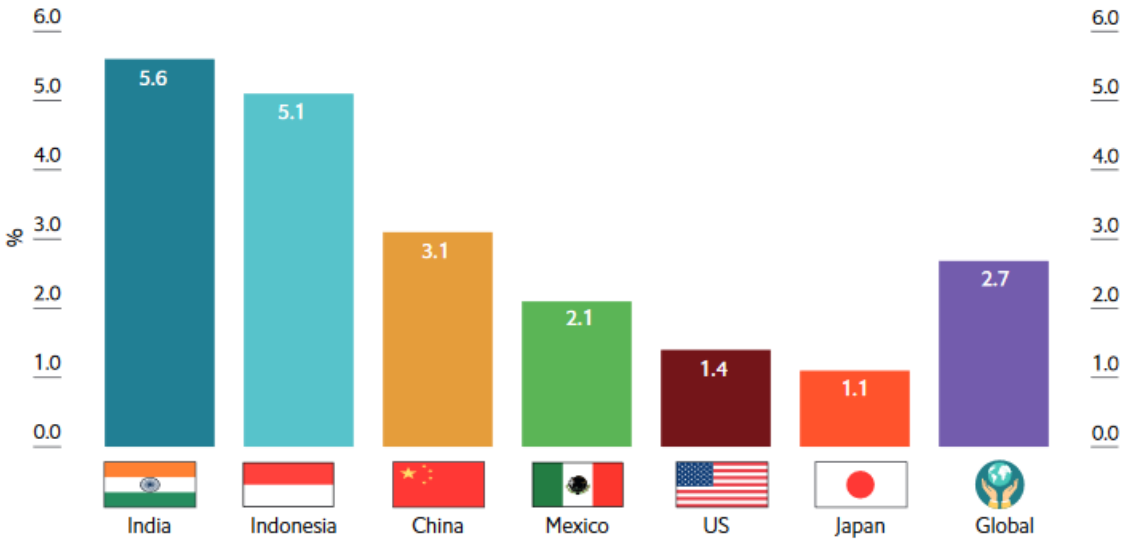

Figure I-1. Average annual growth rate of the sales associated with cooling equipment between 2018 and 2030 [3].

Nowadays, cooling is mainly provided by compression refrigeration systems with electrically driven compressors. Supplying power to these devices comes with considerable costs and environmental implications. Carbon dioxide (CO_2) emissions associated with cooling demand have tripled since 1990 to 1130 million tonnes (Mt), equivalent to the total emissions of Japan [4]. In this context, thermally- not electrically-driven cooling systems could be an interesting alternative for addressing the current climate and energy problems [5].

Of the thermally driven cooling technologies, absorption refrigeration is particularly well-known. It uses heat transformation processes in thermodynamic cycles with refrigerant/absorbent working pairs to produce cooling cleanly and sustainably. Absorption refrigeration systems are particularly suitable for

situations in which there is low grade heat supply available (for example, solar thermal energy, district heating networks, waste heat from some industrial, or cogeneration processes) [6]. In many cases, the huge potential of these sources (the total amount of EU waste heat is estimated to be 3140 TWh [7]) remains unused, which highlights the primary energy saving potential of these systems. Furthermore, absorption refrigeration systems are very useful for reducing the high peak load in the electricity distribution grid due to the cooling demand during summer months. These systems can also use environmentally friendly refrigerants without additional greenhouse gas emissions.

I.2 Working fluids in absorption refrigeration systems

Absorption refrigeration systems use a pair of fluids (namely, refrigerant and absorbent) with different volatilities as the working fluid mixture. The refrigerant is a volatile fluid, and the absorbent can be another fluid or a solution with a non-volatile salt. The performance, efficiency, first cost and operating cost of absorption refrigeration systems are strongly dependent on the properties of the working fluids [6]. Therefore, specific requirements should be imposed on the properties of a refrigerant/absorbent working pair. For instance, the transport properties that influence heat and mass transfer – e.g., viscosity, thermal conductivity, and mass diffusivity – should be favourable, and both fluids must be environmentally friendly and have physicochemical properties such as [8]:

- Refrigerant: high enthalpy of vaporization, moderate vapour pressure compared to atmospheric pressure, low freezing temperature, etc.
- Absorbent: lower vapour pressure than the refrigerant, high affinity with the refrigerant within the operating conditions of the cycle (e.g. negative deviation from Raoult's Law), etc.
- Refrigerant/Absorbent fluid mixture: large difference between the boiling points of the refrigerant and the absorbent (more than 200°C), the absorbent should not crystallize within the system, the mixture must be safe, chemically stable, non-corrosive, low-cost and readily available.

Although many refrigerant/absorbent pairs have been proposed, the most widely used in commercial systems are: Water/LiBr and Ammonia/Water. However, despite its good overall performance, both systems exhibit some drawbacks,

which prevent the development of new cycles or applications, such as solar cooling in hot countries [9] and high-temperature multi-effect cycles [10].

In the H_2O/LiBr working pair, H_2O works as the refrigerant, and an aqueous LiBr solution works as the absorbent fluid. A schematic representation of a basic absorption cycle using this working pair is shown Figure I-2. This figure also shows major components of the cycle, among which the absorber is considered the most critical in terms of overall system performance, size, and first cost [11].

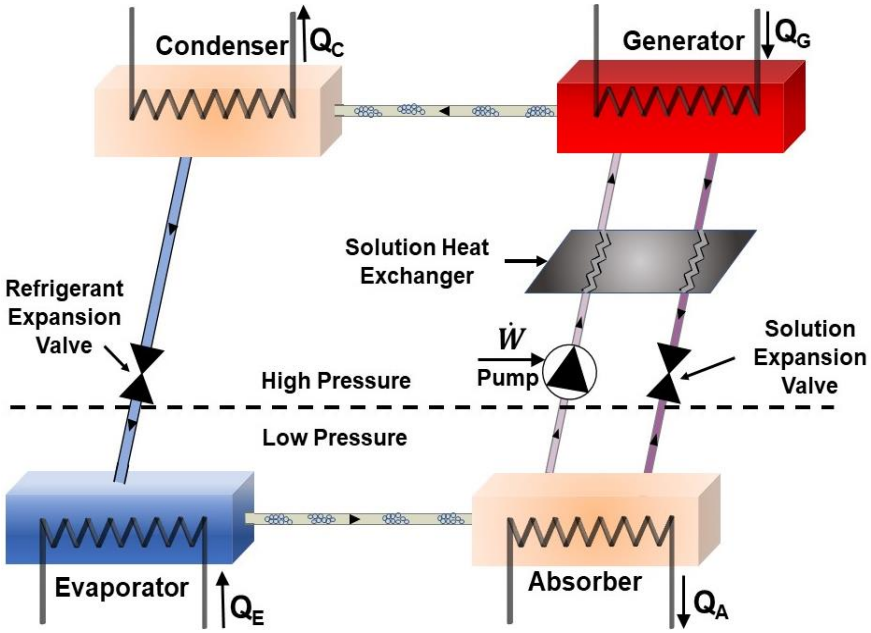

Figure I-2. Schematic representation of a single-effect H_2O/LiBr absorption cycle.

Absorption machines based on H_2O/LiBr are typically configured as water chillers for air-conditioning systems in large buildings [6]. The H_2O/LiBr working mixture presents excellent characteristics such as the non-volatility of the absorbent (LiBr) and the high enthalpy of vaporization of the refrigerant (water). Moreover, this working fluid pair has other advantages such as non-toxicity and high affinity between the absorbent and refrigerant. However, the H_2O/LiBr solution easily crystallizes when the LiBr concentration is high, the absorption temperature is high, or the evaporation temperature is relatively low [8]. The crystallization of LiBr can block the system components and thus shorten the lifetime of the equipment. Other drawbacks include the need for corrosion inhibitors and cooling towers (for heat rejection) and a restricted evaporation temperature range due to the freezing point of water. In this respect, these systems cannot be used for evaporation temperatures below 0ºC. The vapour pressure of water is also very

low so the systems need to be operated at sub-atmospheric conditions. This means that the equipment must be completely sealed.

In the NH_3/H_2O working pair, ammonia works as refrigerant and water as absorbent. The NH_3/H_2O absorption cycle [12] is used mainly for refrigeration purposes since it can produce cold below 0°C due to the low freezing point of ammonia (-77 ºC). This working pair is thermally and chemically stable for a wide range of temperatures and pressures. Moreover, there is no risk of crystallization of the refrigerant/absorbent liquid solution for the operating conditions of the absorption systems. However, the relatively small temperature difference between the boiling points of NH_3 and H_2O makes a *"rectification"* process necessary to *"purify"* the refrigerant vapour at the desorber outlet. To do this, an additional component is introduced into the thermodynamic cycle (namely "rectifier"). Figure I-3 schematically shows an absorption cycle based on this working pair, where it can be seen that the main difference with respect to a cycle using the H_2O/LiBr pair (Figure I-2) is the rectifier.

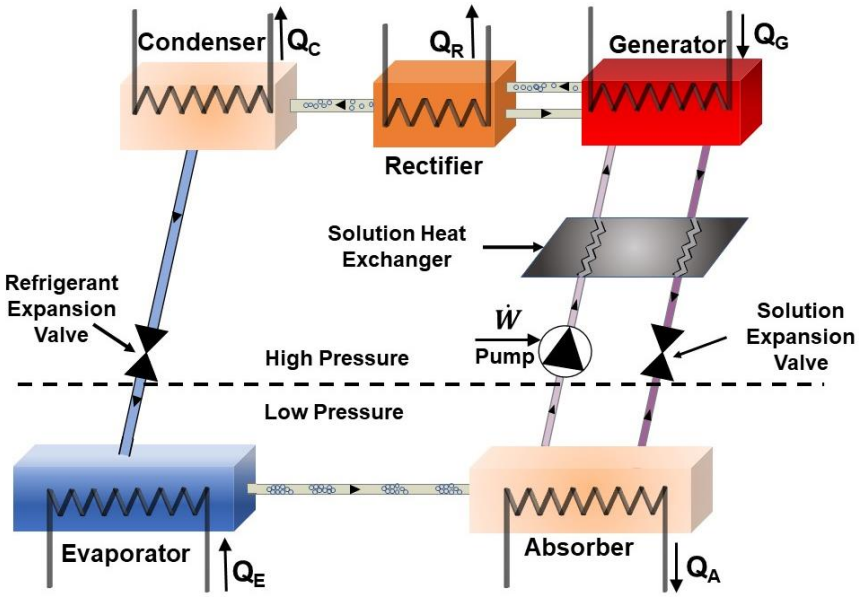

Figure I-3. Schematic representation of a single-stage NH_3/H_2O absorption cycle.

Without a rectifier, the refrigerant vapour leaving the condenser contains water, which accumulates in the evaporator at low temperatures and reduces the cooling capacity of the system. Other drawbacks for this working pair include toxicity and incompatibility with copper-based metals.

Nevertheless, ammonia itself is a cost-effective, natural refrigerant, which is frequently used in large commercial freezing and refrigeration plants, and its behaviour is well known in a wide range of working conditions. Furthermore, ammonia has relatively high latent heat, and low viscosities and heat capacities, which provide good thermodynamics and heat transfer. Thus, considerable effort has been made to find new absorbent liquids for ammonia refrigerant, which overcome the limitations of the NH_3/H_2O systems. In this thesis, we focus on ammonia as the refrigerant.

I.3 Ionic liquids as absorbents in absorption refrigeration systems

Parallel to research efforts to find suitable absorbent substances for refrigeration systems, ionic liquids (ILs) have emerged as alternatives to conventional organic solvents for a broad range of applications [13,14]. ILs are a large family of chemical compounds, which can be classified as a class of molten salts with unique physical and chemical properties, such as negligible vapour pressure, good solubility to many organic or inorganic chemicals, and a wide liquid state range from room temperature to about 300 ºC [15]. Due to their particular chemical structure (large, and asymmetrical ions with highly delocalized charges), many ILs also show low-melting points [13], reduced flammability [16], low corrosion rates and a high gas absorption capacity [5]. Figure I-4 shows the structure of some of the ions present in the most studied ILs in the literature.

Despite their excellent properties, the most outstanding feature of ILs is that they can be synthesized by combining a fairly large quantity of available cations and anions. Thus, ionic liquids can be smartly designed, and their properties can be tuned to meet the specific requirements of a given application [13].

Consequently, ILs have been proposed as alternative, tunable absorbents for absorption refrigeration systems. In particular, the use of IL as a replacement for LiBr in the H_2O/LiBr pair solves the crystallization and metal-compatibility problems of this conventional working pair [8,17]. In the case of the other conventional working pair, NH_3/H_2O, the use of ILs as a replacement for H_2O is driven by the fact that the rectification process is no longer required [18,19].

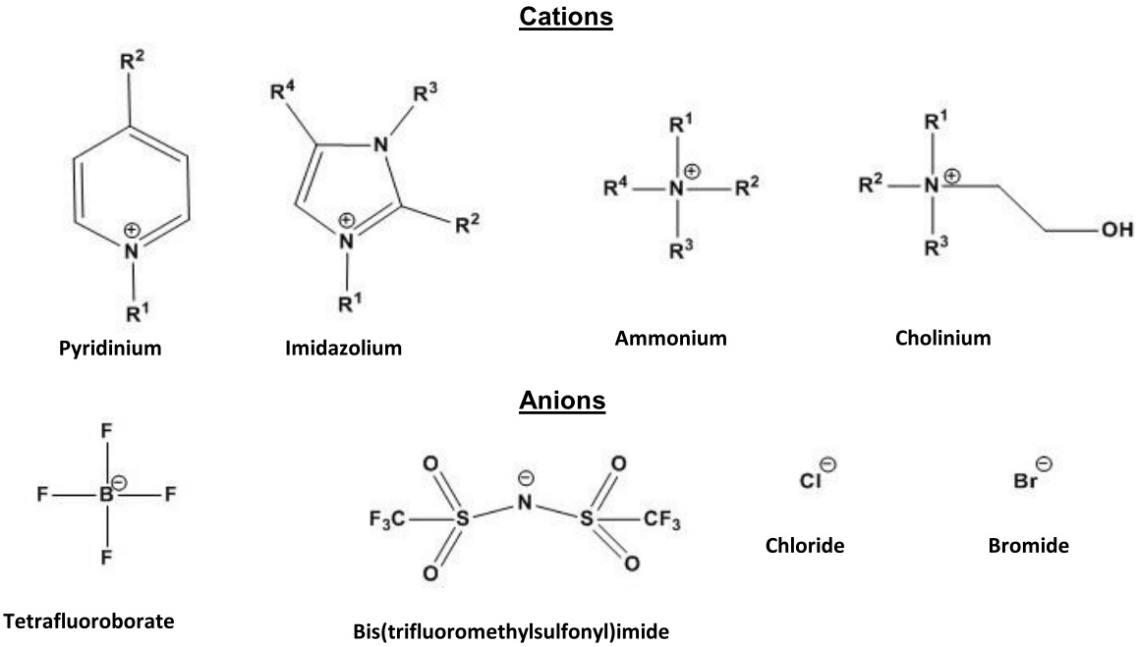

Figure I-4. Chemical structure of some of the cations and anions present in the most studied ionic liquids in the literature [20].

However, despite the promising potential of ILs as absorbents, some drawbacks have also been reported: for example, toxicity [21], biodegradability [22], thermal/chemical stability [16,23–25], high viscosity [26,27], low mass diffusivity [28,29] and, in general, a lack of reliable data on properties. These drawbacks are briefly discussed below.

Toxicity and biodegradability: Besides favourable thermophysical properties, environmental impacts and safety concerns are also important considerations when selecting new working fluid candidates [30]. ILs are environmentally friendly alternatives for conventional volatile solvents because their low vapour pressure reduces air contamination. However, other properties such as their toxicity, biodegradability, and thermal/chemical stability should be fully characterized to determine whether ILs are potential "greener" options [16]. Several studies on their toxicity and biodegradability have shown that some ILs can be hazardous to aquatic and terrestrial ecosystems [21,22] and that imidazolium-based ILs containing, for example, $[BF_4]^-$ or $[PF_6]^-$ anions present high toxicity and low biodegradability.

Thermal stability: The thermal stability of ILs is a key property for absorption refrigeration systems, especially for the development of new high-temperature cycles. Low thermal stability can limit and decrease the performance of the

absorption cycle. Furthermore, in the case of the formation of corrosive and toxic products, operational safety can be also reduced [24]. The range of thermal stability of ILs is typically very large, and decomposition temperature values as high as 400°C have been reported for some ILs [23]. However, other ILs have relatively low thermal stability: for example, [emim][$EtSO_4$] and [bmim][$MeSO_4$] decompose at 50 °C [31]. Furthermore, the decomposition temperatures obtained from thermogravimetric analysis (TGA) using a single temperature ramp experiment, even at low scanning rates, are often overestimations of the long-term thermal stabilities of the ILs [23,24]. Therefore, commonly reported decomposition temperatures should be handled with caution when required for industrial purposes. This is particularly relevant for absorption systems since the use of ILs as absorbents requires prolonged operations at high temperatures under the atmosphere of a given refrigerant (such as ammonia, water, and carbon dioxide).

Chemical stability: The chemical stability of ILs is another factor that considerably limits their potential use as absorbents. In particular, the widely studied imidazolium-based ILs containing $[BF_4]^-$ and $[PF_6]^-$ anions are known to undergo hydrolysis reactions with water [16,25]. These reactions generate toxic fluoride by-products, which limit the use of these ILs to inert and dehydrated systems [19]. Furthermore, the hydrolysis reaction products introduce additional species into the solution that, in turn, can prevent thermodynamic relations and approaches from being used to describe the measured data [16,25]. Therefore, the comparison between the thermophysical properties and, thus, the suitability of different ILs as absorbents, can lead to erroneous conclusions if the additional species have not been recognized adequately and/or explicitly. Despite this, many publications use aqueous solutions of imidazolium based ILs with these anions for purposes of comparison, and very few of those publications have even mentioned the possible occurrence of hydrolysis.

Viscosity: The viscosity values of ILs are higher by several orders of magnitude than those of conventional absorbents such as water or aqueous LiBr solution. For example, the viscosity of basic imidazolium IL 1-butyl-3-methylimidazolium tetrafluoroborate ([bmim][BF_4]) is approximately 100 times that of water at 303.15 K [20]. Thus, when an ionic liquid is used as the absorbent in falling film flows for

absorption refrigeration, its high viscosity may lead to different film flow characteristics than those of the conventional fluid media [32]. This affects the wetting behaviour of the refrigerant/absorbent mixture, which has an impact on how much of the available heat and mass transfer area is used.

Poor wetting directly results in a thicker falling film. The laminar film thickness is also increased by the cubic root of the dynamic viscosity and, thus, with increasing viscosity, the heat transfer resistance in the heat and mass exchangers increases [33]. Also, the high viscosity of the ILs causes a considerable increase in the pressure drop, which can result in higher pumping power requirements to transport the refrigerant/IL mixture through the different components of the absorption cycle [26]. Despite the above, some authors [34] also hypothesize that a high viscosity of the absorbent may have advantages such as a greater residence time of the refrigerant/absorbent solution inside the absorber, which favours the absorption process.

Mass diffusivity: Typical mass diffusivity values of natural refrigerants in ionic liquids have been reported to be considerably lower than in conventional solvents [35–40]. For example, the mass diffusivity of ammonia in [bmim][BF_4] is approximately 17 times less than in water at 303.15 K [39,41]. A low mass diffusivity of the refrigerant in the absorbent is detrimental to the overall performance of the cycle, as a larger mass transfer area is required to complete the mass transfer duty in the absorber. In general, mass diffusivity has received comparatively much less attention than other properties, such as viscosity, because it cannot be measured by a standard experimental technique. Nevertheless, this property is especially important in highly viscous solutions such as those with ILs. In these solutions, the increased viscosity hinders convection in the typical falling film. This causes the mass transfer to be dominated by diffusion so a small diffusion coefficient can limit the cooling capacity of an absorption system [33].

Lack of reliable thermophysical property data: In recent years, there has been a considerable increase in the experimental data available on the properties of ionic liquids. However, data is still limited bearing in mind the large number of ILs available. Also, there are discrepancies in the thermophysical property values of ILs in the literature because purity, sample handling, and measuring methods or

procedures are different [42]. Information on the thermophysical properties of their mixtures with natural refrigerants is even scarcer. In this respect, the thermophysical data in the literature is limited to a small number of ILs. Most of the data focuses on their binary mixtures with water and carbon dioxide, and there is very little on their mixtures with ammonia.

The need for a reliable database of thermophysical properties of ammonia/ILs mixtures can be illustrated by examples from the literature. Wang et al. [43], for instance, recently used a semiempirical heat and mass transfer model to investigate the absorption process of NH_3 vapour in ILs inside plate heat exchangers (PHX). In their study, the mass diffusivity of NH_3 in [emim][SCN], the most promising absorbent liquid, was calculated using an empirical correlation. The correlation was based on diffusivity data reported for NH_3 in [emim][NTf_2] and showed an average relative deviation of 40%. The authors also carried out a sensitivity analysis of transport properties, including mass diffusivity, on the overall heat transfer coefficients, mass transfer flux on the effective mass transfer area, and the area ratio of the plates needed for mass transfer. From their sensitivity analysis, the authors found that a 90% “maximum” decrease in mass diffusivity implies that the PHX used cannot complete the mass transfer duty. But the deviation between the used value and the real value of the mass diffusivity can easily exceed 90%, since the diffusivity values for NH_3 in [emim][NTf_2] have been reported in the literature with a difference of more than an order of magnitude [28,39]. Therefore, in consideration of the potential variation in the mass diffusivity value, it is likely that the PHX used by Wang et al. [43] cannot complete the mass transfer duty.

Despite the considerable contribution of Wang et al’s study [43], which provides a viable methodology for analysing heat and mass transfer during the absorption process of ammonia in ILs, the uncertainty introduced in their results by the calculation of the mass diffusivity can lead to misleading conclusions about the suitability of a given IL as an absorbent. The lack of experimental data and the inconsistency of the few mass diffusivity values reported in the literature highlights the need for high-precision techniques to determine this property.

I.4 Research aspects on the selection of ionic liquids for absorption refrigeration

As illustrated in the previous section, many commercial and non-commercial ILs are identified as absorbents for natural refrigerants (e.g. water, CO_2, ammonia, methanol, ethanol, etc.), and many others are expected in the coming years. However, there is not yet a well-established methodology for selecting a suitable ionic liquid for a specific refrigerant and application. Accordingly, the different research aspects considered in the literature are summarized.

I.4.1 Phase behaviour of refrigerant/IL mixtures

The phase behaviour of refrigerant/IL mixtures is the first step in the screening process for absorbent selection. Figure I-5 illustrates the typical phase behaviour of ammonia with different absorbents (two ionic liquids and water) at ambient temperature. In this figure, vapour pressure is plotted against the ammonia composition in the mixtures, in contrast with the behaviour of the ideal mixture (i.e. Raoult's law). A negative deviation from Raoult's law means that the absorbent has a strong affinity towards the refrigerant. Thereby, the vapour pressure of the suitable absorbent should exhibit a large negative deviation from Raoult's law [19,44,45], at least comparable to or higher than water for the specified concentration range related to the application.

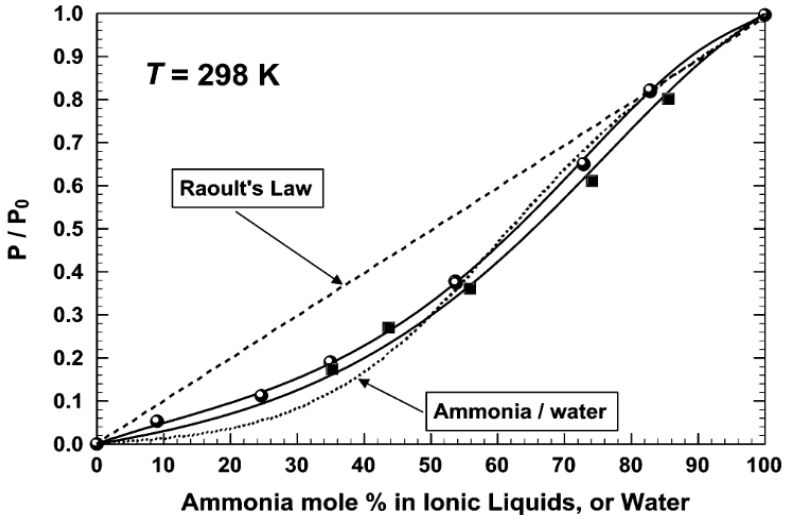

Figure I-5. Normalized (with pure NH_3) vapor pressure plots at 298 K, as a function of NH_3 content (mol %) for NH_3-[hmim][Cl] (circles) and NH_3-[bmim][PF_6] (squares) working pairs [44].

Once the absorbent has been identified by the appropriate phase behaviour, the vapour-liquid equilibria should be obtained in wide temperature and composition. Moreover, thermodynamic properties, such as heat capacity, excess enthalpy and density should be available and used to model the complete thermodynamic properties. Other key aspects such as material compatibility, thermal/chemical stability and safety/environmental risks should be considered carefully.

Thus, the next step in the research is to analyze the thermodynamic performance and operational range of the absorption refrigeration cycle [30,46–48].

I.4.2 Thermodynamic performance of the absorption refrigeration cycle

For this analysis, only thermodynamic data such as vapour-liquid equilibrium (VLE), enthalpy and density of solutions are needed. Various assumptions are made in order to simulate the absorption cycle: for example, the saturation conditions of the liquid streams exiting the absorber and the desorber [46,48]. From these simulations, the main indicators typically used for comparison are the coefficient of performance (COP), the solution circulation ratio (f) and the minimum driving heat temperature for a set of refrigeration and heat rejection temperatures. The influence of these temperatures and the desorber temperature on the performance of the system should also be analyzed.

Most of the studies in the literature are based on vapour-liquid equilibria data and the specific heat capacity data of pure fluids. With these data, the enthalpy of the refrigerant/absorbent solution is estimated using equations of state, such as the Redlich-Kwong [18], or g^E models, such as NRTL [15]. Other properties, such as density are also frequently calculated. As a result, the performance indicators are strongly dependent on the approach used to calculate the relevant thermodynamic properties.

For instance, Figure I-6 shows the COP of the working pair H_2O/[emim][DMP] in an absorption refrigeration cycle calculated by Wang et al. [49] using different VLE models. As can be seen, the values calculated using these models are in the range of between 0.7 and 0.98 at a generator temperature (T_{gen}) of 100 ºC. Moreover, the authors also found that the solution circulation ratio (f) of the NH_3/[bmim][BF_4] calculated by the NRTL model (f = 250) is more than five times that calculated by the UNIFAC model (f = 50).

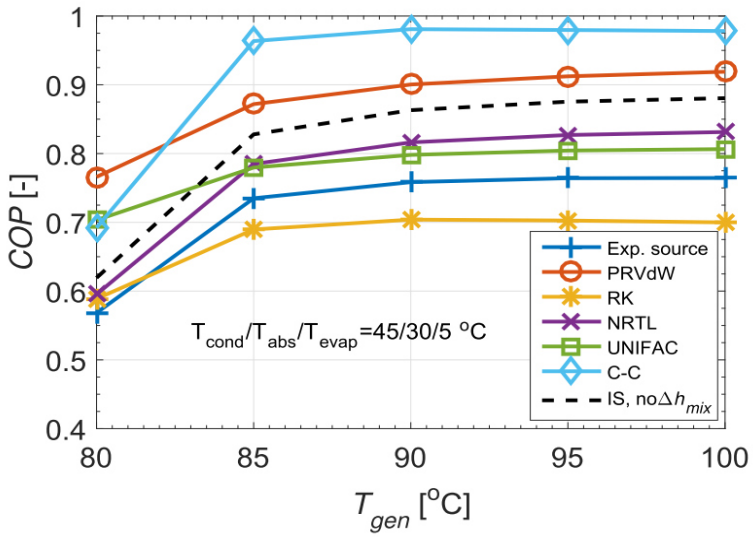

Figure I-6. Coefficient of performance (COP) of the H_2O/[emim][DMP] working pair in an absorption refrigeration cycle when the different VLE models are applied [49].

Therefore, this type of cycle performance analysis should use reliable thermodynamic property data of the working fluid mixture and the appropriate property estimation method.

Despite the above, the thermodynamic analysis of the absorption refrigeration cycle for IL-based working pairs could be useful in the preliminary estimation of the performance of these fluids compared to conventional working pairs. For example, some authors [5,18,33,47,50–52] have found that the COPs of IL-based working pairs are slightly lower but comparable to those of conventional working pairs. However, unlike the COPs, the solution circulation ratio has been found to be significantly higher, which is attributed to the length, and complexity of the ionic liquid structure. A high solution circulation ratio is detrimental to cycle performance and system component size.

Figure I-7 illustrates the COP and solution circulation ratio (f) for different NH_3/ILs working pairs and NH_3/H_2O [18]. It can be seen that the solution circulation ratio of the NH_3/[emim][NTf_2] pair is approximately ten times higher than that of the NH_3/H_2O pair. Moreover, for a fixed solution mass flow rate, the solution circulation ratio is related to the cooling capacity (Q_E); it is lower when the cooling capacity is high, and vice versa [33]. Thus, for a fixed solution mass flow rate, Q_E is expected to be significantly lower for IL-based working pairs than for the conventional working pairs.

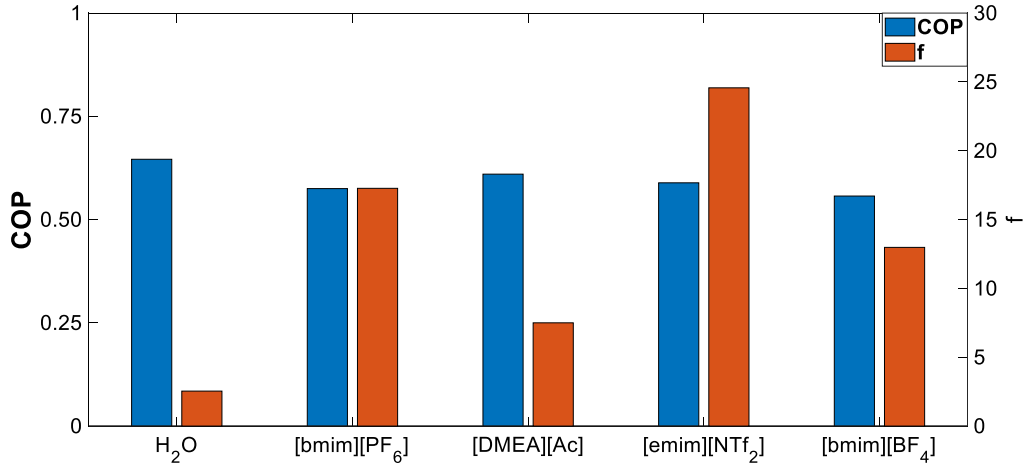

Figure I-7. COP and solution circulation ratio (f) for different Ammonia /ILs pairs and the conventional working pair Ammonia/H_2O [18].

Once the thermodynamic performance of the working pairs has been analyzed, the next step is to study the heat and mass transfer processes in the absorber and desorber.

I.4.3 Heat and mass transfer phenomena in ab/desorption processes

As well as thermodynamic properties, transport properties such as viscosity, thermal conductivity, surface tension and mass diffusivity of the mixtures are needed to study the heat and mass transfer processes in the absorber and desorber.

As mentioned above, ionic liquids often exhibit unfavourable transport properties for absorption systems. The influence of these properties on heat and mass transfer performance is quite noticeable, which makes them one of the main limitations for effective implementation of ILs in absorption cycles.

Illustratively, Figure I-8 (a) shows the poor wetting behaviour observed for a mixture of [DEMA][$MeSO_3$] with water. The low wettability of the solution on the horizontal tube bundle reduces the heat and mass transfer area and increases the mass transfer resistance. This behaviour was experimentally observed by Römich et al. [53] in a commercial absorption chiller (SK Sonnenklima), initially designed for water/LiBr. The authors stated that the high viscosity of pure IL and the low concentration in water (5-20%) were the main causes for this poor wetting behavior. Consequently, the water absorption rate was reduced so the cooling capacity decreased.

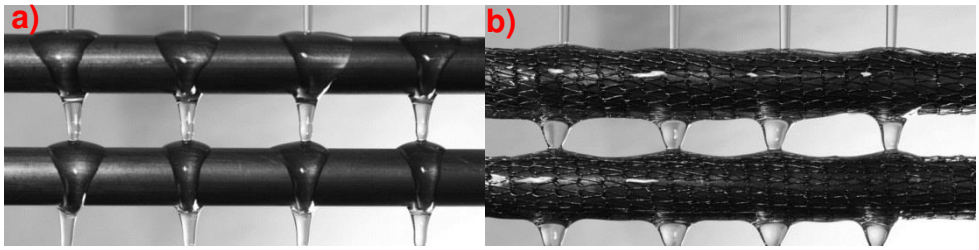

Figure I-8. Falling film flow of a solution H_2O/IL in horizontal tubes within an absorber initially designed for water/LiBr:(a) observed poor wetting behavior; (b) improved wetting behaviour after attaching a fine metal mesh.

However, the unfavourable high viscosity of IL-based working pairs can be overcome by developing new concepts for absorbers and desorbers, which ensure good hydrodynamics for heat and mass transfer. For example, Römmich et al. [53] achieved better wetting of the horizontal tubes by attaching a fine metal mesh, as shown in Figure I-8 (b). Nevertheless, increasing fundamental knowledge of heat and mass transfer in cycle components is essential if new concepts for these components are to be efficiently developed. This knowledge can be increased using appropriate models.

In the literature, there are several analytical and numerical models that discuss simultaneous heat and mass transfer processes in falling film absorption under certain boundary conditions. However, these more complex models require the input of several thermophysical properties of the working pairs investigated, such as density, viscosity, thermal conductivity and mass diffusivity, in addition to the VLE data and enthalpy of the solution. Since there is very little experimental data on these properties for natural refrigerant/IL mixtures, the calculations are usually performed using different correlations for these properties [43].

However, as shown in the section above, the use of correlations to obtain transport properties in ILs, such as mass diffusivity, can introduce highly uncertainty in the results of the models used to perform the heat and mass transfer analysis. Moreover, the uncertainty of the results can be further increased if other correlations are also used to calculate the additional properties required for the study. Consequently, the interpretation of these results can lead to erroneous conclusions about the suitability of an IL.

Furthermore, as the models used to analyze the heat and mass transfer processes are not yet mature, it is recommended that theoretical investigations should be validated using experimental data [33].

I.4.4 Experimental test of the IL-based absorption chiller

Very few experimental studies have been made on absorption refrigeration systems using ILs. Besides, most of the studies that have been reported in the literature focus on the investigation of Water/IL systems. For example, Römich et al. [53] examined the performance of a commercial absorption chiller (SK Sonnenklima) using Water/[DEMA][$MeSO_3$] in a test bench. They reported that the COP for water/[DMEA][$MeSO_3$] is close to that achieved with the conventional working pair Water/LiBr in the same thermal conditions. However, the cooling capacity was around 1.3 kW, much lower than the nominal capacity (10 kW).

Subsequently, Kühn et al. [54] reported experimental results for various Water/ILs tested in a small scale absorption chiller prototype with a glass shell at the Technische Universität Berlin. For the best ILs tested, with COPs comparable to Water/LiBr, the cooling capacity (Q_E) was considerably lower (see Figure I-9).

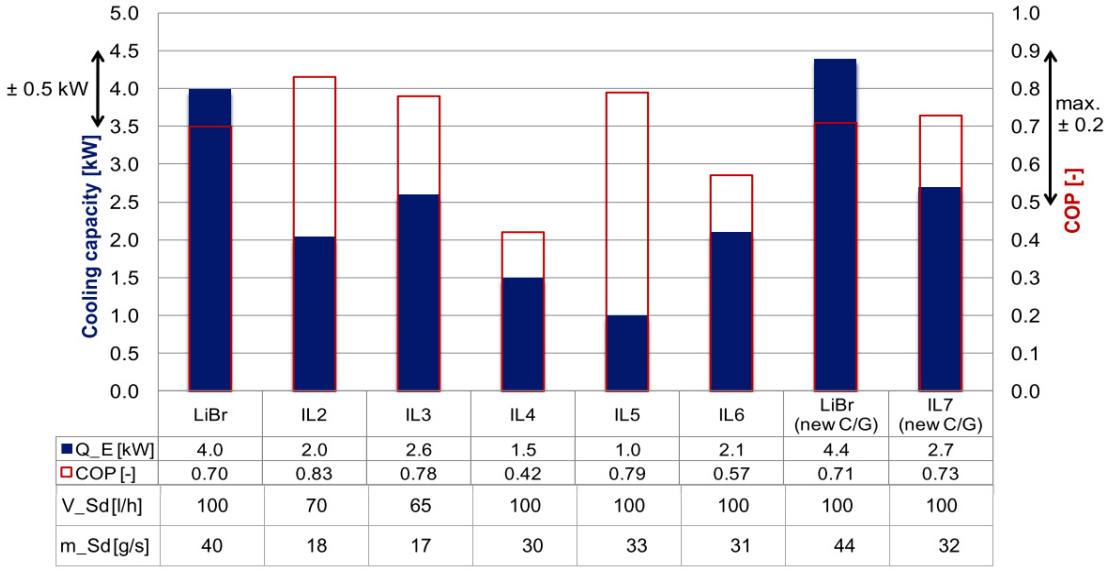

	LiBr	IL2	IL3	IL4	IL5	IL6	LiBr (new C/G)	IL7 (new C/G)
Q_E [kW]	4.0	2.0	2.6	1.5	1.0	2.1	4.4	2.7
COP [-]	0.70	0.83	0.78	0.42	0.79	0.57	0.71	0.73
V_Sd [l/h]	100	70	65	100	100	100	100	100
m_Sd [g/s]	40	18	17	30	33	31	44	32

Figure I-9. Experimental cooling capacity and COP for different water/ILs pairs and for the conventional water/LiBr pair [54].

Previous experimental studies [33,54] show that the reduced cooling capacity for water/ILs systems is the result of a mass transfer inhibition due to unfavourable transport properties. In particular, the cooling capacity has been reported to be strongly dependent on the mass diffusivity of the refrigerant in the IL [33,55,56].

Therefore, in addition to thermodynamic properties, the experimental results indicate that transport properties such as viscosity and mass diffusivity should be considered when selecting a favourable IL for the application.

I.5 Experimental studies on the absorption process of ammonia

In an original study, Kojima and Kashiwagi [57] used a holographic real-time interferometry technique to study the absorption process of ammonia in a pool-type absorber. During the absorption process, the time evolution of ammonia concentration profiles in the absorbent was determined. In particular, the field of view covered by the technique was a small area near the vapour-liquid interface, around 20 mm inside the liquid bulk, as shown in Figure I-10.

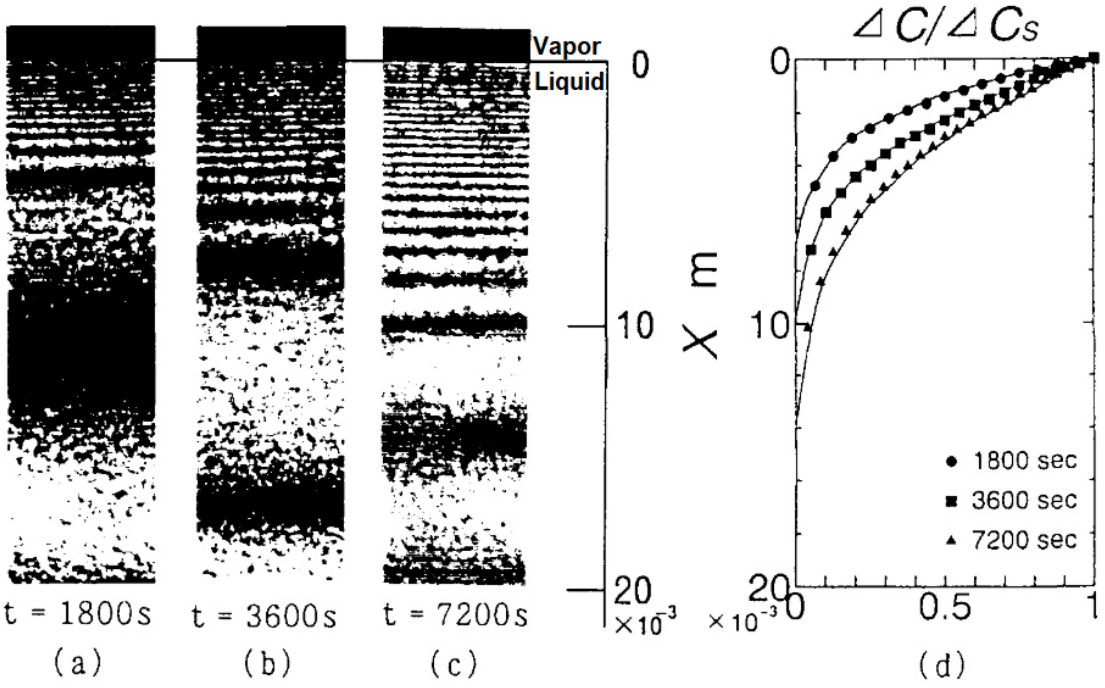

Figure I-10. Interferograms and concentration distributions obtained by interference fringes in the study by Kojima and Kashiwagi [57].

The time-dependent distribution of the ammonia concentration (Figure I-10 d)) was obtained by simply counting the number of interference fringe shifts in the field of view at each instance (Figure I-10 a), b), and c)). Finally, the mass diffusivity was obtained by fitting the experimental distribution of ammonia concentration to a theoretical model based on the one-dimensional (1-D) unsteady diffusion equation. The main hypotheses of the mass diffusion model used were: (1) the vapour-liquid interface is saturated with ammonia throughout the absorption process, and (2) the contact time between the ammonia and the absorbent is

short. The authors reported the mass diffusivity of ammonia in various absorbents, such as water, lithium thiocyanate (LiSCN), sodium thiocyanate (NaSCN), lithium nitrate ($LiNO_3$), lithium bromide (LiBr), and aqueous lithium bromide solutions ($LiBr/H_2O$). They also investigated the effect of additives on enhancing the absorption.

Subsequently, Mahmoud [58] and Mustafa [59] analyzed the absorption process of ammonia vapour in a stagnant pool of ammonia/water mixture using three different experimental approaches: the pressure drop method (PDM), the interface heat flux method, and optical interferometry. They compared the absorption rate values obtained from the three experimental methods used and found that the results of PDM and interferometry show reasonable agreement but are in disagreement with those obtained using the interface heat flux method.

The pressure drop method stands out for its simple design and wide experimental range [60]. A schematic representation of the setup based on the PDM used by Mahmoud [58] is depicted in Figure I-11.

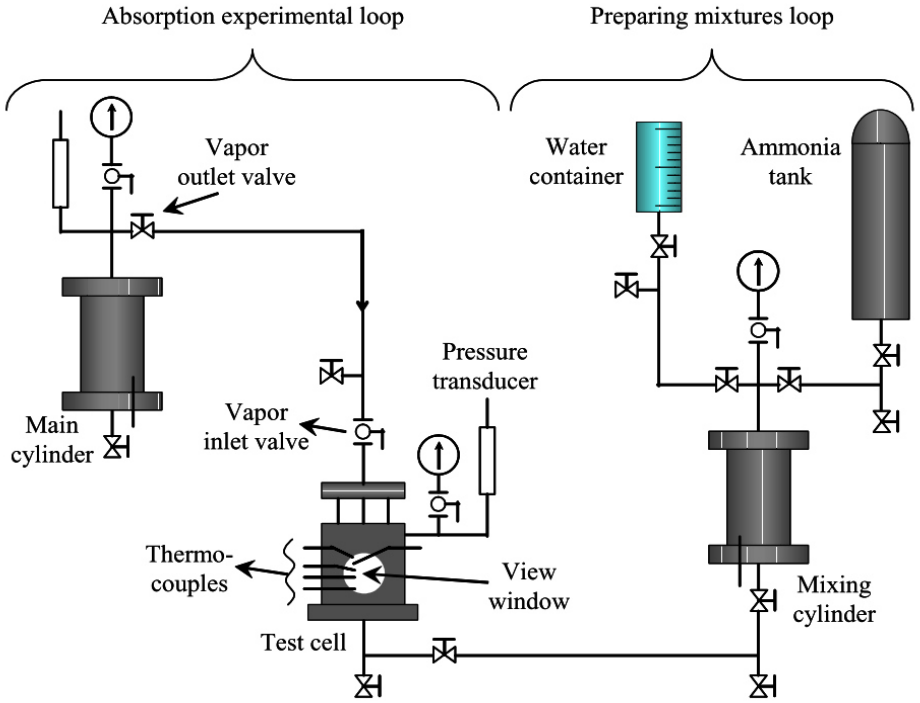

Figure I-11. Schematic of the experimental setup based on the Pressure Drop Method used by Mahmoud [58].

The main components of the setup are the test cell, in which the absorption process takes place, and the main cylinder, which contains the ammonia vapour that feeds the test cell during the absorption process.

The use of PDM provides, among other data, the time evolution of the temperature, pressure, and mass of the refrigerant absorbed during the absorption process. Therefore, the absorption rate, which is defined as the ammonia mass absorbed per unit of interfacial area over time, can be easily obtained. The absorption rate is a key magnitude related to the heat and mass transfer mechanisms between the refrigerant vapour and the absorbent liquid during the absorption process.

However, despite its versatility, the PDM does not provide any information on the spatial distribution of the refrigerant concentration in the liquid mixture during the absorption process. Therefore, the authors used a Mach-Zehnder interferometer to visualize the heat and mass transfer near the vapour-liquid interface. In this case, the field of view covered by the optical technique was around 12 mm inside the liquid mixture, as shown in Figure I-12.

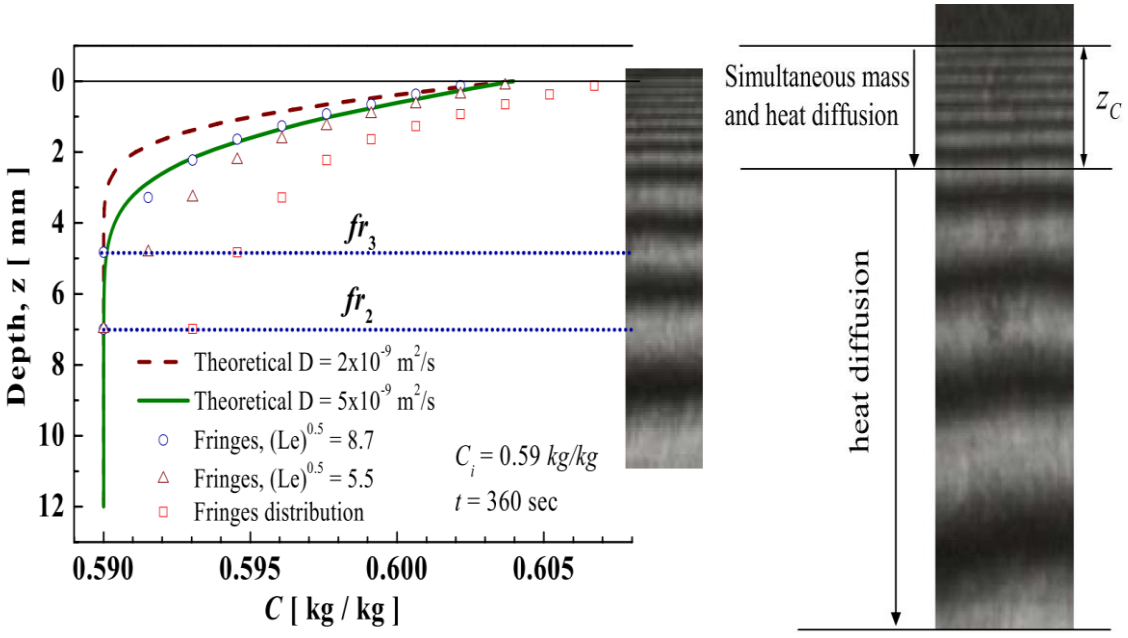

Figure I-12. Visualization of the heat and mass transfer during the absorption process of ammonia in ammonia/water mixture using optical interferometry by Mustafa [59].

The interferograms obtained allowed the authors to identify two diffusion layers at short absorption times. In the first layer, near to the interface, the simultaneous mass and heat diffusion occurs, while in the other layer far from the interface, only heat is diffused. The ammonia concentration profiles were obtained by simply counting the number of interference fringe shifts in the field of view. In their respective studies, Mahmoud [58], and Mustafa [59] did not determine the mass

diffusivity but did provide a better description of the observed concentration profile. To identify the most appropriate mass diffusivity value from the literature, the authors also used a model based on a 1-D unsteady diffusion equation valid at short absorption times. However, unlike the model used by Kojima and Kashiwagi [57], the mass diffusion model used by Mahmoud [58] and Mustafa [59] did consider the variation in time of the concentration at the vapour-liquid interface. In particular, the ammonia concentration at the interface was determined assuming an instantaneous equilibrium between the vapour and liquid phases at the temperature and pressure at each instant of time during the absorption process. The authors [58,59] found a disagreement between the concentration distribution obtained by fringe analysis and that obtained by the mass diffusion model. The disagreement was attributed to the effects of heat on fringe formation.

More recently, our research group [28,61] investigated the behaviour of the absorption process and determined the mass diffusivity of ammonia in three selected ionic liquids. The ionic liquids studied were: 1-ethyl-3-methylimidazolium bis(trifluoromethylsulfonyl)imide ([emim][NTf_2]), 1-(2-hydroxyethyl)-3-methylimidazolium tetrafluoroborate ([EtOHmim][BF_4]), and 1-(2-hydroxyethyl)-3-methylimidazolium bis(trifluoromethylsulfonyl)imide ([EtOHmim][NTf_2]). The absorption process of ammonia in the ionic liquids studied took place at 30ºC and a pressure of 3, 4, and 5 bar.

The experimental setup used a mass flow controller, which allows more ammonia to enter the system during the absorption process to keep the pressure constant. The readings of the mass flow controller show the mass of ammonia absorbed in the ionic liquid as a function of time during the absorption process. Finally, the mass diffusivity of ammonia in the ionic liquids studied was obtained using a non-linear regression procedure between the absorbed mass and the mass diffusion model developed by Yokozeki [62].

Like the mass diffusion model used by Kojima and Kashiwagi [57], the mass diffusion model developed by Yokozeki [62] assumes a constant saturation concentration at the vapour-liquid interface throughout the absorption process. However, unlike the model used by Kojima and Kashiwagi [57], it is valid when

the contact time between the refrigerant vapour and the absorbent is long in comparison with the height of the absorbent in the absorption cell.

I.6 Motivation

Previous experimental studies on the absorption process show that optical techniques for direct visualization of diffusion phenomena near the vapour-liquid interface are powerful tools for investigating the absorption process. Optical techniques have been widely used in several branches of science and engineering for monitoring online process due to their accuracy, high resolution, instantaneous response and non-intrusive nature [63,64]. Interferometry is one of these techniques, which is used to measure the variations in the refractive index of a transparent medium [65]. It is well-known that the refractive index of the liquid phase changes over time during the vapour-liquid absorption process [66]. Therefore, useful information about the absorption process can be extracted by monitoring the refractive index variation fields with optical interferometry and a suitable processing method.

In recent years, advancements in lasers and charge-coupled devices (CCD) have permitted optical interferometry to drastically increase the accuracy of the measurement, from the typical, not very accurate interferograms, such as those used by Kojima and Kashiwagi [57] or Mahmoud [58], to high-resolution digital images. Illustratively, Figure I-13 shows the evolution of the typical interferograms obtained during the absorption process of vapour in absorbent liquids in some experimental studies from the literature [57,58,67].

At the same time, more sophisticated image processing methods have become available that can be easily implemented in computational packages such as MATLAB® [68]. One of these methods is Optical Digital Interferometry (ODI). This method has been successfully used to determine diffusion and thermodiffusion coefficients, and to visualize heat and mass transfer in liquid mixtures [65,69,70]. The unique feature of the ODI method is that it traces the transient path of the system throughout the 2D cell cross-section and the diffusion process [71].

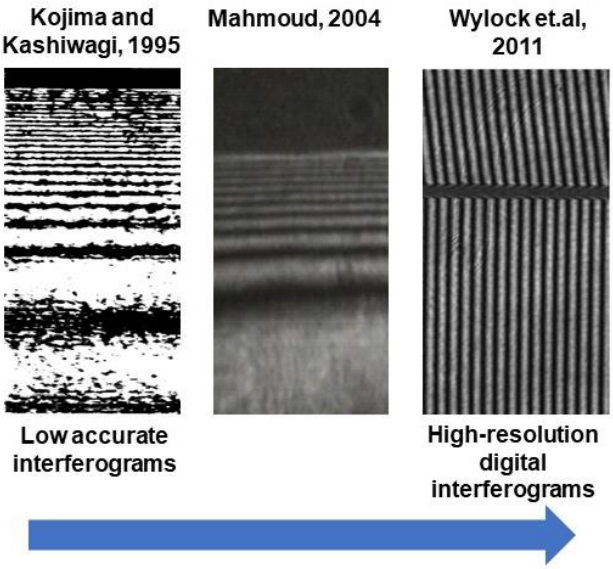

Figure I-13. Evolution of typical interferograms obtained during the absorption process of vapour in absorbent liquids.

Therefore, the application of the ODI method can help reveal more valuable and higher quality information about the absorption process of ammonia in ILs. For example, it can show the time evolution of the ammonia concentration profiles in the ILs during the absorption process. These profiles can be used to assess whether a specific boundary condition or model is suitable for describing ammonia mass diffusion during the absorption process correctly. Moreover, the time evolution of ammonia concentration profiles is also useful for the development and validation of more complex heat and mass transfer models that can be used for screening suitable ILs as absorbents for this natural refrigerant.

The ODI method can also be used to determine the mass diffusivity of natural refrigerants in ILs, an essential transport property, before going on to make a detailed study of the heat and mass transfer performance of new working pairs based on ILs, so that different types of absorbers can be properly designed with ionic liquids as absorbents.

I.7 Objectives

The main objective of this thesis is to study the absorption process of ammonia into ionic liquids to determine (1) the time evolution of the absorption rate and (2) the time evolution of concentration profiles of the ammonia refrigerant in ionic liquids. These experimental data are useful for developing and validating the heat

and mass transfer models used to describe the absorption process of natural refrigerants in ionic liquids.

In this thesis, the Pressure Drop Method was selected to study the absorption process due to its simplicity and flexibility. It was combined with Optical Digital Interferometry because it can accurately and non-intrusively determine the time evolution of the concentration profiles in the absorbent.

The theoretical work includes the modelling of the absorption process using different mass diffusion models, and the estimation of the ammonia mass diffusivity in the absorbents.

To achieve the above-mentioned objective, we set the following specific objectives:

1. To develop and implement a new experimental setup based on the Pressure Drop Method and an optical system (Mach-Zehnder interferometer) and study the absorption of ammonia into selected ionic liquids.
2. To analyze thermal and pressure-drop behaviour during the absorption of ammonia into the selected ionic liquids.
3. To determine the time evolution of the absorption rate of ammonia vapour into the selected ionic liquids using the Pressure Drop Method.
4. To understand the Optical Digital Interferometry method and develop the methodology for determining mass diffusivity in a binary liquid system of the natural refrigerant, water, and an ionic liquid.
5. To determine and visualize the time evolution of the ammonia concentration profiles in the ionic liquids selected during the absorption process using Optical Digital Interferometry.
6. To model the ammonia mass diffusion in the ionic liquids selected during the absorption process using different assumptions and boundary conditions at the vapour-liquid interface.
7. To calculate the mass diffusivity of ammonia in ionic liquids using different thermodynamic models and empirical correlations.
8. To investigate the relevance to the performance of the absorption process of the solubility and mass diffusivity of ammonia in selected ionic liquids.

I.8 Thesis structure

This thesis is divided into six chapters: The first chapter discusses the background, justification and objectives of the thesis. A short description of the absorption refrigeration systems, the conventional working pairs, their limitations, and the potential use of ILs as absorbent liquids is given. It also discusses the need for an experimental investigation into the absorption process and further highlights the importance of the mass diffusivity of natural refrigerants in ionic liquids. Then, some previous studies on the absorption process of ammonia in absorbents are described. Of the methods presented, Optical Digital Interferometry and the Pressure Drop Method stand out.

In the second chapter, the time evolution of the rate of absorption of ammonia vapour into selected ionic liquids is determined. To do this, the first step in the methodology consisted of selecting the ionic liquids to be used in the absorption experiments. For the selection of ionic liquids, the solubility and transport properties of ammonia/ionic liquids mixtures were considered. Then, the Pressure Drop Method, the experimental setup, and the experimental procedure are described in detail. Then, the treatment of the raw experimental thermodynamic data collected in this thesis is explained. The thermal and pressure-drop behaviour of the mixtures is presented, and their trends discussed. Then, the time evolution of the absorption rate is presented and discussed.

The third chapter is devoted to mass diffusivity, which is an essential transport property in absorption processes. First, the fundamental concepts related to diffusion, measurement methods, and models for the estimation of mass diffusivities are presented. Then, a literature review is provided on measuring and modelling mass diffusivity in working fluid mixtures used in absorption technology.

In the fourth chapter, the Optical Digital Interferometry method is applied to determine the mass diffusivity of water in the ionic liquid, 1-(2-hydroxyethyl)-3-methylimidazolium tetrafluoroborate. The experimental work in this chapter will enable us to become familiar with an advanced optical technique, the corresponding image processing steps, and the use of mass diffusion models.

This experience will serve as a basis for modifying and applying the ODI method in the study of the absorption process in chapter five.

In chapter five, the absorption process of ammonia into ionic liquids is investigated using the ODI method. In particular, the absorption experiments described in the second chapter were visualized with a Mach-Zehnder interferometer to obtain new *spatio-temporal* data of the absorption process. Therefore, in this chapter, the use of the ODI method is first described so that the time-evolution of the ammonia concentration profiles in the absorbent can be determined. Then, the mass diffusion during the absorption process of ammonia in ionic liquids is modelled using two mass diffusion models which have different key assumptions and boundary conditions. Subsequently, the ODI method for the absorption of ammonia in water is validated, and then the experimental results obtained using the two mass diffusion models are discussed. After that, the estimation capability of the models chosen to describe the experimental mass diffusivity of ammonia in ionic liquids is assessed. Then, the relevance to the performance of the absorption process of the solubility and mass diffusivity of ammonia in selected ionic liquids is investigated.

Finally, the concluding chapter presents the main findings and some recommendations for future work.

UNIVERSITAT ROVIRA I VIRGILI
THEORETICAL AND EXPERIMENTAL STUDY OF THE ABSORPTION PROCESS OF AMMONIA IN IONIC LIQUIDS FOR ABSORPTION REFRIGERATION SYSTEMS
Ronny Rives Sanz

Chapter II
Experimental determination of the absorption rate of ammonia vapour into the selected ionic liquids

In this chapter, the time evolution of the rate of absorption of ammonia vapour in selected ionic liquids was determined. To do this, the first step in the implemented methodology consisted of the selection of the ionic liquids used in the absorption experiments. For the selection of ionic liquids, the solubility and transport properties of ammonia/ionic liquids mixtures will be considered. Then, the Pressure Drop Method, the experimental setup implemented, and the experimental procedure used were described in detail. After that, the treatment of the raw experimental thermodynamic data collected in this thesis is explained. Thus, thermal and pressure-drop behaviour of the studied mixtures were presented, and their trends discussed. Finally, the time evolution of the absorption rate of ammonia in the absorbent studied is presented and discussed.

II.1 Selection of the ionic liquids used as absorbents for ammonia refrigerant

The selection of ionic liquids for the investigation of the ammonia absorption process is the first step of our methodology. In particular, we have selected three ionic liquids with different physicochemical characteristics, which exhibit opposite solubility and viscosity trends. Furthermore, the selection was also made considering the availability of experimental data on solubility and diffusivity with ammonia. Figure II-1 shows the corresponding chemical structures and a more detailed explanation of the selection for each of the ILs used are provided below.

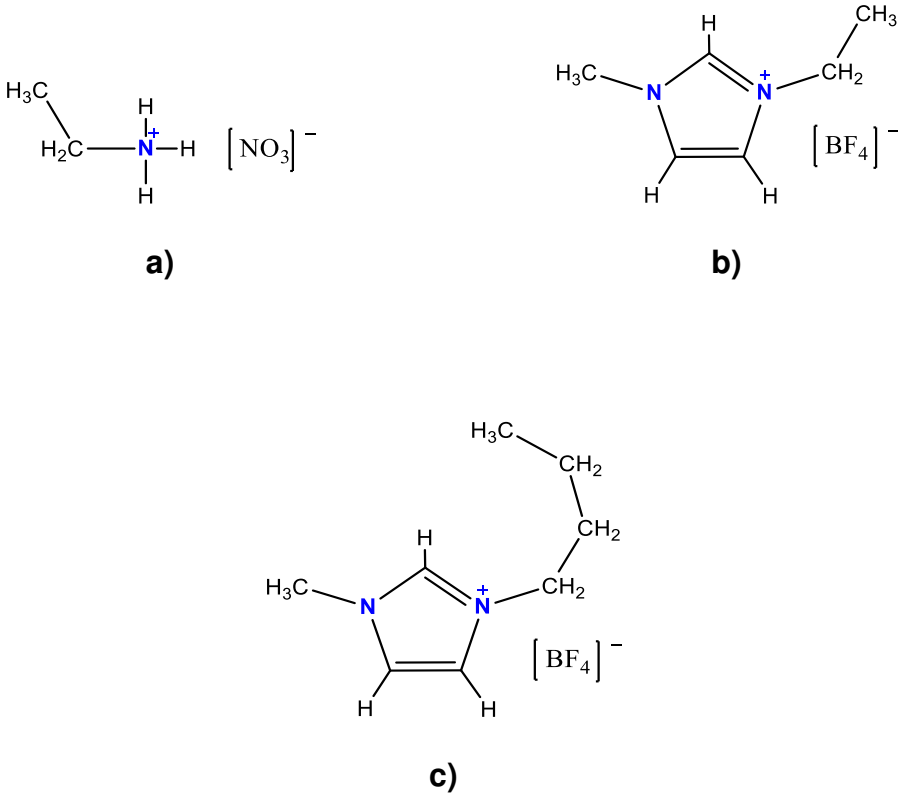

Figure II-1. Chemical structures of the selected ionic liquids: a) ethylammonium nitrate; b) 1-ethyl-3-methylimidazolium tetrafluoroborate; c) 1-butyl-3-methylimidazolium tetrafluoroborate.

- **Ethylammonium nitrate**

  Ethylammonium nitrate (EAN) belongs to the family of alkyl ammonium nitrates, which are among the most studied ionic liquids since the beginning of the 20th century. EAN is structurally one of the simplest ILs and shares many properties with water, such as micelle formation, aggregation of

hydrocarbons, and negative enthalpy and entropy of dissolution of gases [72]. Furthermore, its extensive three-dimensional network of hydrogen bonds has been reported to be fairly similar to the one of liquid water [73]. EAN show a relatively low molecular weight, viscosity, and toxicity compared to other ILs [74,75]. Considering the above, it is interesting to evaluate the potential of EAN as a replacement of H_2O in the conventional working pair NH_3/H_2O for absorption refrigeration systems. Therefore, our research group has recently measured the vapour-liquid equilibria (VLE) of NH_3/EAN mixtures [76]. Thermodynamic simulation of a single-stage absorption cycle was also performed. Also, at this time, some other important properties like density and viscosity of the NH_3/EAN mixtures, are being measured. Viscosity data for pure IL are already available [74].

- **1-ethyl-3-methylimidazolium tetrafluoroborate**

1-ethyl-3-methylimidazolium tetrafluoroborate ([emim][BF_4]) is one of the simplest imidazolium-based ILs, which have been widely and favourably used in different applications. In particular, [emim][BF_4] has previously been investigated by our research group as a potential absorbent not only for ammonia [31] but also for 2, 2, 2-trifluoroethanol [30]. Furthermore, it has also been proposed as an absorbent for water [77]. VLE data for the NH_3/[emim][BF_4] mixture is already available in the literature [78]. Viscosity data for pure [emim][BF_4] are also available [79]. In this thesis, the previous information on the absorption process of ammonia vapour in [emim][BF_4] is complemented with new experimental data.

- **1-butyl-3-methylimidazolium tetrafluoroborate**

1-butyl-3-methylimidazolium tetrafluoroborate ([bmim][BF_4]) is also an imidazolium-based ILs. For this IL, it has been observed that ammonia vapour can be almost completely desorbed at the absorption temperature [36]. It suggests an easy regeneration step of this IL absorbent by desorption, which may be facilitated by heating or vacuum. Although [bmim][BF_4] shows a considerable high molecular weight and viscosity [20], it is structurally simpler than other imidazolium-based ILs. VLE data for the NH_3/[bmim][BF_4] mixture are already available in the literature [39,51,78]. In

this thesis, the investigation of the absorption process of ammonia in [bmim][BF_4] has a twice fold purpose. On the one hand, [bmim][BF_4] is used for comparison, since diffusion data for ammonia in this ionic liquid are available from two different literature sources [36,39]. On the other hand, it is known that the solubility of ammonia in [bmim][BF_4] is higher than in [emim][BF_4] [78], but its viscosity is also higher [20,79]. Consequently, according to the relationship between viscosity and diffusivity, the diffusivity of ammonia in [emim][BF_4] is expected to be higher than in [bmim][BF_4]. Therefore, a joint analysis of the absorption process of ammonia vapour in [emim][BF_4] and [bmim][BF_4] would be useful to find the balance between solubility and diffusivity that a suitable absorbent should exhibit.

II.2 The pressure drop method

Once the ILs have been selected, the next step is the selection of a proper experimental method for determining the ammonia absorption rate. We have found in the literature that the Pressure Drop Method (PDM) is easy to implement, provides great experimental flexibility, and has previously been used for the determination of the absorption rate of ammonia in aqueous solutions [58,59,80,81]. Therefore, this method can be conveniently used to validate our results with those of the literature using the NH_3/H_2O working pair as a reference before determining the absorption rate in ILs.

The PDM states that in a closed isothermal system, all changes in the system pressure are due to the vapour absorption into the liquid phase. Consequently, the mass uptake by the absorbent liquid is determined indirectly by measuring the system pressure during the absorption process. This method requires rather careful calibrations and can only be used for refrigerant vapours whose properties are well-known.

The PDM can be implemented using different experimental setups [82]. Figure II-2 shows a schematic representation of the experimental setup implemented in this chapter to determine the absorption rate of ammonia in the selected ILs. The main components of the experimental apparatus are the absorption cell (see Figure II-3 for more details) that contains the absorbent liquid and a cylindrical tank where the ammonia vapour is stored at a higher pressure. The absorption

cell and the cylindrical tank are connected by a valve that is initially closed. The absorption process starts when the ammonia vapour and the absorbent liquid are brought into contact by opening the valve. After opening the valve, the phases come into contact, and the absorption process of ammonia vapour into the absorbent begins due to good chemical affinity existing between both chemical compounds. Subsequently, the system pressure drops as ammonia passes from the vapour phase to the liquid phase.

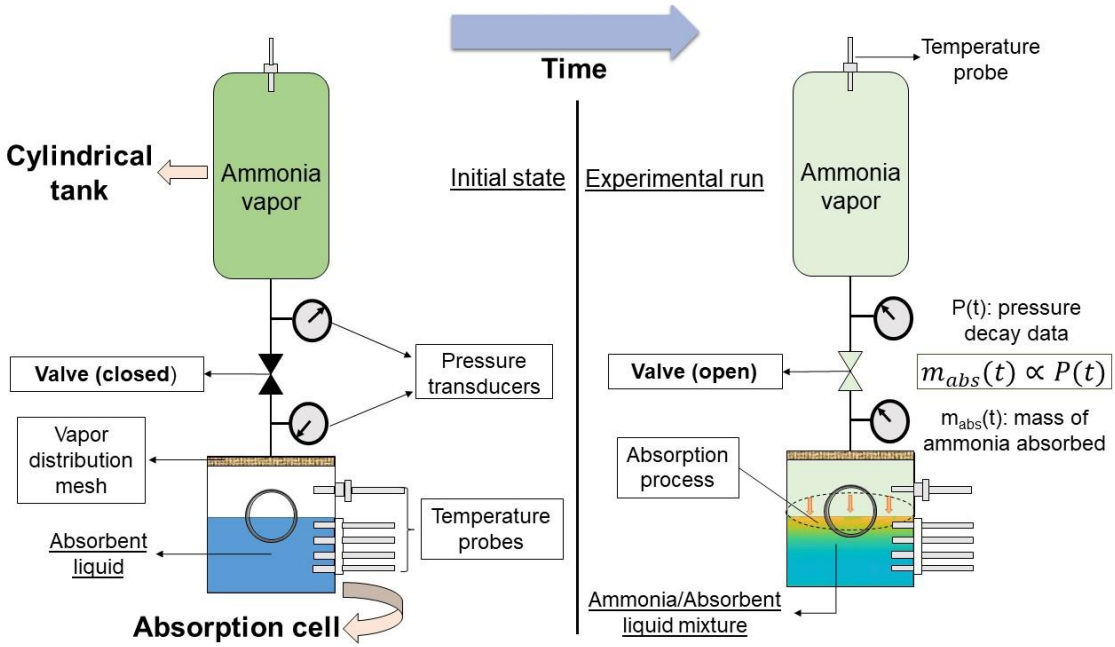

Figure II-2. Schematic representation of the experimental setup used to determine the absorption rate by the pressure drop method.

In the PDM, pressure readings are used to determine the mass of ammonia in the vapour phase at each time instance. For this, it is necessary to know the temperature and the volume of the absorption cell, the cylindrical tank and the connecting tubes. Furthermore, a common assumption in the literature is that the volume of the liquid phase remains constant during the absorption process [58,59]. Then, the mass of ammonia absorbed in the liquid phase in each time instance is obtained from the instantaneous mass of ammonia in the vapour phase, and the initial mass of ammonia loaded in the experimental setup. In the next step, a mathematical function is used to express the mass of ammonia absorbed as a function of time. Finally, the absorption rate is determined by taking the derivative with respect to time of the mathematical function used.

The PDM has been used to analyze the effect of different factors in the absorption process of ammonia vapour in aqueous solutions. Such factors include the temperature, pressure, and ammonia concentration of the solutions. However, in our study, we are more interested in using this method to evaluate the suitability of different ionic liquids as potential absorbents for ammonia refrigerant. Therefore, in the first stage, it is more convenient to simplify the experiments as much as possible to save resources, research efforts, and time. Then, once the most suitable ionic liquids for the absorption of ammonia have been identified, more detailed studies considering the influence of the aforementioned factors can be carried out with this method.

The main simplification of the experiments carried out in this chapter consists in limiting the analysis to those experimental situations in which it can be considered that NH_3 is present only under conditions of infinite dilution in the ILs selected. In this way, the variation of the thermophysical properties of the NH_3/ILs binary mixture during the absorption process can be neglected. Furthermore, the thermophysical properties obtained in this thesis, such as mass diffusivity, can be taken as a limiting value, since as the ammonia concentration in the absorbent increases, the viscosity of the mixture is expected to decrease and therefore, the diffusivity to increase.

Moreover, the reliability of the results obtained with the PDM depends largely on the design features of the experimental setup [58,59,82]. The relative sizes of the absorption cell and cylindrical tank, the interface area, and the location of the data acquisition system probes are some of the main factors that affect the reproducibility of the results. Thus, in the next section, the implemented experimental setup is described in detail.

II.2.1 Experimental setup

The absorption cell is the main component of the entire experimental device because it is where the absorption process occurs. A schematic representation of the cross-section of the absorption cell used for the experiments is shown in Figure II-3. The absorption cell represents a static pool type absorber, in which the absorbent liquid is quiescent, and no convective movement affects the transport of the absorbed vapour.

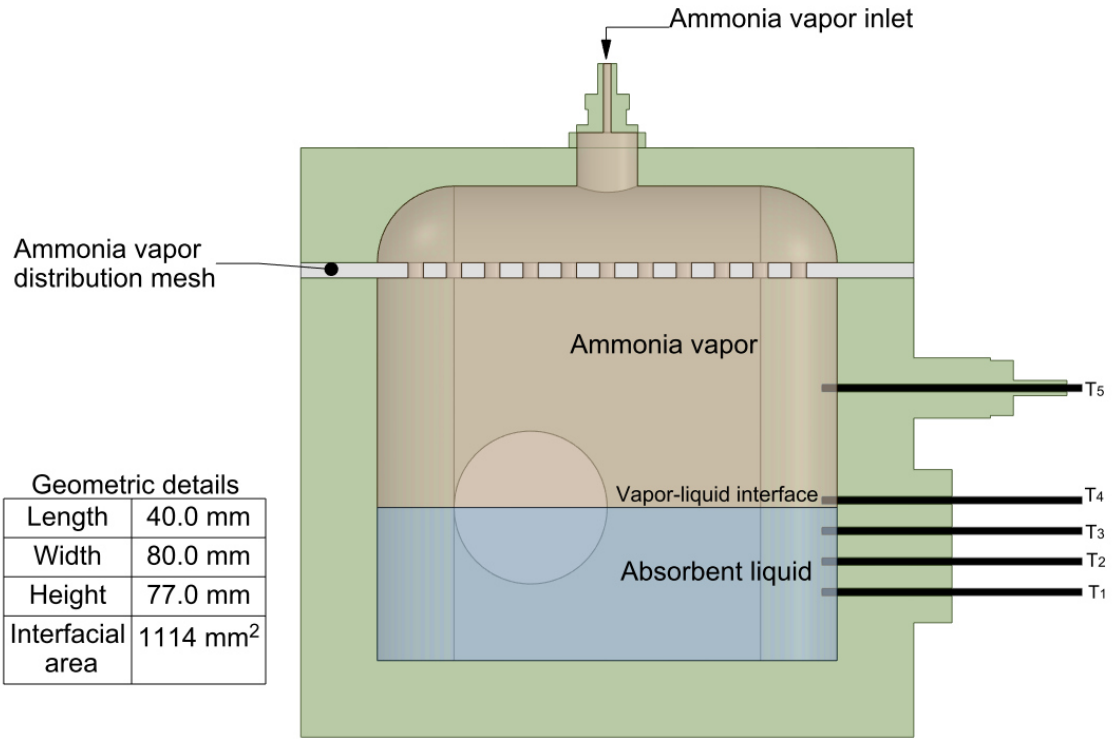

Geometric details

Length	40.0 mm
Width	80.0 mm
Height	77.0 mm
Interfacial area	1114 mm^2

Figure II-3. A schematic representation of the cross-section of the absorption cell.

At the top of the absorption cell, a Teflon® mesh was introduced to achieve a uniform distribution of the ammonia vapour over the entire vapour-liquid interface. The absorption cell is equipped with two optical sapphire windows (model SAW24, diameter 25.40 mm, thickness 2.30 mm, from Lasing S.A) for the visualization of the absorption process. Three pressure transducers (Wika, model S20) measure the system pressure, two in the absorption cell and another one in the cylindrical tank. The process temperature is measured with five Pt-100 probes, one is placed in the vapour phase and the other four at equidistant depths in the liquid phase. The probes in the liquid phase allow us to obtain a temperature profile for the investigation of the thermal behaviour of the mixture under analysis. Also, another Pt-100 probe is located into the cylindrical tank. The temperature of the experiment is controlled by a circulating bath (Huber, model Pilot One), which pumps distilled water through a copper cooling-coil located around the absorption cell. The experimental temperature range was from 293.15 K to 303.15 K with an uncertainty lower than ±0.5 K.

The cylindrical tank is used to feed the absorption cell with superheated ammonia vapour throughout the experimental run. The cylindrical tank has a temperature probe and a pressure transducer to measure temperature and pressure,

respectively. Stainless steel is extensively used in all the components due to the outstanding corrosion-resistant properties and high strength capabilities. The 3.175 mm (1/8") tubing used has an admissible very high working pressure. The treaded connections utilize 1/8" nominal pipe thread (NPT), which provides a superior seal when the threads are wrapped with Teflon tape before tightening.

The data acquisition system is based on converting electrical signals that come from the measured medium to readable values through some logic steps. The temperature measuring loop starts with the low voltage electrical signal that comes from the measured medium by a four-wire temperature probe, Pt-100. The pressure-measuring loop starts by the transducer in which the pressure change of the measured medium causes the internally installed diaphragm to deform. This deformation, strain, is converted to low voltage electrical signal within the transducer itself. The pressure transducers and temperature probes are connected to a data logger (Keysight/Agilent 34972A) via different channels. Then, a basic language-written program converts the electrical signals output to readable pressure and temperature values. All temperature probes and pressure transducers were previously calibrated to establish their gains and offsets. Temperature probes have been calibrated according to the procedure described in the ITS-90 guide, while the pressure transducers have been calibrated according to the EA-10/17 calibration guide.

II.2.2 Adjustment of the experimental setup. Determination of the volumes of the components

Once the ILs and experimental method (PDM) have been selected, and the experimental setup described, the next step is the adjustment of the experimental setup.

The adjustment began with the verification and eradication of leaks in the experimental setup. To do this, the experimental setup was charged with nitrogen gas until the target pressure (≈500 kPa) was reached. Then, the reading of the pressure transducers was monitored for approximately one hour. If the measured pressure dropped, this meant there was a leak somewhere in the experimental setup. These leaks were found by a simple method, for example, by applying liquid detergent on the tubing connections and observing the formation of bubbles. Then, the tubing connections where bubbles were observed were

adjusted, and this procedure was repeated until the system pressure remained constant.

Then, the next step was to accurately determine the volume of the absorption cell, the cylindrical tank, and the connecting tube between both components. To do this, the entire experimental setup was filled again with nitrogen gas from the external reservoir. All the valves were closed, and the initial pressure reading (P_i) was taken. After that, an auxiliary cylindrical tank of the known volume was added to the experimental setup. The volume of the auxiliary cylinder is 157.06 cm^3, which was determined using a gravimetric method. Subsequently, the valve connecting the auxiliary tank and the experimental setup was opened, allowing the nitrogen gas to expand into the auxiliary cylinder, and then a new pressure reading (P_f) was taken. If the deviation from the ideal behaviour of nitrogen gas is small, the following expression can be used to relate the pressure, temperature, and volume of the gas in the experimental setup:

$$P_i V_i / T_i = P_f V_f / T_f \qquad \text{II-1}$$

where P is the pressure, V the volume, T the temperature, and the subscripts i and f stand for the initial and final states, respectively.

In Eq. II-1, V_i is the volume of the absorption cell, the cylindrical tank and the connecting tubes, while V_f includes in addition to the volume of these components, the volume of the auxiliary cylinder:

$$V_f = V_i + V_{aux\_cyl} \qquad \text{II-2}$$

where V_{aux_cyl} is the volume of the auxiliary cylindrical tank. Therefore, by substituting Eq. II-2 into Eq. II-1 and solving for the initial volume, we have:

$$V_i = \frac{P_f V_{aux\_cyl}}{T_f} / \left(\frac{P_i}{T_i} - \frac{P_f}{T_f}\right) \qquad \text{II-3}$$

According to Eq. II-3, the initial volume can be calculated from the measured temperatures, pressures and the known volume of the auxiliary cylindrical tank. To determine the volume of the absorption cell (or the cylindrical tank by subtracting from the calculated V_i), the inlet valve of the absorption cell is kept closed, and the procedure above described is repeated. A total of five measurements were taken in each case.

Table II-1 and Table II-2 show the measured values of temperature and pressure as well as the calculated volumes of the (absorption cell + cylindrical tank + connecting tubes) and the cylindrical tank, respectively. The total volume is 408 ±11 cm^3, while the volume of the cylindrical tank is 330 ±7 cm^3.

Table II-1. Measured temperature and pressure and calculated volume of the absorption cell + cylindrical tank + connecting tubes.

Experimental run	T_i/ ºC	P_i/ kPa	T_f/ ºC	P_f/ kPa	V_i/ cm^3
1	26.2	633.3	25.5	454.1	401.2
2	25.7	421.1	25.6	300.9	394.1
3	25.7	297.9	25.5	215.3	411.0
4	25.8	213.6	25.6	154.6	412.8
5	25.9	153.9	25.7	112.1	422.6

Table II-2. Measured temperature and pressure and calculated volume of the cylindrical tank.

Experimental run	T_i/ ºC	P_i/ kPa	T_f/ ºC	P_f/ kPa	V_2/ cm^3
1	24.5	299.2	24.1	203.8	337.1
2	25.2	618.5	24.4	414.6	321.7
3	24.9	412.9	24.3	278.4	327.2
4	24.8	277.8	24.6	187.4	327.9
5	25.0	186.9	24.9	127.6	338.2

II.3 Experimental procedure

In this section, the procedure for measuring the absorption rate is presented. It is divided into three main stages: preparation of samples and equipment; experimental protocol; and cleaning of the experimental setup.

II.3.1 Preparation of samples and equipment

Anhydrous ammonia (purity 99.98%, CAS no. 7664-41-7) was obtained from Carburos Metálicos and was used directly without any further purification. Ionic liquids: Ethylammonium Nitrate ([EAN], purity > 97%, CAS no. 22113-86-6), 1-Ethyl-3-methylimidazolium tetrafluoroborate ([emim][BF_4], purity > 98%, CAS no. 143314-16-3), and 1-Buthyl-3-methylimidazolium tetrafluoroborate ([bmim][BF_4], purity > 99%, CAS no. 174501-65-6) were supplied by the company Iolitec. All the ionic liquids were dried in a vessel under vacuum and stirred for at least 24 hours to reduce their water content. Furthermore, water is used as a reference for the validation of the PDM for absorption rate measurements. Thus, deionized water with a milli Q reagent-grade was obtained from the laboratories of the Universitat Rovira i Virgili (URV), and it was degassed to avoid the formation of bubbles, which can seriously affect the absorption rate of ammonia into the absorbent.

Before starting each experimental run, non-condensable gases trapped in the setup were removed by applying vacuum to the whole setup. For this, a vacuum pump (Comecta-Ivymen) was used, which allowed obtaining a pressure of 5 kPa throughout the setup. Once the non-condensable gases were evacuated, all the valves of the setup were closed. The next step consisted in the introduction of the ammonia vapour and the absorbent liquid, in the cylindrical tank and the absorption cell, respectively. The ammonia vapour was taken directly from an external reservoir until the desired pressure (≈1 atm) in the cylindrical tank was reached. Meanwhile, the absorbent liquid was injected using a syringe, and its mass was obtained on a digital mass balance Mettler AE 260 DeltaRange (resolution ± 0.1 mg). Then, the absorbent liquid was carefully introduced into the absorption cell through the injection line. After the absorbent liquid is inserted into the absorption cell, all the lines are correctly connected. At this point, we were able to start performing measurements of temperature and pressure.

II.3.2 Experimental protocol

At this stage, the ammonia vapour is brought into contact with quiescent absorbent liquids in a pool-type absorber to initiate the absorption process. In particular, the experimental protocol consists of a series of consecutive steps that are described below:

1. Once the absorbent liquid is inside the absorption cell, and the ammonia is inside the cylindrical tank, the initial temperature and pressure readings are taken with the valve that separates both components closed.
2. Then, the valve that separates the absorption cell and the cylindrical tank is opened. Consequently, the ammonia vapour expands into the absorption cell, and the absorption process begins.
3. The ammonia vapour feed was continuous, keeping the valve open throughout the experiment. Therefore, the total volume of ammonia vapour included the volume of the cylindrical tank and the volume of vapour in the absorption cell. The volume of vapour in the absorption cell can be determined from the calculated volume of the absorption cell and the volume of absorbent liquid.
4. Temperature and pressure data were recorded throughout the absorption process until 15 hours. In particular, the temperature was recorded at different depths in the ammonia/absorbent solution.
5. When the absorption process occurs, the pressure drops as a consequence of the dissolution of the ammonia in the absorbent liquid. Thus, the pressure decay data can be used to determine the mass of ammonia vapour absorbed at each time instance, from which the absorption rate can be obtained as described below in section II.6.

II.3.3 Cleaning of the experimental set-up

Cleaning the equipment is the last step in the experimental procedure implemented to determine the absorption rate of ammonia vapour in the absorbent liquids studied. To do this, we have injected clean, pre-heated water several times, and then we have extracted it to remove the refrigerant/absorbent liquid mixture from inside the absorption cell. Once no traces of ionic liquids were observed in the water exiting the absorption cell, its pH was checked using an indicator paper. If the paper turned blue (high pH), which is indicative of the

presence of ammonia, we continued injecting clean water until we observed a yellow colour (neutral pH) of the indicator paper. Once this condition is reached, acetone is used to remove all the water from the absorption cell. Finally, the vacuum pump is turned on for at least 15 minutes to remove the remaining acetone and ammonia.

II.4 Determination of the absorption rate from the experimental data

The absorption process is sensitive to the initial experimental conditions that determine the total pressure drop (therefore, the ammonia vapour absorbed) in the experimental setup [59]. The relation between the initial experimental conditions and pressure in the experimental setup can be appreciated schematically in Figure II-4.

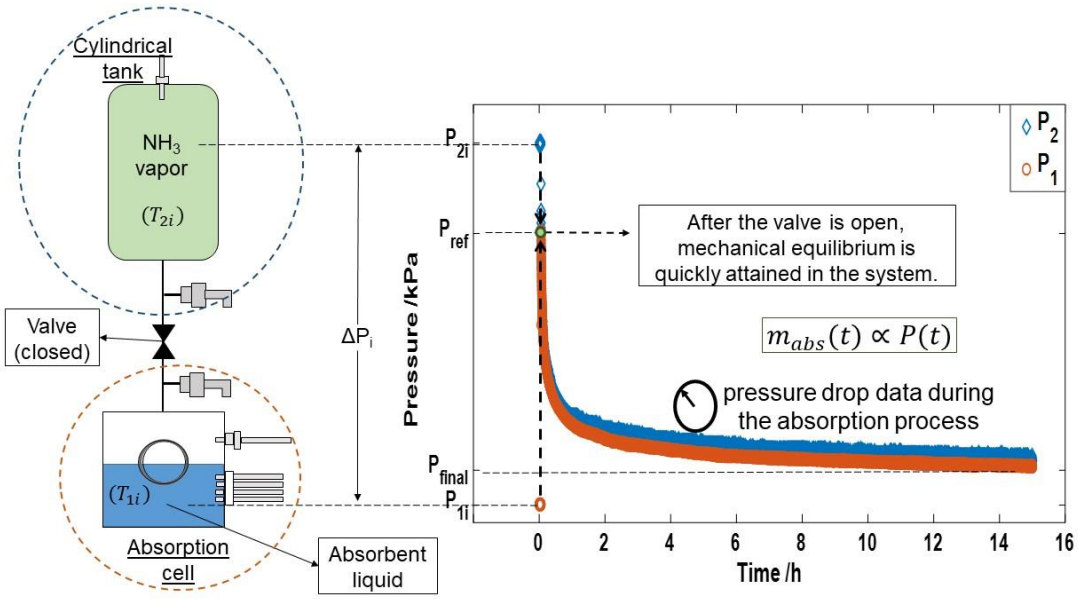

Figure II-4. The relation between the initial experimental conditions and the pressure in the experimental setup prior to the beginning of the absorption experiments.

The initial experimental conditions of the absorption experiments performed can be summarized as follows:

- There is a known amount of the absorbent liquid at temperature, T_{1i}, and pressure, P_{1i} ($\sim 5kPa$), in the absorption cell.
- There is an unknown amount of ammonia vapour at temperature, T_{2i}, and pressure, P_{2i} ($\sim 101.32\ kPa$), in the cylindrical tank.

- The ammonia vapour and the absorbent liquid are separated by a closed valve which does not allow contact between them.

Thus, the initial mass of ammonia vapour in the cylindrical tank can be obtained as follows:

$$m_{NH3_i} = \frac{P_{2i} * V_2 * MW_{NH3}}{Z_i * R * T_{2i}} \quad \text{(II-4)}$$

where: V_2 is the volume of the cylindrical tank, MW_{NH3} the ammonia molar mass, Z_i the initial ammonia compressibility factor, and R the universal constant of gases.

The vapour-liquid absorption process is triggered by opening the inlet valve of the absorption cell. Immediately, the pressure in the cylindrical tank drops, meanwhile, the pressure in the absorption cell increases. After the valve is opened, mechanical equilibrium is quickly attained in the system, which means that the pressure in the absorption cell equals the pressure in the cylindrical tank. The pressure at which there would be mechanical equilibrium in the system (P_{ref} in Figure II-4) is an intermediate pressure between the initial pressure in the cylindrical tank, $P_{2\mathrm{i}}$, and the initial pressure in the absorption cell 1, $P_{1\mathrm{i}}$. In the PDM, this reference pressure (P_{ref}) is used to calculate the pressure drop in the system, $P_d = P_{ref} - P(t)$.

As the absorption process takes place, first, the system pressure drops abruptly, then more slowly and, finally, it remains virtually unchanged. At any time, the instantaneous mass of ammonia vapour (m_{NH3_f}) in the system can be determined from the measured temperature (T_f) and pressure (P_f). For this, we have used two different strategies depending on the volatility of the absorbent liquid used.

1. For the experiments performed with water (volatile fluid) as absorbent liquid:

   On the assumption that there is an instant equilibrium condition during the absorption process, two parameters of the vapour phase are needed to obtain the others [81]. Thus, the specific volume of the vapour phase at any time instance during the absorption process can be obtained from the measured pressure, $P(t)$, and ammonia vapor temperature, T_2 (here, the temperature in the absorption cell 2), using Tillner-Roth and Friend

equation of state [83]. Once the specific volume of the vapor phase has been obtained, the vapour mass in the total vapour volume at any time can be calculated as:

$$m_v(\mathrm{t}) = \frac{V_V}{v(t)} \qquad \text{II-5}$$

where: $v\ (m^3/kg)$ is the vapour specific volume at the time, t, and $V_V(m^3)$ is the total volume of vapor, which includes the volume of vapor in the absorption cell, and the volume of the cylindrical tank. The volume, V_V, can be considered constant since the total ammonia absorbed is too small to cause a noticeable rise in the liquid level [81]. Then, the mass of ammonia vapour absorbed in the water at any time instance during the absorption process can be calculated as follow:

$$m_{NH3_{abs}}(\mathrm{t}) = m_{NH3_i} - \omega * m_v(t) \qquad \text{II-6}$$

where ω is the ammonia mass fraction in the vapour phase, which is also obtained using the Tillner-Roth and Friend equations.

2. For the experiments performed with ionic liquids (non-volatile fluids) as absorbent liquid:

   In this case, the vapour phase can be considered as pure ammonia vapour due to the non-volatility of the ILs. Therefore, the ammonia vapour mass at any time instance during the absorption process was calculated as:

$$m_{NH_3}(\mathrm{t}) = \frac{\mathrm{P(t)} * V_V * M_{NH3}}{\mathrm{Z(t)} * R * T_2} \qquad \text{II-7}$$

   where $Z(t)$ is the ammonia compressibility factor which depends on temperature and pressure. Then, the mass of ammonia vapour absorbed in ionic liquids at any time instance during the absorption process is:

$$m_{NH3_{abs}}(\mathrm{t}) = m_{NH3_i} - m_{NH_3}(\mathrm{t}) \qquad \text{II-8}$$

As mentioned, Eq.s II-6 and II-8 allow us to determine the time evolution of the mass of ammonia absorbed during the absorption process. Then, the variation of the absorbed mass over time can be expressed using some appropriate mathematical function. Finally, the absorption rate of ammonia in the absorbent can be determined simply by differentiating the obtained function with respect to time. Thus, the absorption rate ($\dot{m}_{NH3_{abs}}(t)\ /g\ s^{-1}m^{-2}$) of ammonia vapour in

quiescent absorbent liquids (both, water and ILs) per unit of interfacial area (S) in a pool-type absorber using the pressure drop method can be calculated as:

$$\dot{m}_{NH3_{abs}}(\mathrm{t}) = \frac{1}{S}\frac{\mathrm{d}(m_{NH3_{abs}}(\mathrm{t}))}{\mathrm{dt}} \qquad \text{II-9}$$

II.5 Thermal behaviour during the absorption process of ammonia vapour in the absorbent liquids studied

During the absorption process, heat is released at the vapour-liquid interface, and thus, the temperature in the absorber tends to increase. It is well-known that the solubility of ammonia in ionic liquids decreases with increasing temperature [18,51,78]. Therefore, knowledge of the expected rise in temperature for a given absorbent liquid is imperative for the proper design of the absorber to transfer the released heat to some external circuit (outside air or cooling water).

Illustratively, Figure II-5 display the temperature rise detected by the temperature probe closest to the vapour-liquid interface during the absorption process of ammonia vapour in the absorbent liquids studied at 303.15 K. As can be seen, the behaviour of the curves shows certain similarities. However, it is also possible to appreciate significant differences. In all curves, the temperature rises immediately after the valve is opened (and consequently the ammonia vapour expands and comes into contact with the absorbent liquid in the absorption cell), reaches a maximum value in a short time, and then gradually decreases. Initially, there is a high availability of absorbent liquid molecules in the vapour-liquid interface that favours the absorption process, and hence there is a considerable increase in temperature. Then, as the absorption process progresses, the interface tends to become saturated with ammonia, and the absorbent molecules begin to decrease and, therefore, the temperature decrease [59]. Subsequently, ammonia molecules penetrate the liquid phase via molecular diffusion, allowing "free" absorbent molecules to absorb more ammonia molecules at the interface until equilibrium is reached.

Despite the common behaviour, the differences in the curves shown in Figure II-5 are obvious. For instance, it is observed that the maximum value of the temperature rise varies from approximately 1 K for [bmim][BF_4] to 3.5 K for EAN. The temperature rise depends on several thermophysical properties, mainly, the

heat of absorption, density, specific heat, thermal conductivity, and mass diffusivity. Furthermore, the value of the temperature rise will also depend on the efficiency of the external thermal control system. However, since all experiments were carried out under the same conditions, the observed value is useful for the sake of comparison. As can be seen, the temperature rise value for EAN is comparable to that of H_2O, while, the value of [emim][BF_4] is comparable to that of [bmim][BF_4], especially for times greater than two minutes. The noticeable differences for shorter times may be due to the predominant role of the thermal and mass diffusivities of each particular mixture at this early stage of the absorption process.

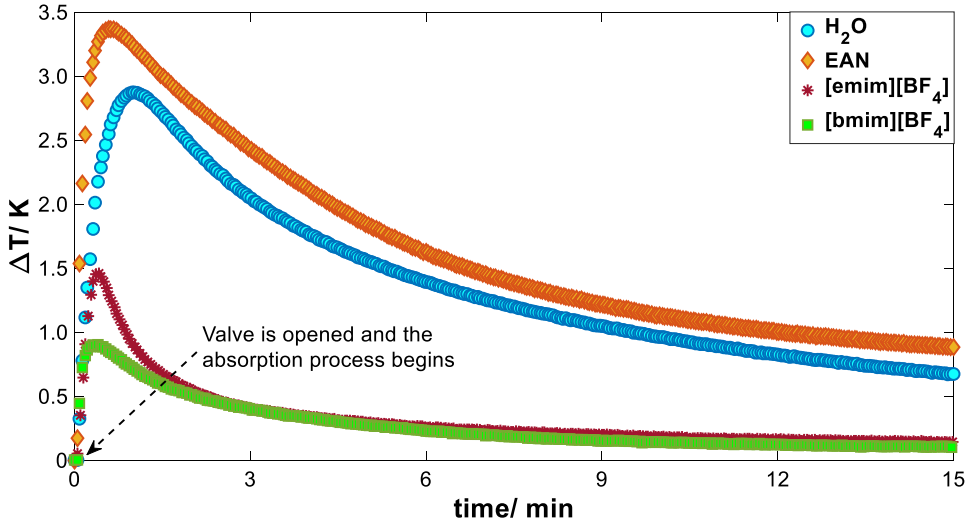

Figure II-5. Temperature rise, ΔT, at the temperature probe closest to the vapor-liquid interface during the absorption process of ammonia in the absorbent liquids studied at 303.15 K.

Table II-3 summarizes the observed rise in temperature for all the experiments performed in this thesis. As can be seen, in all cases, the temperature rise increases with decreasing the temperature in the absorption cell. However, in the case of the absorption in water, the temperature rise is practically the same for both temperatures studied. In the cases of the absorption in EAN, the initial temperature of the absorption cell has a strong influence on the temperature rise. While at 303.15 K, the relative increase is 1.1%, it can be as much as 1.8% at 303.15 K. This is indicative of high heat of absorption for the NH_3/EAN mixture at this temperature. Temperature rise during the absorption process of ammonia in [bmim][BF_4] is also quite sensitive to the initial temperature of the absorption cell.

In this case, the relative increase in temperature at 293.15 K (0.6%) doubles the relative increase at 303.15 (0.3%). The rise in temperature during the absorption process of ammonia in the absorbent liquids studied follow the order: EAN > H_2O > [bmim][BF_4] > [emim][BF_4].

Table II-3. Temperature rise during the absorption process of ammonia vapour in the absorbent liquids studied at a different initial temperature in the absorption cell, T_{1i}, and the pressure difference between the cylindrical tank and the absorption cell, ΔP_i.

Absorbent liquid	ΔP_i/ kPa	T_{1i}/ K	ΔT/ K
H_2O	94.1	293.2	3.0
H_2O	88.7	303.2	2.9
EAN	95.1	293.2	5.3
EAN	86.2	303.2	3.4
[emim][BF_4]	110.5	293.2	1.9
[emim][BF_4]	102.9	303.2	1.5
[bmim][BF_4]	98.3	293.2	1.6
[bmim][BF_4]	101.1	303.2	0.9

As mentioned, the absorption cell is provided with several temperature probes located within the liquid bulk. Thus, the design of the absorption cell not only allows us to follow the time evolution of temperature during the absorption process but also lets us trace the spatial distribution of this variable. Although it is outside the scope of this thesis, this valuable information can be used in future work to study the thermal conductivity or heat absorption of refrigerant/absorbent liquid mixtures using an inverse approach [59].

Illustratively, Figure II-6 shows the temperature behaviour at different locations in the absorption cell during the absorption process of ammonia vapour in EAN at 293.15 K. The spatial distribution of temperature in the remaining experiments is quite similar to that shown here. The temperature curves shown in Figure II-6 corresponds to the five probes installed in the absorption cell (see Figure II-3). The distances shown are determined from the position of the vapour-liquid interface. The thermal behaviour shown in Figure II-6 can be explained as follow.

During the absorption process, heat is released at the vapour-liquid interface that diffuses into the liquid and vapour bulks. The temperature rise perceived by the probes located in different places of the absorption cell differs in magnitude and detection time due to the thermal diffusivity of the liquid and vapour phases, and the action of the external thermal control system. As can be seen, the temperature probes closer to the interface perceive a higher and faster temperature rise than the rest of the probes. In Figure II-6, T_4 is the closest probe to the vapour-liquid interface, while T_5 is in the vapour bulk and the other probes (T_3, T_2, and T_1) are in the liquid bulk at different depths in descending order, respectively. In this case, the relative increase in temperature is 0.2%, 0.4%, 1.0%, 1.8%, and 0.2% for T_1, T_2, T_3, T_4, and T_5, respectively.

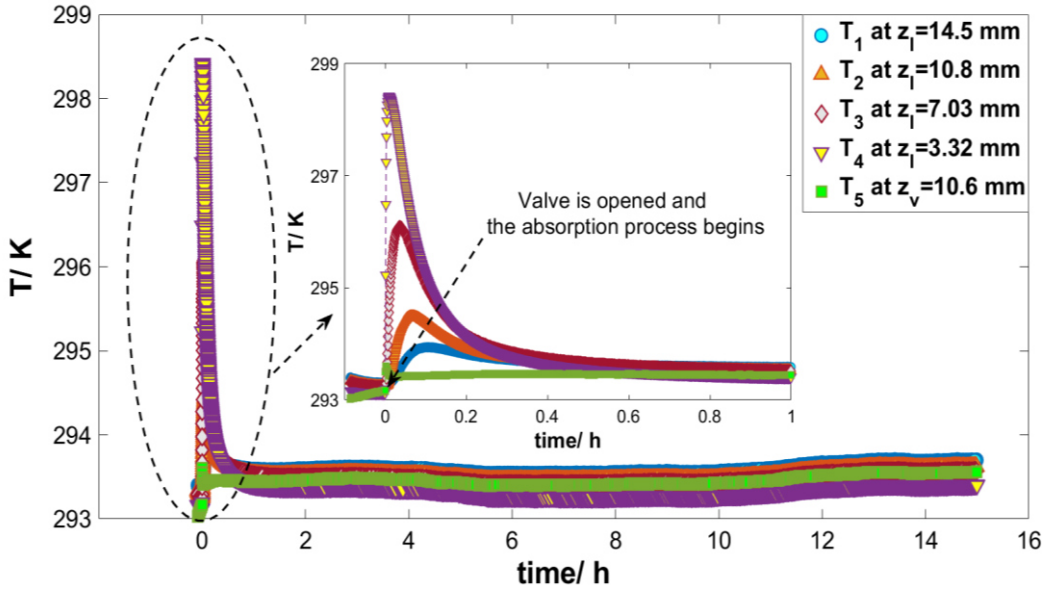

Figure II-6. Temperature behaviour in the absorption cell during the absorption process of ammonia vapour in EAN at 293.15 K.

II.6 Pressure-drop behaviour during the absorption process of ammonia vapour in the absorbent liquids studied

The experimental setup implemented was based on the pressure drop method. Therefore, the pressure in the system changes during the entire absorption process. Figure II-7 shows the pressure-drop behaviour during the absorption process of ammonia vapour in H_2O at 293.15 K.

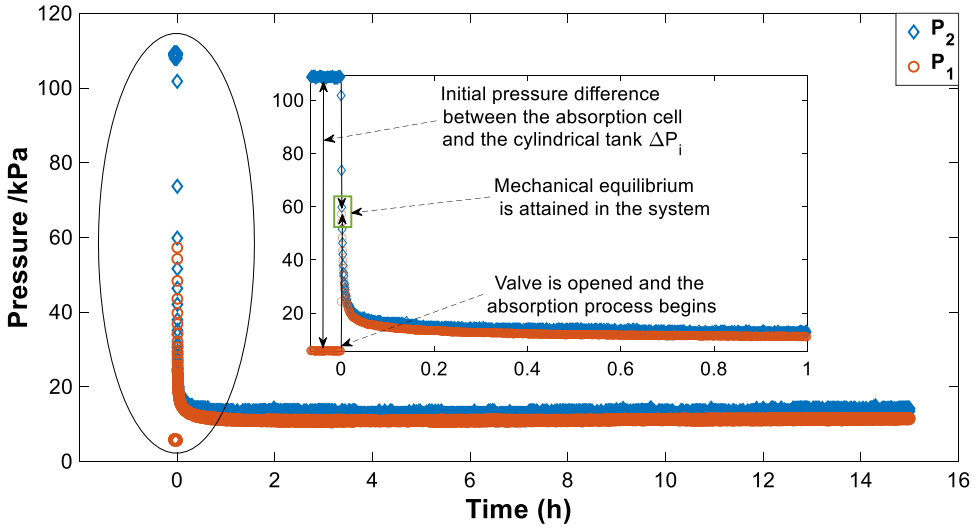

Figure II-7. Pressure behaviour in the experimental setup during the absorption process of ammonia vapour in the water at 293.15 K.

As can be appreciated, initially, there is a pressure difference between the absorption cell and the cylindrical tank. When the contact valve is opened, the pressure in the absorption cell increases immediately, the opposite being right in the case of the cylindrical tank. Afterwards, mechanical equilibrium is quickly attained in the system. Later, as the absorption process progresses, the pressure in the absorption cell decreases. Finally, after a certain time, the system pressure remains practically constant until the end of the experimental run.

However, unlike the case of temperature, the behaviour of the system pressure is different for each ammonia vapour/absorbent liquid pair studied. The total pressure drop in the system depends on the ammonia absorption capacity of the absorbent liquid, while the rate at which the pressure decreases depends on the mass diffusivity. Moreover, the pressure-drop behaviour also depends on the experimental conditions, such as initial pressure difference and temperature. To compare the pressure-drop behaviour during the absorption process in all cases of slightly different initial pressure, we have normalized the pressure readings as:

$$P_2^*(t) = \frac{P_2(t)}{P_{2i}} \qquad \text{II-10}$$

where P_{2i} is the initial pressure in the cylindrical tank and $P_2(t)$ are the pressure readings at a time *t* during the absorption process. For the sake of clarity, only the pressure in the cylindrical tank is considered.

Figure II-8 displays the normalized pressure curves during the absorption process in ammonia vapour in the four absorbent liquids studied. The general impression is that the pressure drop in H_2O and EAN is much more significant than in [bmim][BF_4] and [emim][BF_4]). Therefore, it is convenient to group the absorbent liquids into two groups. In one of these groups are the two ionic liquids with relatively low absorption capacity ([bmim][BF_4] and [emim][BF_4]), and in the other group, H_2O and EAN. The similarities between the curves of each group are evident. However, here, our interest lies in the differences.

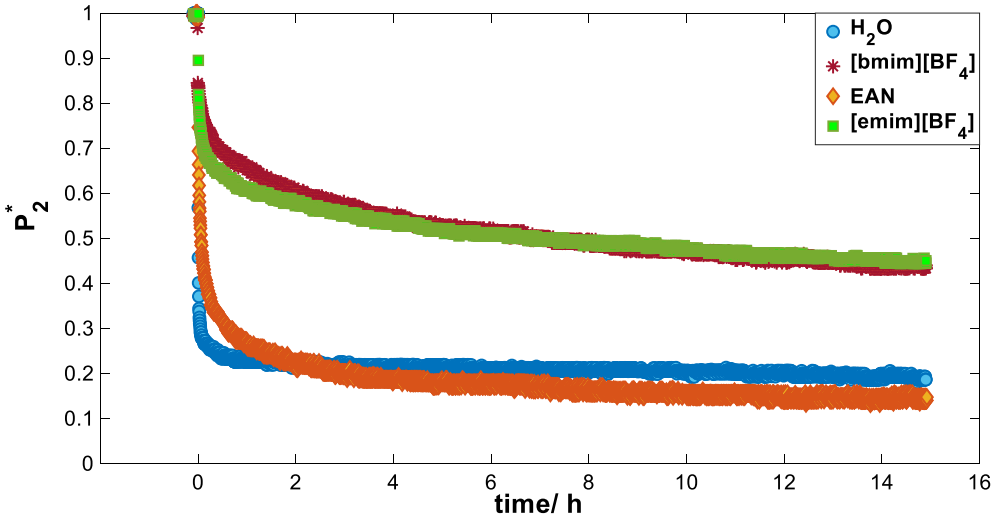

Figure II-8. Pressure behaviour in the cylindrical tank during the absorption process of ammonia vapour in H_2O, EAN, [emim][BF_4], and [bmim][BF_4] at 303.15 K.

In the group of the imidazolium-based ILs, it can be observed the pressure drop is approximately the same. After 15 hours from the beginning of the absorption process, the pressure in the cylindrical tank is close to half of the initial pressure. It is important to note that the pressure decay is faster in the case of the absorption in [emim][BF_4], especially during the first hours of the absorption process. The pressure behaviour shown in these two curves suggests that the ammonia absorption capacity of these ILs should be quite similar while the mass diffusivity of ammonia vapour should be higher in [emim][BF_4] than in [bmim][BF_4].

In the case of the absorption of ammonia in H_2O and EAN, the pressure at the end of the experiment (after 15 hours from the beginning of the absorption process) is close to one-fifth of the initial pressure. Therefore, it is expected that

both H_2O and EAN exhibit a high ammonia absorption capacity. However, it is essential to note that while the H_2O appears to have reached the maximum absorption capacity rapidly, the EAN is still absorbing ammonia after 15 hours from the beginning of the absorption process. The high absorption capacity of the EAN may be due to the presence of the ammonium group in the cation of this IL, which suggests the formation of hydrogen bonds with ammonia. As for the rate of pressure decrease, it can be seen that it is higher in the case of H_2O than in the EAN. Therefore, it is expected that EAN has a greater absorption capacity than H_2O and that the mass diffusivity of ammonia vapour in H_2O is higher than in EAN.

From the behaviour of the pressure curves shown in Figure II-8, the ammonia absorption capacity of the studied absorbent liquids, at 303.15 K, is expected to follow the descending order: EAN>H_2O> [bmim][BF_4]> [emim][BF_4]. While, at the same temperature, the mass diffusivity of ammonia vapour in the absorbent liquids studied is expected to follow the order: H_2O> EAN> [emim][BF_4]> [bmim][BF_4].

Furthermore, we have identified three different stages of the absorption process from the pressure measurements. In the first stage, called the incubation period (or interface-filling) [84–86], pressure drops significantly due to the high availability of “free” absorbent liquid molecules at the vapour-liquid interface. The second stage is the transition period, where the pressure drop in the system slows down due to the increase in ammonia molecules at the vapour-liquid interface. In the last stage, called linear decay period, the measured pressure decays slowly, and smoothly with time, and molecular diffusion is considered the dominant mass transfer mechanism [87].

We also observed that the time evolution of pressure during the absorption process could be reliably fitted to an exponential function of two terms:

$$P(t) = m_1 \exp\left(-\frac{t}{k_1}\right) + m_2 \exp\left(-\frac{t}{k_2}\right) + P_{eq} \qquad \text{II-11}$$

where the coefficients m_1, m_2, k_1, k_2, and P_{eq} can be obtained by regression of the pressure-time data. This type of equation has been used previously to fit pressure-time history during the dissolution of carbon dioxide and methane in heavy oils [84]. The first exponential term in equation II-11 fits the pressure-time

curve during the incubation and transition periods and the second exponential term fits the tail of the pressure-time curve. Although a 3-term exponential fit could have been used (one term for each stage of the absorption process), the quality of the fit using a two-term equation is satisfactory for the cases studied here. An advantage of using equation II-11 is the elimination of the need to experimentally measure equilibrium pressure provided sufficient pressure history is recorded to obtain reliable values of the regression parameters [84].

To illustrate the different stages during the absorption process, pressure-time curves during the absorption process of ammonia vapour in EAN and [bmim][BF_4] at 303.15 K are shown in Figure II-9. In this figure, the results of the fitting procedure using Eq. II-11 are also shown.

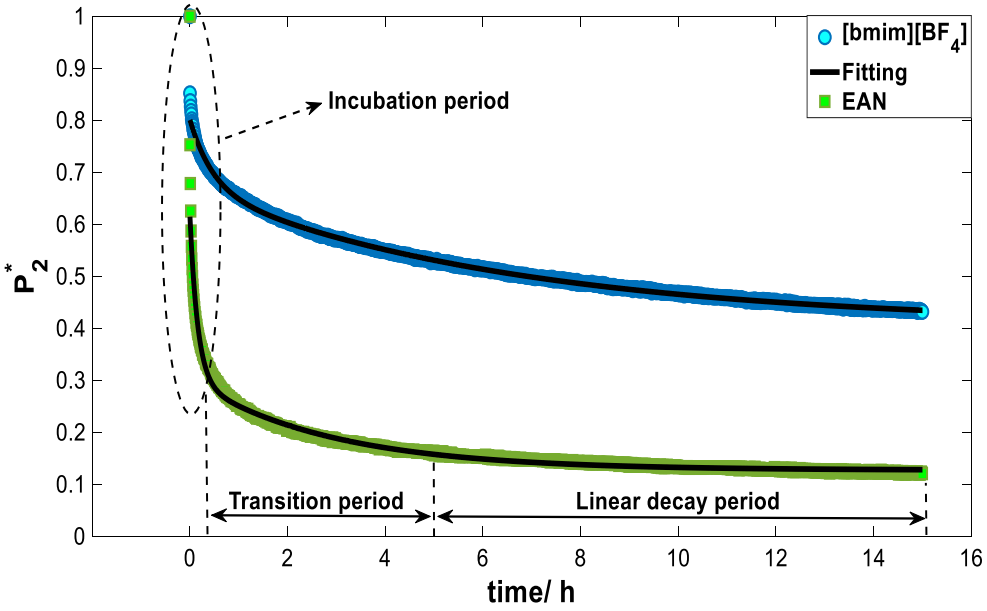

Figure II-9. Observed periods during the absorption process of ammonia vapour in EAN, and [bmim][BF_4], at 303.15 K, from pressure decay measurements.

As can be seen, the incubation and transition periods for the EAN curve are more clearly defined than for the [bmim][BF_4] curve. The duration of each period depends on the absorbent liquid used. In general, the incubation period is very short and is of the order of 15 minutes after the start of the absorption process. The limits of the linear decay period can be determined using some criteria about the linearity of the curve. For example, Du et al. [87] determined the limits of this period adopting a cut-off value for the linear correlation coefficient (R^2 = 0.900).

Once the limits of the incubation and linear decay periods are known, the transition period can be established.

II.7 Absorption rate measurements

The initial pressure (and thus the ammonia vapour mass) is slightly different in each experiment. Therefore, for the sake of comparison, the absorbed mass of ammonia vapour at each time instance, $m_{NH3_{abs}}(t)$, is normalized as:

$$m^*_{NH3_{abs}}(t) = \frac{m_{NH3_{abs}}(t)}{m_{NH3_i}} \qquad \text{II-12}$$

where m_{NH3_i} is the initial ammonia vapor mass in the cylindrical tank. In this way, the normalized absorbed mass of ammonia gives a measure of how much ammonia of the initial total is absorbed.

Figure II-10 shows the normalized absorbed mass of ammonia vapour in the four absorbent liquid studied at 303.15 K. Here again, it is convenient to group the absorbent liquids into two groups to facilitate analysis. In the first group, imidazolium-based ILs can be included, and in the other, H_2O and EAN.

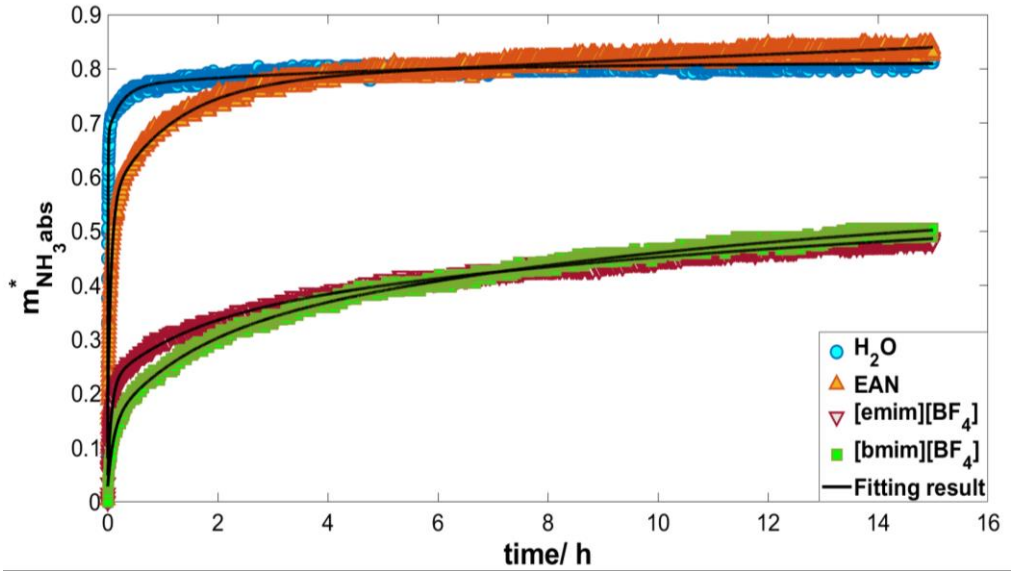

Figure II-10. Absorbed mass of ammonia as a function of time during the absorption process in EAN, H2O, [emim][BF4], and [bmim][BF4], at 303.15 K.

In the case of the imidazolium based ILs, about half of the initial mass of ammonia vapour is absorbed. Both fluids, [bmim][BF_4] and [emim][BF_4], display a similar behaviour. At the beginning of the absorption process, [emim][BF_4] absorbs faster

than [bmim][BF_4], but at the end of the experiment (15 hours), the latter absorbs more ammonia than the first.

In the case of the absorption of ammonia vapour in water and EAN, the absorbed mass is greater than 80% of the initial mass of ammonia vapour. This confirms the great absorption potential of these fluids. At the beginning of the absorption process, H_2O absorbs faster (this means a higher mass diffusivity). However, after 6 hours of the beginning of the absorption process, it is observed that EAN absorbs more ammonia than H_2O. In general, the behaviour of the curves shown in Figure II-10 is in good agreement with that of the pressure curves displayed in Figure II-8.

Then, the experimental mass of ammonia absorbed can be fitted to a function of the form:

$$m_{NH3_{absfit}}(t) = \mathrm{a} \cdot \exp(bt) + c \cdot \exp(dt) + e \cdot \exp(ft) + g \qquad \text{II-13}$$

where the coefficients a, b, c, d, e, f, and g were determined by a non-linear least-square regression method using MATLAB® [88]. The fitting results are represented by solid black lines in Figure II-10.

It is observed that the proposed equation successfully reproduces the temporal behaviour of the absorbed mass of ammonia vapour in each absorbent liquid studied. The coefficients of Eq. II-13 and goodness of the fitting (R^2 and RMSE) are listed in Table II-4.

Once we have determined the coefficients, we can determine the absorption rate of ammonia vapour by differentiating equation II-13 with respect to time:

$$\dot{m}_{NH3_{abs}}(\mathrm{t}) = \frac{1}{S}\frac{\mathrm{d}(m_{NH3_{absfit}}(\mathrm{t}))}{\mathrm{dt}} = \frac{1}{S}(\mathrm{a} \cdot \mathrm{b} \cdot \exp(bt) + c \cdot \mathrm{d} \cdot \exp(dt) + e \cdot \mathrm{f} \cdot \exp(ft)) \qquad \text{II-14}$$

where S is the interfacial area.

Table II-4. Coefficients of equation II-13 and goodness of the fitting procedure (R^2 and RMSE).

Coefficient	T = 293.15 K			
	H_2O	EAN	[emim][BF_4]	[bmim][BF_4]
a	7.064E+00	1.139E+00	-1.349E-02	-5.672E-02
b	1.421E-08	8.981e-08	-3.340E-05	-3.229E-05
c	-1.987E-01	-4.362E-02	-7.052E-03	-1.828E-02
d	-6.642E-02	-3.361E-04	-4.187E-03	-3.179E-03
e	-1.638E-02	-1.087E-01	-1.251E-02	-2.254E-02
f	-1.106E-03	-5.993E-03	-4.256E-04	-3.271E-04
g	-4.916E-01	-9.472E-01	3.825E-02	1.020E-01
R^2	8.756E-01	9.872E-01	9.564E-01	9.962E-01
RMSE	1.228E-03	1.187E-03	9.850E-04	9.951E-04
Coefficient	**T = 303.15 K**			
	H_2O	EAN	[emim][BF_4]	[bmim][BF_4]
a	1.129E+00	1.830E+00	-6.370E-02	-6.554E-02
b	1.059E-07	1.295E-07	-1.928e-05	-2.544E-05
c	-1.401E-01	-7.810E-02	-3.023E-02	-2.711E-02
d	-3.935E-02	-4.336E-03	-1.838E-04	-2.526E-03
e	-1.909E-02	-4.350E-02	-4.714E-02	-3.327E-02
f	-4.924E-04	-2.398E-04	-3.705E-03	-1.983E-04
g	-9.412E-01	-1.679E+00	0.1525E-01	1.314E-01
R^2	9.430E-01	9.908E-01	9.962E-01	9.974E-01
RMSE	1.166E-03	1.199E-03	1.093E-03	1.024E-03

To validate our results, we have compared the obtained absorption rate of ammonia in H_2O at 293.15 K with those of Mustafa [59]. Figure II-11 displays the variation of the absorption rate of ammonia in H_2O at 293.15 K during the first 600 seconds of the absorption process. As can be seen, at the very beginning of the absorption process, the observed value of the absorption rate is around 12 g m^{-2} s^{-1} in both works.

However, a few seconds after the beginning of the absorption process, the behaviour of the curves is different. This difference may be due to the experimental conditions in both works. In particular, Mustafa [59] used a thermally insulated absorption cell, while in this thesis, the temperature in the absorption cell is actively controlled. However, after 300 seconds, the absorption rate curves

show the same behaviour. Despite the differences, in general, there is a good agreement between the two studies. Therefore, it is considered that the implemented methodology is suitable to determine the absorption rate of ammonia vapour in selected ionic liquids.

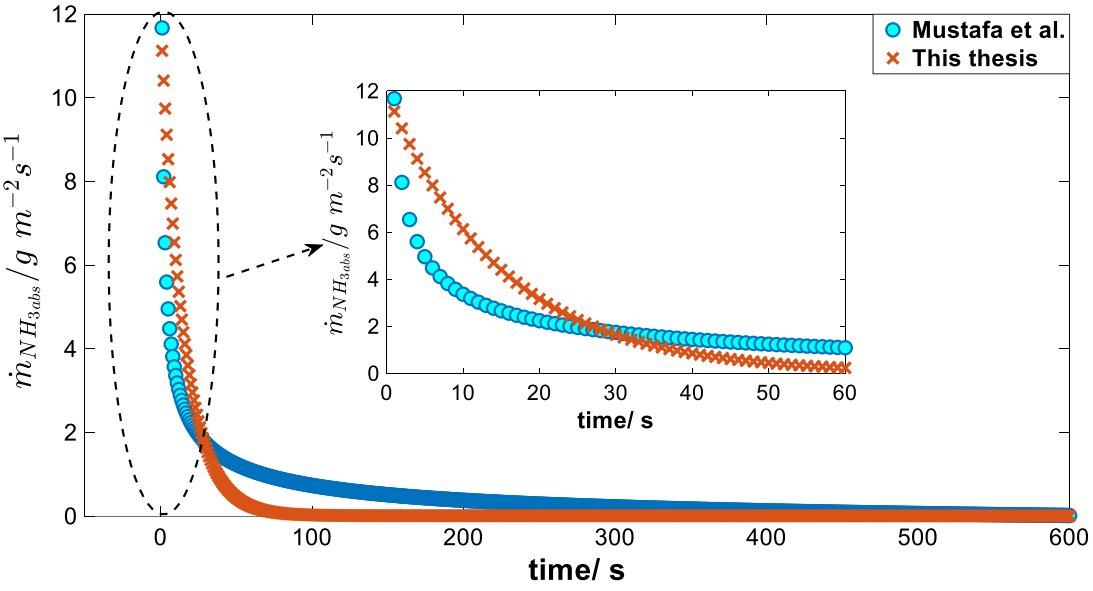

Figure II-11. Time evolution of the absorption rate of ammonia vapour in H_2O at 293.15 K.

Figure II-12 depicts the absorption rate during the absorption process of ammonia vapour in the ionic liquids studied at 303.15 K.

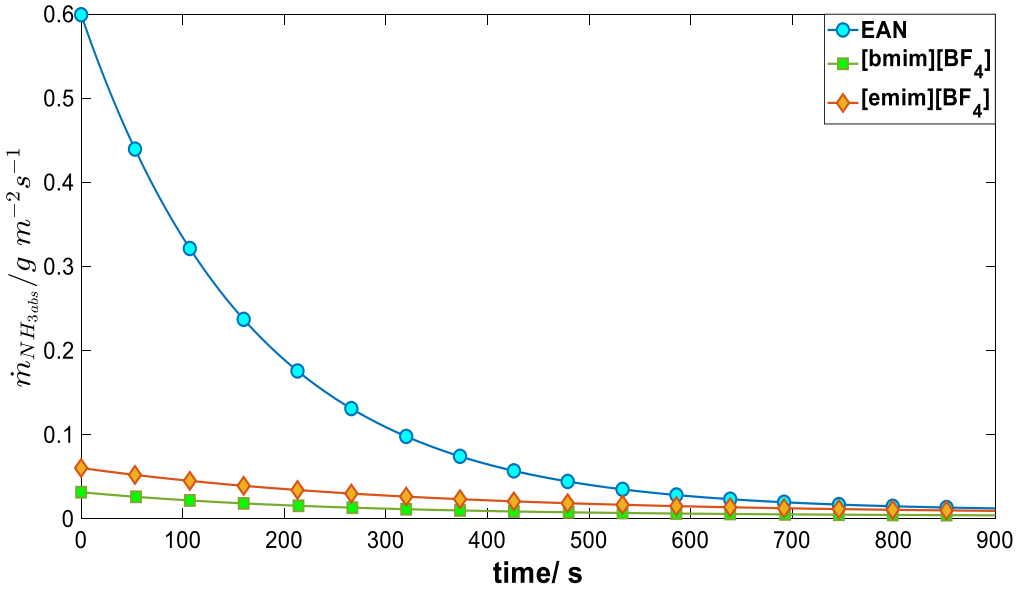

Figure II-12. Time evolution of the absorption rate of ammonia vapour in the ionic liquids studied at 303.15 K.

The general impression is that the absorption rate behaviour in ionic liquids is similar to those of H_2O. Nonetheless, the absorption rate of ammonia in ionic liquids is several times lower than in H_2O. Furthermore, among the three ionic liquids studied, EAN shows the highest absorption rate of ammonia, followed by [emim][BF_4], and, lastly, [bmim][BF4]. As can be seen, the absorption rate of ammonia vapour in EAN is six times higher than in the other ILs studied.

It was found that the absorption rate of ammonia in the absorbent liquids studied decreases with increasing temperature. As mentioned, the absorption rate is an important magnitude closely related to heat and mass transfer mechanisms in absorption systems. Furthermore, the results of the absorption rate can be interpreted in terms of the mass diffusivity, according to Fick's First Law. The absorption rate is the mass flux of ammonia vapour diffusing from the vapour phase into the liquid phase at the vapour-liquid interface due to a concentration gradient:

$$\dot{m}_{NH3_{abs}} = D_{NH3-AL} \nabla c_{NH3} \qquad \text{II-15}$$

where D_{NH3-AL} is the mass diffusivity of ammonia in the absorbent liquid, and ∇c_{NH3} the concentration gradient of ammonia in the system. Thus, at the same initial conditions (same concentration gradient), the absorption rate gives an indication of the mass diffusivity. From the above, the mass diffusivity is expected to follow the order: H_2O> EAN> [emim][BF_4]> [bmim][BF_4], which is consistent with the thermal and pressure behaviour observed during the absorption process.

II.8 Conclusions

This chapter deals with the experimental determination of the absorption rate of ammonia vapour in absorbent liquids. For this purpose, a dual-chamber absorption system was implemented. The methodology used to determine the absorption rate was based on the pressure drop method. In total, four absorbent liquids have been studied, H_2O, and three ionic liquids: EAN, [emim][BF_4] and [bmim][BF_4]. Absorption experiments were performed at two temperatures, 293.15 K and 303.15 K, and lasted 15 hours from the beginning of the absorption process. In particular, the following conclusions were drawn:

- The maximum value of the temperature rise during the absorption process varies from 0.9 K for [bmim][BF_4] at 303.15 K to 5.3 K for EAN at 293.15

K. Therefore NH_3/EAN mixtures are expected to show high heat of absorption at this temperature.

- Pressure behaviour during the absorption process is different for each ammonia/absorbent liquid pair analyzed. After 15 hours of the beginning of the absorption process, the pressure is close to half of the initial pressure for the cases of absorption in [emim][BF_4], and [bmim][BF_4] In the cases of the absorption of ammonia in H_2O and EAN, the pressure at the end of the experiment is close to one-fifth of the initial pressure.
- Three different stages of the absorption process from the pressure measurements were identified: incubation, transition, and linear decay periods.
- The absorption rate of ammonia in H_2O at the very beginning of the absorption process was observed to be around 12 g m^{-2} s^{-1}. The results are in an acceptable agreement with the literature.
- The absorption rate of ammonia in ionic liquids is several times lower than in H_2O. Among the ionic liquids studied, EAN shows the highest absorption rate of ammonia (around 0.6 g m^{-2} s^{-1}), followed by [emim][BF_4] (0.06 g m^{-2} s^{-1}), and, lastly, [bmim][BF4] (0.03 g m^{-2} s^{-1}).

Chapter II

Chapter III
Mass diffusivity: Concepts, measurement, and modelling

This chapter is devoted to the mass diffusivity as an essential transport property in absorption refrigeration systems. The main concepts related to diffusion, experimental measurement methods, and models for the estimation of mass diffusivities are presented. Then, a review of the literature on measurements and modeling of mass diffusivity in working fluid mixtures used in absorption technology is provided.

III.1 Diffusion fundamentals

Diffusion is the process by which matter is transported from one part of a system to another as a result of random molecular motions [89]. It can be the main transport process in the absence of mixing by mechanical means or convection and is relevant for many industrial instances. Such instances include, but are not limited to, absorption refrigeration systems, biotechnology, distillation, solvent-solvent extraction, and the sequestration of CO_2 in saline aquifers and depleted oil and gas reservoirs [90].

In general, diffusion in liquids is a slow process, which is characterized by a small magnitude compared to other transport mechanisms, such as convection. However, this is precisely the main reason for its importance. In many industrial processes, diffusion occurs sequentially with different phenomena and is usually the rate-determining step in the sequence. For example, diffusion often limits the efficiency of commercial distillations and the rate of industrial reactions using porous catalysts [91].

On a microscopic scale, molecular diffusion describes the relative motion of individual molecules in a mixture induced by their thermal energy causing random, irregular movements [92]. In addition to the inherent kinetic energy of a molecule, both experiment and theory have shown that diffusion can result from pressure gradients (pressure diffusion), temperature gradients (thermal diffusion), external force fields (forced diffusion), and concentration gradients [93]. In all cases, the resulting net diffusion flux is established in the decreasing direction of the potential gradient. In this thesis, only diffusion phenomena caused by a concentration gradient are considered since it is the main driving force in absorption refrigeration systems. In the case of a concentration gradient, species will diffuse from regions of higher to lower concentration until uniformity of the system is reached [92].

On a macroscopic scale, as early as 1855, Adolf Fick developed a description of diffusion in binary liquid mixtures based on two phenomenological laws. He observed that the mass diffusion flux of a component in a liquid mixture was proportional to its concentration gradient, analogous to heat diffusion flux in

Fourier's Law. Thus, for a binary mixture of A and B, Fick's First Law of diffusion can be written as:

$$J_A = -D_{AB}\nabla c_A \qquad \text{III-1}$$

Here, J_A is the molar flux of solute A having concentration c_A. The proportionality constant, D_{AB}, between the flux and concentration gradient (potential) is the mutual diffusion coefficient or mass diffusivity with dimensions of (length)^2 (time)$^{-1}$. Typical values for mass diffusivities in gases and liquids are in the order of 10^{-5} m^2·s^{-1} and 10^{-9} m^2·s^{-1}, respectively [91].

In the previous definition of the diffusion flux, a frame of reference of *no net mole flow* is considered:

$$J_A + J_B = 0 \qquad \text{III-2}$$

where J_B is the molar flux of solvent B. Alternatives frames of reference, such as those moving with the local center of mass or the local center of volume, can also be adopted. Nevertheless, great care must be taken to select the correct frame of reference to adequately describe the diffusion phenomena in each system. For binary system diffusion coefficients are identical in any frame of reference, the problem starts from ternaries,

Meanwhile, Fick's Second Law can be derived from Fick's First Law and the requirement of mass conservation in the system. Fick's Second Law relates the time-dependent concentration changes with the concentration of each component in the system as follows:

$$\frac{\partial c_A}{\partial t} = D_{AB}\nabla^2 c_A \qquad \text{III-3}$$

To solve this partial differential equation, one initial condition and two boundary conditions must be defined over the control volume. Particular solutions for some practical geometries are available and can be found in the literature [89].

III.1.1 Mutual, self-, and tracer diffusion coefficients

The term D_{AB} introduced above refers to the diffusion of one constituent in a binary system. In this thesis, preference has been given to the term *mass diffusivity* over the *mutual diffusion coefficient* to be consistent with most of the relevant literature for engineering processes. Besides, in many scientific and

engineering applications, it is common to assume that there is only a small amount of solute (A) diffusing into an infinitely large amount of solvent (B). Under these conditions, a mutual diffusion coefficient at infinite dilution, D_{AB}^{0}, is used to describe the diffusion process, and in engineering work, it is assumed to be a representative value even for concentrations of A of 5 to 10 mole % [93]. This leads to a simplification in the treatment of the diffusion model since there is no need to consider the functional dependence of the mass diffusivity on the concentration of the solute [90].

In addition to the mutual diffusion coefficient, there are two other important definitions of the diffusion coefficient, which are also frequently used: self-, and tracer diffusion coefficients. Although they are all related, the difference is given by the nature of the diffusion process itself. The relationship between these coefficients are schematically depicted in Figure III-1.

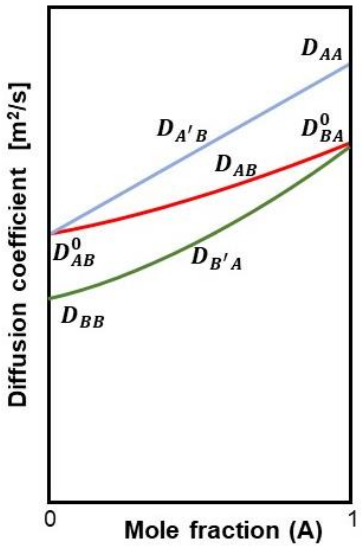

Figure III-1. Relationship between mutual, self and tracer diffusion coefficients in a binary mixture A + B (adapted from the literature [93]*).*

Self-diffusion coefficient, denoted by D_{AA}, is a measure of mobility of a species in itself. In the special case that A and B are similar in molecular weight, polarity, and so on, the self-diffusion coefficients of pure A and B will be approximately equal to the mutual diffusivity. In a binary system where A and B are the less mobile and more mobile components respectively, their self-diffusion coefficients can be used as rough lower and upper bounds of the mutual diffusion coefficient in some systems: $D_{AA} < D_{AB} < D_{BB}$ [94].

Tracer diffusion coefficients (sometimes referred to as intradiffusion coefficients), denoted as $D_{A'B}$, relating to the diffusion of a labelled component within a homogeneous mixture. Like mutual diffusion coefficients, tracer diffusion coefficients can be a function of composition [93]. As concentration varies, tracer diffusivities approach mutual diffusivities at the dilute limit, and they approach self-diffusivities at the pure component limit. That is, at the limit of dilute A in B $D_{A'B} \rightarrow D_{AB}^{0}$ and $D_{B'A} \rightarrow D_{BB}$; likewise, at the limit of dilute B in A, $D_{B'A} \rightarrow D_{BA}^{0}$ and $D_{A'B} \rightarrow D_{AA}$ [94].

Neither the tracer diffusivity nor the self-diffusivity has much practical value except as a means to understand ordinary diffusion and as order-of-magnitude estimates of mutual diffusivities [94].

III.1.2 Chemical potential gradient as a driving force for diffusion

As mentioned, Fick's diffusion laws state that the flux of a diffusing component is proportional to the concentration gradient, with D_{AB} being the constant of proportionality. However, diffusion is affected by more than just the concentration gradient, e.g., the intermolecular interactions of the molecules which can give complex composition dependence of the behaviour in addition to that from temperature and pressure. Thus, fluxes may not be linear in the concentration gradient; and Fick's laws do not always adequately describe diffusion. This is especially true for multicomponent systems where the presence of non-zero cross-coefficients in the Fick matrix lends to characteristics quite different from the corresponding binary system [95]. In multicomponent systems, it is possible to have a diffusion flux of a component even in the absence of a composition gradient for that component (this phenomenon is known as osmotic diffusion). Furthermore, species may not diffuse at all in the presence of a concentration gradient for that component (known as diffusion barrier), or even species may diffuse opposite to their concentration gradient (known as reverse diffusion) [93]. Therefore, a more fundamental approach is to consider the chemical potential gradient as the driving force for diffusion, instead of the concentration gradient [93,96].

An alternative description of diffusion phenomena using the chemical potential gradient as the driving force is the generalized Maxwell-Stefan (M-S) formalism

[95,97]. The M-S formalism, which was derived from the kinetic gas theory and later extended to liquid systems, describes diffusion fluxes in terms of gradients in chemical potential (μ_i) and Maxwell-Stefan diffusion coefficients ($Đ_{ij}$) [98]:

$$\frac{x_i}{RT}\nabla_{T,P}\mu_i = \sum_{j=1}^{n}\frac{x_i J_j - x_j J_i}{c\, Đ_{ij}} \qquad \text{III-4}$$

Here $\nabla_{T,P}\mu_i$ is the chemical potential gradient at constant temperature (T) and pressure (P); c is the molar concentration; R is the gas constant; and x_i, x_j, and J_i, J_j denote the mole fraction and molar flux of component i and j, respectively.

Unlike mutual diffusion coefficients defined by Fick's laws (or simply Fick diffusivity), which depend on the frame of reference, $Đ_{ij}$ is independent of the frame of reference, and thus, commonly used in computational predictions. Moreover, the relationship between the M-S diffusivity and the Fick diffusivity can be obtained after the algebraic treatment of equation III-4. It can be demonstrated that for a binary system, the diffusion flux of component 1 can be written as [98]:

$$J_1 = -cĐ_{12}\Gamma\nabla x_1 = -cD_{12}\nabla x_1 \qquad \text{III-5}$$

where D_{12} is the Fick diffusion coefficient, and thus, $D_{12} = Đ_{12}\Gamma$. Since the Fick diffusion coefficient was defined in terms of a concentration gradient instead of a chemical potential gradient, a thermodynamic correction factor Γ is introduced to account for the nonideal behaviour of the binary mixture as follows:

$$\Gamma = 1 + x_1\frac{\partial \ln \gamma_1}{\partial x_1} \qquad \text{III-6}$$

Here, x_1 and γ_1 are the mole fraction and activity coefficient of component 1 in the mixture, respectively. Nevertheless, according to the Gibbs-Duhem equation, Γ is the same regardless of whether activities and mole fractions of either component 1 or 2 are used in equation III-6 [93]. Moreover, the required activity coefficient can be obtained using several thermodynamic models based on excess Gibbs energy (g^E). Such a model can be, for example, NRTL, Wilson, or UNIQUAC models [98]. By definition, the thermodynamic factor is equal to unity for a pure component and an ideal mixture, regardless of the state of matter. For gases, Γ is almost always close to unity (except at high pressures), but in the case of liquid mixtures, significant deviations from unity are observed. With the use of equation III-6, the Fick and the Maxwell-Stefan diffusivities can be transformed into one another. Therefore, both approaches may be employed in

the description of diffusion fluxes once information on either type of diffusivity is available [92].

III.1.3 Effect of concentration on diffusion in liquid mixtures

The concentration dependence of binary diffusion coefficients in liquid mixtures is not simple. In some systems, this dependence is quite remarkable, since the diffusion coefficients of the pure compounds may differ by more than an order of magnitude [99]. In contrast, the concentration dependence is much weaker for systems in which the two limiting diffusion coefficients are in the same order. Also, the shape of the diffusion-concentration curves differs from one system to another. In some cases, it varies linearly between the two limiting diffusion coefficients, while in others, strong positive or negative deviations from linearity are observed [93].

Although considerable research efforts have been made on the concentration dependence of the diffusion coefficient, there is no satisfactory theoretical interpretation for all liquid systems [93,99]. Nevertheless, several correlations have been proposed to estimate the diffusion coefficients of concentrated binary liquid mixtures [99–105]. In most of these correlations, the thermodynamic factor (Γ) is introduced, which has a strong influence on the concentration dependence of the diffusion coefficient. In this sense, it has been suggested that Γ be raised to a fractional power because it often overcorrects the diffusion coefficient [93]. Furthermore, in general, the developed correlations originate from different theories of diffusion and their formulation involves properties other than concentration, such as viscosity and temperature. Thus, here, the concentration dependence of the diffusion coefficient is considered through the theories and practical correlations presented in section III.3

III.1.4 The effect of temperature on diffusion in liquid mixtures

The temperature dependence of binary diffusion coefficients is simpler than the concentration dependence. In general, the diffusion coefficient increases with increasing temperature. This is consistent with the previous explanation that diffusion describes random molecular motion. At higher temperatures, more thermal energy is available for molecular motion. Despite this general trend, in the literature, several functional forms can be found for the temperature

dependence of the diffusion coefficients. Here we only present some of the most common ones.

The Arrhenius-type equation is probably the most common functional form of the temperature dependence of the mutual as well as self-diffusion coefficients:

$$D_{12} = D_0 \exp\left(-\frac{E_a}{RT}\right) \quad \text{III-7}$$

The temperature dependence of the self-diffusion coefficients in ionic liquids has also been well represented by an equation of the Vogel-Tamman-Fulcher (VTF) type [106,107]:

$$D_{11} = \exp\left(A + \left(\frac{B}{T - T_0}\right)\right) \quad \text{III-8}$$

Another functional form of the temperature dependence of diffusion coefficients is the Speedy-Angell power law:

$$D_{12} = D_0 \left(\frac{T}{T_S} - 1\right)^m \quad \text{III-9}$$

Infinitely dilute binary (and also self-) diffusion coefficients can be correlated with temperature as [93]:

$$\frac{D_{12}^0(T_1)}{D_{12}^0(T_2)} = \left(\frac{T_c - T_1}{T_c - T_2}\right)^n \quad \text{III-10}$$

where T_c is the critical temperature of the solvent (component 2), and the parameter n is related to the heat of vaporization of the solvent.

III.1.5 Effect of pressure on diffusion in liquid mixtures

Transport properties of fluids tend to be a far weaker function of pressure than of concentration or temperature. Therefore, the effect of pressure on liquid diffusion coefficients has received considerably less attention [93]. In general, if an increase in pressure causes an increase in viscosity (or density), and consequently in the resistance to motion provided by the solvent, the observed diffusivity of the solute should decrease [90]. Ultimately, the extent of this reduction, which may not be as pronounced as the effect of temperature, can be significant at higher pressures for some systems and negligible for others. For example, by increasing the pressure from 20 to 30 MPa, the CO_2 diffusion coefficient in ethyl benzoate at 333.16 K is reduced by 26.2% [108], while the

CO_2 diffusion coefficient in methane at 298 K and 353 K only reduced by 2.4% and 3.8%, respectively [109].

III.2 Experimental methods for the determination of mass diffusivities

As mentioned, there are no standard methods for determining the diffusivity of one substance in another. Therefore, a wide variety of experimental methods have been used for this purpose and can be found in the literature [110]. In this section, some of the most common methods used to determine the diffusion coefficient in fluid mixtures relevant to absorption refrigeration systems are described, with special emphasis on ionic liquid-based working pairs. The presented techniques have been used to determine diffusion coefficients in liquid-liquid systems as well as in vapour-liquid systems. The scope of this section is to provide an overview and is therefore not intended to conduct a comprehensive literature review.

III.2.1 Nuclear magnetic resonance

Nuclear magnetic resonance (NMR) is a technique that measures the response of a nuclei to a magnetic field. In particular, in the pulsed-field gradient NMR (PFG-NMR) method, the attenuation of a spin-echo signal resulting from the dephasing of the nuclear spins due to the combination of the translational motion of the spins and the imposition of spatially well-defined gradient pulses is used to measure motion [111]. The attenuation of the signal intensity depends on the diffusion time as well as the gradient parameters as:

$$\ln\left(\frac{I}{I_0}\right) = -D\gamma^2 g^2 \delta^2 (\Delta - \frac{\delta}{3}) \qquad \text{III-11}$$

where I is the spin-echo signal intensity, I_0 the reference intensity (unattenuated signal intensity), D the diffusion coefficient, γ the gyromagnetic ratio of the observed nucleus, g the gradient strength, δ the length of the gradient, and Δ the diffusion time. The diffusion coefficient is obtained from the slope of the plot $\ln\left(\frac{I}{I_0}\right)$ vs $\gamma^2 g^2 \delta^2 (\Delta - \frac{\delta}{3})$.

The NMR method is primarily used for measuring self- and tracer-diffusion coefficients, although NMR in the form of magnetic resonance imaging (MRI) can

provide information on mutual diffusion [111]. It should also be theoretically possible to measure mass diffusivities if individual species are labelled with different NMR active probes [90].

III.2.2 Taylor dispersion

The Taylor dispersion technique (TDT) is one of the most popular methods for measuring mass diffusivities in liquid mixtures. A schematic representation of an experimental setup based on the TDT, and its main components, are shown Figure III-2.

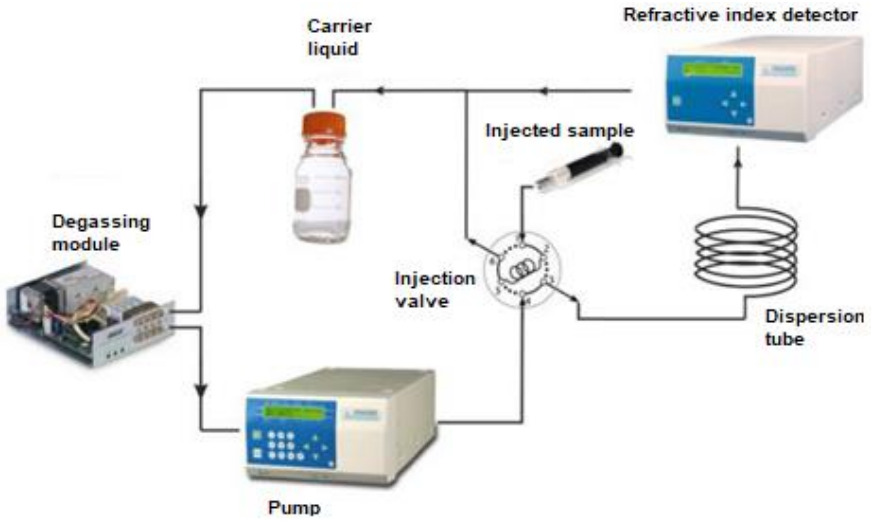

Figure III-2. Schematic of an experimental setup based on the Taylor Dispersion Technique (TDT) [69].

The TDT is based on the diffusive spreading of a small volume of a solution injected into a laminar stream of the same mixture but with a slightly different concentration [69]. The fluid mixture flows in laminar regime (using a pump) through an infinitely long, isothermal tube (dispersion tube), of uniform circular cross-section, with impermeable walls [112]. Due to the combined effects of convective flow and molecular diffusion, the narrow pulse of sample injected ultimately assumes a Gaussian distribution (see Figure III-3), whose temporal variance is dependent on both the average flow velocity and the mass diffusivity [113]. At the end of the tube, the Gaussian shape of the pulse is monitored by means of a suitable detector such as a flow-through spectrophotometer or a refractive index detector [69].

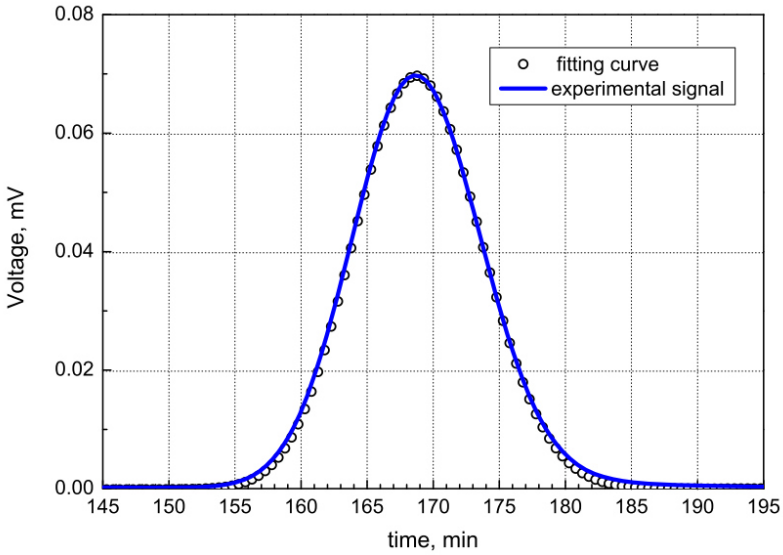

Figure III-3. Dispersion profile (experimental signal) and fitting curve obtained using the TDT [114].

Finally, the Gaussian signal can be interpreted using different methods to calculate the diffusion coefficient of interest. One of these methods is based on fitting the diffusion coefficient in order to minimise the difference between the experimental points and the analytical solution of Taylor's equation [113,115]:

$$c(t) = \frac{m}{\pi R^2 \sqrt{4\pi K t}} \exp\left(-\frac{(L-ut)^2}{4Kt}\right) \qquad \text{III-12}$$

In Eq. III-12, $c(t)$ is the solute concentration in the solvent at time *t*, *m* the mass of solute injected, *R* the inner tube radius, *K* the Taylor dispersion coefficient, L the effective length of the dispersion tube and *u* the cross-section averaged axial velocity. The Taylor dispersion coefficient is related to the diffusion coefficient as follows [41,113]:

$$K = D_{12} + \frac{R^2 u^2}{48 D_{12}} \qquad \text{III-13}$$

The TDT initially developed for binary mixtures, has also been extended to ternary and even quaternary mixtures [114,116]. Some of the advantages of the TDT include the possibility of measurements over a wide range of temperature and pressure; it does not require a calibration procedure with a liquid of known diffusivity, and it is relatively simple in realization because the setup consists of components available on the HPLC (High-performance liquid chromatography) market [116]. In addition, this is a relatively fast method due to the imposition of convection on diffusive transport [90]. However, several experimental constraints

should be implemented to perform TDT as a consistent analytical technique for the determination of diffusion coefficients in liquid systems [115]. In particular, the high viscosity of IL-containing mixtures, especially at high IL concentrations, can lead to several experimental problems, due to the validity of the relationships assumed in the mathematical formulation of the dispersion model [112].

III.2.3 Dynamic light scattering

Dynamic light scattering (DLS) make use of microscopic statistical fluctuations of the electric susceptibility, which may be related to various diffusive processes [117]. Specifically, from the analysis of the time-dependent scattered light intensity, which contains information on the dynamics of microscopic fluctuations in pressure, temperature, and concentration, various properties of fluids, such as the mass diffusivity, can be determined [118].

In macroscopic thermodynamic equilibrium, the equilibration of microscopic fluctuations in temperature and concentration is governed by thermal and mass diffusivities. Then, the mean decay times of both types of fluctuations are analyzed by calculating the time-dependent intensity correlation function ($g^{(2)}$) [119]. If heterodyne conditions can be arranged, the normalized intensity correlation function is simplified. In that case, the correlation function only depends on the transport properties (thermal and mass diffusivities), time, the scattering vector, and some experimental constants [118] as:

$$g^{(2)} = b_0 + b_t \exp(-\frac{\tau}{\tau_{C,t}}) + b_c \exp(-\frac{\tau}{\tau_{C,c}}) \qquad \text{III-14}$$

Here, the decay times of the two exponential functions, $\tau_{C,t}$ and $\tau_{C,c}$, reflect the mean lifetimes of the temperature and concentration fluctuations in the binary mixture. The experimental constants b_0, b_t, and b_c are mainly determined by the intensities of the scattered and the reference light as well as by effects that are caused by imperfect signal collection. $\tau_{C,t}$ and $\tau_{C,c}$ are related to the thermal diffusivity (α) and the mass diffusivity D_{12} according to:

$$\tau_{C,t} = 1/\alpha q^2 \qquad \text{III-15}$$

$$\tau_{C,c} = 1/D_{12} q^2 \qquad \text{III-16}$$

The scattering vector *q* can be determined from the refractive index of the fluid, the laser wavelength in vacuo, and the scattering angle (the angle between the directions of the incident light and the analyzed scattered light in the fluid).

Finally, the mass diffusivity can be obtained using non-linear regression of the correlation function with the experimental data from the correlator (a special-purpose computer which calculates correlation functions in real-time) in the DLS apparatus [117].

The main advantages of DLS techniques include non-intrusiveness and determination of a wide range of transport and other thermophysical properties (which can be determined even simultaneously in some instances). Furthermore, in most cases, these techniques are based on rigorous working equations, where no calibration procedure is needed, and the reliability of the measurements can be easily checked [120]. However, the evaluation of the correlation functions has been reported to be considerably difficult at the limits of the concentration range because the small concentration of one of the components of the mixture results in smaller scattering intensities [121]. Furthermore, the precision of DLS techniques is 2 to 5 times less precise than other common methods for measuring diffusion coefficients, such as interferometric methods [122]. Other disadvantages include the relatively large expense and complexity of the experimental setup [97].

III.2.4 Gravimetric method

The gravimetric method is a simple method, where a certain amount of IL (or other absorbent liquid) is brought into contact with the gas (or vapour) to be absorbed. The experiment is set up by filling the absorption cell with a small amount of absorbent liquid. In this method, the pressure is maintained constant over the course of the experiment, and the absorption cell is placed over a mass balance. As gas dissolves into the IL, the total mass of the sample in the absorption cell will increase, giving a direct measurement of the mass absorbed with time. Then, the mass of the liquid sample (absorbent liquid mass + absorbed vapour mass) is analyzed as a function of time with the help of a mass diffusion model.

This method has been extensively used to measure gas diffusivity in ionic liquids. Most of the literature works use a simplified mass diffusion model, based on Yokozeki's pioneering work for the analysis of time-dependent absorption of gas in lubricant oil [62]. This simplified model assumes:

a) the gas dissolves through a one-dimensional diffusion process.
b) there is a thin boundary layer between the gas and liquid phases, where the thermodynamic equilibrium is instantly established with the saturation concentration and where the concentration is constant in time at a given temperature and pressure.
c) temperature and pressure remain constant during the absorption process.
d) the gas-dissolved liquid is a highly dilute solution, and so the relevant thermophysical properties of the solution do not change.

On the basis of these assumptions, the solution of the one-dimensional unsteady diffusion equation is usually expressed in terms of a series of trigonometric functions that converge satisfactorily at large times [89]:

$$c(z,t) = \mathrm{c_{eq}}\left(1 - \frac{4}{\pi}\sum_{n=0}^{\infty}\frac{(-1)^n}{2n+1}\cos\left(\frac{(2n+1)\pi}{2\mathrm{H}}z\right)\exp\left(-\frac{(2n+1)^2\pi^2 D_{12}t}{4\mathrm{H}^2}\right)\right) \quad \text{III-17}$$

where $c(z,t)$ is the concentration at point *z*, and time *t*; $\mathrm{c_{eq}}$ the saturation concentration; and *H* the liquid height in the absorption cell.

An experimentally determined quantity at a specified time is the total concentration (or mass) of dissolved gas in the absorbent liquid, and not the concentration profile in z. Thus, this space-averaged concentration at a given time, $\bar{c}(t)$, can be calculated from Eq. III-17:

$$\bar{c}(t) = \frac{\int_0^H c(z,t)dz}{H} = \mathrm{c_{eq}}\left(1 - \frac{8}{\pi^2}\sum_{n=0}^{\infty}\frac{1}{(2n+1)^2}\exp\left(-\frac{(2n+1)^2\pi^2 D_{12}t}{4\mathrm{H}^2}\right)\right) \quad \text{III-18}$$

Finally, the mass diffusivity is obtained from a nonlinear regression procedure between the measured mass values and the calculated values from the mass diffusion model (Eq. III-18).

III.2.5 Pressured drop method

As mentioned above, the pressure drop method can be used to determine the time-dependent mass of absorbed vapour in an absorbent liquid in a closed isothermal system. Then, the absorption rate of the vapour in the absorbent liquid

can be determined by a simple mathematical treatment of the data. In this method, the recorded pressure data can also be used to determine the mass diffusivity. To do this, changes in pressure in the absorption cell are recorded over time until equilibrium is reached. Then, using Fick's second law in combination with a mass balance in the liquid phase, the following expression relating the pressure-drop data ($P(t)$) and the mass diffusivity (D_{12}), can be written [123]:

$$\ln\frac{P(t)}{P_0} = \left(\frac{k}{H_{12}}\right)\sum_{n=0}^{\infty}\frac{1}{(2n+1)^2}\left\{exp\left[-\frac{(2n+1)^2\pi^2 D_{12}t}{4L^2}\right]-1\right\} \qquad \text{III-19}$$

where P_0 is the pressure corresponding to a time t, t = 0, H_{12} is the Henry's Law constant for the studied solute in the ionic liquid, L corresponds to the liquid height in the absorption cell, and $k = 8RTV_{IL}\rho_{IL}/\pi VMW_{IL}$ is a parameter that depends on temperature (T), Gas constant (R), the volume of vapor (V), IL density (ρ_{IL}), IL volume (V_{IL}), and IL molecular weight (MW_{IL}).

Then, using a nonlinear regression procedure of the experimental pressure values, the mass diffusivity and Henry constant (if not known) can be simultaneously determined. Figure III-4 shows the typical profiles of the system pressure during the absorption process of CO_2 in ionic liquid [hmim][NTf_2].

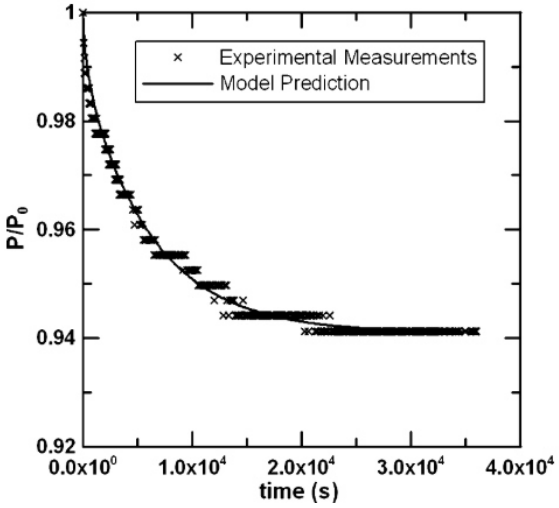

Figure III-4. Typical profiles of the dimensionless pressure (P/P_0), (×) experimental and (-) predicted using the model, versus time (t) during the absorption process of CO_2 in ionic liquid [hmim][NTf_2] at 23 °C obtained in the study by Hou and Baltus [123].

III.2.6 Semi-infinite volume method

The semi-infinite volume (SIV) method is based on a diffusion model mathematically described by Crank [89]. This method was originally implemented

by Camper et al. [124] and has enjoyed certain popularity among various research groups for the measurement of gas diffusion in ionic liquids. In this method, the determination of the mass of gas absorbed as a function of time is carried out by measuring the pressure decay in a short time (generally around 20 minutes). Therefore, the SIV method is essentially a modification of the pressure drop method, and the difference lies in the assumptions made in the development of the diffusion model. A complete analysis of the main assumptions of the SIV method can be found in the study by Camper et al. [124].

The distinctive feature of this method is the assumption that the concentration at the vapour-liquid interface ($C_{x=0}$) is related to the concentration at the interface at time t = 0 ($C_{t=x=0}$) and experimental time by the following equation:

$$C_{x=0} = C_{t=x=0} + k\sqrt{t} \qquad \text{III-20}$$

where k is a fitting parameter. The concentration at the interface, $C_{x=0}$, is determined from the fugacity of the gas phase in the ionic liquid using Henry's Law or the Krichevsky-Kasarnovsky relation. Subsequently, a linear fitting procedure is performed to determine $C_{t=x=0}$ and k from the plot of concentration at the interface as a function of the square root of time ($C_{x=0}\ vs\ t^{0.5}$).

Finally, the mass diffusivity is determined applying another linear regression procedure between the absorbed mass and an experimental parameter (ε) (shown in equation III-18), which includes the contributions of the determined fitting parameters ($C_{t=x=0}$ and k) and time:

$$M_t = \int_0^t \left(D \left.\frac{\delta C}{\delta x}\right|_{x=0}\right) dt = \sqrt{D}\left[2C_{t=x=0}\sqrt{\frac{t}{\pi}} - \frac{1}{2}kt\sqrt{\pi}\right] = \sqrt{D}\varepsilon \qquad \text{III-21}$$

III.2.7 Optical interferometric methods

Optical techniques are recognized as the most accurate instruments to measure mass diffusivities [91]. The use of these techniques implies the optical analysis of the equilibration of macroscopic concentration gradients reflected in the changing refractive index of the studied mixture [121]. These techniques are characterized by their sensitivity, non-intrusiveness and experimental flexibility due to the great variety of optical configurations that can be used. The main limitations are that the media under investigation must be transparent to the light source used [125].

In general, optical techniques for measuring diffusion coefficients can be sub-divided into interferometric and non-interferometric methods. Non-interferometric optical methods, such as schlieren, are simply not precise enough, and cannot be adequately improved [122]. Thus, interferometric methods are widely preferred and classical interferometers, such as Jamin, Mach-Zender, Rayleigh and Gouy, have been routinely employed for measuring diffusivities in liquid mixtures [125]. Among these interferometers, Gouy interferometer is the more highly developed and shows an accuracy better than 0.1% [97]. However, the procedures behind Gouy interferometer are quite complex and involves the use of optical wave theory to obtain correct expressions for the fringe positions [126]. Thus, the information obtained is difficult to interpret, and writing the appropriate computer program for data processing can be a very demanding task.

The Mach-Zehnder and Rayleigh interferometers are recognized as reliable alternatives to the Gouy interferometer [97]. Mach-Zehnder interferometer (MZI), for example, has been used to determine diffusion coefficients in liquids for more than five decades [127]. Compared to the Rayleigh interferometer, MZI does not need the hard-to-get good cylinder lens that the Rayleigh interferometer requires [122]. A schematic representation of the MZI is illustrated in Figure III-5. The main components include a laser source, two beam splitters, two flat mirrors, and a detection and visualization system, such as a charge-coupled device (CCD) camera. The MZI uses measurable changes in the light intensity of the interference pattern to determine the change in the refractive index of transparent media that undergo a physical process, such as diffusion. In more detail, the working principle of an MZI can be summarized as follows.

First, coherent light emitted from a laser source is filtered, expanded, and collimated using a spatial filter with a microscopic objective, and a collimating lens. The collimated beam then hits a beam splitter (BS_1), where half of the amplitude of the incident wave is reflected, and the other half is refracted. One of the resulting beams, which is called the test (or object) beam, is directed to propagate through the working cell containing the fluid mixture under investigation using a mirror (M_1). The second beam, called the reference beam, is directed using another mirror (M_2) through the ambient air. Thus, the optical paths of both beams are different. Recombination of these two beams at a second

beam splitter (BS_2), generates the interference pattern, which can be detected and stored in a CCD camera with the help of an objective lens. Finally, the interference pattern can be processed to extract the optical phase difference between both beams, which contains valuable information about the studied physical process.

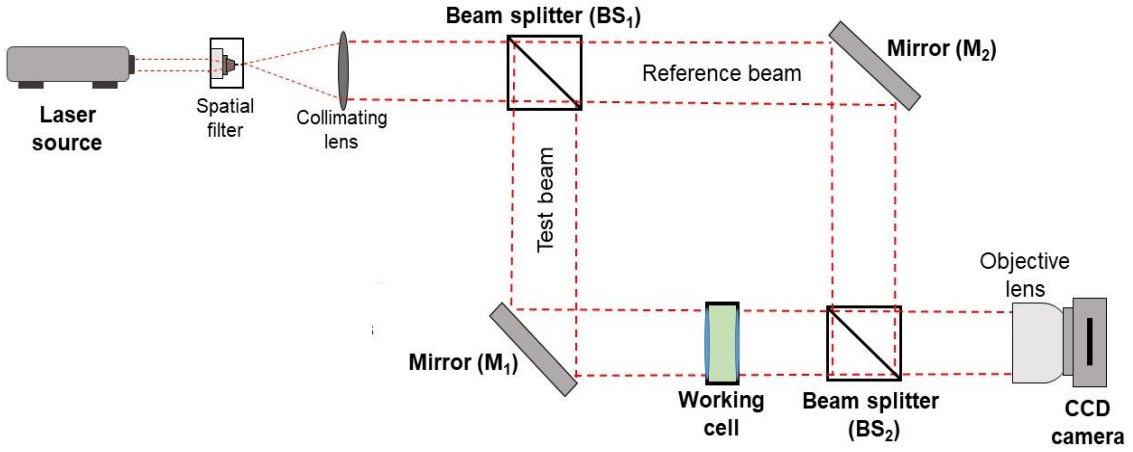

Figure III-5. Schematic representation of the Mach-Zehnder interferometer.

Although the great popularity of classic interference schemes such as MZI or Rayleigh, their design, and alignment is a difficult, expensive, and time-consuming task [128]. Moreover, traditional optical interferometry exhibits certain drawbacks that limit its applicability to various problems of practical interest. For example, Mach-Zehnder interferometry is limited to small deformations of the test beam wavefront compared with the shape of the reference wavefront. For large deformations of the test beam wavefront, the fringe density becomes too high to be resolved by the CCD camera [129].

Furthermore, since the test and reference beams propagate along different optical paths, the optical elements in both arms must be practically identical and, consequently, be free of aberrations, creating output distortions. Therefore, the components used must be of high optical quality, which makes the systems more expensive and hardly applicable to some types of installations [128].

The advent of holographic interferometry at the beginning of the 1970s offered some advantages over classical interferometry, mainly relaxing the need for high optical quality elements and gaining in simplicity, at the expense of a slight decrease in precision [125]. The idea of optical holographic interferometry, unlike its classic counterpart, is based on a two-step approach [128]. In the first step (or

recording step), the interference pattern between the reference and test beams is recorded through grey levels on a photographic plate and is called the hologram. This pattern contains a “coding” of the object phase. In the second step (or reconstruction step), the object (here, the working cell) is removed, and the plate is developed and illuminated by the reference beam only. The diffraction of the reference beam by the interference pattern on the plate provides a “decoding” of the recorded object phase [130]. At the output of a scheme of reconstruction, the interference of the reference and test beams cancel optical aberrations; and the resulting interference field is practically free of aberration of the interferometer [128].

The basic concept of holographic interferometry is similar to that of classical interferometry. The basic optical scheme for recording Mach-Zehnder holograms is the Mach-Zehnder classic interferometer [128]. However, in opposition to classical interferometry, holographic interferometry provides time-differential measurements [129]. The main difference between classical interferometry and holographic interferometry is that in the latter the object beam is compared with itself, or more precisely, with a memory of itself at a reference (preceding) time (registered in the hologram) [131].

Furthermore, the introduction of recent advances in lasers, cameras, computers, and data processing software has led to a considerable evolution in holographic interferometry. In digital holographic interferometry, the holographic plate used in conventional holographic interferometry is replaced by a CCD camera. This implies that the interference pattern of the object and reference beams is now recorded through grey levels by the CCD sensor during the recording step. Then, the diffraction of the reference beam by the recorded interference pattern is carried out numerically instead of physically during the reconstruction step [130]. This results in a much easier experimental technique that requires less cost and experimental effort.

III.3 Models and correlations for the estimation of diffusion coefficients

There is a growing demand for accurate diffusion properties, which experimental measurements alone are not able to satisfy. Moreover, considering the huge

family of ionic liquids, the need to estimate the mass diffusivities becomes evident. The estimation methods for diffusion can be broken down into four general approaches: hydrodynamic theory, kinetic theory, Eyring's absolute reaction rate theory, and semiempirical equations based on these theories [132]. This section presents some of the main theoretical models and correlations developed from these models to estimate diffusion coefficients in binary systems.

III.3.1 Hydrodynamic theory

In the hydrodynamic theory, a diffusing molecule is considered a particle moving through a continuous medium that applies a resistance to flow. Based on this approach, the well-known Stokes-Einstein equation was developed [96]:

$$\frac{D_{12}\mu_2}{T} = \frac{\kappa}{6\pi r_1} \qquad \text{III-22}$$

where D_{12} is the mass diffusivity in $m^2\ s^{-1}$, μ_2 is the viscosity of the solvent in Pa s^{-1}, κ is the Boltzmann's constant (κ = 1.38 x 10^{-23} m^2 kg s^{-2} K^{-1}), T is the temperature in K, and r_1 is the radius of the ''spherical'' solute in m.

The Stokes-Einstein equation is not of practical use in predicting the diffusion coefficient since the radius of the "spherical" solute is generally not known. Instead, this equation can be used to estimate the molecular radius of the solute, once the diffusion coefficient has been measured. Furthermore, this equation is useful for extrapolating the measured diffusivities from one temperature to another, since $D_{12}\mu_2/T$ is a constant for a solute-solvent pair.

In the literature, several empirical modifications of the Stokes-Einstein equation have been proposed, to express the diffusion coefficient as a function of properties that are easier to measure, such as viscosity or volume. The Wilke-Chang equation is the most widely used one, which is defined by [29,38,123,133]:

$$D_{12}/\mathrm{cm^2 s^{-1}} = \frac{7.4\times10^{-8}(\phi M_2)^{1/2}T}{\mu_2 V_1^{0.6}} \qquad \text{III-23}$$

where: M_2 is the molecular weight of solvent (2), in g/mol; T the temperature in K; η_2 the viscosity of solvent (2) in mPa·s; V_1 the molar volume of solute (1) at its normal boiling temperature in cm^3/mol; and ϕ is the solvent association factor, dimensionless.

The association factor addresses the intrinsic characteristics of the solvent association and size. In an attempt to eliminate the solvent association factor and improve the precision of the Wilke-Chang correlation, some modifications have been suggested, such as the Scheibel correlation [35,134]:

$$D_{12} = \mathrm{C}\frac{T\left(1+\left(3\frac{\mathrm{V}_2}{V_1}\right)^{2/3}\right)}{\mu_2 {V_1}^{1/3}} \qquad \text{III-24}$$

where C is an empirical constant, and V_2 is the molar volume of the solvent (2).

III.3.2 Kinetic theory

In the kinetic theory, both the diffusing molecule and the solvent are treated as particles in which the collision between different particles acts to oppose diffusivity.

In general, kinetic theory can provide accurate estimates of the diffusion coefficients for gases, but the situation is considerably less favourable for liquid mixtures. However, several correlations have been developed to estimate diffusivity in liquid systems based on kinetic theory. In particular, an equation based on a combination of kinetic and hydrodynamic theories that have been previously used in gas-ionic liquid systems is the Arnold equation [35,132,134].

$$D_{12} = \left[\frac{0.010}{A_1 A_2}\right]\frac{\left(\frac{1}{M_1}+\frac{1}{M_2}\right)^{1/2}}{{\mu_2}^{1/2}\left({V_1}^{1/3}+{V_2}^{1/3}\right)^2} \qquad \text{III-25}$$

where A_i are abnormality factors to account for nonidealities, both in the solvent phase and in the solute phase.

III.3.3 Eyring's theory of absolute reaction rates

Eyring's theory of absolute reaction rates states that diffusional processes may be modelled analogously to chemical reactions, i.e. a sufficient high initial energy is crucial for a diffusional process to overcome the energy barrier between the position of the molecule considered and an adjacent, vacant lattice site [92]. Based on this theory, a number of empirical correlations for predicting diffusivities in infinitely dilute liquid solutions have been developed. In particular, Akgerman and Gainer [135,136] modified the Eyring's theory of absolute reaction rates to develop an equation for predicting gas diffusivities in liquids as:

$$D_{12} = \left(\frac{\kappa T N_A^{\frac{1}{3}}}{6}\right)\left(\frac{M_2}{M_1}\right)^{\frac{1}{2}}\left(\frac{1}{\mu_2}\right)\left(\frac{1}{V_1 V_2}\right)^{\frac{1}{6}}\exp\left(\frac{E_a^{vis}-E_a^D}{RT}\right) \quad \text{III-26}$$

where N_A is the Avogadro's number, M_1 the molecular weight of the solute (1), V_1 the molar volume of the solute, E_a^{vis} and E_a^D are the activation energies for viscosity and diffusion, respectively. The activation energy for viscosity can be obtained from viscosity measurements at different temperatures using an Arrhenius-type equation. The same applies to the activation energy for diffusion.

III.3.4 Darken and Vignes correlations

In concentrated binary liquid mixtures, D_{12} is typically described by several correlations as a function of composition and some limiting diffusion coefficients. One of the first correlations, which is still used quite frequently, was proposed by Darken [100] as:

$$D_{12} = (x_2 D_1^* + x_1 D_2^*)\left[1 + x_1 \frac{d\ln\gamma_1}{dx_1}\right] \quad \text{III-27}$$

where x_1, x_2 are the mole fractions of componets 1 and 2, respectively; γ_1 is the activity coefficient of component 1; and D_1^*, D_2^* are the tracer diffusion coefficient of components 1 and 2, respectively. Therefore, to use the Darken correlation, one has to know the tracer diffusion coefficient of the components, which is not always available in the literature. It is important to note that in this correlation D_{12} is expressed by a kinetic contribution $(x_2 D_1^* + x_1 D_2^*)$ and a thermodynamic contribution $\left[1 + x_1 \frac{d\ln\gamma_1}{dx_1}\right]$. This last term is the thermodynamic factor, Γ, as defined in Eq. III-6. The thermodynamic factor can be obtained from a g^E model, as described in Annex A.

Later, Vignes [101] conveniently replaced the tracer diffusion coefficients in the Darken equation by the limiting diffusion coefficients at infinite dilution. Vignes correlation is expressed as the product of a geometric average of the composition and a thermodynamic factor as follows:

$$D_{12} = ((D_1^\infty)^{x_2}(D_2^\infty)^{x_1})\Gamma \quad \text{III-28}$$

where D_1^∞, D_2^∞ are the limiting diffusion coefficients at infinite dilution of components 1 and 2, respectively. There are several available correlations for

calculation of diffusion coefficients at infinite dilution with reasonable success [93].

III.3.5 UNIDIF model

In another approach, Hsu and Chen [103] developed a correlation for the mass diffusivity in binary liquid mixtures using statistical thermodynamics and the absolute reaction rate theory. The developed correlation does not involve the use of a thermodynamic factor; instead, it expresses the mass diffusivity as a reference term and an excess term. The reference term is based on a mole fraction average of the logarithm of the limiting diffusion coefficients. Meanwhile, the excess part of the diffusion coefficient is expressed as UNIQUAC equation, which comprises two parts due to the combinatorial and residual contributions. The combinatorial part depends on molecular sizes and shapes. The residual part includes two binary interaction parameters, which can be obtained from experimental data.

In this model, the mass diffusivity in a binary mixture can be expressed as:

$$\ln D_{12} = x_2 \ln D_1^{\infty} + x_1 \ln D_2^{\infty} + 2\left(x_1 \ln \frac{x_1}{\phi_1} + x_2 \ln \frac{x_2}{\phi_2}\right) +$$

$$+2x_1x_2\left[\frac{\phi_1}{x_1}\left(1-\frac{\lambda_1}{\lambda_2}\right)-\frac{\phi_2}{x_2}\left(1-\frac{\lambda_2}{\lambda_1}\right)\right]+$$

$$+x_2q_1[(1-\theta_{21}^2)\ln\tau_{21}+(1-\theta_{22}^2)\tau_{12}\ln\tau_{12}]+$$

$$+x_1q_2[(1-\theta_{12}^2)\ln\tau_{12}+(1-\theta_{11}^2)\tau_{21}\ln\tau_{21}] \qquad \text{III-29}$$

Here, θ_{ji} (for *j* or *i* = 1 or 2) is the local composition parameter, and it is defined by Abrams and Prausnitz [137] as:

$$\theta_{ji} = \frac{\theta_j \tau_{ji}}{\sum_l^2 \theta_l \tau_{li}} \qquad \text{III-30}$$

where θ_j is the average fraction of the surface area *q* of the component *j:*

$$\theta_j = \frac{x_j q_j}{\sum_l^2 x_l q_l} \qquad \textit{III-31}$$

τ_{ji} is the binary interaction parameter defined as:

$$\tau_{ji} = exp\,(-\frac{a_{ji}}{T}) \qquad \textit{III-32}$$

where *T* is the temperature and a_{ji} are the adjustable parameters.

Finally, ϕ_i (for *i* = 1 or 2) is defined as:

$$\phi_i = \frac{x_i \lambda_i}{\sum_l^2 x_l \lambda_l} \qquad \text{III-33}$$

where $\lambda_i = (r_i)^{\frac{1}{3}}$, and r_i are the UNIFAC volume parameters.

Hsu and Chen determined values of the interaction parameters for 49 binary systems. These authors evaluated the performance of their correlation by testing 1042 experimental points and found an average error of 2.3%. They compared their results with those from modified Darken and Vignes correlations for the same systems and concluded that the developed correlation gave superior results.

III.3.6 Cluster diffusion model

More recently, Kamgar et al. [104] developed a correlation to predict mass diffusivities in concentrated solutions. The correlation is based on the cluster diffusion theory proposed by Cussler [102]. In this theory, diffusion is represented through the movement of entire clusters of molecules. The correlation developed by Kamgar et al. expresses the mass diffusivity as a function of temperature (T), viscosity (η) and composition of the solution (x_1,x_2) as follows:

$$D_{12} = \frac{kT}{2\pi\eta(2-n)\beta r_0}\left(\frac{1}{1+Y^*\frac{1}{x_1 x_2}\left(\frac{1}{\Gamma}-1\right)}\right)^{\frac{1}{3-n}} \qquad \text{III-34}$$

where k is the Boltzmann constant, r_0 is the radius of the solute molecule, Γ is the thermodynamic factor, and n, β, Y^*, are the adjustable parameters of the model, respectively. Here, the radius of the solute for the ionic liquid is unknown, so in this work, it is used as another adjustable parameter.

Kamgar et al. [104] evaluated the prediction ability of the developed expression by comparison with the experimental data of 11 binary systems from literature. Moreover, they tested three different approaches to obtain the thermodynamic factor, namely NRTL, Wilson, and numerical integration of the VLE data. They found good agreement with the experimental data for classical binary systems, with an average relative error of 4.24%, 3.47%, and 13.99% when using NRTL, Wilson, and numerical integration, respectively.

III.3.7 Modified group contribution (MGC) model

In the MGC model, the mass diffusivity is described as a diffusion coefficient for an ideal solution, ${D_{12}}^{id}$, modified by a thermodynamic correction factor ψ as:

$$D_{12} = \psi {D_{12}}^{id} \qquad \text{III-35}$$

Here the diffusion coefficient for the ideal solution is written as follows:

$${D_{12}}^{id} = D^* \frac{(x_1 q_2 + x_2 q_1)^a}{(x_1 q_1 + x_2 q_2)^b} \sqrt{T} exp\left(\frac{(x_1 E_{21} + x_2 E_{12})}{RT} - \alpha \frac{298.15(x_1 r_2 + x_2 r_1)^c}{T(x_1 q_1 + x_2 q_2)^d}\right) \qquad \text{III-36}$$

where x_1 and x_2 are mole fractions of components, E_{12} and E_{21} are interaction energies, R is the universal gas constant, T is the temperature, and q_1, q_2, r_1, r_2 are the surface and volume parameters defined above.

The thermodynamic correction factor is related to the thermodynamic factor by:

$$\psi = \Gamma^{\beta} = \left[1 + x_2 \frac{dln\gamma_2}{dx_2}\right]^{\beta} \qquad \text{III-37}$$

where x_2 and γ_2 are the mole fraction and the activity coefficient of the small molecule component, respectively. In this model, there are 7 adjustable parameters, D^*, α, β, a, b, c, and d, used to correlate the experimental data.

III.4 Literature review on mass diffusivity measurements and modelling in absorption fluid mixtures

According to the author's statistics from the NIST ILThermo database [138], prior to November 20th, 2020, 1318 data-points were reported for the mass diffusivity in different refrigerant/IL working pairs. As shown in Figure III-6, data-points for CO_2/ILs working pairs take up the largest portion, followed by the H_2O/ILs working pairs. These two working pairs correspond to more than half of the total data-points. Besides, measurements of the group “Other refrigerants” accounts for 23.7% of the total data-points. In this group, the measurements for fluorinated refrigerants take up the majority, while for alcohols only take quite small percentages.

As the focus of this study, the natural refrigerant NH_3 has 109 mass diffusivity data-points representing 8.3% of the total, which is considerably lower than for other natural refrigerants (CO_2, and H_2O). This fact highlights the need for more

experimental data to further explore the scientific potential of this refrigerant for an IL-based absorption refrigeration cycle.

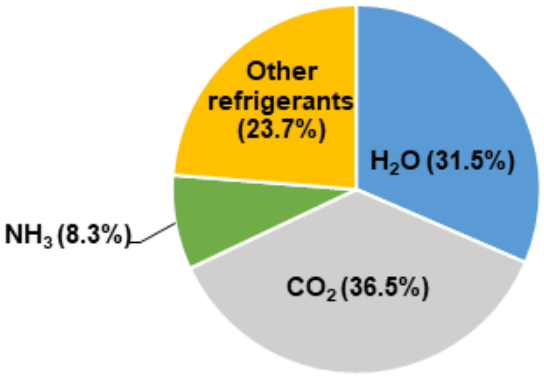

Figure III-6. Statistics of measurements of mass diffusivity for different refrigerants//IL working pairs. Data have been acquired from the NIST ILThermo database [138] *before November 20th, 2020.*

In this section, the measurement methods and estimation models used in some of the most referenced studies in the literature are reviewed. Particular attention is paid to mass diffusivity measurements in natural refrigerant/IL working pairs, although measurements in other mixtures of interest to absorption technology are also covered.

III.4.1 Mass diffusivity in CO_2/ILs working pairs

In pioneering work, Shiflett and Yokozeki [139–141] used a gravimetric method to determine the mass diffusivity of gases such as CO_2 and hydrofluorocarbons (HFC) in various ionic liquids, as potential working pairs in absorption refrigeration systems. For example, in one of their studies [139], the authors determined the CO_2 diffusion coefficients in two ionic liquids at different temperatures (283.15 K, 298.15 K, 323.15 K, and 348.15 K), and pressures below 2 MPa. The temperature dependence of diffusion coefficients was analyzed using an Arrhenius type of equation. Also, the authors observed that the Stokes-Einstein equation provided a good description of the relationship between mass diffusivity and solution viscosity. Finally, measured diffusivities of CO_2 in ILs were found to be 10-100 times lower than typical values found in various organic liquids.

In 2006, Camper et al. [124] implemented the semi-infinite volume (SIV) method for measuring the diffusivity of various gases in ionic liquid ethylmethylimidazolium bis (trifluoromethanesulfonyl) imide. The gases studied

were ethane, ethene, propane, propene, and CO_2. Measurements were made at 303.15 K for all gases, while for CO_2, a temperature range from 303.15 K to 343.15 K was analyzed, in 10 K intervals. In their work, Camper et al. [124] analyzed the influence of the molecular size of the solute and the viscosity of the IL on the variation of the diffusivity in the ionic liquid. The authors observed that the mass diffusivities decreased with increasing IL viscosity and solute molecular size.

After that, Hou and Baltus [123] determined the solubility and diffusivity of CO_2 in five ionic liquids in the temperature range from 283K to 323 K using the pressure drop method. The authors found that, in contrast to the gas solubility results, measured mass diffusivities were determined to be dependent on the ionic liquid cation as well as the anion. Moreover, the authors also observed that CO_2 diffusion coefficients were considerably more sensitive to temperature than were CO_2 solubility in the ionic liquids studied.

Moganty and Baltus [132] also used a gravimetric method to determine the mass diffusivity of CO_2 in eight ILs at 10 °C, 25 °C and 40 °C, and infinite dilute conditions. The results obtained showed that the mass diffusivity is inversely proportional to the square root of the IL viscosity. Most of the values predicted with the Arnold equation showed a deviation of ±30% from measurements, although, in the case of ionic liquids with cation $[emim]^+$, higher deviations (around +50%) were observed. The authors also developed correlations between CO_2 diffusion, some IL properties, and system temperature. These correlations allowed a satisfactory prediction of the mass diffusivities, which show deviations within 25% to the experimentally measured values.

Jalili et al. [142] used the SIV method to determine the mass diffusivities of CO_2 and H_2S in the ionic liquid 1-ethyl-3-methylimidazolium ethylsulfate ([emim][$EtSO_4$]) in a range of temperatures ranging from (303.15 to 353.15) K and pressures up to 1.6 MPa. In their study, the authors indicated that the higher value of the H_2S diffusivity compared to that of CO_2 is due to the lower molecular weight of the former. The authors concluded that the mass diffusivity of both gases in the studied IL increase with decreasing IL viscosity and with increasing temperature. These authors have continued investigating the diffusion of other gases in various ILs using the SIV method [38,143,144].

Moya et al. [145] determined the mass diffusivity of CO_2 in ionic liquids using a gravimetric method at different temperatures (293 K-323 K) and pressures (1-20 atm). The authors tested several models of diffusivity, which include those based on hydrodynamic theory, kinetic theory of liquids as well as semiempirical correlations. Among the diffusivity models studied, the authors selected a modified Wilke-Chang model as a general expression for the preliminary screening of ionic liquids with favourable CO_2 absorption rates. Unfortunately, the association factor used in this model is unknown for most ILs. Furthermore, the few experimental values reported varying widely from ionic liquid to ionic liquid and from solute to solute. For example, association factor values between 0.15 for CO_2 diffusion [35], and 197.2 for H_2 diffusion [133] in different imidazolium-based ionic liquids have been reported. Therefore, the use of this model for the preliminary screening of ILs would require the knowledge of experimental diffusivity data.

Rausch et al. [119] reported the use of the DLS method to determine the mutual and thermal diffusivities for mixtures of two imidazolium-based ILs with dissolved CO_2 at temperatures from 303.15 to 333.15 K and pressures between 2 and 26 bar. In their study, the mass diffusivity values ranged from 4.4 x 10^{-10} m^2 s^{-1} to 14.04 x 10^{-10} m^2 s^{-1}. The authors found a good agreement with literature data and only slight differences between the diffusivities measured for the two systems at the same temperature and comparable mole fractions of CO_2 were found. Also, the authors observed that the mutual diffusivities increase with increasing mole fractions of CO_2, consistent with decreasing viscosities. This was attributed to the weakening of molecular interactions by the dissolved gas.

After that, Koller et al. [118] investigated the molecular diffusion in binary mixtures of the IL 1-ethyl-3-methylimidazolium tetracyanoborate with dissolved gases using DLS and molecular dynamics (MD) simulations. The gases studied include carbon dioxide (CO_2), nitrogen (N_2), carbon monoxide (CO), hydrogen (H_2), methane (CH_4), oxygen (O_2), and hydrogen sulfide (H_2S). Measurements were performed at temperatures from 298.15 to 363.15 K and pressure up to 63 bar. The obtained diffusivities agreed with literature data for the same or comparable systems as well as with the general trend of increasing diffusivities for decreasing IL viscosities. Also, the authors found that the experimental mutual diffusivities

were well reproduced by the calculated self-diffusivities of the gases in the IL for systems containing small mole fractions of CO_2, N_2, CO, and H_2 below 0.09. The DLS and MD results revealed distinctly larger molecular diffusivities for IL-H_2 mixtures compared to mixtures with all other gases.

As a summary of the literature reviewed, we have found that:

- The diffusivity of CO_2 in ionic liquids decreases as the alkyl chain of their cation increases [123,132–134];
- The introduction of the OH^- group into the cation also leads to a decrease in diffusivity [38,143];
- The diffusivity of CO_2 in pyrrolidinium ILs with the anion $[NTf_2]^-$ is lower than the diffusivity of CO_2 in imidazolium ILs with the same anion [123,146];
- The diffusivity of CO_2 in ionic liquids with the same cation and different anions follows the order: $[NTf_2]^-$> $]BF_4]^-$> $[PF_6]^-$ [123,133,134,139].

III.4.2 Mass diffusivity in H_2O/ILs working pairs

In 2009, Sarraute et al. [147] reported the mass diffusivity of binary mixtures containing ionic liquids with water, methanol, and acetonitrile using a Taylor dispersion technique (TDT). The ILs studied are based on the 1-alkyl-3-methylimidazolium-based cation, with $[Cl]^-$, $[BF_4]^-$, and $[NTf2]^-$, anions. Measurements were performed in the temperature range between 283 K and 333 K. The measured mass diffusivities ranged from 0.57 x 10^{-9} m^2 s^{-1} for [Omim][NTf_2], in water to 3.48 x 10^{-9} m^2 s^{-1} for [emim][NTf_2] in acetonitrile.

The temperature dependence of the measured diffusivities was successfully correlated using Arrhenius-type equations. The authors observed that the diffusivities decrease, for all three solvents, with the number of carbon atoms of the alkyl side chain for the studied ionic liquids. Furthermore, the authors found that the measured diffusion coefficients are not proportional to the inverse of the viscosity, and therefore the Stokes-Einstein equation is invalid in this case. Finally, the diffusion data were correlated using a modified Wilke-Chang equation with a correction parameter, and the standard deviations obtained did not exceed 3%.

Later, Rausch et al. [121] reported the use of DSL for measuring mutual diffusivities in binary mixtures of ionic liquids and molecular liquids over the complete composition range. The fluids studied include two imidazolium based ILs and solvents such as acetone, acetonitrile, dichloromethane, ethanol, methanol, and water. Compared to conventional aqueous solutions of inorganic salts, the obtained values for IL solutions were somewhat lower. Additional measurements for IL + acetone mixtures at temperatures ranging from 278.15 K to 323.15 K showed that the temperature dependence of the mass diffusivity can be represented by Arrhenius functions and is increasing for decreasing mole fractions of acetone.

He at al. proposed a method for estimating mass diffusivities of ionic liquids-water mixtures based on an optofluidic chip. In total, eight 1,3-methylimidazolium ionic liquids-water binary systems were considered in their study, which are shown in Figure III-7. The results showed that the mass diffusivities follow the opposite order to that of the molecular weights of the ILs investigated.

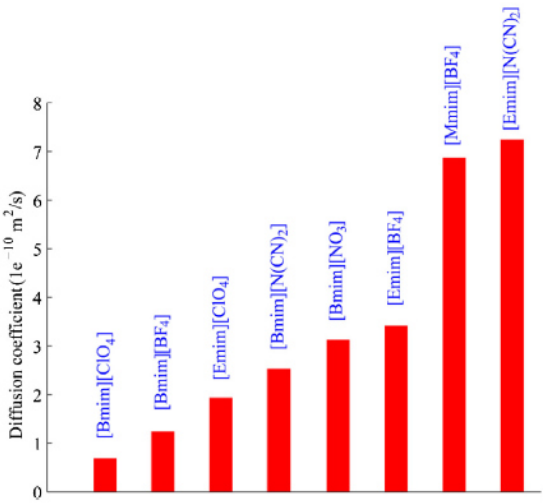

Figure III-7. Mass diffusivities of the eight ILs-water binary systems studied by He et al. [148].

After that, Merkel et al. [149] determined the thermophysical properties of the binary mixtures of water and two ammonium ILs as replacements for the conventional working pair water/LiBr in absorption chillers. The investigated ILs were diethylmethylammonium trifluoromethanesulfonate ([DEMA][OTf]) and diethylmethylammonium methanesulfonate ([DEMA][OMs]). The authors determined the diffusion coefficients of water in the ILs studied using PFG-NMR

in the temperature range from 288 K to 313 K. The obtained diffusion coefficients of water in [DEMA][OTf] were higher than the ones in [DEMA][OMs]. Thus, the authors concluded that [DEMA][OTf] is favorable for better heat and mass transfer in absorption cycles to enhance the efficiency. However, as mentioned above, PFG-NMR is used primarily to determine self and tracer diffusivities, and the determination of mass diffusivity with this technique is not straightforward. Since the authors did not describe any additional procedure, it is likely that their measurements correspond to tracer diffusivity rather than mass diffusivity. Therefore, the selection of the ionic liquid that is considered most favourable for heat and mass transfer may be wrong.

Krannich et al. [37] investigated the suitability as a drying agent of six hygroscopic ILs for technical gas dehydration processes by absorption. In particular, the mass diffusivity of water in the most suitable ionic liquid in their study, [emim][$MeSO_3$], was measured using a gravimetric method at temperatures between (303.2 and 373.2) K. The diffusivity values reported ranged from 2.1×10^{-10} $m^2\cdot s^{-1}$ to 1.2×10^{-9} $m^2\cdot s^{-1}$, with a standard uncertainty of 0.1×10^{-9} $m^2\cdot s^{-1}$.

Chen et al. [105] investigated the mass diffusivities in binary mixtures of water and methanol with ionic liquid 1-methyl-3-methylimidazolium dimethylphosphate ([mmim][DMP]) using digital holographic interferometry. Measurements were performed over a wide range of ionic liquid concentration, at atmospheric pressure of 101.5 kPa, and in the temperature range from 298.15 K to 328.15 K. The mass diffusivity values for both binary mixtures were found to increase with increasing temperature and decrease with increasing IL mass fraction. Chen et al. [105] also satisfactorily used a Modified Group Contribution (MGC) model to determine the mass diffusivity. The activity coefficients used in their work were obtained from VLE data in the literature. The authors found an excellent agreement with the experimental data. They obtained an average absolute relative deviation of 2.05% and 1.78%, for the [mmim]DMP/H_2O and [mmim]DMP/CH_3OH systems, respectively.

More recently, Rocha and Shiflett [40] measured in situ atmospheric water absorption and desorption in three imidazolium ILs using a gravimetric method at temperatures ranging from 283.15 K to 315.15 K and relative humidity 0-70% at 101 kPa. The diffusion coefficients ranged from 0.49×10^{-11} m^2/s to 1.31×10^{-10}

m^2/s. The water diffusivity increases with water concentration in two of the ILs studied. However, the diffusivity of water in [bmim][BF_4] decreases with water concentration. Diffusing radius calculations using the Stokes-Einstein relationship support the hypothesis about the formation of water/BF_4^- clusters/networks in the [bmim][BF_4] system that increase in size with increasing water concentration.

III.4.3 Mass diffusivity in NH_3/ILs working pairs

In 2012, Bedia et al. [36] used a gravimetric method to determine the mass diffusivity of ammonia (NH_3) in four ILs: [EtOHmim][BF_4], [choline][NTf_2], [MTEOA][$MeOSO_3$] and [EtOHmim][DCA]. The selection of these ILs was based on the calculated absorption capacity of ammonia by quantum-chemical COSMO-RS. The analysis of the suitability of the ILs studied was performed considering both kinetic and thermodynamic aspects in the absorption-desorption cycles. Diffusivity measurements were performed at three temperatures, 293 K, 303 K, and 313 K. The mass diffusivity of ammonia ranged from 0.37×10^{-10} m^2 s^{-1} in [MTEOA][$MeOSO_3$] at 293 K to 12.5×10^{-10} m^2 s^{-1} in [choline][NTf_2] at 303 K. In general, the authors observed an opposite trend for diffusivity and absorption capacity. Among the studied ILs, the authors selected [choline][NTf_2] as the most suitable solvent for the absorption of NH_3, because this IL shows the best compromise between absorption capacity and diffusivity.

Then, as mentioned in Chapter I, our research group [28,61] determined the mass diffusivity of ammonia in three ionic liquids: [emim][NTf_2], [EtOHmim][BF_4], [EtOHmim][NTf_2], at 303.15 K, and three different pressures, 3 bar, 4 bar, and 5 bar. The mass diffusivity of ammonia in [emim][NTf_2] was the highest among the ILs investigated and ranged from 4.7×10^{-9} m^2 s^{-1} at P = 3 bar to 5.7×10^{-9} m^2 s^{-1} at P = 5 bar. The mass diffusivity of ammonia in [EtOHmim][BF_4], the IL with the highest ammonia solubility among the ILs investigated, ranged from 5.2×10^{-10} m^2 s^{-1} at P = 3 bar to 1.2×10^{-9} m^2 s^{-1} at P = 5 bar.

After that, Turnaoglu and Shiflett [39] determined the mass diffusivity of NH_3 vapour in three imidazolium-based ILs using a gravimetric method at temperatures of 283.15, 298.15, 323.15, and 348.15 K and pressures up to 0.7 MPa. The authors observed that the values obtained for the mass diffusivities of NH_3 in the ILs studied were approximately 3 to 5 times lower than the masss diffusivity of NH_3 in the conventional absorbent, water. Finally, the authors used

the Stokes-Einstein equation to correlate the diffusivity of NH_3 in ILs with the solution viscosity. The molecular radius of NH_3 calculated with the Stokes-Einstein equation shows good agreement with a maximum error of less than 5%, suggesting the suitability of this equation to relate diffusivity and solution viscosity. However, since the viscosity of the solution was calculated with an empirical model, the results of using the Stokes-Einstein equation were inconclusive.

More recently, our research group [150] has reported diffusion coefficients of the ions in mixtures of ammonia/ionic liquid (1-(2-hydroxyethyl)-3-methylimidazolium tetrafluoroborate) using PFG-NMR. The reported diffusion values include measurements for the pure ionic liquid, and various concentrations of ammonia, covering a temperature range from 293.15 K to 333.15 K, and at two different pressures, 2.5 bar and 6.0 bar. The reported values, which are not mass diffusivity values, are useful to describe the interactions at the molecular level of the binary NH_3/IL mixtures. In this regard, the authors observed that regardless of the ammonia concentration in the mixture the changes in the diffusion coefficients were small. This was considered to be indicative that the average size of the ions did not vary significantly in the presence of ammonia. Therefore, the authors concluded that in the studied mixture, there is little interaction between ammonia and ionic liquid.

It is not possible to make a direct comparison of the mass diffusivities of ammonia in IL because the few experimental data available correspond to different experimental conditions. Also, like in the case of CO_2/IL working pair, the reported values correspond to average diffusivities for the absorption process where the absorbent concentration changes considerably. For example, the absorption curves used by Bedia et al. [36] to determine the mass diffusivity involved a wide range of concentrations ranging from zero (pure ionic liquid) at the beginning to molar fractions of ammonia that exceeded 50% at the end of a typical experimental run. In the case of measurements made by our research group [28,61], the absorption curves also involved a wide concentration range, from an initial zero concentration up to 45% mole fraction at the end of the absorption process. In the study by Turnaoglu and Shiflett [39], the concentration range in the absorption experiments was narrower than in the previous studies, less than

10% in mole fraction. Therefore, it is necessary to consider the ammonia concentration in the ammonia / IL solution when comparing the mass diffusivities of different ILs.

III.4.4 Mass diffusivity in other fluid mixtures relevant to absorption technology

Diffusivity values for other fluid mixtures relevant to absorption refrigeration systems have also been reported.

In particular, for NH_3 based systems, Kojima and Kashiwagi [57] used holographic interferometry to determine the mass diffusivity in several absorbent liquids. However, despite their great contribution, the data processing method used by these authors seems somewhat dated today because, for example, the concentration of NH_3 in the liquid mixture was determined by a simple (visual) fringe counting procedure. Furthermore, considering the low resolution of the obtained interferograms, the reported diffusion data has high associated uncertainty.

After that, Frank et al. [41] reported diffusion coefficients of binary mixtures, of CO_2 and NH_3 dissolved in water and methanol using the Taylor Dispersion technique. The measurements were performed at temperatures from 293 to 333 K, and the ammonia mole fraction ranged from 0 to 0.312. The temperature dependence of the measured diffusivities was correlated using Arrhenius-type equations. Also, the authors found that the modified Stokes-Einstein equation and the Wilke-Chang equation show typical error of up to 30% for estimating diffusion coefficients in dilute systems.

Richter et al. [151] reported the successful application of digital holographic interferometry to investigate the mass diffusivities in mixtures of methanol and ionic liquid 1-butyl-3-methylimidazolium hexafluorophosphate ([bmim][PF_6]). Measurements were performed at several ionic liquid concentration at 25 ºC. The authors observed very low values of diffusion coefficient, in the order of 2×10^{-11} $m^2\ s^{-1}$, at high ionic liquid concentrations. The required measuring time was found to be quite long, up to 4 days. Furthermore, the concentration dependence of the diffusion coefficient was fitted to a second-order exponential decay function.

Peng et al. [152] measured ternary diffusion coefficients of diethylene glycol (DEG) and lithium bromide (LiBr) in an aqueous glycol-salt solution containing DEG + LiBr + H_2O using TDT. In their work, the studied fluids are relevant for dehumidification systems based on liquid desiccants, and also, for absorption refrigeration systems. Diffusion measurements were done for temperatures of 303.15, 308.15, and 313.15 K at solute concentrations of 10, 15, and 20 wt%. Also, a modified Batchelor equation was satisfactorily used to represent the dependence of the diffusion coefficient on temperature and concentration with an average deviation of 5.1%.

More recently, He et al. [29] used the semi-infinite volume method to determine the diffusion coefficients of six hydrofluorocarbons in three ILs in the temperature range from 303.2 K to 343.2 K. Their work was performed explicitly considering the potential application of the fluids studied for absorption refrigeration systems. The measured diffusivities of hydrofluorocarbons in ILs were found to be an order of magnitude smaller than those of gases in traditional solvents due to the high viscosity of ILs. Furthermore, the authors observed that the effect of temperature on the absorption rate of hydrofluorocarbons in ILs was positive, meanwhile negative for the absorption capacity. The measured diffusion coefficients were satisfactorily correlated using the Wilke-Chang equation. The average absolute relative deviations between the experimental results and the predicted values for the gases in the ionic liquids studied were around 20% for all the systems studied. Other studies by He's research group related to the diffusion of gases in ionic liquids based on the semi-infinite volume method are available elsewhere [153,154].

In addition to those mentioned above, other methods have been used to some extent to measure diffusion coefficients in potential refrigerant/ILs working pairs. For example, mass diffusivities for CO_2 in several ionic liquids were determined from the permeability of immobilized IL membranes by a lag-time technique [35,155]. Later, CO_2 diffusivity in ionic liquid [emim][NTf2] at 303 K was determined from the temporal change of infrared spectra [156].

More recently, the classical diaphragm cell method has also been used to determine the mass diffusivities in binary mixtures of ethanol + ionic liquid ethyl-methyl-imidazolium-di-ethyl-phosphate ([emim][DEP]) in the range of ionic liquid

mass fraction from 0.72 to 0.845, and at temperatures ranging from 42ºC to 55ºC [55].

III.5 Conclusions

In this chapter, the main concepts, experimental measurement methods, and models for the estimation of the mass diffusivity in binary mixtures relevant for absorption refrigeration systems were presented.

Most of the mass diffusivity values reported for refrigerant vapours in ionic liquids were obtained using conventional methods, such as the gravimetric or the semi-infinite volume methods. These methods, unlike the optical interferometric methods, do not provide any description about the concentration profiles of the refrigerant in the absorbent.

Experimental mass diffusivity data for NH_3/ILs mixtures are the scarcest compared to the data available for other mixtures of natural refrigerants/ILs.

In general, increasing the length of the alkyl side chain of the cation was found to decrease the mass diffusivity of natural refrigerants in ILs. Moreover, the mass diffusivity of natural refrigerants in ILs decreases with increasing molecular weight of the IL. This trend is the opposite of that usually followed by the solubility of these refrigerants. Unlike the solubilities, mass diffusivities of natural refrigerants in ILs are strongly dependent on the IL cation as well as the anion.

In the literature related to absorption heat pump and refrigeration system, there is confusion between the different (mass-, self-, tracer-) diffusion coefficients. A higher tracer diffusion coefficient value for a refrigerant/IL mixture does not necessarily imply better characteristics for heat and mass transfer. Furthermore, a direct comparison of average effective diffusivities without considering the concentration of the absorbent/refrigerant solution can lead to misleading conclusions when screening ionic liquids as absorbents.

The Wilke-Chang correlation was found to better describe the mass diffusivity of refrigerants in absorbent liquids compared to other correlations. Improving the estimation capability of theoretical models and empirical correlations for the estimation of mass diffusivity is essential to reduce the research effort in the screening of ILs as absorbents.

Chapter IV
Application of the Optical Digital Interferometry method to measure the mass diffusivity in aqueous ionic liquid solutions[1]

In this Chapter, it is used the Optical Digital Interferometry (ODI) method to determine the mass diffusivity in an aqueous mixture of ionic liquid 1-(2-hydroxyethyl)-3-methylimidazolium tetrafluoroborate. The experimental procedure, the image processing steps, and the working equations are addressed. From the measurements, the dependencies on concentration and temperature of the mass diffusivity are discussed. Finally, we evaluated the suitability of four different estimation models to describe our measurements.

[1] Part of this chapter is adapted from: R. Rives, A. Mialdun, V. Yasnou, V. Shevtsova, A. Coronas, *Experimental determination and predictive modelling of the mutual diffusion coefficients of water and ionic liquid 1-(2-hydroxyethyl)-3-methylimidazolium tetrafluoroborate*, J. Mol. Liq. 296 (2019) 111931. doi:10.1016/j.molliq.2019.111931.

IV.1 Optical Digital Interferometry (ODI) method

In Chapter III, we have shown the suitability of optical interferometry to determine mass diffusivities in mixtures containing ionic liquids. In common literature related to the application of optical techniques, the mass diffusivity has been determined using a data processing method described by Bochner and Pipman [157]. This data processing method relies on the determination of the distance of two peaks in a concentration difference profile. The basic assumption of this method is that the diffusing process and the concentration difference profile are symmetrical.

However, it has been observed that the concentration difference profile is asymmetrical and that the degree of asymmetry changes over time [158]. Besides, this method lacks the means to detect the differences between the experiment and the ideal physical model. Moreover, this method requires the visualization of the full profile of the concentration (optical phase) in the diffusion cell to determine the position of the extrema (peaks) in the experimental curve. Therefore, the diffusion cell must be provided with large optical windows, which is technically feasible for the investigation of diffusion in liquid mixtures (at low pressures) without major complications. However, in the study of gas-liquid systems, such as those intended to study vapor absorption processes, the size of the optical windows is limited by the pressure to be applied within the measurement volume. Thus, the data processing method used previously by Richter et al. [151] and Chen et al [105] lacks applicability in our current experimental setup (see section II.2.1).

Consequently, alternative approaches should be used to overcome the inherent and practical limitations of the typical data processing method used in the literature [105,151]. Such alternative method could be based on fitting a theoretical mass diffusion model to the experimental concentration profiles [65,158]. This approach was used by Kojima and Kashiwagi [57], although with the experimental limitations mentioned above, especially those related to the quality of the interferograms and their processing. In this approach, the experimental values used in the fitting procedure can be only a portion of the full concentration profile. Because of this, the field of view covered by the technique, and thus, the size of the optical windows, can be reduced and cover only part of the diffusion path in the working cell. One of the data processing methods, in

which diffusion coefficients are determined using this approach, is the Optical Digital Interferometry (ODI) method [159,160].

The ODI method is based on sensing the refractive index changes of a fluid mixture to determine diffusion coefficients [160]. The unique feature of the ODI method is the ability to track the time-dependent evolution of temperature and concentration fields in the entire cell cross-section, and not just in distinctive points [71]. Therefore, this method has very attractive features for studying the absorption process of ammonia vapor in absorbent liquids. First, it allows us to use an approach similar to that of the literature [57], which is the only antecedent found aimed at studying the absorption process, and within this general objective, to determine the mass diffusivity of ammonia refrigerant in absorbent liquids. However, now the measurement tool is much more powerful, with higher quality optical elements and reliable computer-aided processing of digital fringe patterns. Second, the ODI method can be used combined with an interferometer scheme based on the Mach-Zehnder arrangement. In this regard, the relatively wide spacing between the test beam and the reference beam in the MZI provides better applicability to study the absorption process, allowing simultaneous observation of the fringe pattern and the object itself. Also, there are antecedents on the use of the MZI to investigate heat and mass transfer during the absorption process of NH_3 vapor in NH_3/H_2O solutions [58,59].

The ODI method, originally developed to study thermodiffusion phenomena, has also been successfully extended to determine mass diffusivity values in binary and ternary liquid systems [65,70,161]. Furthermore, the diffusion measurements obtained with this method have been used for the reconstruction of the binodal curve in the partially miscible mixture of methanol + cyclohexane [71]. The ODI method was first validated using the measured diffusion coefficient of a binary mixture of water + ethanol [159]. Afterwards, comprehensive validation campaigns using *Fontainebleau* benchmark values for three binary mixtures have been performed [65]. In these campaigns, the diffusion coefficients measured using the ODI method were compared with other diffusion values obtained using conventional and novel techniques. In all cases, an excellent agreement was observed for both diffusion and Soret coefficients, with typical deviations in the range of 1%-3%.

In general terms, the ODI method is based on the relationship between the refractive index changes, $\Delta n(x,z,t)$, with temperature and concentration of a transparent fluid mixture [65]:

$$\Delta n(x,z,t) = \left(\frac{\partial n}{\partial T}\right)_{C,\lambda} \Delta T(x,z,t) + \left(\frac{\partial n}{\partial C}\right)_{T,\lambda} \Delta C(x,z,t) \qquad \text{IV-1}$$

where λ is the wavelength of the laser source used, $\Delta T(x,z,t)$ and $\Delta C(x,z,t)$ are the temperature and concentration changes at time t and point (x, z), here x-axis is the horizontal and z-axis is the vertical direction. The derivative terms $\left(\frac{\partial n}{\partial T}\right)_{C,\lambda}$ and $\left(\frac{\partial n}{\partial C}\right)_{T,\lambda}$ are the optical contrast factors for the temperature and the concentration, which are evaluated by keeping the other property constant. At the same time, $\Delta n(x,z,t)$ may be obtained from the optical phase distribution, $\Delta\varphi(x,z,t)$, which is measured by interferometry:

$$\Delta n(x,z,t) = \frac{\lambda}{2\pi L}\Delta\varphi(x,z,t) \qquad \text{IV-2}$$

Here L is the optical path in the fluid mixture inside the diffusion cell.

The experimental output of the ODI method is an interference (or fringe) pattern, from which $\Delta\varphi(x,z,t)$ can be extracted. To do this, two main techniques are generally used; the phase-shifting method and the Fourier-transform method [162]. The phase-shifting (PSI) method consists of acquiring a minimum of three phase-shifted images and calculating the phase with an algorithm. The Fourier-transform (FFT) method consists of introducing a fringe carrier in order to be able to extract the fringe phase with Fourier analysis from only one image [129]. PSI is considered more sensitive, but FFT has the advantage of being more robust to external disturbances and requires only one snapshot to extract phase information [127,160]. Thus, in this thesis, the Fourier-transform method was adopted. Using this method imposes some requirements, such as a fringe pattern dense enough to provide a distinguishable peak in the Fourier domain without losing fringe contrast. More details on specific requirements of the Fourier transform method can be found elsewhere [163].

After applying the Fourier transform to the initial fringe pattern, the result is a spectrum of fringes in the spatial frequency domain. A typical spectrum consists of a central peak with information about the background intensity of the

interferogram and two sidebands with information about the optical phase. Then the next step is to filter out the central peak and one of the sidebands and shift the remaining sideband to the center of the spectrum. The distance of this shift corresponds to the spatial frequency of the initial (or reference) interference pattern. This operation eliminates the fringe carrier frequency from the spectrum and leaves only information about the change of fringe density with respect to the initial state, and value of the optical phase related to this change. In addition to determining the spatial carrier frequency, the reference interferogram has its phase distribution map, which must be evaluated in a separate step and then subtracted from the phase map of interest. In this way, the method applies the holography principle and tracks the only posterior optical phase variation in the set of images following the reference image [160].

In the next step, the inverse Fourier transform is applied to the filtered and shifted spectrum. As a result of this step, the optical phase distribution of the fringe pattern can be obtained. However, the optical phase calculated in this way is discontinuous and wrapped in the range (-π, π). Thus, an unwrapping procedure should be applied to construct the continuous natural phase, $\Delta\varphi(x,z,t)$. Next, the refractive index changes can be calculated using equation III-23. Then, under isothermal conditions, the concentration change maps can be easily obtained using equation III-22. Subsequently, the concentration change maps are horizontally averaged to obtain a one-dimensional concentration profile. Finally, by fitting the experimental concentration profile to a mass diffusion model, the mass diffusivity value can be obtained as a regressed parameter.

IV.2 Application of the ODI method to the experimental determination of the mass diffusivity in an aqueous ionic liquid solution

The previous section highlights the enormous potential of the ODI method for the determination of mass diffusivity during the absorption process of ammonia vapor in absorbent liquids. However, this method requires fairly careful experimental procedures to avoid undesirable disturbances in the measurements. Furthermore, the mathematical formalism behind the method is quite challenging, and the data processing steps can be cumbersome for researchers unfamiliar

with the subject. Therefore, it is advisable to first become familiar with the method before tackling a complex process such as the absorption process.

Following this reasoning, the ODI method can be used in a "simpler" problem of diffusion in a binary liquid mixture. In this case, unlike the absorption process, diffusion takes place without heat transfer or the presence of two phases (liquid and vapor). Consequently, the need to separate the contributions of concentration and temperature to changes in the refractive index is eliminated [65]. However, this training allows acquiring familiarity with the experimental requirements of the method and with mathematical tools such as the Fourier transform or the use of different boundary conditions in the formulation of the diffusion model. Then, the experience gained by applying the method to liquid mixtures can be extended to studies that involve more complex physical phenomena, such as those involved in the absorption process.

Based on the above, we have applied the ODI method to the determination of mass diffusivities in an aqueous ionic liquid mixture. In particular, the investigation has been carried out during a research stay at the Université Libre de Bruxelles in the research group "Non-linear phenomena in fluids", led by Dr. Valentina Shevtsova (currently at the Mondragon University, Spain). This research group has extensive experience in the use of optical methods for the determination of mass diffusion coefficients in liquid mixtures, references can be found anywhere [65,159,164]. Some of the results of this investigation have been already published in the Journal of Molecular Liquids (Volume 296, 15 December 2019, 111931) and other results are expected to be published soon in the Journal of Chemical Thermodynamics.

In the next sections, the use of the ODI method to measure mass diffusivities in a binary mixture H_2O + ionic liquid [EtOHmim][BF_4] is discussed. Here, the experimental procedure, the image processing steps, and the working equations are addressed. Measurements were performed over the entire range of ionic liquid mass fraction, and at four temperatures between 298.15 K and 313.15 K. Also, we evaluated the suitability of four different estimation models to describe our measurements, namely Vignes, UNIDIF, Cluster Diffusion, Modified Group Contribution. These estimation models, unlike the other correlations presented in

sections from III-3.1 to III.3-3, can be used to investigate the concentration dependence of the mass diffusivity.

IV.2.1 Materials

For the experimental measurement of the mass diffusivity, a closed diffusion cell with interferometric probing was used. Ionic liquid [EtOHmim][BF_4] (1-(2-hydroxyethyl)-3-methylimidazolium tetrafluoroborate, >98%, CAS Number: 374564-83-7, Molecular Weight: 213.97) supplied by Iolitec, and Water extra pure, deionized, supplied by Acros Organics were used without further purification. It is worth mentioning that the water was degassed to avoid the formation of bubbles, which can seriously affect the concentration distribution of the components inside the diffusion cell. Before starting the experiments, mixtures of H_2O + [EtOHmim][BF_4] were prepared gravimetrically with an accuracy of ±0.005 g. For each experimental run, two solutions with a small mass fraction difference of 1% were treated as one pair for the diffusion measurement at the mean composition. We have set the mean compositions of the mixtures in intervals of 0.1 over the entire range of ionic liquid mass fractions. Thus, a total of 22 samples were prepared, including pure components.

IV.2.2 Creation of diffusion field

Figure IV-1 depicts schematically the evolution of the diffusion field during a typical experimental run using the ODI method for the determination of mass diffusivity in the binary liquid mixtures of H_2O + [EtOHmim][BF_4].

In the first step, two solutions of the same liquid mixture, with a slight difference in concentration (e.g., 1% w/w), are injected into the diffusion cell. A narrow concentration range is required primarily for two reasons. First, to be able to approximate the diffusion coefficient as constant, and second, due to the limitations in the resolution of the optical system. A large concentration gradient causes the test beam to deflect in the interface area, generating a horizontal black stripe in the interferogram pattern. In addition, under isothermal conditions, the density gradient must be in the same direction as gravity to avoid mass transport due to convection. Thus, the lighter solution must be injected from the top, while the heavier solution from the bottom of the diffusion cell.

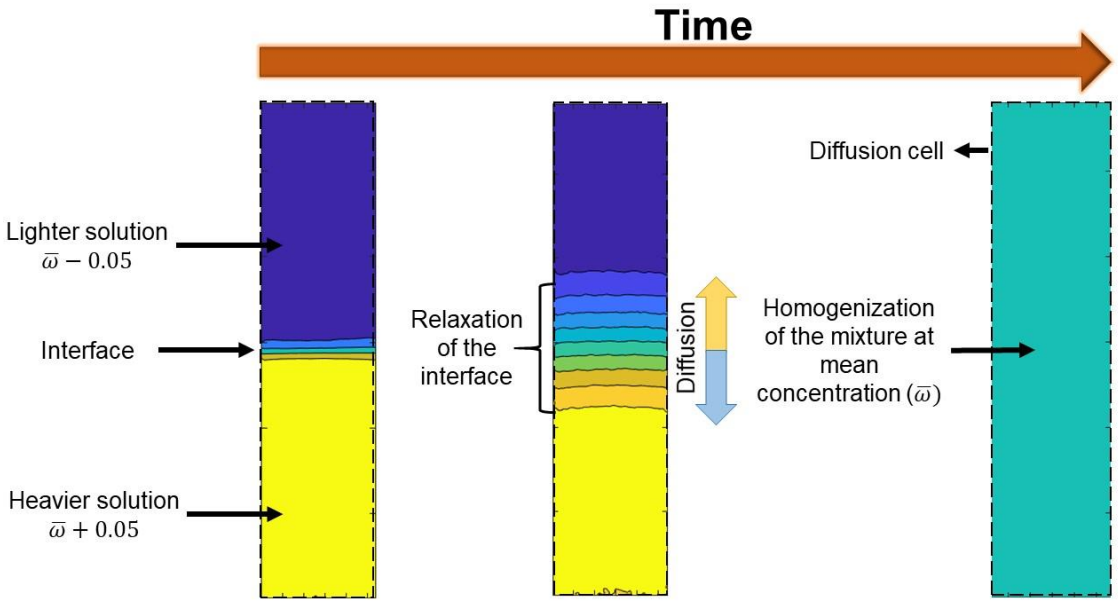

Figure IV-1. Schematic representation of the evolution of the diffusion field.

At the beginning of a typical experimental run, the diffusion field is characterized by a sharp interface and two well-defined zones with the injected solutions. As time passes, a relaxation of the interface occurs due to the diffusive transport of matter within the cell. At this moment, there are three zones within the diffusion field, two occupied by each of the injected solutions and a third where the mixing process is taking place. After that, diffusive transport causes the area occupied by the mixing process to occupy more and more space within the diffusion cell over time. Finally, after a long enough time, the liquid mixture inside the cell will reach spatial homogeneity at the mean concentration, and the diffusion process caused by the initial concentration gradient will cease.

IV.2.3 Setup and experimental procedure

The schematic design of the diffusion cell used for the experiments is shown in Figure IV-2. The optical path length inside the liquid bulk is L = 5.0 mm, the total height is H = 20.0 mm, and the width of the cell is W = 5.0 mm. The location of the diffusion cell in the experimental set-up can be appreciated in Figure IV-3. The experimental procedure was established as follows. At the beginning of each experimental run, the cell was filled with the heavier solution through the bottom inlet. We let the heavier solution flow into the cell for some time just to ensure that it removes any residual liquid from previous experiments. At the end of this phase, the injection of the lighter solution

was injected from the top inlet until it reaches mid-height. After that both liquids are injected into the cell simultaneously by a syringe pump through the orifices in the bottom (a denser liquid) and top (a lighter liquid) walls. The quality and thickness of the interface depend on the injection flow rate. While a high injection flow rate deforms the interface, a slow filling of the cell produces a wide interface. After several tests, a flow rate equal to 2 ml per hour was chosen for the experiments. It provides a fairly good interface sharpness, a typical example of which can be seen in the first snapshot in Figure IV-4.

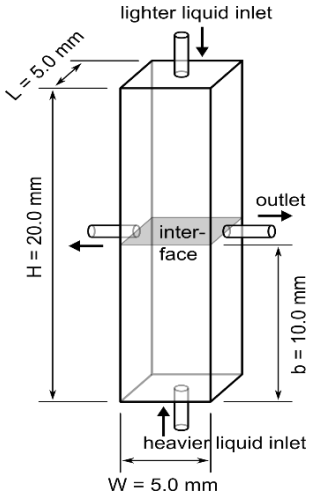

Figure IV-2. Schematic of the diffusion cell.

The injection systems consist of a dual syringe pump from kdScientific, model KDS 200/200P. The diffusion cell and all optical components were maintained inside a thermally insulated box equipped with an active thermal control system. The temperature inside the box was regulated between 298.15 K to 313.15 K with residual fluctuations below 0.1 K.

An optical arrangement based on a Mach–Zehnder interferometer was employed to sample refractive index changes inside the diffusion cell. A sketch of the experimental set-up is shown in Figure IV-3. The light source was an expanded and collimated laser beam with a wavelength of λ = 670 nm. The resulting interferogram was recorded by a CCD camera with a 1280 x 1024 pixels sensor. The resolution of the imaging system was around 15.7 μm per pixel. The image acquisition time step was varied from 10 s at the beginning of the experiment to 300s at the end. Then the set of images was analyzed to extract an optical phase, from which the refractive index change profiles were obtained. Finally, mutual

diffusion coefficients were evaluated by fitting an analytical solution to the obtained experimental data.

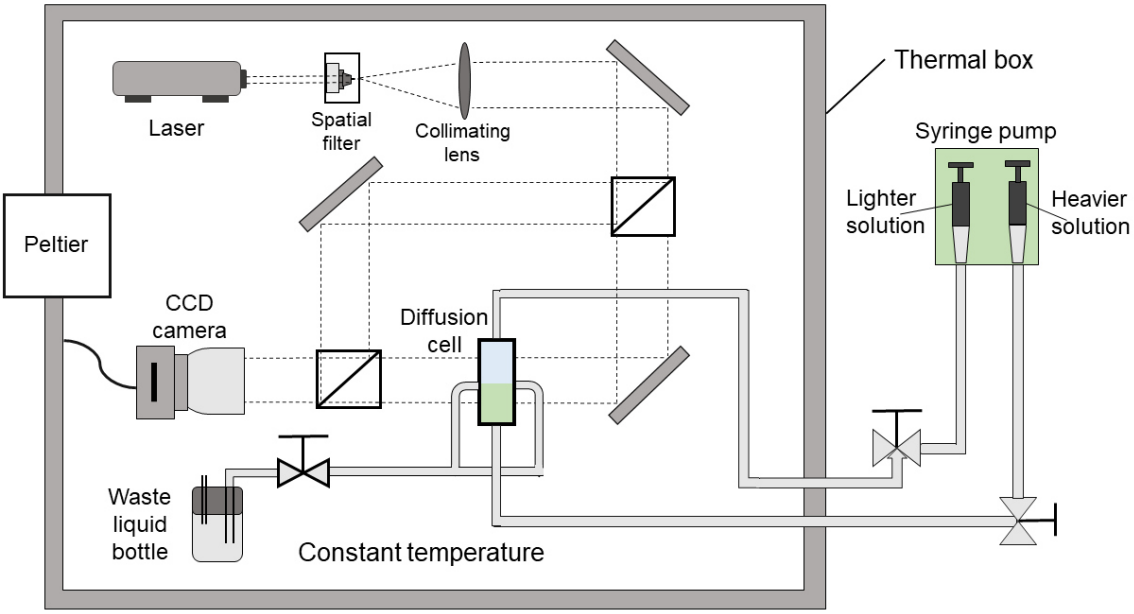

Figure IV-3. Schematic of the experimental set-up.

IV.2.4 Image processing and determination of refractive index profiles

As mentioned above, the experimental output of the ODI method is an interferogram. Figure IV-4 shows original experimental interferograms, corresponding to a variation of the refractive index at different time instances. In the first picture (at the beginning of the experiment), the interface is quite sharp. In the second image (after 15 minutes), the relaxation of the interface clearly indicates that a diffusion process is taking place. Here, 2D Fourier transform technique was employed for the extraction of an optical phase from the interferograms. The image processing consists of applying the 2D Fourier transform to the interferogram, selecting one of the lateral peaks in the Fourier domain, moving the selected peak towards the origin and applying the inverse Fourier transform. More detailed descriptions will be given in the next chapter and are also available in the literature [65]. After these steps, the results are a set of two-dimensional (2-D) phase map images wrapped into [0, 2π] range; an example is shown in the fourth snapshot in Figure IV-4.

The next step in the image processing, is the selection of two phase images, one to be processed and the other as the reference. For a proper estimation of an

optical phase, a reference image is needed. This reference image will be subtracted from each of the following images to separate the value of interest. The selection of a proper reference image is a very important step because the presence of tiny refractive index imperfections can lead to data corruption. Ideally, the reference image should provide a pure background with no traces of refractive index differences in the diffusion cell, which is difficult to achieve in practice. We have thus decided to use the very last image of the experiment as the reference [71].

To minimize the computational cost, first, we made the subtraction of the reference phase image from the other phase image and only then we proceeded to perform the unwrapping. The unwrapping procedure was based on the simple pixel-to-pixel comparing principle but with a specifically oriented unwrapping path. The unwrapping was oriented from the region with the best phase quality toward the regions with the worst phase quality [165]. Wrapped and unwrapped phase maps after subtraction of the reference image are shown in the last two pictures in Figure IV-4 at t = 15 min.

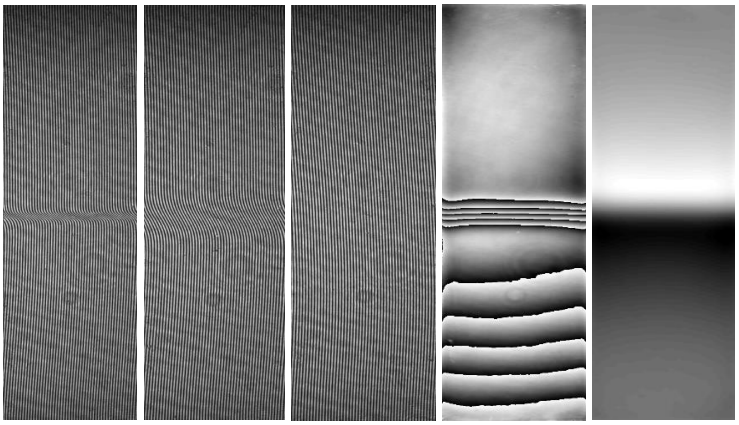

Figure IV-4. Transient diffusion fields: the three pictures on the left are fringe images at t = 0, 15 min and 15 hours, respectively; the following two pictures show the wrapped and unwrapped phase at t = 15 min after the beginning of the experiment.

Then, the 2-D unwrapped phase map ($\Delta\varphi(x,z)$) was converted into a map of refractive index ($\Delta n_{exp}(x,z)$) by applying the relation:

$$\Delta n_{exp}(x,z) = \frac{\lambda}{2\pi L}\Delta\varphi(x,z) \qquad \text{IV-3}$$

where *x*, *z* are the horizontal and vertical directions, respectively; *L* = 5.0 mm is the optical path length inside the liquid bulk and λ is the wavelength.

The ODI technique gives a unique possibility of increasing measurement accuracy by providing information about composition distribution along the whole diffusion path. It provides a two-dimensional refractive index field, although the distribution itself is almost one-dimensional. To apply 1D mathematical description of measurements, the 2-D map of the refractive index is averaged in the horizontal direction. The averaging also increases the reliability of the extracted profiles because it suppresses local noise, which is otherwise observable, without applying additional filters.

IV.2.5 Working equations

Mutual diffusion coefficients were determined by fitting an analytical solution to the experimental refractive index profiles. For this purpose, two different routes were followed. In each case, the mathematical description of the experiment is different, but both led to accurate fitting results. Therefore, the resulting mutual diffusion coefficient values using these routes did not deviate significantly from each other. In both routes, the calculated refractive index profile $\Delta n_{cal}(z,t)$ is expressed as:

$$\Delta n_{cal}(z,t) = \Delta n_0 * f(z,t,D_{12}) \qquad \text{IV-4}$$

where Δn_0 is the initial refractive index difference between the top and bottom solutions; and $f(z,t,D_{12})$ is the function presenting the solution of the diffusion problem with initial and boundary conditions of the diffusion cell. This function depends on spatiotemporal variables and the unknown diffusion coefficient. The form of this function for the considered geometry and initial conditions here is shown below.

IV.2.5.1 Long-time model

When the diffusion time is long, the diffusing fronts reach the ends of the cell, and the problem should be considered as occurring in a finite medium. In this case, the function $f(z,t,D_{12})$ can be expressed as:

$$f(z,t,D_{12}) = \frac{2}{\pi}\sum_{n=1}^{\infty}\frac{1}{n}\sin\left(\frac{n\pi b}{H}\right)\cos\left(\frac{n\pi z}{H}\right)\exp\left(-\frac{n^2\pi^2}{H^2}D_{12}t\right) \qquad \text{IV-5}$$

where b is the distance between the initial interface and the bottom of the diffusion cell, H is the height of the cell, D_{12} is the mutual diffusion coefficient and t is the time.

Then, the mutual diffusion coefficient is obtained by minimization of the deviation between experimental and calculated refractive index profiles as:

$$\Phi = \sum_{i,j}[\Delta n_{exp}(z_i, t_j + t_0) + \Delta n_{cal}(z_i, t_{\text{end}} + t_0) - \Delta n_{cal}(z_i, t_j + t_0)]^2 \quad \text{IV-6}$$

Mutual diffusion coefficient and initial refractive index difference are determined as the result of minimization. Here, t_{end} is the timestamp of the last image, which was taken as a reference. In this equation, t_0 is an empirical parameter introduced to consider that the initial distribution of the refractive index recorded in the experiment does not have a perfect stepwise shape at the interface, as it is assumed by the analytical solution. In other words, t_0 is the first time instance at which the theoretical profile coincides with the experimental one. Therefore, three unknown parameters were concurrently fitted:D_{12}, Δn_0 and t_0.

IV.2.5.2 Short-time model

The other route followed to obtain the mutual diffusion coefficients considers that the diffusion fronts does not reach the top and bottom of the diffusion cell. In this case, the diffusion process can be considered as occurring in an infinite medium. In this case, function $f(z,t,D)$ in equation IV-5 can be expressed as:

$$f = \frac{1}{2}\left[erfc\left(\frac{z-b}{2\sqrt{Dt}}\right) - 1\right] \quad \text{IV-7}$$

The fitting procedure for extracting the mutual diffusion coefficients and the other fitting parameters is similar to the long-time model.

IV.2.6 Experimental diffusion results

In this chapter, the mass diffusivity of a binary mixture H_2O + [EtOHmim][BF_4] at temperature 298.15-313.15 K was measured using optical digital interferometry. As detailed in section IV.2.5, two different routes were used to determine the mass diffusivity from experimentally sampled data. As an example, fitting results are discussed for the experimental measurement at T = 308.15 K and ω = 0.500 kg kg^{-1}.

Figure IV-5(a) shows refractive index profiles at two instances, one of which (the black curve) corresponds to the profile at an early stage of diffusion, and the other one corresponds to the upper limit of the short-time model. The diffusion front reached the top and bottom of the diffusion cell at the observation time t = 3 hours,

which means that the experimental data at later times can only be used for the long-time model. Note that the diffusion experiments lasted for about 15 hours.

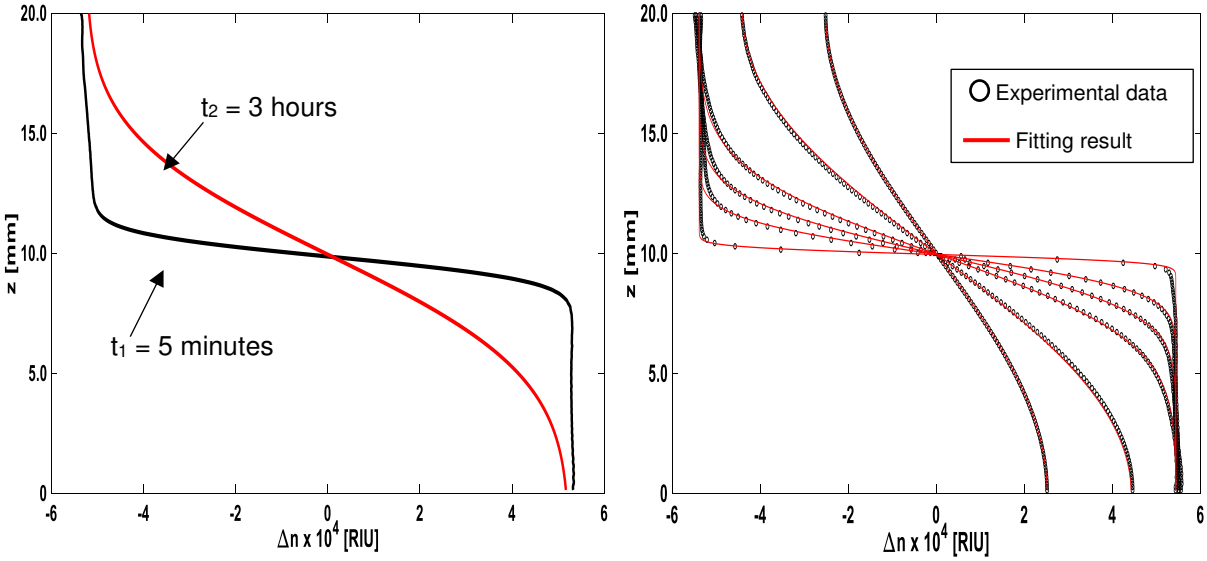

a) b)

Figure IV-5. Variation of the refractive index (Δn(z, t)) along the cell in different time instances for the mixture H_2O + [EtOHmim][BF_4]. a) Experimental data on short-time scale; b) Experimental data and fitting by long-time model.

Figure IV-5(b) illustrates the fitting result of the long-time model. The successive curves show the time evolution of the refractive index change along the cell height. The fitting results obtained by the short-time and long-time models are very similar, i.e. D = [7.53 and 7.57] x 10^{-10} m^2 s^{-1}, respectively.

Table IV-1 presents the experimental results of the mass diffusivity and its uncertainties at different IL mass fractions and temperatures.

Table IV-1. Measured mass diffusivities of H_2O + [EtOHmim][BF_4] mixtures at different IL mass fraction, ω, and temperature, T.

ω	D_{12} x 10^{10}/ m^2 s^{-1}			
	T = 298.15 K	T = 303.15 K	T = 308.15 K	T = 313.15 K
0.0060	10.19 ±0.05	11.03 ±0.05	11.87 ±0.05	12.72 ±0.05
0.1000	8.93 ±0.05			
0.2000	7.84 ±0.04	8.74 ±0.05	9.74 ±0.04	10.47 ±0.04
0.3000	6.92 ±0.04			
0.4000	5.87 ±0.05			
0.5000	5.80 ±0.03	6.37 ±0.03	7.57±0.04	8.80 ±0.03
0.6000	5.74 ±0.03			
0.7000	5.70 ±0.03			
0.8000	5.34 ±0.05	6.12 ±0.05	7.11 ±0.05	7.83 ±0.06
0.9000	4.05 ±0.10			
0.9975	2.04 ±0.10	2.21±0.11	2.42 ±0.11	3.01 ±0.13

IV.2.6.1 Concentration and temperature dependences of the mass diffusivity

One of the targets of our research was aimed at the examination of the concentration dependence of the mass diffusivity. Figure IV-6 shows the measured mass diffusivity of H_2O + [EtOHmim][BF_4] as a function of IL mass fraction. We found that with the increase of IL mass fraction the mass diffusivity value diminishes. It can be related to the opposite effect of the viscosity on the diffusion process in binary solutions. The viscosity of this IL is considerably higher than that of H_2O, therefore, by increasing the IL mass fraction the solution viscosity increases rapidly.

Over the concentration range the mass diffusivity displays different types of behavior. For IL content in the mixture below 0.40, the mass diffusivity decreases almost linearly with mass fraction. For the composition range $0.40 < \omega < 0.80$, mass diffusivity decreases very slowly. This behaviour is relevant for absorption systems, which generally work in this composition range (0.50-0.80 of absorbent

mass fraction). At a higher content of [EtOHmim][BF_4] (ω > 0.80), the mass diffusivity decreases sharply because the viscosity of the solution increases abruptly. It is worth emphasizing that the viscosity of the pure ionic liquid is several tens of times greater than that of water in the studied temperature range.

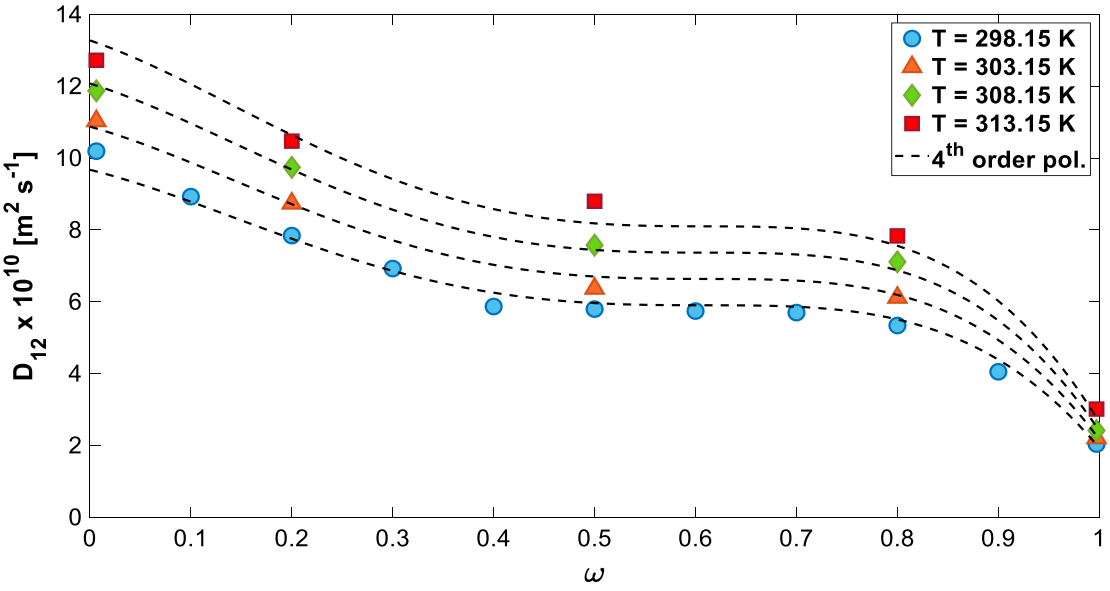

Figure IV-6. Measured mass diffusivity at different temperatures as a function of composition; ω is the mass fraction of ionic liquid.

Composition dependence of the measured mass diffusivity can be very well correlated with fourth-order polynomials, which are represented by dashed lines in Figure IV-6. The similarity in the behavior of the curves at the four experimental temperatures is clear. According to our results, the concentration and temperature dependence of the mutual diffusion coefficient can be described as:

$$D_{12}(\omega, \mathrm{T}) \times 10^{10} = D_0[1 + \alpha(\mathrm{T} - T_0)] \qquad \text{IV-8}$$

where:

$$D_0(\omega) \times 10^{10} = a\omega_1^4 + b\omega_1^3 + c\omega_1^2 + d\omega_1 + D_1^{\infty} \qquad \text{IV-9}$$

Here, *a*, *b*, *c*, *d* are the polynomial coefficients; D_1^{∞} represents the diffusion coefficient of [EtOHmim][BF_4] at infinite dilution in H_2O at reference temperature T_0 (in this study, T_0 = 298.15 K); and α is an empirical parameter, which gives a sense of the percentage of the diffusion coefficient variation per temperature variation of 1 K. Coefficients of equations IV-8 and IV-9 were obtained by least

square regression from measured diffusion coefficients. These coefficients and quality of fit (R^2) are listed in Table IV-2.

Table IV-2. Coefficients of equations IV-8 and IV-9.

Coefficient	a	b	c	d	D_1^{∞}	α	R^2
Value	-50.42	75.85	-26.18	-6.993	9.673	0.02482	0.9918

The absolute relative deviation (ARD) was used as the main criterion to evaluate the prediction ability of equation IV-8.

$$ARD/\% = \frac{100}{N}\sum_{i=1}^{N}\left|\frac{D_{exp}-D_{cal}}{D_{exp}}\right| \qquad \text{IV-10}$$

where *N* is the number of experimental diffusion points.

At the four studied temperatures, the ARD was found to be always less than 4.2%.

We have also investigated the effect of the temperature on the mass diffusivity of H_2O + [EtOHmim][BF_4] at selected compositions ω = (0.006; 0.20; 0.50; 0.80; 0.9975). As expected, with the increase of the temperature the mass diffusivity grows up due to intensified molecular thermal motion. Figure IV-7 shows the mass diffusivity of the studied mixture as a function of temperature at the selected compositions.

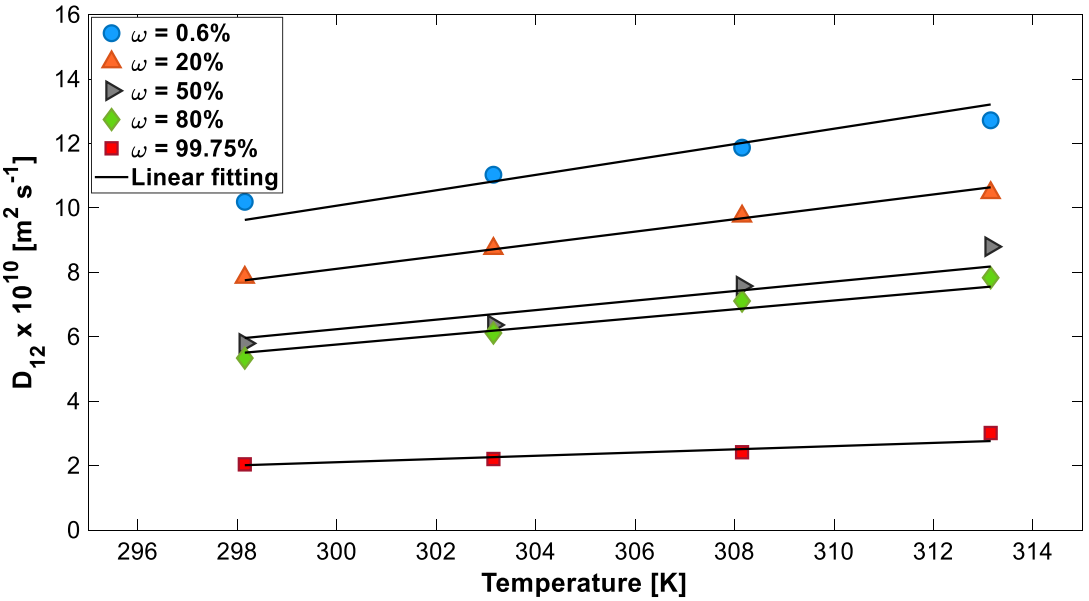

Figure IV-7. Measured mass diffusivity at different IL mass fractions (ω).

In Figure IV-7, it is possible to appreciate the linear relationship between the mass diffusivity and temperature in the studied experimental conditions. Wong et al. [166] also reported the linear dependency for [emim, (1-ethyl-3-methylimidazolium)]-based ionic liquids in water at infinite dilution for temperatures ranging from 303.2 to 323.2 K using Taylor dispersion method. Here, the largest but still reasonable deviation was observed in the case ω = 0.9975 (ARD = 4.9%). Thus, a linear fitting provides correct and important trends for the temperature dependence of the mass diffusivity.

IV.2.7 Results of the models and correlations for the estimation of the mass diffusivity

As mentioned, we have measured the mass diffusivity for the mixture H_2O + [EtOHmim][BF_4] at different IL mass fractions and temperatures. In total, we have 26 experimental points in the full range of concentration. In particular, mass diffusivities at T = 298.15 K were measured at intervals of 0.10 IL mass fraction. As soon as we recognized that the concentration dependence of the mass diffusivity for this mixture can be reliably fitted by fourth-order polynomials, the need for a larger number of experimental points vanished. Thus, we used these polynomials to obtain the mass diffusivity at intervals of 0.10 of IL mass fraction for the other 3 experimental temperatures, T = (303.15; 308.15; and 313.15) K. From this point on, the calculated mass diffusivities were treated as experimental points. Therefore, instead of 26 experimental diffusion points, we extended them to 44 experimental points.

Prior to comparing the performance of the different models and correlations considered, we need to determine the binary interaction parameters. First, we determined these binary parameters by means of VLE data regression using g^E models. In this case, the parameters obtained from VLE data (see in Annex A, Tables A1 and A2 for NRTL and Wilson models, respectively) are used to calculate the thermodynamic factor, Γ. Next, we used the binary parameters as adjustable parameters with experimental diffusion data. The obtained best-fit parameters for this correlation are listed in the Annex B. A comparison between the results using both strategies is made, and some conclusions are drawn.

In this chapter, we examined four estimation models and binary parameters for each of them, except for UNIDIF model, were estimated using two different methodologies. The results of the analysis are summarized in Table IV-3. The numbers in brackets represent the number of adjustable parameters that are used in each model. It follows from the data in this table that the use of binary interaction parameters from diffusion data considerably improves the prediction ability of all the models, even in the simplest case of Vignes correlation. In line with literature data, our study confirms that among the analyzed models, the MGC model using the NRTL equations, provides the best predictions.

Table IV-3. Comparison of the error (ARD%) of the models used for the estimation of mass diffusivity.

Model	From VLE data		From diffusion experiments	
	NRTL	Wilson	NRTL	Wilson
Vignes	76.8 (0)	70.4 (0)	17.2 (5)	26.5 (4)
Cluster	18.3 (5)	18.7 (5)	4.1 (10)	3.4 (9)
MGC	7.9 (7)	8.8 (7)	2.1 (12)	3.4 (11)
UNIDIF			13.9 (2)	

In order to highlight the performance of the MGC model, we present in Figure IV-8 our experimental data and those calculated by this model using NRTL equations. Not only can this model provide estimates of the mass diffusivity for the H_2O + [EtOHmim][BF_4] mixture with great precision, but it is also capable of reproducing the behavior of the mass diffusivity as a function of concentration.

Finally, we have used the regressed binary parameters from diffusion data to calculate the excess Gibbs energy and the thermodynamic factor. Again, the behavior of the excess Gibbs energy and the thermodynamic factor are opposed as in the case when using binary parameters from VLE data. We have found that the predictive model with the best estimates of the mass diffusivity, i.e. MGC with NRTL equations, corresponds to the minimum excess Gibbs energy, and thus the maximum thermodynamic factor. Perhaps, it is a general trend, but, on this step, we cannot prove it as an examination of different liquid mixtures is required.

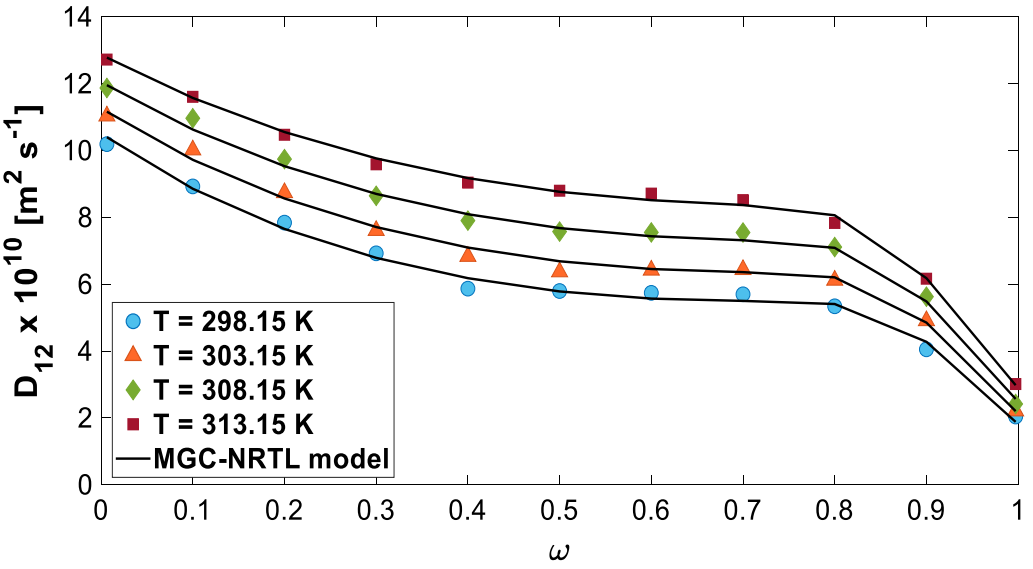

Figure IV-8. Mass diffusivity for mixture H_2O + [EtOHmim][BF_4]. Symbols: experimental data. Lines: calculations by the MGC model and NRTL equations with binary parameters from diffusion data.

IV.3 Conclusions

This chapter deals with the application of an advanced optical technique, in particular optical digital interferometry, to determine the mass diffusivity of a binary mixture of H_2O + [EtOHmim][BF_4]. Diffusion measurements were performed in the entire range of ionic liquid mass fraction and at temperatures ranging from 298.15 K to 313.15 K.

As the general trend, the mass diffusivity of H_2O + [EtOHmim][BF_4] decreases with increasing the ionic liquid mass fraction. It was found that the rate of the decrease is essential only in regions that are IL-poor or IL-rich. In the mid-range, $0.4<\omega<0.8$, the mass diffusivity is nearly constant. It was also shown that the measured diffusion coefficients could be perfectly described using fourth-order polynomials as a function of the IL mass fraction.

We have also studied the dependence of the mass diffusivity of H_2O + [EtOHmim][BF_4] on temperature. The results showed an almost linear increase in the diffusion coefficient with temperature. Linearity is slightly deviated with increasing the mass fraction of the ionic liquid.

Four estimation models were employed to describe the mutual diffusion coefficients of this mixture: Vignes, UNIDIF, Modified Group Contribution, and

Cluster diffusion. The binary interaction parameters of each of these models, except for UNIDIF model, were calculated using two different methodologies. In the first, binary parameters were determined by VLE data regression. In the second, binary parameters were treated as adjustable parameters with experimental diffusion data.

Among the four examined predictive models, the MGC model provides the best estimates of the mass diffusivity: an overall ARD from experimental data of 7.9% using binary interaction parameters regressed from VLE data and 2.1% using binary parameters regressed from diffusion data.

It is expected that the other estimation models presented in this chapter and, which themselves require experimental diffusion data, can also be employed to predict the diffusivities at temperatures which are experimentally more challenging.

The experience acquired during the investigation of mass diffusivity in this binary liquid mixture has served as the basis for the modification and adaptation of the ODI method for its application to the study of the absorption process.

UNIVERSITAT ROVIRA I VIRGILI
THEORETICAL AND EXPERIMENTAL STUDY OF THE ABSORPTION PROCESS OF AMMONIA IN IONIC LIQUIDS FOR ABSORPTION REFRIGERATION SYSTEMS
Ronny Rives Sanz

Chapter V
Study of the absorption process of ammonia in ionic liquids using optical digital interferometry

Modern science strives to construct its picture of the world not from speculations but so far as possible from facts. It verifies its constructs by recourse to observation.

Ernst Mach [167]

The insight into a physical process is always improved if a pattern produced by or related to this process can be observed by visual inspection [167]. Thus, in this Chapter, the absorption process of ammonia in ionic liquids is investigated using Optical Digital Interferometry (ODI). To this end, the information obtained by the Pressure Drop Method of the experiments described in Chapter II is complemented with new information obtained from the visualization of the absorption process with a Mach-Zehnder interferometer. Thus, in addition to temperature and pressure, records of the refractive index change over the field of view are also analyzed. From the experimental profiles of the refractive index change, the time evolution of the ammonia concentration profiles in the absorbent are obtained. Then, the ammonia mass diffusion in the absorbent during the absorption process is described using two mass diffusion models. After that, the experimental results of the time evolution of the ammonia concentration profiles in the absorbent are presented and discussed. In particular, the validation of the ODI method for the absorption of ammonia in water is performed, and then, the results for the ionic liquids selected using both mass diffusion models are addressed. Also, the capability of selected models to estimate the mass diffusivity of ammonia in ionic liquids is addressed. Finally, a comparison of solubility and mass diffusivity of ammonia in the ILs selected is performed.

V.1 Description of the Optical Digital Interferometry method to determine the time evolution of the ammonia concentration profiles in the absorbent

As mentioned in Chapter II, when ammonia vapor and an absorbent liquid, out of thermodynamic equilibrium, come into contact, the ammonia vapor begins to be absorbed in the liquid due to the chemical affinity between the compounds. As a result, temperature, pressure, and the spatial distribution of ammonia concentration in the absorbent changes over time until equilibrium is reached. In turn, changes in concentration cause changes in the refractive index which can be visualized with an appropriate optical system, such as the Mach-Zehnder interferometer used in this thesis (Figure V-1), obtaining valuable information on the absorption process.

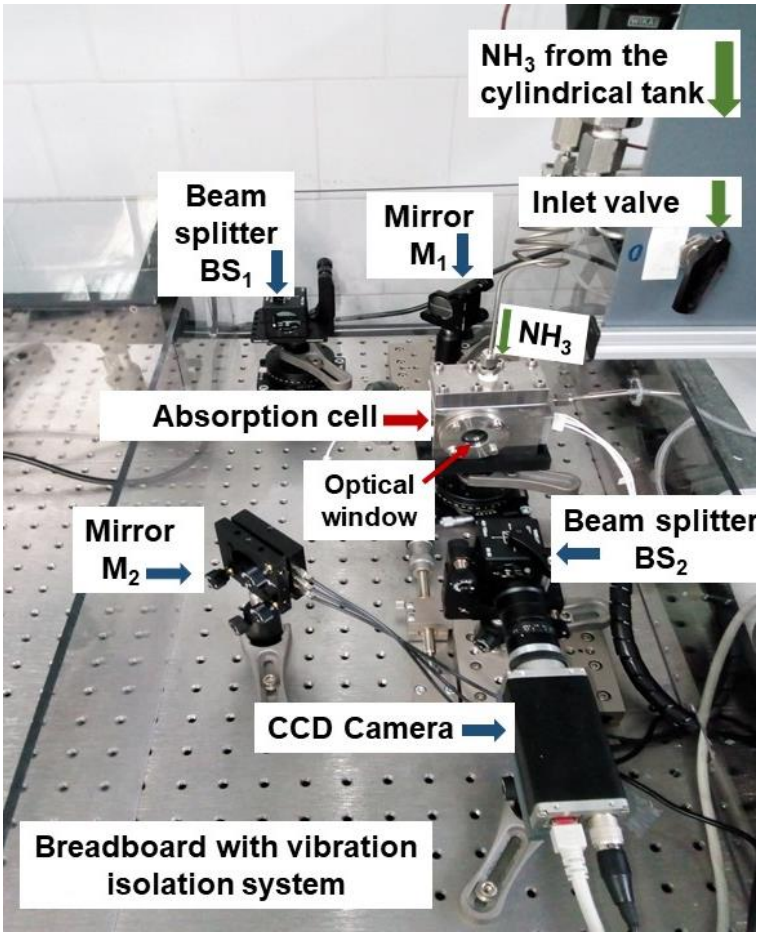

Figure V-1. A picture of the implemented setup with the optical measuring system (Mach-Zehnder interferometer).

As described in Chapters III and IV, the experimental output of the ODI method is an interferogram, such as those shown in Figure V-2. In this figure, two

experimental interferograms at different instances during the absorption process are shown. For visualization, the absorption cell is provided with optical windows (Figure V-1) allowing the test beam of the MZI to pass through the liquid bulk where the absorption process is taking place. The horizontal black strip observed corresponds to the area of the vapor-liquid interface. The meniscus shape of the interface deflects the test beam light in this area, and thus, this area appears in black in the interferograms [67].

Before opening the inlet valve of the absorption cell (see Figure V-1), the interference fringes are vertical in the liquid phase, as shown Figure V-2 (a). In our optical system, one of the mirrors (M_2 in Figure V-1) was tilted to produce a linear optical phase difference in the horizontal direction. Thus, vertical interference fringes are observed even if the fluids in the absorption cell show optical uniformity.

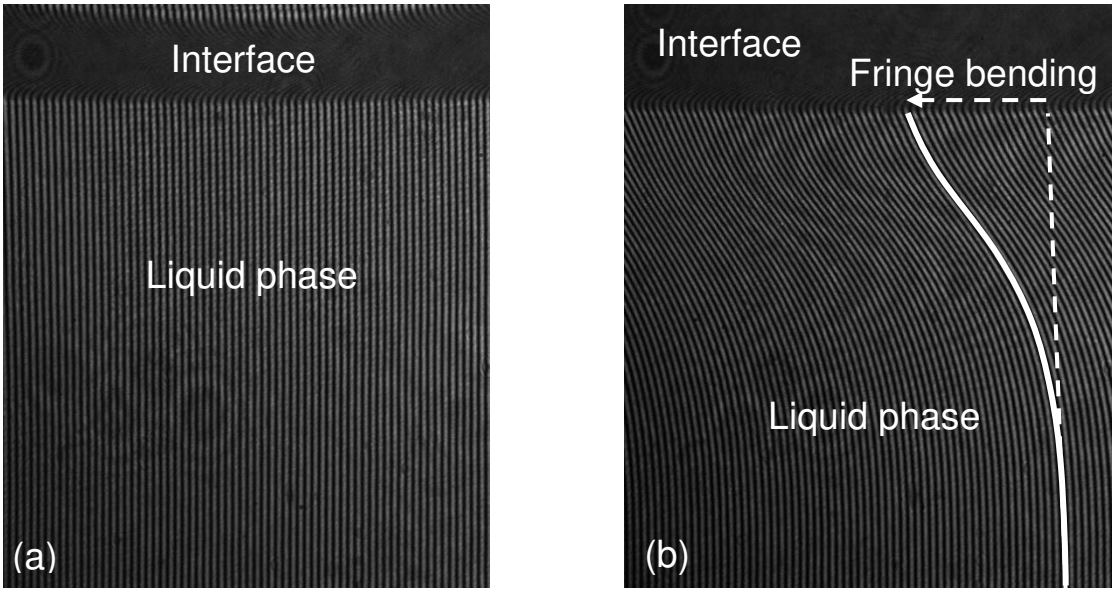

Figure V-2. Experimental output of the ODI method for the determination of the time evolution of the ammonia concentration profiles in ionic liquids: (a) In a time instance prior to start the absorption process; (b) During the absorption process.

Then, as soon as the ammonia absorption process starts, an additional optical phase difference is established between both arms of the interferometer. The additional optical phase difference is due to the local distribution of the refractive index of the liquid phase. If the change in the refractive index of the liquid phase is homogeneous, the fringes deform uniformly. On the contrary, if the change is not homogeneous, the fringes deform unevenly.

An interferogram recorded 20 minutes after starting the absorption process is presented in Figure V-2 (b), observing how the fringes are bent in the region of the image corresponding to the liquid phase just below the interface. This means that the variation of the refractive index is greater in that region, than in a deeper region of the cell. Moreover, a thickening of the interface area is also observed, as between Figure V-2 (a) and (b). This thickening is mainly observed during the early stages of the absorption process and lasts a few minutes. After that time, it was observed that the meniscus thickness remained stable until the end of the absorption experiments (15 hours).

At the scale of the interferogram, the optical phase difference between the reference beam and the test beam of the MZI lead to a time and space evolution of the fringe positions. By following this evolution, the MZI is an accurate instrument to detect local variations of the refractive index during the mass absorption in the liquid [67]. In this way, the implemented experimental setup enables to visualize the formation and evolution of the concentration diffusion layer inside the liquid phase. Moreover, it is possible to quantify the refractive index variation, and consequently, the ammonia concentration change in the liquid phase by extracting the optical phase difference from the obtained interferograms.

V.1.1 Determination of the experimental profiles of the refractive index change

Here, the optical phase extraction was performed using the Fourier transform technique [168]. For this reason, the interferometer was aligned to obtain a narrow fringe pattern [65]. To illustrate the use of this technique, the main image processing steps are schematically shown in Figure V-3.

First, the two-dimensional (2D) Fourier transform is applied to each experimental interferogram (Figure V-3 (a)). The result is a spectrum with three peaks in the Fourier domain (Figure V-3 (b)). The next step, consists in selecting one of the lateral peaks in the Fourier domain using a Gaussian filter, and then, moving the selected peak towards the origin (Figure V-3 (c)).

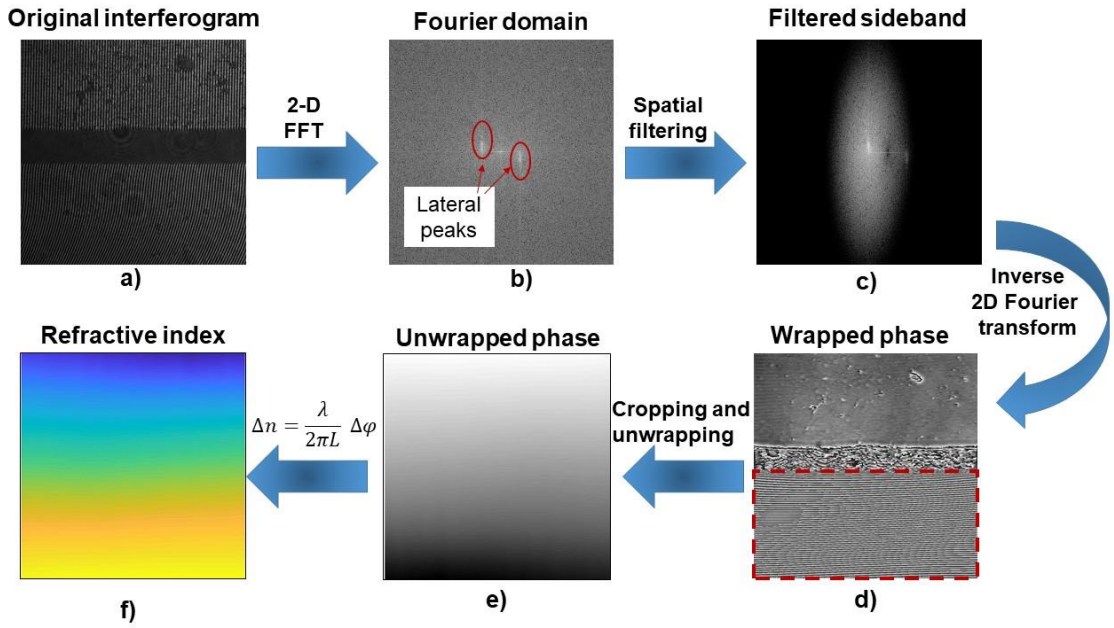

Figure V-3. Image processing steps: (a) a fringe image (experimental output); (b) image after applied 2D fast Fourier transform (FFT); (c) filtered sideband; (d) wrapped phase map; (e) unwrapped phase map of liquid phase in the field of view of the absorption cell; (f) refractive index variation field in the absorbent liquid/ammonia mixture.

In the next step, the inverse Fourier transform is applied to the filtered sideband, and the result is an optical phase map wrapped in the range [0, 2π] (Figure V-3 (d)). After that, the wrapped phase map is cropped, and an unwrapping procedure is applied. Thus, an unwrapped optical phase map as shown in Figure V-3 (e) is obtained. Finally, the unwrapped optical phase map is converted into a refractive index map (Figure V-3 (f)) by applying the relationship between optical phase and refractive index.

A code in MATLAB® [68], using a *fast Fourier transform* (FFT) algorithm has been developed to implement the above steps. Further details on the mathematical description of the optical phase extraction and the unwrapping procedure are described in Annex C.

The ODI method gives a unique possibility of increasing measurement accuracy by providing information about composition distribution along the diffusion path. It provides a two-dimensional refractive index field, although the distribution itself is almost one-dimensional (1-D). To apply 1-D mathematical description of measurements, the 2-D map of the refractive index change (Figure V-3 (f)) is

averaged in the horizontal direction. The averaging also increases the reliability of the extracted profiles because it suppresses local noise, which is otherwise observable, without applying additional filters. In addition to changes in concentration, other factors can alter the refractive index of the mixtures. Annex D provides a brief analysis of the influence of these factors.

V.1.2 Description of the optical system

As mentioned, we have implemented an experimental setup with an optical system based on the Mach-Zehnder interferometer (see Figure V-1) to investigate the absorption process of ammonia in the ionic liquids selected. The initial adjustment of a Mach-Zehnder interferometer (MZI) is considered in the literature as one of the greatest difficulties when using this technique due to its sensitivity to external disturbances. Thus, the initial adjustment of an MZI usually involves many steps and, as a good practice, the alignment of the optical elements should be checked daily before beginning work with the technique.

In our optical system, the light source used was a filtered, expanded, and collimated He-Ne laser (Thorlabs, HRS015B), with a wavelength λ = 632.8 nm. The collimated beam was divided by a beam splitter (BS_1), where half of the amplitude was refracted, and the other half transmitted. Then, the resulting beams traveled through different optical paths in the experimental setup. The two beams are recombined at a second beam splitter (BS_2) and imaged on a CCD camera (Basler, piA1000-60gm) by an objective lens (Fujinon, HF75HA-1B).

The resulting interferogram was recorded by a CCD camera with a 1000 x 1000 pixels sensor. The resolution of the imaging system was around 11.5 µm per pixel. The image acquisition time step was varied from 30 s at the beginning of the absorption process to 300s at the end.

All optical elements are mounted on mechanical platforms that allow the accurate adjustment of their position. Moreover, one mirror (M_2 in Figure V-1) is connected to a piezoelectric controller for its movement in the order of micrometers that facilitates the obtention of interference fringes with good visibility. In addition, due to the sensitivity of Mach-Zehnder interferometer, it is mounted with the absorption cell on a special optical table (Nexus Breadboard, 750 mm x 900 mm x 60 mm) with vibration isolation system.

V.2 Modelling the ammonia mass diffusion during the absorption process

Modelling the ammonia mass diffusion in ionic liquids during the absorption process is a quite demanding task due to the presence of complex physical phenomena. Such phenomena include the possible evolution of the heat of absorption, liquid convection due to the local temperature difference, as well as the free convection due to the density difference, and the possible change in thermophysical properties of the liquid [169]. Nevertheless, the effect of such complex phenomena can be minimized with a well-designed experimental setup and suitable experimental conditions. In the literature [38,60,132,169–171], different mathematical models based on a simplified mass diffusion process have been used to describe the time-dependent behavior of the absorption process. These models and their solutions are dissimilar in terms of the interface thermodynamic conditions, simplifying assumptions and parameter estimation algorithms [60]. In this thesis, the following assumptions are considered:

1. The ammonia refrigerant dissolves through a one-dimensional diffusion process, and no convective movements affects the liquid phase in the absorption cell [38,60,132,169–171].
2. For the diffusion analysis, the temperature in the absorption cell is considered constant [84]. In the experimental setup implemented, the dimensions of the absorption cell and the capacity of the thermal control circuit facilitate a rapid heat transfer between the ammonia/absorbent solution and the external fluid of the thermal bath, which allows to keep the temperature constant at practical effects during the absorption process.
3. The ammonia/absorbent solution is a highly dilute solution, and thus, the relevant thermophysical properties of the solution do not significantly change during the absorption process [169].
4. The expansion in the volume of the liquid phase caused by the absorption of the ammonia vapor is negligible. Therefore, the height of the liquid phase in the absorption cell is assumed to be constant during the absorption process [84].

5. Absorbents are considered as non-volatile. This assumption is acceptable in the case of water because, the mass fraction of water in the vapor phase is quite small (always less than 8%) at the experimental conditions studied. Furthermore, our interest is to establish a methodology for the investigation of the absorption process of ammonia vapor in (novel) absorbents, which are non-volatile to meet the requirements of the absorption refrigeration systems. Therefore, the control volume of our mass diffusion model is only the liquid phase (represented by dashed black line in Figure V-4.

Based on the above assumptions, the ammonia concentration into the liquid phase can be obtained using Fick's second law as:

$$\frac{\partial c}{\partial t} = D_{12}\frac{\partial^2 c}{\partial z^2} \qquad \text{V-1}$$

where c [mol m^{-3}] is the ammonia concentration in the liquid phase; z [m] is the vertical position along the height of the absorbent liquid in the absorption cell; t [s] is time; and D_{12} [m^2 s^{-1}] is the mass diffusivity of ammonia in the absorbent. Figure V-4 displays a schematic of the absorption cell and the boundary conditions (BCs) used to model the mass diffusion during the absorption process.

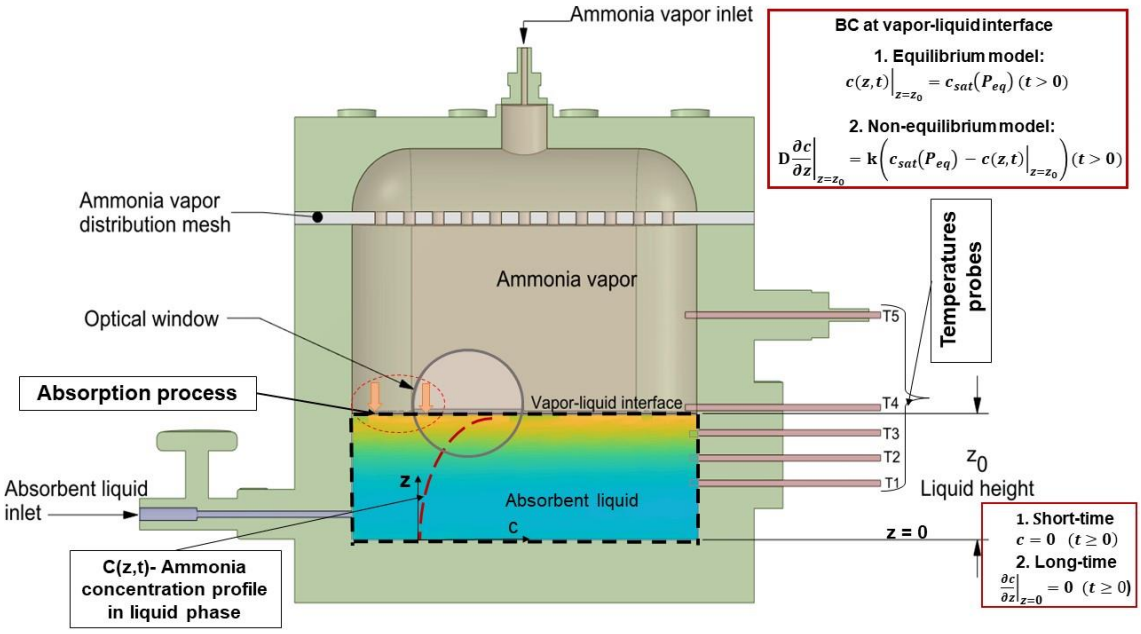

Figure V-4. Schematic of the absorption cell and the boundary conditions used to model diffusion during the absorption process.

In order to solve Eq. V-1, an initial and two boundary conditions are required. Prior to the beginning of the absorption process, the absorbent contains no ammonia (i.e. the absorbent is pure fluid). Thus, in all the experiments, the initial condition is given by:

$$c(z,t)|_{t=0} = 0 \qquad (0 \leq z \leq z_0) \qquad \text{V-2}$$

Regarding boundary conditions, one can be conveniently located at the bottom of the absorption cell and the other at the vapor-liquid interface, respectively.

In particular, at the bottom of the absorption cell, two different options can be considered depending on the contact time and the mass transfer rate between the vapor and liquid phases.

The first option considers that the diffusion front does not reach the bottom of the absorption cell. This condition prevails when the absorption cell is long, or the time of contact between the phases is short. For this reason, the mass diffusion model is called short-time model. In this model, the diffusion can be considered as occurring in a semi-infinite medium and the boundary condition is expressed as:

$$c = 0 \qquad (z = 0 \quad and \quad t \geq 0) \qquad \text{V-3}$$

The second option considers that the contact time is long, and the diffusing front reaches the bottom of the absorption cell. In this case, diffusion occurs in a finite medium, and the mass diffusion model is called the long-time model. Since the bottom of the absorption cell is a rigid and impermeable boundary, there can be no mass transfer across the bottom of the cell. Thus, the Neumann boundary condition can be applied:

$$\frac{\partial c}{\partial z}\Big|_{z=0} = 0 \qquad (t > 0) \qquad \text{V-4}$$

At the vapor-liquid interface, three main boundary conditions are found in the literature, namely, equilibrium, quasi-equilibrium, and non-equilibrium [60,170,172]. Tharanivasan et al. [170] examined the effects of these three different boundary conditions on the determined diffusion coefficients of CO_2-heavy oil and CH_4-heavy oil systems using the Pressure Drop Method (PDM). These authors found that the mass diffusivity obtained using different boundary conditions can differ up to two orders. Furthermore, these authors concluded that

the most appropriate boundary conditions may be different depending on the pair of fluids studied. The quasi-equilibrium boundary condition can be considered as intermediate between the equilibrium and non-equilibrium conditions. Therefore, the adoption of these last two boundary conditions seems very reasonable to evaluate the proposed methodology to determine the time evolution of the ammonia concentration profiles in the absorbent. These models are described in the following subsections.

V.2.1 Equilibrium mass diffusion model

The main assumption of this model is the existence of a thin boundary layer between the vapor and liquid phases, where the thermodynamic equilibrium is established at the saturation concentration [28,57,67,84].

$$c(z,t)|_{z=z_0} = c_{sat}(P_{eq}) \qquad (t > 0) \qquad \text{V-5}$$

At first glance, this assumption seems rudimentary. However, it is the most common boundary condition in the literature related to measurements of gas diffusivity in ILs [28,39,141,145,169,173]. Furthermore, as the absorption process progresses, the concentration at the vapor-liquid interface tends to the equilibrium concentration. Therefore, the equilibrium model is more suitable for advanced stages of the absorption process.

The short-time solution of the Eq. V-1, subjected to the initial (Eq. V-2) and BCs defined in Eqs V-3 and V-5 is given by Crank [89]:

$$c^*(z,t) = erfc\left(\frac{z_0 - z}{2\sqrt{D_{12}t}}\right) = erfc(\xi) \qquad \text{V-6}$$

where z_0 is the height of the liquid in the absorption cell, $c^*(z,t) = c(z,t)/c_{eq}$, and c_{eq} is the equilibrium concentration. $c^*(z,t)$ provides a useful indicator of the degree of saturation that the refrigerant/absorbent mixture reaches during the absorption process.

The long-time solution of Eq. V-1, subjected to the initial (Eq. V-2) and boundary conditions defined in Eq.s V-4 and V-5 is conveniently expressed in dimensionless variables as [170]:

$$c^*(z,t) = 1 - \frac{4}{\pi}\sum_{n=0}^{\infty}\frac{(-1)^n}{2n+1}\cos\left(\frac{(2n+1)\pi}{2}z^*\right)\exp\left(-\frac{(2n+1)^2\pi^2}{4}\tau\right) \qquad \text{V-7}$$

where $z^* = z/z_0$, and $\tau = t \cdot D_{12}/z_0^2$ is the mass-transfer Fourier number.

V.2.2 Non-equilibrium mass diffusion model

In this model, the ammonia mass transfer flux at the interface is assumed to be proportional to the difference between the saturation concentration under the equilibrium pressure and the existing concentration at the interface [170]:

$$D \left.\frac{\partial c}{\partial z}\right|_{z=z_0} = k\left(c_{sat}(P_{eq}) - c(z,t)|_{z=z_0}\right) \quad \text{V-8}$$

where k [$m^2\ s^{-1}$] is the mass transfer coefficient, and 1/k represents the interfacial resistance. This boundary condition is more realistic than the equilibrium condition. Furthermore, the use of this boundary condition enables the simultaneous experimental determination of other important mass transfer parameters, such as the mass transfer coefficient k, from a single test [174]. This parameter is typically lumped into the heat transfer coefficient, neglecting its importance in the analysis of absorption systems [33].

In this case, the short-time solution of the mass diffusion model is [89]:

$$c^*(z,t) = \mathrm{erfc}(\xi) - \exp(\mathrm{h}(\mathrm{z}_0 - \mathrm{z}) + \mathrm{h}^2 \mathrm{D}_{12} t)\ \mathrm{erfc}\left(\xi + \mathrm{h}\sqrt{D_{12}t}\right) \quad \text{V-9}$$

where $h = k/D_{12}$.

Meanwhile, for the long-time approach, the solution is expressed as [170]:

$$c^*(z,t) = 1 - 4\sum_{n=1}^{\infty} \frac{\sin\lambda_n}{2\lambda_n + \sin 2\lambda_n} \cos(\lambda_n z^*)\, e^{-\lambda_n^2 \tau} \quad \text{V-10}$$

where λ_n (n = 1,2,3, ...) represents the eigenvalues, which are the positive roots of the characteristic equation:

$$\tan\lambda_n = \frac{k_D}{\lambda_n} \quad \text{V-11}$$

Here, $k_D = kz_0/D_{12}$, which is the mass-transfer Biot number.

Physically, the non-equilibrium model approaches the equilibrium model when k_D is large enough, noting that $1/k_D$ represents the ratio of the interfacial resistance 1/k for the mass transfer to the bulk resistance z_0/D_{12} for the molecular diffusion [170].

V.2.3 Determination of the mass diffusivity of ammonia in the ionic liquid and the mass transfer coefficient, based on the mass diffusion model

In general, the short- and long-time solutions, both led to accurate results despite the differences in the mathematical description of diffusion phenomena. However, the application of the short-time approach lacks a physical sense for the equilibrium model in the early stages of the absorption process. Furthermore, it has been reported that the long-time model provides conditions for more precise estimates of diffusion coefficients from the experimental point of view [85]. However, applying the long-time approach to the non-equilibrium model also makes no physical sense for the specific conditions of our experimental setup. Therefore, in this thesis, two different approaches were used to describe ammonia mass diffusion during the absorption process. In particular, we have used the long-time solution for the equilibrium model, and the short-time solution for the non-equilibrium model.

The use of long-time solutions requires dealing with the infinite series presented in equation V-7 for the equilibrium model. Fortunately, it has been found that only the first few terms are sufficient in practical applications [36,139]. Shiflett and Yokozeki [139] found that, after the sum of the first 10 terms, the numerical contribution to concentration became less than 10^{-12}. Furthermore, Bedia et al. [42] found that for their diffusivity measurements of ammonia in ionic liquids, only the first three terms in the series contributed significantly to changes in concentration. Nevertheless, to increase the precision in the early stages of the absorption process, and to leverage the full potential of the ODI method, we have considered the first 100 terms in the infinite series solution for the equilibrium model.

Once the working equations for the distribution of the ammonia concentration have been established, the next step is to relate the concentration to the refractive index. To do so, it is needed to determine the changes in ammonia concentration of the liquid phase.

As mentioned above, initially, there is no ammonia in the absorbent. Thus, the change in ammonia concentration in the absorbent between the initial or

reference time, $t_{ref} = 0$, and any other time during the absorption process, t, can be expressed as:

$$\Delta c^*(z,t) = c^*(z,t) - c^*\left(z, t_{ref} = 0\right) = c^*(z,t) - 0 = c^*(z,t) \qquad \text{V-12}$$

Then, the changes in ammonia concentration can be related to changes in refractive index of the liquid phase. On the assumption that these two quantities are linearly related for the concentration ranges found in the experiments [158], the refractive index variation profile can be calculated as:

$$\Delta n_{cal}(z,t) = m \cdot \Delta c^*(z,t) \qquad \text{V-13}$$

where m is the mean value of the derivative of the refractive index on concentration (so-called concentration contrast factor) for the experimental concentration range. Since this factor is unknown for the mixtures studied, it is determined simultaneously with the mass diffusivity using a non-linear regression procedure. In particular, these parameters are obtained using a non-linear least squares minimization of the deviation between experimental ($\Delta n_{exp}(z,t)$) and calculated ($\Delta n_{cal}(z,t)$) refractive index profiles as:

$$\Phi = \sum_{i,j}[\Delta n_{exp}(z_i, t_j + t_0) + \Delta n_{cal}(z_i, t_{\text{ref}} + t_0) - \Delta n_{cal}(z_i, t_j + t_0)]^2 \qquad \text{V-14}$$

The mass diffusivity, D_{12}, and the concentration contrast factor, m, are determined as result of the minimization of Eq. V-14. In this equation, t_0 is an empirical parameter introduced to consider that the reference time (which corresponds to the last image just before the absorption process begins) is not necessarily located at the very beginning of the absorption process. Therefore, three unknown parameters were concurrently fitted:D_{12}, m, and t_0. In addition, in the case of the non-equilibrium model, a fourth parameter, the mass transfer coefficient, k, is also determined from the regression procedure.

Several minimization algorithms can be found in the literature and are available in commercial software packages such as MATLAB ® [88]. In this thesis, the Nelder-Mead (simplex) [65,116] and Levenberg-Marquardt [60] algorithms were used to determine the unknown parameters. The minimization procedure was based on the sequential application of both algorithms to benefit from their respective advantages. Thus, we divided the fitting procedure into two steps to accelerate the convergence. The first step was aimed at searching for good initial

guesses using the Nelder-Mead (simplex) algorithm. The second step is the iterative process to minimize Φ, which uses the initial guess of the first step. The second step was performed using the Levenberg-Marquardt algorithm.

In the next step, the standard uncertainty (standard deviation) of the fitted parameters was obtained. In a non-linear regression model, the standard uncertainty of the fitted parameters, can be obtained from the diagonal of variance-covariance matrix. If the model Jacobian, J, has full column rank, the estimated variance-covariance matrix, CovB, can expressed as [88]:

$$\mathrm{CovB} = (\mathrm{J}' \cdot \mathrm{J})^{-1} \cdot \mathrm{MSE} \qquad \text{V-15}$$

where: J' is the Jacobian transpose, and $\mathrm{MSE} = (\mathrm{R}' * \mathrm{R})/(\mathrm{N} - \mathrm{p})$ is the mean squared error. Here, R' and R are the residuals matrix and its transpose, respectively; N is the number of observations, and p is the number of estimated parameters.

Finally, the expanded uncertainty, $U(D_{12})$, can be obtained from the standard uncertainty in the mass diffusivity as:

$$U(D_{12}) = k \cdot u(D_{12}) \qquad \text{V-16}$$

where k = 2 is the confidence coefficient, which corresponds to a degree of confidence of 95%.

V.3 Experimental results of the time evolution of the ammonia concentration profiles in the absorbent

As mentioned in Chapter III, traditional methods for determining the mass diffusivity provide time-dependent data, such as the absorbed mass in the gravimetric method or the pressure decay in the pressure drop method. These time-dependent data are usually used to determine an average effective diffusivity over the concentration range observed during the absorption process. However, the use of an average effective diffusivity determined with these methods may not be appropriate to describe the evolution of the spatial distribution of the refrigerant concentration within the absorbent. This has been confirmed for the absorption of gases in heavy oils, since a different trend was observed in terms of penetration distance and concentration distribution using a magnetic resonance imaging (MRI) technique [175].

Unlike traditional methods, the ODI method allows us to directly visualize the evolution of the refractive index fields, and thus, the concentration fields within the refrigerant/absorbent liquid solution. Thus, providing valuable spatio-temporal data that can be used to determine the mass diffusivity of refrigerant vapor in the absorbent at a given concentration. In this regard, the shapes of the concentration-distance curves at different times, obtained with the ODI method, contain relevant information on the mechanisms of mass transfer during the absorption process. For example, from the analysis of the shapes of these curves, the concentration-dependence of the mass diffusivity for concentrated solutions can readily be deduced [89]. Furthermore, this information can also be used to validate mass transfer approaches such as two-film theory, penetration theory, or surface renewal theory, which are typically addressed at the (global) scale of the gas-liquid contactor, but rarely at the (local) scale of the vapor-liquid interface [67]. In this section, the experimental results of the time evolution of the ammonia concentration profiles in the absorbent are presented and discussed.

V.3.1 Validation of the ODI method for the absorption of ammonia in water

Here, the diffusivity measurements for the NH_3/H_2O system are used as a reference to validate the ODI method. In the validation, the two mass diffusion models described in section V.2, equilibrium, and non-equilibrium, are considered.

As mentioned, the equilibrium model assumes that the vapor-liquid interface is always saturated with NH_3 at equilibrium pressure. Therefore, this model provides a spatial distribution of the concentration relative to the (assumed) equilibrium concentration at the interface.

Figure V-5 shows the experimental and calculated profiles of the concentration during the absorption process of NH_3 in H_2O, at 293.15 K. The successive curves show the time evolution of the ammonia concentration profiles in the field of view. In the initial stages of the absorption process, the NH_3 concentration is zero in the lower region of the field of view, while the interface is assumed to be saturated. Therefore, in these stages, the maximum difference between the concentrations of the interface and the lower region of the field of view is observed. Then, this difference is reduced as the diffusion front reaches the lower region of the field of view throughout the absorption process. After a long enough

time, the concentration should be uniform across the field of view, as the system reaches equilibrium. In this study, at the end of the experiments ($\tau = 0.1464 \rightarrow t \approx 15\ h$), some differences can be observed between the concentrations at the interface and at the lower region of the field of view, which indicates that the equilibrium state is not reached.

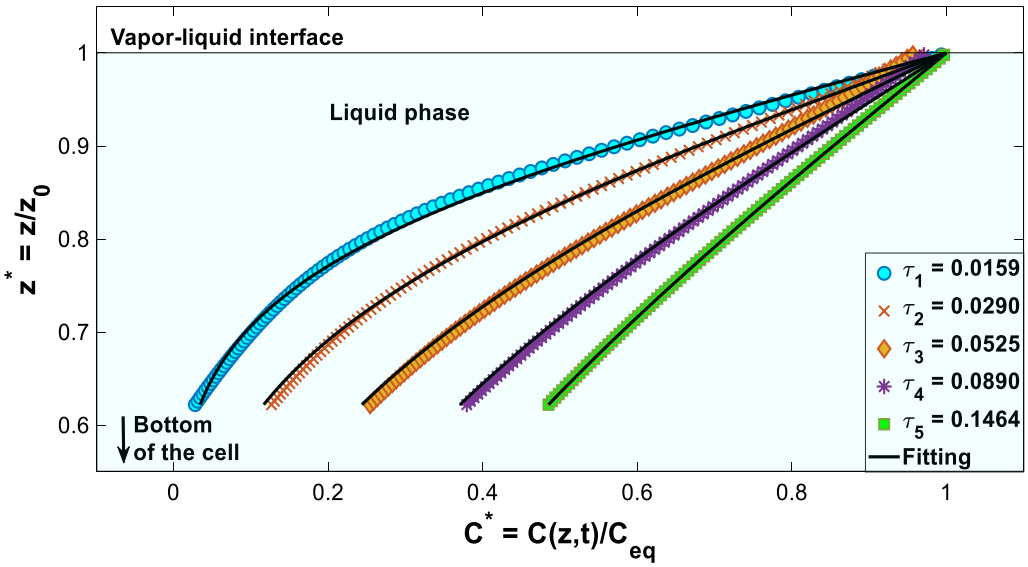

Figure V-5. Concentration distribution ($C^*(z, t)$) in the field of view of the absorption cell obtained using the equilibrium model at different time instances during the absorption process of NH_3 in H_2O at 293.15 K.

Furthermore, it is also observed that the equilibrium model represents more accurately the experimental concentration profiles for advanced times of the absorption process. This is because, as time increases, the concentration at the interface approaches the (assumed) equilibrium concentration and the model represent the mass diffusion process more realistically. In this regard, the most notable difference between the model and the experimental data is observed near the interface at shorter times. This difference is mainly due to thermal effects that affect the distribution of the refractive index and thus, of the concentration in the field of view. Despite this, in general, the equilibrium model is able to satisfactorily reproduce the experimental NH_3 concentration profiles in the liquid phase.

Unlike the equilibrium model, the non-equilibrium model considers the variation in concentration at the interface throughout the absorption process. Here, the non-equilibrium model is considered valid for short times of the absorption process, in which the diffusion front does not reach the lower region of the field

of view. Consequently, the NH_3 concentration is zero in that region for the time interval considered. In particular, the determination of the time period in which this model is valid can be determined from the analysis of the experimental interferograms and the corresponding optical phase maps.

Illustratively, Figure V-6 shows the evolution of the diffusion layer during the absorption process of NH_3 in H_2O at 303.15 K at different time instances. Two regions of similar size can be identified on the upper interferogram. In the region closest to the vapor-liquid interface, it can be observed that the fringes bend to the left as a consequence of the diffusion of NH_3 into the H_2O bulk. While in the region furthest from the interface and therefore closest to the lower region of the field of view, the fringes remain vertical. This suggests the existence of a layer within the liquid phase where diffusive transport of matter takes place and another where the liquid bulk is not affected by diffusion and therefore, only pure H_2O is present.

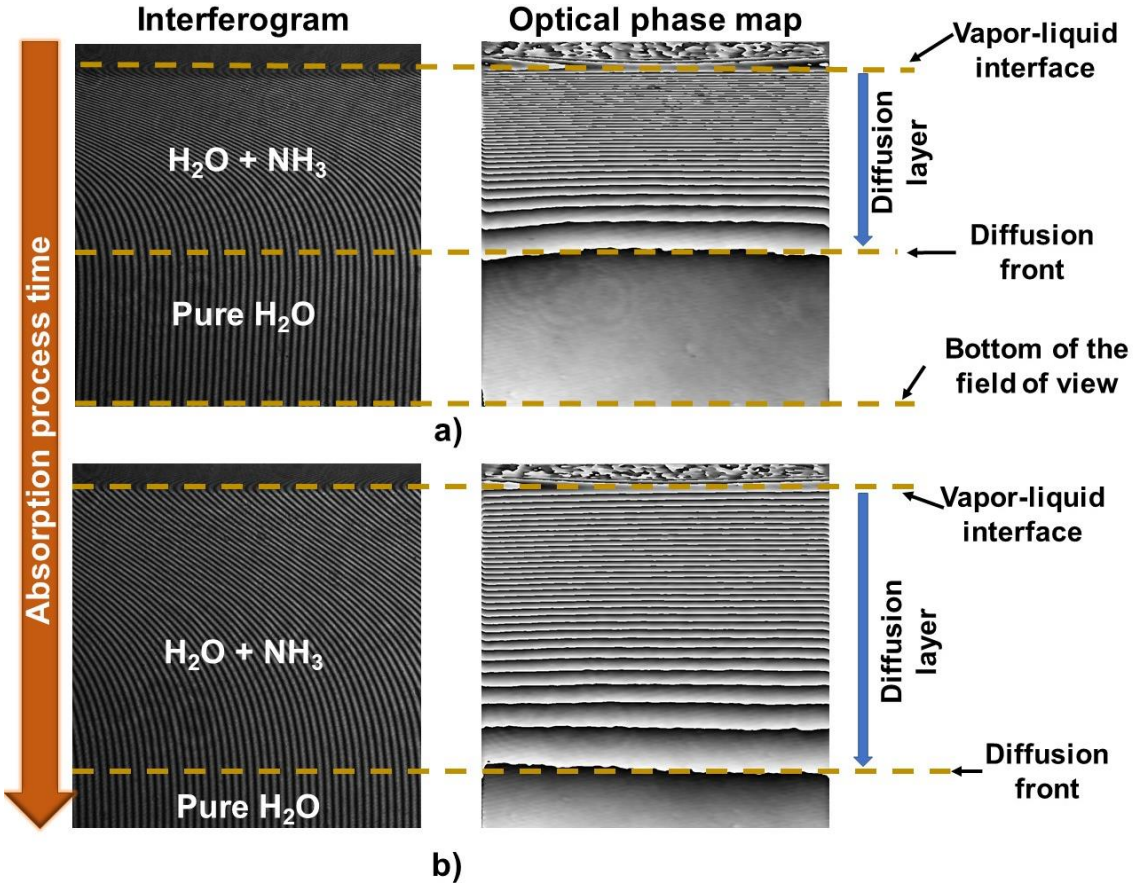

Figure V-6. Evolution of the diffusion layer at different time instances during the absorption process of NH_3 in H_2O at 303.15 K. a) At 40 minutes; b) At 60 minutes.

However, as the absorption process progresses, the mass diffusion layer increases in thickness as can be seen in Figure V-6 (b), and after a sufficient long time the diffusion front reaches the lower region of the field of view. We have determined the upper limit of the short time range to be $\tau = 0.0106$ ($t \approx 75\ minutes$).

Once the period of time in which the non-equilibrium model is considered valid has been determined, the next step is to visualize the experimental concentration profiles during the absorption process in this time interval.

Figure V-7 shows the observed concentration profiles and the fitting results for this model during the absorption process of NH_3 in H_2O, at 303.15 K. As can be seen, the concentration difference between the interface and the lower region of the field of view increases with time. As the absorption process progresses and more NH_3 passes from the vapor phase to the liquid phase, this difference grows. The concentration difference increases until the diffusion front reaches the lower region. Thereafter, the concentration difference gradually begins to decrease as the interface tends to saturate and the diffusion front continues to reach the lower region of the field of view. Moreover, Figure V-7 also shows that the non-equilibrium diffusion model is able to satisfactorily reproduce the experimental concentration profiles in the liquid phase.

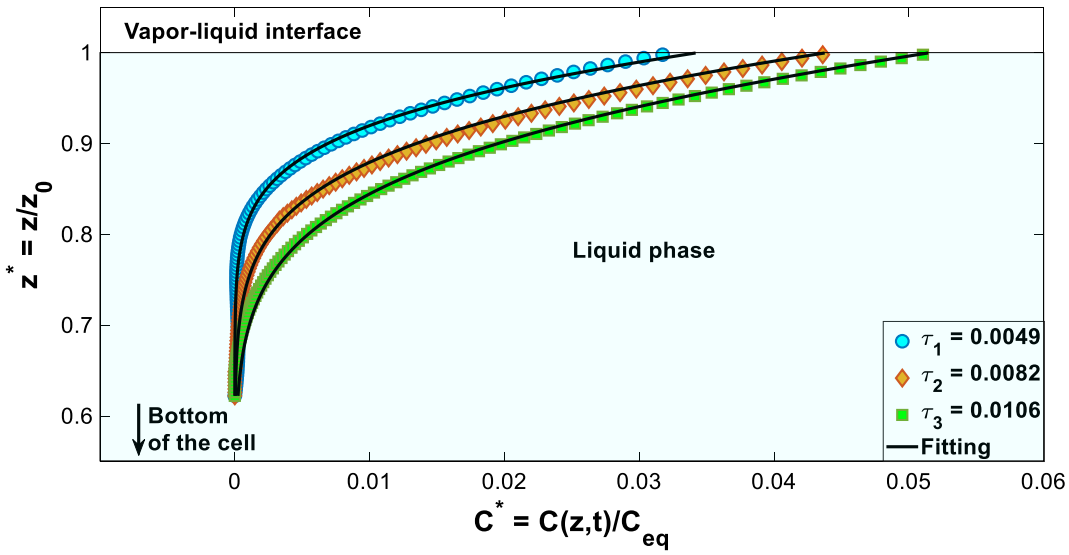

Figure V-7. Concentration distribution ($C^*(z, t)$) in the field of view of the absorption cell obtained using the non-equilibrium model at different time instances during the absorption process of NH_3 in H_2O at 303.15 K.

Once the concentration profiles during the absorption of NH_3 in H_2O have been observed using the two mass diffusion models, the next step is to compare the obtained mass diffusivity values. As mentioned, the determination of the mass diffusivity was performed by minimizing the differences between the calculated and experimental refractive index variation profiles (see Eq. V-14). Table V-1 lists the results of the diffusivity values obtained together with the literature ones.

Table V-1. Comparison between reported and determined mass diffusivity values (D_{12} x 10^9 [m^2 s^{-1}]) of NH_3 in H_2O at different temperatures and pressures.

T/ K	Literature[1]		This thesis		
	D_{12} x 10^9/ m^2 s^{-1}	P/ kPa	D_{12} x 10^9/ m^2 s^{-1}	P[2]/ kPa	Diffusion model
293.2	1.51 [41]	101.32	1.80 ±0.10	12.74	Equilibrium
			1.42 ±0.12	13.84	Non-equilibrium
303.2	1.90 [41]	101.32	2.26 ±0.08	22.78	Equilibrium
			1.98 ±0.10	27.07	Non-equilibrium

[1] *Measurements were performed using a Taylor Dispersion Technique.*
[2] *Average pressure in the time interval used in the determination of the mass diffusivity.*

In general, an overestimation of the mass diffusivity value is observed using the equilibrium model. The overestimation may be due to the assumption of an equilibrium concentration at the vapor-liquid interface from the beginning of the absorption process. Nevertheless, the relative deviations between the experimental and reported values are around +20 %, which is still a reasonable agreement. In the case of the non-equilibrium model, our results are closer to the literature values. The relative deviations are -5.3% and 4.2% at 293.15 K and 303.15 K, respectively. As expected, the use of a more realistic boundary condition at the vapor-liquid interface lead to a more precise determination of the mass diffusivity.

In Table V-1 are also listed the experimental pressure in our measurements. The values from the literature were obtained at atmospheric pressure. Although the mass diffusivity dependence on pressure is weak [39], this property could have influenced the small differences between the values obtained for the non-equilibrium model and those reported in the literature. Despite this, based on the

observed deviations, it is considered that the ODI method describes with enough precision the mass diffusion phenomena during the absorption process of ammonia vapor in water. Therefore, the described methodology was considered validated and used to determine the mass diffusivity of ammonia in the ionic liquids studied. The results for the equilibrium and non-equilibrium diffusion models are shown in the following subsections, respectively.

V.3.2 Results for the ionic liquids selected using the equilibrium mass diffusion model

As discussed, the equilibrium mass diffusion model provides an acceptable description of the diffusion phenomena during the absorption process of NH_3 in H_2O. Furthermore, the equilibrium model is the most widely used in the literature to determine the mass diffusivity of refrigerant vapor in ionic liquids. Therefore, it is used here to compare our results with the experimental values available in the literature.

As an example, fitting results are discussed for the experimental measurements that corresponds to the absorption process of NH_3 in [emim][BF_4] at 303.15 K. Figure V-8 shows the time evolution of the refractive index change profiles during the absorption process.

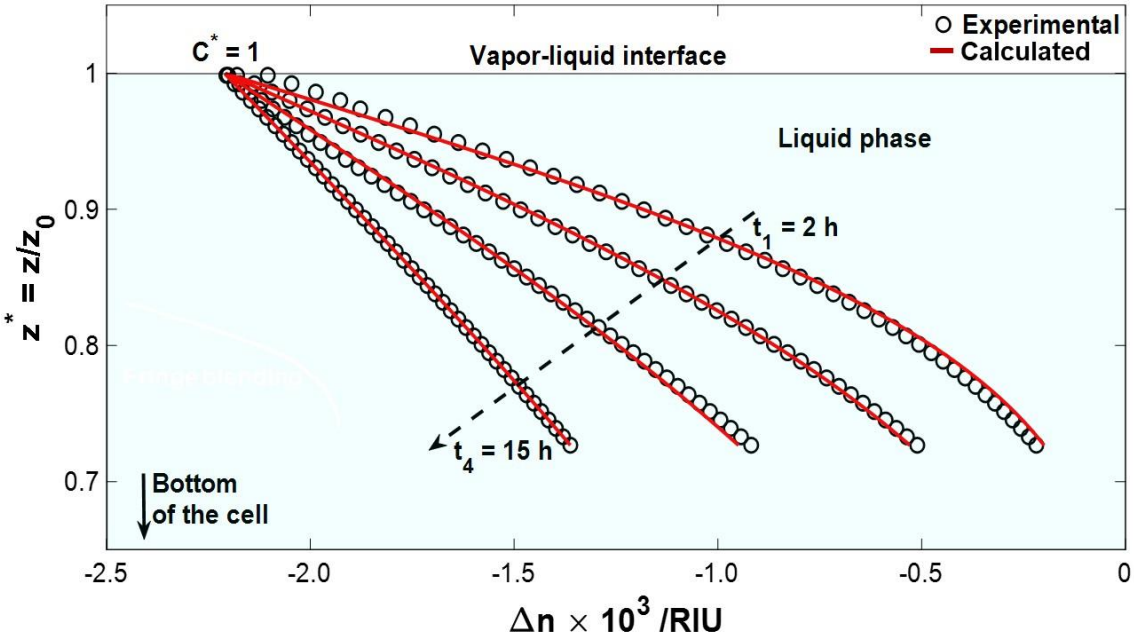

Figure V-8. Evolution of the refractive index change (Δn) profiles in the field of view of the absorption cell using the equilibrium diffusion model during the absorption process of NH_3 in [emim][BF_4] at 303.15 K.

As expected, the model represents more accurately the experimental profiles of the refractive index variation for advanced times of the absorption process. Moreover, the absolute variation of the refractive index is around 2.2 x 10^{-3} refractive index units (RIU).

Figure V-9 shows the time evolution of the refractive index change profiles during the absorption process of NH_3 in EAN at 303 K, after six hours from the beginning of the absorption process.

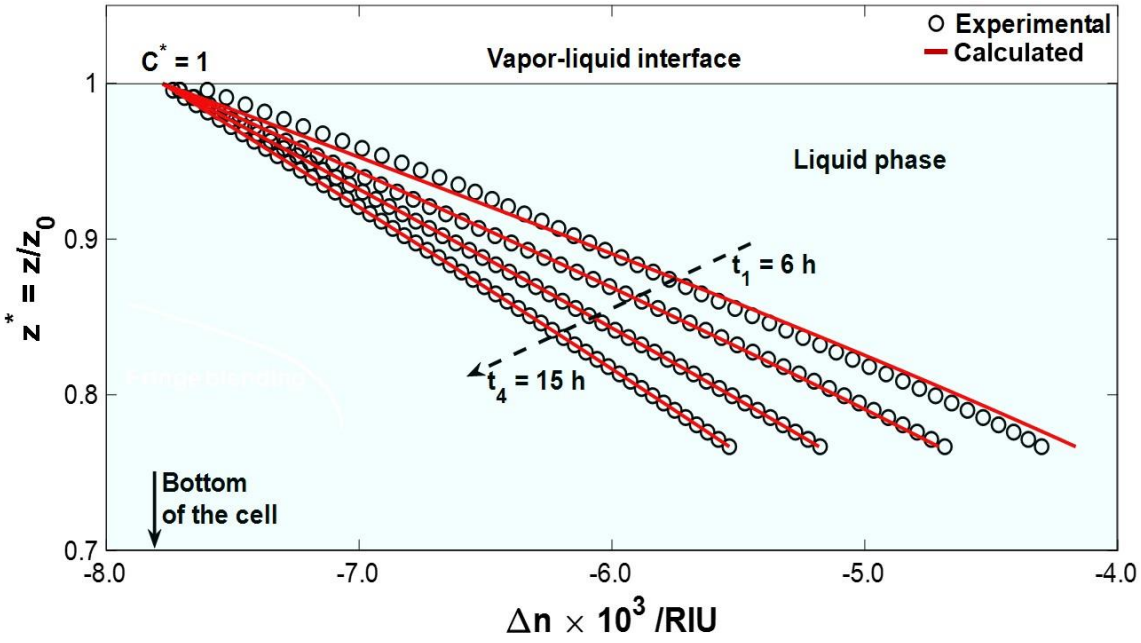

Figure V-9. Evolution of the refractive index change (Δn) profiles in the field of view of the absorption cell using the equilibrium diffusion model during the absorption process of NH_3 in EAN at 303.15 K.

As can be seen, from this moment on, the variation of the refractive index in the field of vision follows a virtually linear distribution. Moreover, the absolute variation of the refractive index in the time interval shown is much greater in EAN than during the entire absorption process in [emim][BF_4]. This may suggest that the concentration contrast factor, which is the variation of the refractive index with concentration, for the NH_3/EAN mixture is higher than for the NH_3/[emim][BF_4] mixture. However, it is necessary to consider that the amount of NH_3 dissolved in EAN is greater than in [emim][BF_4] at the same temperature. According to our measurements of the absorption rate described in Chapter II, after 15 hours from the beginning of the absorption process, at 303 K, the mass fraction of NH_3 (ω_{NH3}) in EAN is ω_{NH3} = 0.64%, while in [emim][BF_4] ω_{NH3} = 0.43%. Therefore, the

concentration contrast factor of NH_3/[emim][BF_4] mixture is greater than that of the NH_3/EAN.

Table V-2 presents the experimental results of the mass diffusivity and its uncertainties at different temperatures and pressures for the equilibrium model. The value of D_{12} in the ionic liquids studied follows the order [EAN] > [emim][BF_4]> [bmim][BF_4], in accordance with the absorption rate results discussed in Chapter II. In particular, our diffusivity values ranged from 4.86 x 10^{-10} m^2 s^{-1} at 293 K for [bmim][BF_4] to 9.01 x 10^{-10} m^2 s^{-1} at 303 K for EAN. Moreover, the mass diffusivity of NH_3 in the ILs studied increases with temperature.

Table V-2. Experimental mass diffusivity (D_{12} x 10^{10} /m^2 s^{-1}) of NH_3 in the ILs studied at different temperatures and pressures using an equilibrium mass diffusion model.

Ionic liquid	T/ K	Literature		This thesis	
		D_{12} x 10^{10} / m^2 s^{-1}	P/ kPa	D_{12} x 10^{10} / m^2 s^{-1}	P[3]/ kPa
EAN	293.2	-		7.39 ±0.12	16.9
EAN	303.2	-		9.01 ±0.08	15.7
[emim][BF_4]	293.2			6.23 ±0.10	60.7
[emim][BF_4]	303.2			8.68 ±0.10	61.7
[bmim][BF_4]	293.2	2.10[4] [36]		4.86 ±0.11	59.5
[bmim][BF_4]	303.2	7.51[5] [36]		5.26 ±0.10	52.7
		1.0[6] [39]	50		

[3] *Average pressure in the time interval used in the calculation of the mass diffusivity in this thesis.*
[4] *Average effective diffusivity reported at the partial pressure of ammonia in a gas mixture of NH_3/N_2, and x_{NH3} ≈ 0.3 using a gravimetric method.*
[5] *Average effective diffusivity reported at the partial pressure of ammonia in a gas mixture of NH_3/N_2 using a gravimetric method.*
[6] *Average effective diffusivity reported at 298 K, 50 kPa, and x_{NH3} = 0.16 using a gravimetric method.*

For comparison with our values, literature values are also listed in Table V-2. In the cases of the NH_3/EAN and NH_3/[emim][BF_4] mixtures, no references are available, while for the NH_3/[bmim][BF_4] mixture we have found different results in the literature. In particular, Bedia et al. [36] reported an average effective mass diffusivity $\bar{D}_{12} = 2.10 \times 10^{-10} m^2 s^{-1}$ at 293 K, and after that, Turnaoglu and Shiflett [39] reported $\bar{D}_{12} = 1.0 \times 10^{-10} m^2 s^{-1}$ at 298 K, which represents only 47.6% of the value reported by Bedia et al. at lower temperature. This difference

may be given by the amount of ammonia dissolved in the IL, $x_{NH3} \approx 0.3$ at 293.15 K, and $x_{NH3} = 0.16$ at 298 K, in the studies of Bedia et al., and Turnaoglu and Shiflett, respectively. However, Turnaoglu and Shiflett [39] also reported $\overline{D}_{12} = 1.4 \times 10^{-10} m^2 s^{-1}$ at 298 K, P = 128 kPa, and $x_{NH3} = 0.31$, indicating inconsistency of the values reported in these studies even though both use a gravimetric method.

As can be seen in Table V-2, the diffusivity values obtained are in the same order as the literature values. In particular, compared to the values of Bedia et al. [36], our diffusivity at 293.15 K is higher, while at 303 K it is lower. Whereas in comparison with Turnaoglu and Shiflett [39] our results are quite higher. Moreover, in general, our values are closer to those of Bedia et al. than to those of Turnaoglu and Shiflett. In the next subsection we discuss the results obtained with the non-equilibrium model, which more realistically describes the diffusion phenomena during the absorption process.

V.3.3 Results for the ionic liquids selected using the non-equilibrium mass diffusion model

Figure V-10 shows the time evolution of the refractive index change profiles during the absorption process of NH_3 in the ionic liquid [bmim][BF_4] at 293.15 K. As can be seen, the non-equilibrium model successfully reproduces the experimental refractive index change profiles in the liquid phase. In this regard, the most notable differences between the model and the experimental data is observed near the vapor-liquid interface region. In this region, the absorption thermal effects affect the experimental profiles of the refractive index change. Nonetheless, this model is very useful to visualize the penetration depth of NH_3 at different instances during the absorption process. In this case, we have determined the upper limit of the short time range to be around $\tau = 0.0028$ ($t \approx 225\ minutes$).

Table V-3 shows the results obtained for the mass diffusivity and mass transfer coefficient using the non-equilibrium model.

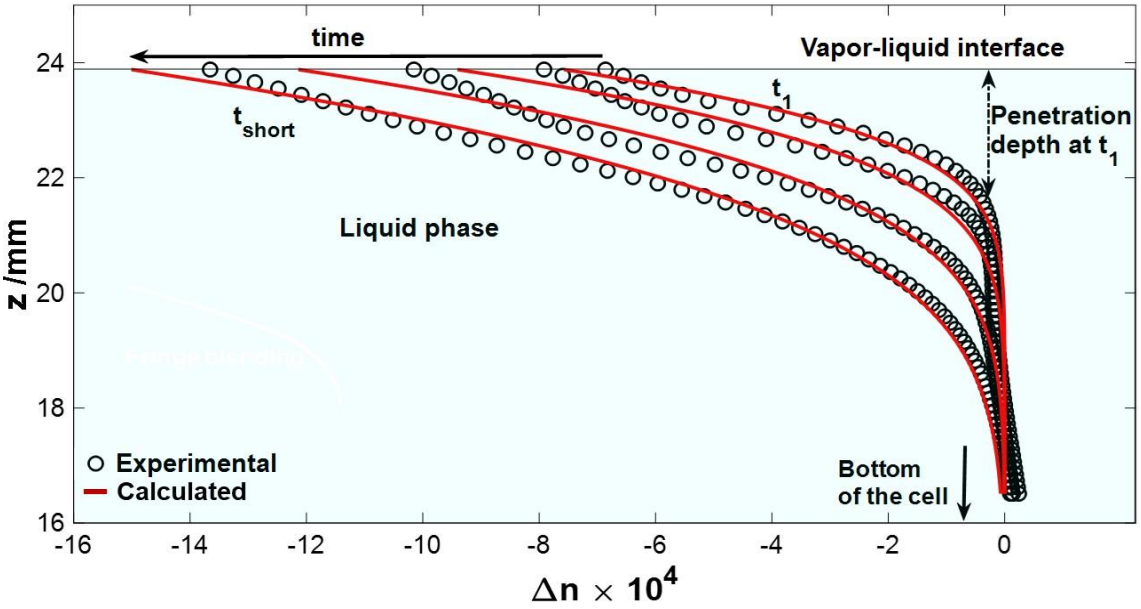

Figure V-10. Evolution of the refractive index change (Δn) profiles in the field of view of the absorption cell using the non-equilibrium diffusion model during the absorption process of NH_3 in [bmim][BF_4] at 293.15 K.

Table V-3. Experimental mass diffusivities (D_{12} x 10^{10} [m^2 s^{-1}]) and mass-transfer coefficient (k x 10^7 [m^2 s^{-1}]) of NH_3 in the ILs studied at different temperatures and pressures using a non-equilibrium diffusion model.

Ionic liquid	T/ K	Literature		This thesis		
		D_{12} x 10^{10} / m^2 s^{-1}	P/ kPa	D_{12} x 10^{10} / m^2 s^{-1}	k x 10^7 /m s^{-1}	P^7/ kPa
EAN	293.2	-		3.81 ±0.12	16.03	25.1
EAN	303.2	-		5.71 ±0.11	19.92	28.7
[emim][BF_4]	293.2	-		3.34 ±0.10	11.52	76.4
[emim][BF_4]	303.2	-		4.98 ±0.10	14.88	79.9
[bmim][BF_4]	293.2	2.10[8] [36]		1.18 ±0.11	9.98	70.5
[bmim][BF_4]	303.2	7.51[9] [36] 1.0[10] [39]	50	3.22 ±0.10	10.56	69.7

[7] *Average pressure in the time interval used in the calculation of the mass diffusivity in this thesis.*
[8] *Average effective diffusivity reported at the partial pressure of ammonia in a gas mixture of NH_3/N_2, where $x_{NH3} \approx 0.3$ using a gravimetric method.*
[9] *Average effective diffusivity reported at the partial pressure of ammonia in a gas mixture of NH_3/N_2.*
[10] *Average effective diffusivity reported at 298 K, and $x_{NH3} = 0.16$ using a gravimetric method.*

The diffusivity values obtained are considerably lower than for the equilibrium model and closer to those reported in the literature. In particular, the values obtained are quite close to the expected trend of the measurements of Bedia et al [36]. Although at 303 K the difference is quite remarkable, if the strong dependence of diffusivity with concentration is considered, a value close to that reported by these authors could be expected. Compared to Turnaoglu and Shiflett [39], our diffusivity value is still considerably higher.

Table V-3 also shows the values obtained for the mass-transfer coefficient (k). The values obtained ranged from 9.98 x 10^{-7} m s^{-1} for [bmim][BF_4] at 293.15 K to 19.92 x 10^{-7} m s^{-1} for EAN at 303.15 K. Furthermore, the relationship between the mass transfer coefficients and the mass diffusivity values obtained follows a trend closer to the linear than to the square-root. This suggests that the simple two-film theory may provide an acceptable description of mass transfer for the mixtures studied in our measurement system [91]. Moreover, mass-transfer Biot numbers (k_D), calculated from the diffusivities and mass transfer coefficients, show that the bulk resistance to the molecular diffusion is larger than the interfacial resistance to the mass transfer [170]. k_D ranged from 63 for [emim][BF_4] at 303.15 K to 200 for [bmim][BF_4] at 293.15 K.

V.4 Estimation of mass diffusivity of ammonia vapor in ionic liquids

So far, the importance of mass diffusivity is limited, while priority was given to VLE and viscosity data. As a result, diffusion data and models in liquid mixtures are still scarce and lack the required level of accuracy [92]. Hence, there is great interest in improving the accuracy of the models and correlations, such as those shown in Chapter III, to estimate gas diffusivities in liquids. Here, we have evaluated the accuracy of some of the most widely applied correlations to describe gas diffusivity in ionic liquids.

The correlations evaluated here are appropriate only for dilute solutions. Therefore, among the values reported in the literature for the mass diffusivity of ammonia in ionic liquids, only the experimental data for dilute solutions have been considered. In this thesis, dilute solutions are considered those that have less than 10% mole fraction of ammonia. Thus, in addition to our experimental data,

11 data-points reported by Turnaoglu and Shiflett [39] were considered to evaluate the accuracy of the correlations used. The correlations evaluated include some of those shown in section III.3, such as Wilke-Chang, Scheibel, Arnold, Akgerman-Gainer, and also other empirical correlations developed for the diffusion of gases, mainly CO_2, in ionic liquids. In all cases, the absolute relative deviation (ARD), the maximum relative deviation (MRD), and the coefficient of determination (R^2) were used as the main criteria to evaluate the estimation capability of these correlations:

$$ARD/\% = \frac{100}{N}\sum_{i=1}^{N}\left|\frac{D_{exp}-D_{cal}}{D_{exp}}\right| \qquad \text{V-17}$$

$$MRD/\% = 100 \cdot \max\left|\frac{D_{exp}-D_{cal}}{D_{exp}}\right| \qquad \text{V-18}$$

$$R^2 = 1 - \frac{\sum_{i=1}^{N}\left[y(i)_{calc}-y(i)_{exp}\right]^2}{\sum_{i=1}^{N}\left[y(i)_{calc}-\bar{y}_{exp}\right]^2} \qquad \text{V-19}$$

We found that the Scheibel, Arnold, and Akgerman-Gainer correlations were unable to reproduce the behavior of ammonia diffusivity in the ionic liquids studied. Illustratively, Figure V-11 shows the ability of Arnold's correlation to describe experimental measures of diffusivity.

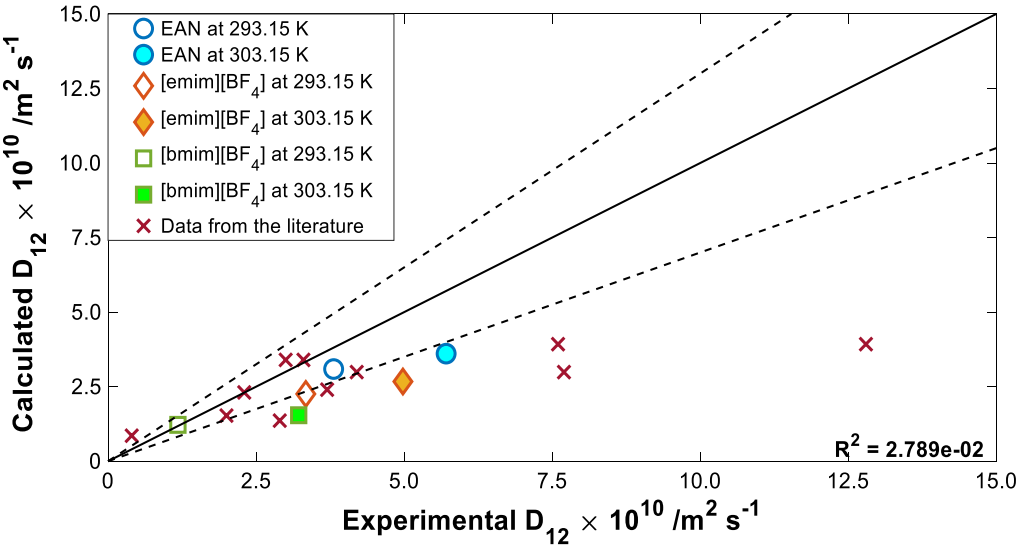

Figure V-11. Experimentally determined diffusivities versus diffusivities calculated by Arnold correlation.

The Arnold correlation contains an empirical fitting parameter (the abnormality factors, A_1A_2); therefore, we adjusted this parameter to fit the ionic liquid data.

We found that the optimal value of A_1A_2 is 2.421 for the diffusivity of NH_3, while A_1A_2 has been reported in the literature to be equal to 0.714 for the diffusivity of CO_2 in ionic liquids [35].

As can be seen, many of the predicted data points fall well below the experimental values. This behaviour is more pronounced for higher diffusivity values. In this case, the average relative deviation is close to 38%, while the maximum relative deviation is close to -114%, with an unacceptable R^2 = 2.789E-02. These typical lower values of R^2 have been previously reported in the literature for the diffusion of CO_2 in imidazolium ILs [134].

We have also assessed the estimation capability of the Wilke-Chang correlation, and the results are plotted in Figure V-12. In general, this correlation provides better estimates than the previous ones, with a higher R^2 = 4.524e-01, and deviations from the experimental data of the order of 48% and 75% for ARD, and MRD, respectively.

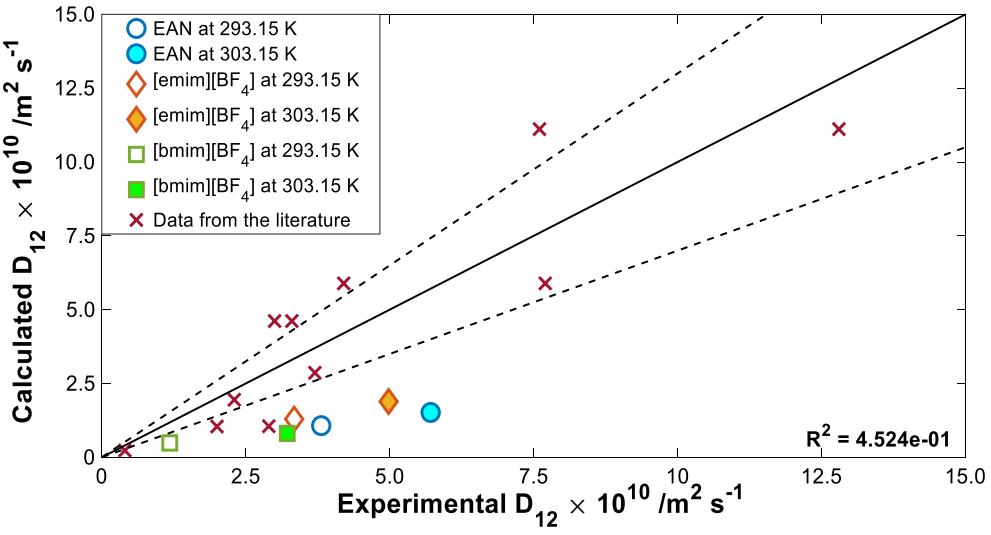

Figure V-12. Experimentally determined diffusivities versus diffusivities predicted by Wilke-Chang correlation.

In this correlation, the association factor (ϕ in equation III-25) is an adjustable parameter, which is determined by a non-linear regression procedure of the experimental data. Since ϕ is only related to the physicochemical character of the solvent, there should be an association factor for each ionic liquid studied [38]. Despite this, several authors used a common value for ϕ for the diffusion of gases (CO_2 [35,132] and H_2 [133]) in different ILs. In this thesis, in consideration

of the limited availability of experimental data, a common value of ϕ is used to describe the diffusivity of ammonia in the different ionic liquids studied.

We have determined ϕ to be equal to 1.73, which is between the value for ethanol (ϕ = 1.5), and for methanol (ϕ = 1.9). Typical ϕ values in ionic liquids are considerably higher compared to traditional solvents. The relatively low value of ϕ obtained for the Wilke-Chang correlation could be indicative of the inappropriateness of using this conventional solvent correlation for ILs [35]. Nevertheless, other authors have also found similar values of ϕ for the diffusion of gases in ionic liquids. For example, He at al. [29] reported a value of ϕ = 2.4 for the diffusion of hydrofluorocarbons in ionic liquid [hmim][NTf_2], a value lower than for water (ϕ = 2.6). Furthermore, Hou and Baltus [123] suggested that the poor agreement between the diffusivities measured and those predicted using the Wilke-Change correlation could be due to the fact that ϕ is temperature-dependent for gas-ILs systems. Here, to investigate the possible influence of the temperature on ϕ, and hence, on the estimation capability of the Wilke-Chang correlation, we assumed an Arrhenius-type dependence for ϕ:

$$\phi = \phi_0 \exp\left(\frac{\phi_1}{RT}\right) \qquad \text{V-20}$$

where ϕ_0, and ϕ_1 are the adjustable parameters of the Wilke-Chang correlation with temperature-dependent association factor.

The results of this modified Wilke-Chang correlation are depicted in Figure V-13. The adjustable parameters were found to be ϕ_0 = 2.332e-05, and ϕ_1 = 30.90. Thus, ϕ = 4.92 at 303.15 K, which is a more appropriate value since large values for the association factor were found to be characteristic of the ionic association nature in ionic liquids [38].

As can be seen in the figure, the use of a temperature-dependent association factor improves the prediction ability of the Wilke-Chang correlation. In this case, R^2 = 6.398E-01, ARD = 30%, and MRD = 62%. However, like the original, the modified correlation also underestimates the diffusivity. This may be because both correlations assume a greater dependence on viscosity ($D_{12} \propto \mu^{-1}$) than that observed for ionic liquids ($D_{12} \propto \mu^{-0.6}$) [35].

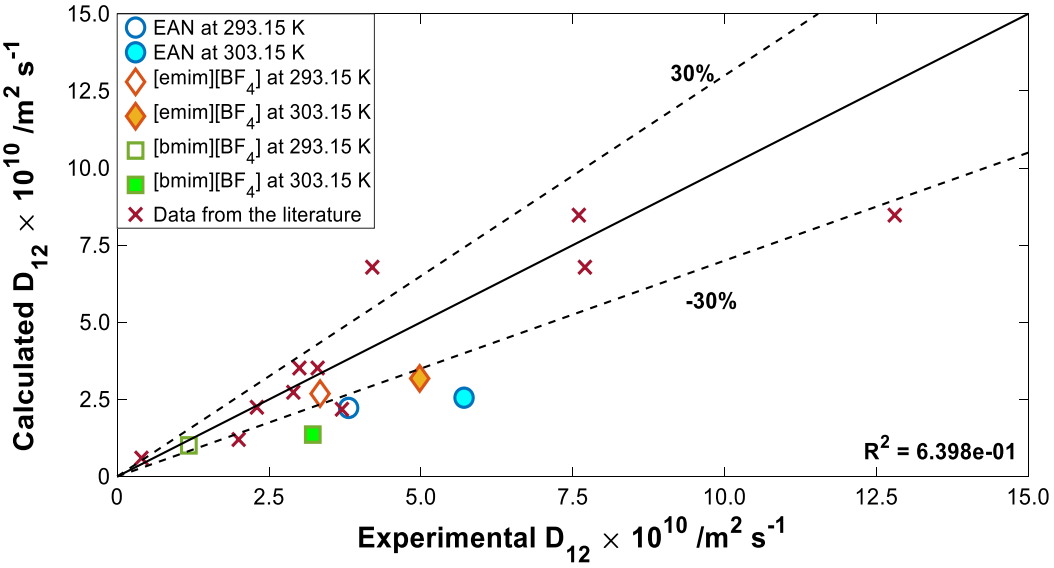

Figure V-13. Experimentally determined diffusivities versus diffusivities predicted by a modified Wilke-Chang correlation with temperature-dependent association factor.

As shown in Figures V-11 to V-13, previous correlations, which were originally developed for conventional solvents, did not perform satisfactory for ammonia diffusivity in ionic liquids. Thus, new empirical correlations have recently been proposed to describe gas diffusivity in ionic liquids [35,123,132].

Morgan et al. [35] developed a correlation, which expresses mass diffusivity as a function of the solvent viscosity and solvent and solute molar masses and molar volumes:

$$D_{12} = \lambda_0 \mu_2^{\lambda_1} M_1^{\lambda_2} M_2^{\lambda_3} \bar{V}_1^{\lambda_4} \bar{V}_2^{\lambda_5} \qquad \text{V-21}$$

where the constants λ_i are adjustable parameters. After a statistical analysis of their experimental data, Morgan et al. [35] found that not all the parameters had a significant influence on the estimation of mass diffusivity. Therefore, the authors simplified their correlation, finally arriving at an expression for diffusivity that was only a function of the viscosity of the solvent and the molar volume of the solute.

After that, Hou and Baltus [123] developed another correlation for gas diffusivities in imidazolium-based ILs using the IL viscosity, molar mass, density, and temperature:

$$D_{12} = \lambda_0 \mu_2^{\lambda_1} M_2^{\lambda_2} \rho_1^{\lambda_3} T^{\lambda_4} \qquad \text{V-22}$$

In this correlation, the effect of temperature is included explicitly and not as in the Morgan correlation that only does it implicitly in viscosity.

In another experimental study, Moganty and Baltus [132] found that their diffusivity values could not be represented by a single equation. Therefore, these authors developed two correlations on the basis of anion class.

For ionic liquids with the anion bis((trifluoromethyl)sulfonyl)imide ($[NTf2]^-$), the diffusivity was correlated with viscosity, temperature, and activation energy of viscosity, E_a^{vis}:

$$D_{12} = \lambda_0 \mu_2^{\lambda_1} \exp\left(\frac{\lambda_2 E_a^{vis}}{T}\right) \quad \text{V-23}$$

For the ionic liquids with anion other than $[NTf_2]^-$, viscosity, molecular weight, and density were found to be statistically significant in representing the gas diffusivity:

$$D_{12} = \lambda_0 \mu_2^{\lambda_1} M_2^{\lambda_2} \rho_1^{\lambda_3} \quad \text{V-24}$$

We have assessed the estimation capability of the Morgan, Hou-Baltus, and Moganty-Baltus correlations to estimate the mass diffusivity of ammonia in ionic liquids. In all cases, the results were superior to those observed for the correlations developed for conventional solvents. Furthermore, all these new correlations yield similar results for the experimental data considered here, $R^2 \approx 0.76$; ARD ≈ 22%, and MRD ≈ 62%. Although, in the particular case of the Moganty-Baltus correlation, we have observed that equation V-24 performed better than equation V-23 even for ionic liquids with the $[NTf_2]^-$ cation. Thus, we only used equation V-24 to estimate the mass diffusivity of ammonia in the ionic liquids studied when evaluating the accuracy of the Moganty-Baltus correlation. Despite their better performance, these new correlations involved a significant number of adjustable parameters if the availability of experimental data is considered. Therefore, based on these correlations, we have made some modifications in order to reduce the number of adjustable parameters. The resulting correlation is shown in equation V-25:

$$D_{12} = \frac{1.58\times10^{-3}}{\mu_2^{\lambda_1}} \left(\frac{T\bar{V}_2}{\bar{V}_1 M_2}\right)^{\lambda_2} \quad \text{V-25}$$

where λ_1, and λ_2 are the two adjustable parameters of the modified correlation.

Unlike the Morgan and Moganty-Baltus correlations (and similar to the Hou-Baltus correlation), the modified correlation explicitly correlates the mass diffusivity with temperature. It also groups the precursor properties in two terms. One term involves only the ionic liquid viscosity and the other includes, in addition to temperature, the molar volumes of ammonia and ionic liquid, and the molar mass of the latter. The value (1.58×10^{-3}) in the numerator of equation V-25 was taken from Morgan et al. [35]. We found the values of the adjustable parameters to be λ_1 = 0.7951, and λ_2 = -1.5440. The results of the modified correlation with these parameters are depicted in Figure V-14.

A glance at this figure, reveals better estimation capability that the correlations developed for conventional solvents. In this case, R^2 = 6.850e-01, ARD = 28% and MRD = 58%, results slightly higher than those of the Wilke-Chang correlation with the temperature-dependent association factor. Nonetheless, the correlation also underestimates some experimental values, especially for our diffusivity values at T = 303.15 K. This suggests that the temperature dependence of diffusivity may be somewhat stronger than that found using the modified correlation.

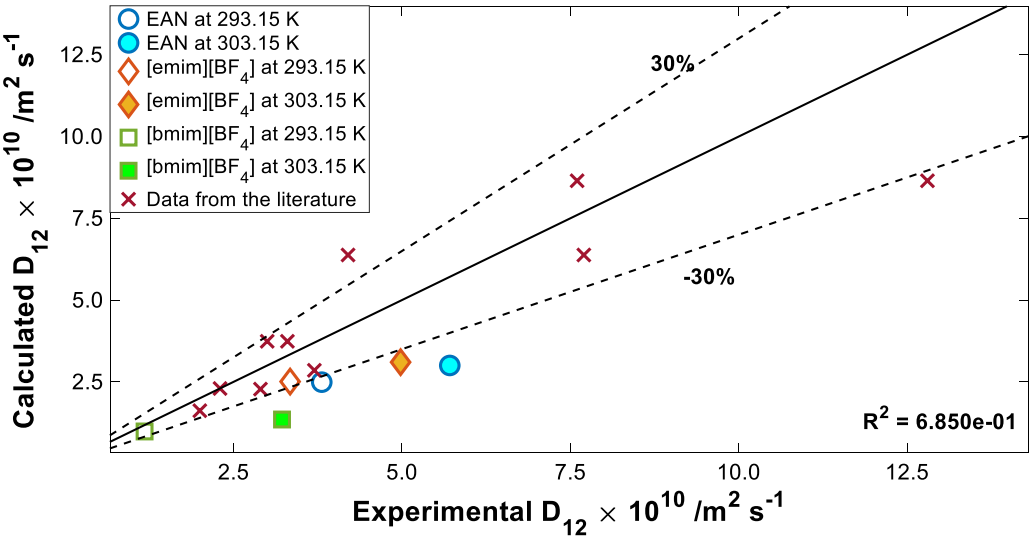

Figure V-14. Experimentally determined diffusivities versus diffusivities predicted by the modified empirical correlation.

In all the above correlations, it is apparent that there is an intrinsic relationship between the mass diffusivity of ammonia and the viscosity of the ionic liquid. To

shed some light on this topic, we have used the Hayduk and Cheng correlation [35,93,123,132]:

$$D_{12} = A\mu^{B} \qquad \text{V-26}$$

where A, and B are adjustable parameters.

Figure V-15 shows the experimental values of ammonia diffusivity as a function of the viscosity of the ionic liquid, and the fitting results using the Hayduk and Cheng correlation. We have determined the adjustable parameters for our experimental data set and found that A = 3.6858, while B = -0.7424, with R^2 = 5.276e-01, ARD = 34%, and MRD = 56%. The value of the exponent (parameter B) in the Hayduk-Cheng correlation is close to that found for the viscosity in the modified empirical correlation (0.7951). In Figure V-15, the decreasing trend of diffusivity with increasing viscosity can be clearly observed. The dependence of diffusivity on the viscosity of ionic liquids follows a negative power trend with an exponent much less than 1, which is consistent with the literature. However, the absolute value of B in this study is higher than that found for the diffusion of CO_2 in ionic liquids, which has been reported between 0.35 and 0.66 [132]. This is indicative that the mass diffusivity of ammonia has a stronger dependence on the viscosity of ionic liquids than that of CO_2.

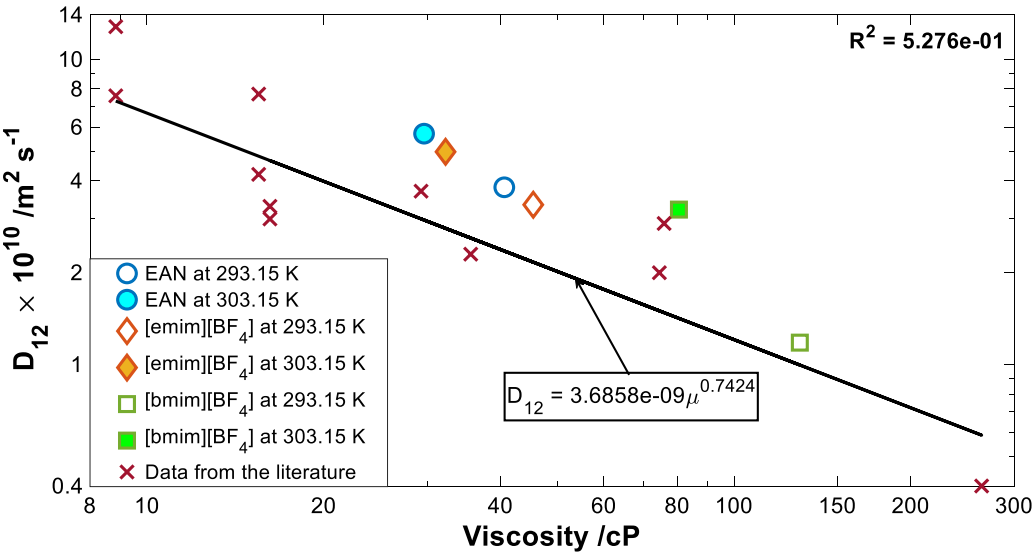

Figure V-15. Experimentally determined diffusivities as a function of viscosities of the studied ionic liquids. The solid line represents the fitting results using the Hayduk-Cheng equation.

To the best of the author's knowledge, this is the first time that these correlations have been used to estimate the mass diffusivity of ammonia in ionic liquids.

V.5 Investigation of the relevance to the performance of the absorption process of the solubility and mass diffusivity of ammonia in selected ionic liquids

This section analyzes the relevance of the solubility and mass diffusivity of ammonia in the ionic liquids selected for the absorption process based on some thermodynamic and transport properties of the studied mixtures, and the performance of an absorption cycle obtained from of a mass balance model in the components of the cycle.

V.5.1 Solubility and transport properties data for the NH_3/absorbent mixtures studied

In the literature, great attention has been paid to the investigation of the solubility of natural refrigerants in ionic liquids. However, this is not the case for the transport properties and, in particular, for the mass diffusivity of ammonia in ionic liquids, as discussed in Chapter III.

In general, transport properties determine the rates of heat and mass transfer between the refrigerant and the absorbent in the components of the absorption cycle. In particular, since mass transfer is slow compared to heat transfer, it is expected to be dominant, and it should, therefore, be more relevant predicting the performance of absorption systems [56].

Mass transfer processes are usually characterized by dimensionless numbers, such as the Schmidt number (Sc), which is defined as:

$$Sc = \frac{\mu}{\rho D_{12}} = \frac{\nu}{D_{12}} \qquad \text{V-27}$$

where μ is the dynamic viscosity, ρ the density, D_{12} the mass diffusivity, and $\nu = \frac{\mu}{\rho}$ the kinematic viscosity. This dimensionless number represents the ratio of the momentum diffusivity to mass diffusivity and is the analogue to the Prandtl number in heat transfer. The use of Sc number for the screening analysis of ILs is very convenient because it groups the viscosity and the mass diffusivity into a single term. A small value of Sc is desired, since this means that the kinematic

viscosity is small compared to the mass diffusivity, which could lead to better heat and mass transfer performance.

To calculate the Sc number for the NH_3/absorbent mixtures studied, density, viscosity and mass diffusivity data are needed. Here, the mass diffusivity data were obtained from our results using the ODI method, while, viscosity and density data were taken from the literature [74,176]. Furthermore, the viscosity and density values correspond to those of the pure ionic liquid. Therefore, the calculated Sc values can be interpreted as a limiting value for Sc.

Table V-4 lists the Schmidt numbers (Sc) and the Henry's constants (which are usually used to represent solubility data) of NH_3 into the ILs studied at 293.15 K and 303.15 K. The lower the Henry's constant (k_H) value, the greater the solubility of the refrigerant in the absorbent. Here, the k_H values for EAN were calculated following a similar procedure to that of Turnaoglu and Shiflett [39] and using our VLE data [76]. The Henry's constants for [emim][BF_4] and [bmim][BF_4] at the temperatures studied were taken from the literature [78].

It can be seen that, although the solubility of ammonia in water is comparable to that in EAN, the transport properties (represented by Sc) of water are tens of times lower than for ionic liquids. Therefore, in this comparison, we focused our analysis on the properties of the ionic liquids studied as potential absorbents for ammonia refrigerant.

Table V-4. Schmidt (Sc) numbers and Henry's constants (k_H) of NH_3 in ionic liquids: EAN, [emim][BF_4], [bmim][BF_4], at two temperatures: 293.15 K, and 303.15 K.

	T = 293.15 K		T = 303.15 K	
Absorbent	k_H / kPa	Sc	k_H / kPa	Sc
Water	73.9	707	118.17	564
EAN	56.0	23624	84.8	17380
[emim][BF_4]	610.5	24848	1099.2	17722
[bmim][BF_4]	416.2	75628	800.4	47363

Among the ionic liquids studied, the k_H values of NH_3 in EAN are much lower than in the others. It is also observed that the k_H values for [bmim][BF_4] are lower than, yet comparable to, those of [emim][BF_4]. Meanwhile, Sc values for EAN are also

lower than for the other IL studied, but unlike the k_H values, comparable to those of [emim][BF_4]. In this sense, other ILs with the same $[emim]^+$cation and different anions have been reported to show favourable kinetics behavior for ammonia absorption [28,43]. Furthermore, [bmim][BF_4] presents the least favourable transport properties, with Sc values between two and three times higher than those of EAN and [emim][BF_4] at the studied temperatures.

Analysis of the data in Table V-4 shows an opposite trend for solubility and transport properties with temperature for all ILs studied. However, the influence of temperature on the properties analyzed is different for each ionic liquid. The variation of k_H from 293.15 K to 303.15 K represents 51%, 80%, and 92% of the corresponding value at 293.15 K for EAN, [emim][BF_4], and [bmim][BF_4], respectively. In the case of the Sc values, the variations are -26%, -29%, and -37% for EAN, [emim][BF_4], and [bmim][BF_4], respectively. Therefore, the properties of [bmim][BF_4] are more sensitive to variations in temperature than the other ILs in the temperature range studied.

V.5.2 Influence of mass diffusivity in the absorption process of ammonia in the ionic liquids selected

As mentioned in Chapter I, absorption refrigeration systems using NH_3/ILs show a detrimentally high solution circulation ratio compared to the conventional NH_3/H_2O working pair. The solution circulation ratio depends on the equilibrium concentration and on the deviation from that equilibrium, due to the mass transfer resistances. In turn, the equilibrium concentration is determined by the solubility of the refrigerant in the absorbent, while the mass transfer resistances are determined by transport properties of the working mixtures such as mass diffusivity. These properties determine how much of the absorption potential can be utilized [33].

So far, researchers have placed more importance on the solubility than the mass diffusivity of the refrigerant in the absorbent. However, in practice, large deviations from steady state are frequently observed [33,53]. Furthermore, as in real absorption machines, the areas available for heat and mass transfer are limited, and therefore the residence time of the solution within the absorber, the mass diffusivity, which determines the rate of the absorption process, may play a preponderant role compared to solubility.

To illustrate this, we rely on the mass diffusivity values determined in this chapter in subsection V.3.3 using the ODI method, and also on the experiments described in Chapter II in section II.7 devoted to the determination of the absorption rate of ammonia in selected ionic liquids. Furthermore, since in general the thermodynamic and transport properties of EAN are much more favourable than those of imidazolium-based ionic liquids, we have used the latter to make the comparison.

Figure V-16 shows the observed degree of saturation that is reached during the absorption process of ammonia in [emim][BF_4] and [bmim][BF_4] at 303.15 K. Here, the degree of saturation is defined as the real concentration in the ammonia/ionic liquid solution during the absorption process over the concentration under saturated conditions (that is, the solubility of ammonia in the ILs at a given temperature and equilibrium pressure).

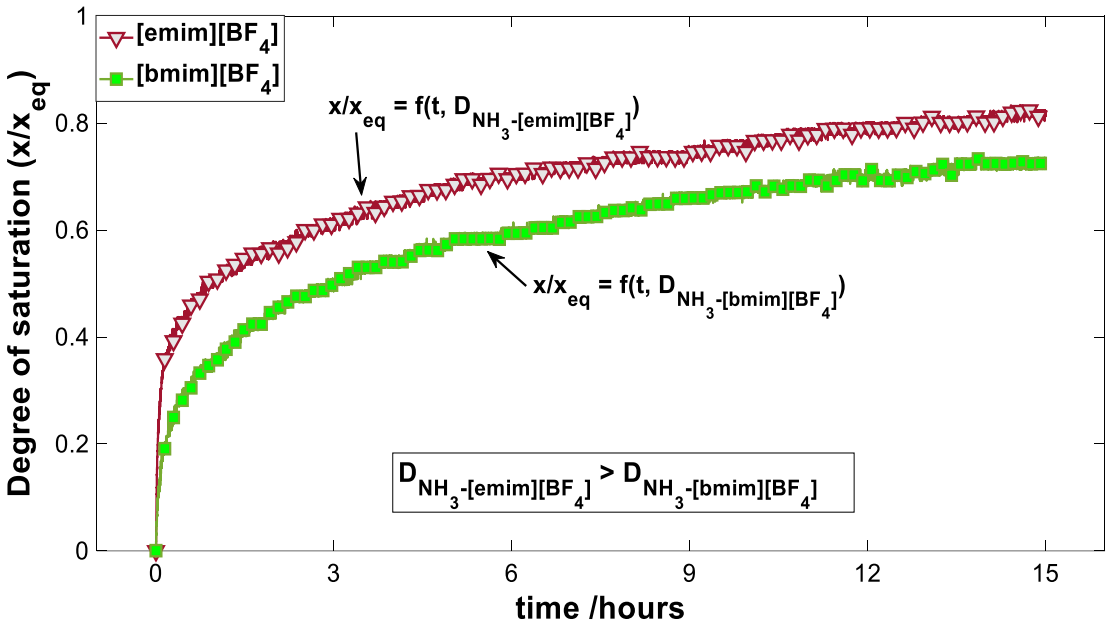

Figure V-16. Absorption completion of NH_3 in [emim][BF_4] and [bmim][BF_4] at 303.15 K.

As shown, the degree of saturation is a function of time and mass diffusivity of ammonia in the ionic liquid. Thus, the higher mass diffusivity of ammonia in [emim][BF_4] leads to a more complete absorption process than in [bmim][BF_4]. This is observed throughout the absorption process, where on average the degree of saturation in [emim][BF_4] is 10.2 percentage points higher than in [emim][BF_4], with a maximum difference of 17.9 percentage points around 55 minutes after the beginning of the absorption process. Therefore, it must be

considered that in an absorption machine, under the same operating conditions, it is easier to reach saturation at the absorber outlet, when [emim][BF_4] is used than when [bmim][BF_4] is used as absorbent for ammonia refrigerant.

Despite its importance, the degree of saturation reached by the absorbent/refrigerant solution after the absorption process is not usually considered when evaluating the thermodynamic performance of the absorption cycle. Wang et al. [47], for instance, found that the COP of an absorption heat pump using NH_3/[emim][BF_4] and NH_3/[bmim][BF_4] working pairs was quite similar, while the solution circulation ratio was considerably more favourable for NH_3/[bmim][BF_4].

However, using experimental VLE data reported by Li et al. [78] for both working pairs, and our experimental results on the degree of saturation, we found that the solution circulation ratio varies to a greater extent and in a more unfavorable manner for NH_3/[bmim][BF_4] than for NH_3/[emim][BF_4].

Table V-5 shows the degree of saturation and the corresponding solution circulation ratio at different instances during the absorption process of ammonia in [emim][BF_4] and [bmim][BF_4] at 303.15 K. The values of the solution circulation ratio (f) shown in this table were obtained from the modelling of a single stage absorption refrigeration cycle using both working pairs, based on mass balances in each component of the cycle.

Table V-5. Calculated solution circulation ratio (f) and experimental degree of saturation (x/x_eq) during the absorption process of ammonia in ionic liquids [emim][BF4] and [bmim][BF4] at 303.15 K.

time/ h	[emim][BF_4]		[bmim][BF_4]		Δx/x_eq /%	Δf/ %
	x/x_eq	f	x/x_eq	f		
0.25	0.381	30.79	0.238	39.90	60.08	-22.83
0.5	0.437	26.79	0.293	32.43	49.15	-17.39
0.75	0.482	24.32	0.325	29.22	48.31	-16.77
1	0.511	22.92	0.357	26.56	43.14	-13.70
2	0.567	20.66	0.456	20.81	24.34	-0.72
3	0.610	19.20	0.498	19.07	22.49	0.68
5	0.686	17.07	0.584	16.25	17.47	5.05
10	0.757	15.47	0.672	14.14	12.65	9.41
15	0.812	14.42	0.725	13.10	12.00	10.08

Moreover, the following assumptions and operating conditions were considered to model mass balances in the absorption cycle:

- Temperature of the solution at the outlet of the absorber, T_A = 30 ° C, which correspond to one of the experimental temperatures in this thesis.
- Temperature of the refrigerant at the outlet of the evaporator, T_E= 10°C.
- Temperature of the solution at the outlet of the generator, T_G=100°C.
- Temperature of the refrigerant at the outlet of the condenser, T_C=40°C.
- Fixed mass flow of the refrigerant at the inlet of the evaporator, 1 kg/s.
- The refrigerant leaving the condenser and the evaporator is saturated liquid and saturated vapor, respectively.

These operating conditions correspond to those used by Yokozeki and Shiflett [18,44] for other NH_3/IL-based working pairs in absorption refrigeration cycles. A comparison between our results (f = 12.85) and those reported by Yokozeki and Shiflett [44] (f = 12.98) using the VLE data reported by the these authors for the NH_3/[emim][BF_4] working pair revealed excellent agreement.

We have also determined the solution circulation ratio for the NH_3/[emim][BF_4] and NH_3/[bmim][BF_4] working pairs using VLE data from Li et al. [78], and considering that saturation is reached at the absorber outlet. In accordance with Wang et al. [47], the results show a better circulation ratio for NH_3/[bmim][BF_4] (f = 9.49) than for NH_3/[emim][BF_4] (f = 11.72). However, once we have considered the degree of saturation, which reflects the influence of mass diffusivity on the rate at which the absorption process occurs, we have found that the solution circulation ratio may be more favourable for the NH_3/[emim][BF_4].

In particular, from Table V-5 it is observed that the degree of saturation is much higher for the NH_3/[emim][BF_4] pair at the beginning of the absorption process. Consequently, the solution circulation ratio is considerably more favourable for this working pair than for the NH_3/[bmim][BF_4] pair. After three hours of the beginning of the absorption process, although the degree of saturation for the NH_3/[emim][BF_4] pair is still higher (due to the higher diffusivity) than for the NH_3/[bmim][BF_4] pair, the solution circulation ratio is more favourable for the last working pair due to its higher ammonia solubility. Despite this, the solution circulation ratio for both working pair is comparable until the end of the absorption experiments (15 hours). Thus, considering the much more favourable transport properties, [emim][BF_4] should be more suitable for its use as absorbent for ammonia in absorption refrigeration systems than [bmim][BF_4].

V.6 Conclusions

In this chapter, we have implemented an optical system based on the Mach-Zehnder interferometer to investigate the absorption process of ammonia in ionic liquids. In particular, the experimental profiles of the refractive index change, and thus, the ammonia concentration profiles in the absorbent were obtained using a processing method based on Optical Digital Interferometry. Two mass diffusion models based on a one-dimensional unsteady state diffusion equation were used to describe the ammonia mass diffusion in the ionic liquids during the absorption process. The two mass diffusion models, namely, equilibrium model and non-equilibrium model, are dissimilar in the key assumptions and boundary conditions used.

The experimental method was validated using the working pair H_2O/NH_3 as reference fluid mixture. The relative deviations obtained were around 20% and 5%, for the equilibrium and non-equilibrium mass diffusion models, respectively. Both diffusion models are capable of successfully reproducing the experimental profiles of the ammonia concentration in the absorbent. Nonetheless, the precision of the equilibrium model improves as more time passes after the start of the absorption process. While the application of non-equilibrium is restricted to short times of the absorption process in which the diffusion front does not reach the bottom of the field of vision.

A quantitative comparison between the experimental mass diffusivity and literature values was performed. Globally, a reasonable agreement is observed, although the measured values somehow overestimate the values of the literature. In all cases, the determined mass diffusivity of ammonia in the ionic liquids studied increased with temperature.

In the case of the equilibrium model, the mass diffusivity of ammonia vapor in the ionic liquids studied varies from 2.49×10^{10} m^2 s^{-1} to 9.01×10^{10} m^2 s^{-1} and follows the order: [EAN] > $[emim][BF_4]$ > $[bmim][BF_4]$.

In the case of the non-equilibrium model, the mass diffusivity of ammonia vapor in the ionic liquids studied ranges from 1.18×10^{10} m^2 s^{-1} to 5.71×10^{10} m^2 s^{-1} and follows the order: [EAN]>$[emim][BF_4]$>$[bmim][BF_4]$. Moreover, the non-

equilibrium model shows a better agreement with the literature than the equilibrium model.

The accuracy of several models and empirical correlations for the estimation of the mass diffusivity of ammonia in ionic liquid have been evaluated. Among the correlations investigated, a modified empirical correlation with R^2 = 6.850e-01, ARD = 28% and MRD = 58%, provide the best results. The mass diffusivity of NH_3 was found to have a stronger dependence on the viscosity of ionic liquids than that of CO_2.

Finally, an investigation of the relevance to the performance of the absorption process of the solubility and mass diffusivity of ammonia in selected ionic liquids studied was performed. The transport properties represented by the nondimensional number of Schmidt of water are tens of times lower than for ionic liquids studied. Among the ILs investigated, EAN shows the most favorable thermodynamic and kinetic characteristics for ammonia absorption. The properties of [bmim][BF_4] are more sensitive to variations in temperature than the other ILs in the temperature range studied.

The influence of the mass diffusivity on the absorption process, reflected by degree of saturation reached by the solution during the absorption process, was also analyzed. For the analysis, a model based on the mass balances in the components of an absorption cycle were used. The results revealed comparable solution circulation ratio for NH_3/[emim][BF_4] and NH_3/[bmim][BF_4] working pairs. Furthermore, considering the much more favourable transport properties of [emim][BF_4], it should be more suitable for ammonia absorption than [bmim][BF_4]. The analysis performed illustrates the importance of considering favourable mass diffusivity in addition to good solubility characteristics when selecting ILs as absorbents.

Chapter VI
Conclusions and Recommendations

VI.1 Conclusions

This thesis studies the absorption process of ammonia in ionic liquids for absorption refrigeration systems. It combines experimental and theoretical work to determine the time evolution of the absorption rate and the concentration profiles of ammonia refrigerant in ionic liquids using the Pressure Drop Method and Optical Digital Interferometry, respectively. These experimental data are useful for developing and validating mass transfer models during the absorption process of ammonia in ionic liquids.

For the experimental investigation, we selected three ionic liquids – EAN, [emim][BF_4] and [bmim][BF_4] – to illustrate the importance of considering mass diffusivity in addition to solubility in the screening analysis of ionic liquids as absorbents.

The experimental setup was based on the pressure drop method (PDM) to determine the time evolution of the absorption rate of ammonia in selected ionic liquids. To determine the time evolution of the absorption rate, experiments lasting 15 hours from the start of the absorption process were performed on each selected IL at two temperatures: 293.15 K and 303.15 K. The experiments were performed at infinite dilution conditions. In addition to the ILs selected, water was used as a reference to validate the PDM and determine the absorption rate.

The thermal and pressure-drop behaviours of the mixtures during the absorption process were analyzed using the raw experimental data. The rise in temperature observed during the absorption process of NH_3 in EAN was comparable to that of water, or even higher. We also recorded the temperature at different depths in the liquid phase so that we could investigate the thermal diffusivity of the mixtures. The drop in pressure during the absorption process was different for

each NH_3/IL pair analyzed. At the end of the experiments, the pressure was close to half of the initial pressure for the cases of absorption in [emim][BF_4], and [bmim][BF_4]. The pressure measurements revealed three different stages in the absorption process: incubation, transition, and linear decay.

Then, the absorption rate of NH_3 in water was determined to validate the PDM. At the very beginning of the absorption process it was observed to be around 12 g m^{-2} s^{-1}, which was in agreement with the literature. Therefore, the PDM was considered to have been validated and was used to determine the absorption rate of NH_3 in the selected IL. It was more than 20 times lower than in water and followed the order: EAN> [emim][BF_4] > [bmim][BF4].

The third chapter discussed mass diffusivity as an essential transport property in absorption refrigeration systems. It first focused on some of the main concepts of diffusion, and then the experimental measurement methods and the models for estimating this property were presented. Optical interferometry methods stand out from other methods for their non-intrusiveness in the process as well as for their high precision. Finally, we provided a review of the literature on mass diffusivity measurement and modeling in working fluid mixtures used in absorption technology. There is much less data available on the experimental diffusivity of NH_3/IL mixtures than of other mixtures of natural refrigerants/ILs. Moreover, the prediction ability of theoretical models and the empirical correlations for estimating mass diffusivity must be improved to facilitate the research into the screening analysis of ILs as absorbents.

We found that Optical Digital Interferometry (ODI) is a powerful method for studying the absorption process of NH_3 in ILs. However, it requires careful experimental procedures, familiarity with some mathematical tools, and knowledge of the essential steps so that the interferograms can be properly processed. Therefore, the method needs to be understood well before the absorption process is addressed. Therefore, we used this method to determine the mass diffusivity in binary liquid mixtures of the natural refrigerant, water, and the ionic liquid [EtOHmim][BF_4].

The mass diffusivity of water + [EtOHmim][BF_4] decreased when the ionic liquid mass fraction increased. It was found that the rate of the decrease of the mass diffusivity is essential only in regions that are IL-poor or IL-rich. The measured

mass diffusivities were described using fourth-order polynomials as a function of the IL mass fraction. The results showed an almost linear increase in the diffusion coefficient with temperature. Linearity deviated slightly as the mass fraction of the ionic liquid increased.

Four estimation models were used to describe the mass diffusivity of the mixture: Vignes, UNIDIF, modified group contribution, and cluster diffusion. With the exception of UNIDIF, the binary interaction parameters of each of these models were calculated using two different methodologies. In the first, binary parameters were determined by VLE data regression. In the second, binary parameters were treated as adjustable parameters with experimental diffusion data.

Of the four predictive models examined, the MGC model provides the best mass diffusivity estimates. The overall ARD from experimental data was 7.9% using binary interaction parameters regressed from VLE data and 2.1% using binary parameters regressed from diffusion data. It is expected that the other estimation models presented, which themselves require experimental diffusion data, can also be employed to predict the diffusivities at temperatures which are experimentally more challenging.

Finally, we leveraged the experience gained during the investigation of mass diffusivity in the aqueous ionic liquid solution to modify and adapt the ODI method so that we could study the absorption process of NH_3 in ILs. In particular, the absorption experiments based on the Pressure Drop Method and described in Chapter II, were visualized with a Mach-Zehnder interferometer, and analyzed using the ODI method.

Two mass diffusion models based on a one-dimensional unsteady state equation were used to describe the ammonia mass diffusion phenomena as a result of the absorption process. The ODI method was validated using the working pair H_2O/NH_3 as a reference fluid mixture. The relative deviations obtained were around 20% and 5% for the equilibrium and non-equilibrium models considered. Both models were capable of successfully reproducing the experimental profiles of of the ammonia concentration in the absorbent depending on the time analyzed during the absorption process.

Reasonable agreement with the literature values was observed for the NH_3/[bmim][BF_4] mixture, especially for the non-equilibrium model. The measured mass diffusivity increased with temperature. The mass diffusivity of ammonia vapor in the ionic liquids studied using the non-equilibrium model ranged from 1.18 x 10^{10} m^2 s^{-1} to 5.71 x 10^{10} m^2 s^{-1} in the order: [EAN]>[emim][BF_4]>[bmim][BF_4]. Mass-transfer coefficient values ranged from 9.98 x 10^{-7} m s^{-1} for [bmim][BF_4] at 293.15 K to 19.92 x 10^{-7} m s^{-1} for EAN at 303.15 K.

The performance of several models and empirical correlations in the estimation of the mass diffusivity of ammonia in ionic liquid was tested. Among the correlations investigated, we obtained a modified empirical correlation that provided the best results with R^2 = 6.850e-01, ARD = 28% and MRD = 58%. The mass diffusivity of NH_3 was found to have a stronger dependence on the viscosity of ionic liquids than that of CO_2.

The importance of the solubility and mass diffusivity of ammonia in the ionic liquids to the absorption process was studied. We analyzed the influence of the mass diffusivity on the absorption process, reflected by the degree of saturation reached by the solution during the absorption process. For the analysis, the model used was based on the mass balances in the components of an absorption cycle. The results revealed comparable solution circulation ratios for NH_3/[emim][BF_4] and NH_3/[emim][BF_4] working pairs. Furthermore, considering its much more favourable transport properties, [emim][BF_4] should be more suitable for ammonia absorption than [bmim][BF_4].

The results obtained in this thesis show the potential of optical digital interferometry for studying the absorption process of natural refrigerants in ionic liquids by direct visualization of the process.

Furthermore, this research is essential if we are to be able to identify, model and predict time-dependent data from the absorption process of ammonia refrigerant in ionic liquids. This thesis provides new experimental data on the mass diffusivity of natural refrigerants in ILs, information that is essential if we are to proceed to the detailed study of the heat and mass transfer performance of these working pairs and, therefore, to the proper design of IL-based absorption systems.

VI.2 Recommendations

Below there are some recommendations for improving the methodology used and taking better advantage of the capabilities of the experimental technique. They are:

1. Quantify the contributions of solubility and diffusivity to the performance of absorption refrigeration systems by implementing a heat and mass transfer model for a given absorber geometry using the determined mass diffusivity values.
2. Perform simulations of absorption cycles using NH_3/IL working pairs by varying the operating conditions of the cycle and considering the deviation from equilibrium state at the absorber outlet. Perform a sensitivity analysis of the influence of mass diffusivity on the overall performance of the absorption cycle for the NH_3/ILs working pairs studied
3. Improve the thermal design of the experimental setup
    - Design the thermal system so that heat transfer from the fluid mixture to the external thermal control circuit is one-dimensional and in the vertical direction towards the bottom of the absorption cell. Thus, a thermal diffusion layer will develop within the fluid mixture in the same direction as the mass diffusion layer, allowing a one-dimensional analysis of simultaneous heat and mass transfer. In addition to the temperature probes already installed in the absorption cell, this will ultimately facilitate the simultaneous determination of the mass and thermal diffusivities using an inverse approach.
    - Locate two additional temperature probes in the absorption cell, one at the inlet and the other at the outlet of the external thermal control circuit. In this way, the amount of heat that is extracted from the fluid mixture will be known, and the heat of absorption of the fluid mixture can be estimated.
    - Control more precisely the temperature of the absorption process by using an external thermal circuit for the cylindrical tank of ammonia vapor.
4. Use more realistic diffusion models of the absorption process
    - Use more realistic boundary conditions at the vapor-liquid interface. This can be achieved by considering a time-dependent saturation concentration instead of a constant saturation concentration when

formulating the 3rd type (Robin) boundary condition at the vapor-liquid interface for the non-equilibrium model.

- Use a maximum likelihood approach instead of a least-square method for estimating mass diffusivity, and the other fitting parameters.
- Develop a mass diffusion model that considers evaporation for volatile absorbent liquids.
- Perform simulations to estimate the influence of the meniscus shape of the vapor-liquid interface on the mass transfer mechanism.

References

[1] European Comission, An EU strategy on heating and cooling, Brussels, 2016. doi:10.1017/CBO9781107415324.004.

[2] International Renewable Energy Agency, Heating & Cooling, (2020). https://www.irena.org/heatingcooling (accessed May 2, 2020).

[3] C. Griffin, D.H. Fisher, S.A. Haider, E. Labalme, D. Saini, S. Constantino, V. Garg, M. Jain, S.R. Kapul, A. Green, G. Owen, The Cooling Imperative. Forecasting the size and source of future cooling demand, London, 2019. http://www.eiu.com/graphics/marketing/pdf/TheCoolingImperative2019.pdf.

[4] OECD/IEA, The Future of Cooling Opportunities for energy-efficient air conditioning Together Secure Sustainable, 2018. https://www.iea.org/reports/the-future-of-cooling.

[5] M. Seiler, A. Kühn, F. Ziegler, X. Wang, Sustainable cooling strategies using new chemical system solutions, Ind. Eng. Chem. Res. 52 (2013) 16519–16546. doi:10.1021/ie401297u.

[6] K.E. Herold, R. Radermarcher, S.A. Klein, Absorption chillers and heat pumps, Second edi, CRC Press, Boca Raton, FL, 2016.

[7] M. Pärssinen, M. Wahlroos, J. Manner, S. Syri, Waste heat from data centers: An investment analysis, Sustain. Cities Soc. 44 (2019) 428–444. doi:10.1016/j.scs.2018.10.023.

[8] J. Sun, L. Fu, S. Zhang, A review of working fluids of absorption cycles, Renew. Sustain. Energy Rev. 16 (2012) 1899–1906. doi:10.1016/j.rser.2012.01.011.

[9] M.U. Siddiqui, S.A.M. Said, A review of solar powered absorption systems, Renew. Sustain. Energy Rev. 42 (2015) 93–115. doi:10.1016/j.rser.2014.10.014.

[10] Y.T. Kang, Y. Kunugi, T. Kashiwagi, Review of advanced absorption cycles: Performance improvement and temperature lift enhancement, Int. J. Refrig. 23 (2000) 388–401. doi:10.1016/S0140-7007(99)00064-X.

[11] J.D. Killion, S. Garimella, A critical review of models of coupled heat and mass transfer in falling-film absorption, Int. J. Refrig. 24 (2001) 755–797. doi:10.1016/S0140-7007(00)00086-4.

[12] W. Wu, B. Wang, W. Shi, X. Li, An overview of ammonia-based absorption chillers and heat pumps, Renew. Sustain. Energy Rev. 31 (2014) 681–707. doi:10.1016/j.rser.2013.12.021.

[13] N. V. Plechkova, K.R. Seddon, Applications of ionic liquids in the chemical industry, Chem. Soc. Rev. 37 (2008) 123–150. doi:10.1039/b006677j.

[14] S.T. Handy, ed., Applications of ionic liquids in science and Technology, InTech, Rijeka, 2011.

[15] X. Zhang, D. Hu, Performance simulation of the absorption chiller using water and ionic liquid 1-ethyl-3-methylimidazolium dimethylphosphate as the working pair, Appl. Therm. Eng. 31 (2011) 3316–3321. doi:10.1016/j.applthermaleng.2011.06.011.

[16] M.G. Freire, C.M.S.S. Neves, I.M. Marrucho, J.A.P. Coutinho, A.M. Fernandes,

References

Hydrolysis of tetrafluoroborate and hexafluorophosphate counter ions in imidazolium-based ionic liquids, J. Phys. Chem. A. 114 (2010) 3744–3749. doi:10.1021/jp903292n.

[17] M. Khamooshi, K. Parham, U. Atikol, Overview of Ionic Liquids Used as Working Fluids in Absorption Cycles, Adv. Mech. Eng. 5 (2013) 620592. doi:10.1155/2013/620592.

[18] A. Yokozeki, M.B. Shiflett, Vapor-liquid equilibria of ammonia + ionic liquid mixtures, Appl. Energy. 84 (2007) 1258–1273. doi:10.1016/j.apenergy.2007.02.005.

[19] A. Cera-Manjarres, D. Salavera, A. Coronas, Vapour pressure measurements of ammonia/ionic liquids mixtures as suitable alternative working fluids for absorption refrigeration technology, Fluid Phase Equilib. 476 (2018) 48–60. doi:10.1016/j.fluid.2018.01.006.

[20] J. Salgado, T. Regueira, L. Lugo, J. Vijande, J. Fernández, J. García, Density and viscosity of three (2,2,2-trifluoroethanol + 1-butyl-3-methylimidazolium) ionic liquid binary systems, J. Chem. Thermodyn. 70 (2014) 101–110. doi:10.1016/j.jct.2013.10.027.

[21] Y. Zhao, J. Zhao, Y. Huang, Q. Zhou, X. Zhang, S. Zhang, Toxicity of ionic liquids: Database and prediction via quantitative structure-activity relationship method, J. Hazard. Mater. 278 (2014) 320–329. doi:10.1016/j.jhazmat.2014.06.018.

[22] A. Romero, A. Santos, J. Tojo, A. Rodríguez, Toxicity and biodegradability of imidazolium ionic liquids, J. Hazard. Mater. 151 (2008) 268–273. doi:10.1016/j.jhazmat.2007.10.079.

[23] S. Aparicio, M. Atilhan, F. Karadas, Thermophysical properties of pure ionic liquids: Review of present situation, Ind. Eng. Chem. Res. 49 (2010) 9580–9595. doi:10.1021/ie101441s.

[24] M. Villanueva, A. Coronas, J. García, J. Salgado, Thermal stability of ionic liquids for their application as new absorbents, Ind. Eng. Chem. Res. 52 (2013) 15718–15727. doi:10.1021/ie401656e.

[25] D.G. Archer, J.A. Widegren, D.R. Kirklin, J.W. Magee, Enthalpy of solution of 1-Octyl-3-methylimidazolium tetrafluoroborate in water and in aqueous sodium fluoride, J. Chem. Eng. Data. 50 (2005) 1484–1491. doi:10.1021/je050136i.

[26] Y. Jo, S. Kim, Y.K. Joshi, A.G. Fedorov, P.A. Kohl, Thermodynamic analysis of an absorption refrigeration system with ionic-liquid/refrigerant mixture as a working fluid, Energy. 44 (2012) 1005–1016. doi:10.1016/j.energy.2012.04.048.

[27] S.K. Swarnkar, S. Srinivasa Murthy, R.L. Gardas, G. Venkatarathnam, Performance of a vapour absorption refrigeration system operating with ionic liquid-ammonia combination with water as cosolvent, Appl. Therm. Eng. 72 (2014) 250–257. doi:10.1016/j.applthermaleng.2014.06.020.

[28] H.M. Ariyadi, A. Cera-Manjarres, A. Coronas, Absorption Behaviour and Diffusivity of Ammonia in Ionic Liquids, in: 5th IIR Int. Conf. Thermophys. Prop. Transf. Process. Refrig., International Institute of Refrigeration, Seoul, South Korea, 2017: pp. 1–8. doi:10.18462/iir.tptpr.2017.0129.

[29] M. He, S. Peng, X. Liu, P. Pan, Y. He, Diffusion coefficients and Henry's constants of hydrofluorocarbons in [HMIM][Tf2N], [HMIM][TfO], and [HMIM][BF4], J. Chem. Thermodyn. 112 (2017) 43–51. doi:10.1016/j.jct.2017.04.009.

[30] D.S. Ayou, M.R. Currás, D. Salavera, J. García, J.C. Bruno, A. Coronas, Performance analysis of absorption heat transformer cycles using ionic liquids based on imidazolium cation as absorbents with 2,2,2-trifluoroethanol as refrigerant, Energy Convers. Manag. 84 (2014) 512–523. doi:10.1016/j.enconman.2014.04.077.

[31] H.M. Ariyadi, Thermodynamic study on absorption refrigeration systems using ammonia/ionic liquid working pairs, Universitat Rovira i Virgili, 2016.

[32] F.F. Zhang, F.F. Zheng, Y.L. Yin, X.H. Wu, G. Chen, Falling film flow of [EMIm]Ac ionic liquid aqueous solution on horizontal tubes considering the Marangoni effect, Exp. Therm. Fluid Sci. 107 (2019) 130–139. doi:10.1016/j.expthermflusci.2019.05.010.

[33] R. Kühn, T. Meyer, F. Ziegler, Experimental investigation of ionic liquids as substitute for lithium bromide in water absorption chillers, Energy. 205 (2020) 117990. doi:10.1016/j.energy.2020.117990.

[34] F. Ziegler, Options for New Working Pairs-Perceptions and Misperceptions, in: Int. Sorption Heat Pump Conf., University of Maryland, Department of Mechanical Engineering, Center for Environmental Energy Engineering - United States/United States, College Park, MD, USA, 2014.

[35] D. Morgan, L. Ferguson, P. Scovazzo, Diffusivities of Gases in Room-Temperature Ionic Liquids: Data and Correlations Obtained Using a Lag-Time Technique, Ind. Eng. Chem. Res. 44 (2005) 4815–4823. doi:10.1021/ie048825v.

[36] J. Bedia, J. Palomar, M. Gonzalez-Miquel, F. Rodriguez, J.J. Rodriguez, Screening ionic liquids as suitable ammonia absorbents on the basis of thermodynamic and kinetic analysis, Sep. Purif. Technol. 95 (2012) 188–195. doi:10.1016/j.seppur.2012.05.006.

[37] M. Krannich, F. Heym, A. Jess, Characterization of Six Hygroscopic Ionic Liquids with Regard to Their Suitability for Gas Dehydration: Density, Viscosity, Thermal and Oxidative Stability, Vapor Pressure, Diffusion Coefficient, and Activity Coefficient of Water, J. Chem. Eng. Data. 61 (2016) 1162–1176. doi:10.1021/acs.jced.5b00806.

[38] M. Shokouhi, H. Sakhaeinia, A.H. Jalili, A.T. Zoghi, A. Mehdizadeh, Experimental diffusion coefficients of CO2 and H2S in some ionic liquids using semi-infinite volume method, J. Chem. Thermodyn. 133 (2019) 300–311. doi:10.1016/j.jct.2019.02.022.

[39] T. Turnaoglu, M.B. Shiflett, 110th Anniversary: The First Thermodynamic and Kinetic Analysis of Ammonia in Imidazolium-Based Ionic Liquids Using a Gravimetric Microbalance, Ind. Eng. Chem. Res. 58 (2019) 4644–4655. doi:10.1021/acs.iecr.9b00274.

[40] M.A. Rocha, M.B. Shiflett, Water Sorption and Diffusivity in [C2C1im][BF4], [C4C1im][OAc], and [C4C1im][Cl], Ind. Eng. Chem. Res. 58 (2019) 1743–1753. doi:10.1021/acs.iecr.8b05689.

[41] M.J.W. Frank, J.A.M. Kuipers, W.P.M. van Swaaij, Diffusion Coefficients and Viscosities of CO2 + H2O, CO2 + CH3OH, NH3 + H2O, and NH3 + CH3OH Liquid Mixtures, J. Chem. Eng. Data. 41 (1996) 297–302. doi:10.1021/je950157k.

[42] A. Cera-Manjarres, Experimental determination and modelling of thermophysical properties of ammonia/ionic liquid mixtures for absorption refrigeration systems, Universitat Rovira i Virgili, 2015.

References

[43] M. Wang, L. He, C.A. Infante Ferreira, Ammonia absorption in ionic liquids-based mixtures in plate heat exchangers studied by a semi-empirical heat and mass transfer framework, Int. J. Heat Mass Transf. 134 (2019) 1302–1317. doi:10.1016/j.ijheatmasstransfer.2019.02.063.

[44] A. Yokozeki, M.B. Shiflett, Ammonia Solubilities in room temperatures ionic liquids, Ind. Eng. Chem. Res. 46 (2007) 1605–1610.

[45] D. Zheng, L. Dong, W. Huang, X. Wu, N. Nie, A review of imidazolium ionic liquids research and development towards working pair of absorption cycle, Elsevier, 2014. doi:10.1016/j.rser.2014.04.046.

[46] L. Dong, D. Zheng, N. Nie, Y. Li, Performance prediction of absorption refrigeration cycle based on the measurements of vapor pressure and heat capacity of H2O + [DMIM] DMP system, Appl. Energy. 98 (2012) 326–332. doi:10.1016/j.apenergy.2012.03.044.

[47] M. Wang, C.A. Infante Ferreira, Absorption heat pump cycles with NH3– ionic liquid working pairs, Appl. Energy. 204 (2017) 819–830. doi:10.1016/j.apenergy.2017.07.074.

[48] W. Wu, H. Zhang, T. You, X. Li, Thermodynamic Investigation and Comparison of Absorption Cycles Using Hydrofluoroolefins and Ionic Liquid, Ind. Eng. Chem. Res. 56 (2017) 9906–9916. doi:10.1021/acs.iecr.7b02343.

[49] M. Wang, T.M. Becker, C.A.I. Ferreira, Assessment of vapor–liquid equilibrium models for ionic liquid based working pairs in absorption cycles, Int. J. Refrig. 87 (2018) 10–25. doi:10.1016/j.ijrefrig.2017.09.021.

[50] A. Yokozeki, Theoretical performances of various refrigerant-absorbent pairs in a vapor-absorption refrigeration cycle by the use of equations of state, Appl. Energy. 80 (2005) 383–399. doi:10.1016/j.apenergy.2004.04.011.

[51] A. Yokozeki, M.B. Shiflett, Ammonia solubilities in room-temperature ionic liquids, Ind. Eng. Chem. Res. 46 (2007) 1605–1610. doi:10.1021/ie061260d.

[52] A. Yokozeki, M.B. Shiflett, Water solubility in ionic liquids and application to absorption cycles, Ind. Eng. Chem. Res. 49 (2010) 9496–9503. doi:10.1021/ie1011432.

[53] C. Römich, N. Merkel, N. Schaber, T. Schubert, M. Koch, A comparison between lithium bromide - water and ionic liquid - water as working solution for absorption refrigeration cycles, in: Proceeding 23rd IIR, International Institute of Refrigeration, Prague, Czech republic, 2011: p. 287.

[54] A. Kühn, M. Seiler, M. Radspieler, O. Kotenko, Ionic liquids as new absorbents for absorption chillers and heat pumps, in: A. Kühn (Ed.), Therm. Driven Heat Pumps Heat. Cool., Deutsche Nationalbibliothek, Berlin, 2013: p. 215.

[55] T. Meyer, U. Schulze, Experimental Data on Mutual Mass Diffusivities of Binary Mixtures of Ethanol and [EMIM][DEP], Chem. Eng. Technol. 42 (2019) 1414–1420. doi:10.1002/ceat.201900027.

[56] T. Meyer, F. Ziegler, A characteristic mass fraction difference in absorption chillers, Int. J. Refrig. 97 (2019) 67–72. doi:10.1016/j.ijrefrig.2018.09.021.

[57] M. Kojima, T. Kashiwagi, Mass Diffusivity Measurements for Ammonia-Vapour Absorption Processes, in: 19th Int. Congr. Refrig., 1995: pp. 353–360.

[58] I. Mahmoud, Mass and heat transfer during absorption of ammonia vapour into

ammonia-water mixture, Saga University, 2004. doi:10.1016/j.ijheatmasstransfer.2003.12.014.

[59] H. Mustafa, Experimental and Analytical Investigation of Ammonia Vapor Absorption Into a Ammonia-Water Solution, Saga University, 2007.

[60] S.R. Etminan, B.B. Maini, Z. Chen, Determination of mass transfer parameters in solvent-based oil recovery techniques using a non-equilibrium boundary condition at the interface, Fuel. 120 (2014) 218–232. doi:10.1016/j.fuel.2013.11.027.

[61] H.M. Ariyadi, A. Coronas, Absorption Process Behavior and Theoretical Performance of Ammonia/Ionic Liquid Mixtures for Absorption Refrigeration Applications, in: Int. Sorption Heat Pump Conf., 2017: pp. 1–2.

[62] A. Yokozeki, Time-dependent behaviour of gas absorption in lubricant oil, Int. J. Refrig. 25 (2002) 695–704. doi:10.1016/S0140-7007(01)00066-4.

[63] P.K. Panigrahi, K. Muralidhar, Imaging Heat and Mass Transfer Processes: Visualization and Analysis, Springer, 2012. doi:DOI 10.1007/978-1-4614-4791-7.

[64] S. Verma, Y.M. Joshi, K. Muralidhar, Optical interferometers: Principles and applications in transport phenomena, Interferom. Princ. Appl. (2012) 353–414. doi:10.1086/652467.

[65] A. Mialdun, V. Shevtsova, Measurement of the Soret and diffusion coefficients for benchmark binary mixtures by means of digital interferometry, J. Chem. Phys. 134 (2011) 1–12. doi:10.1063/1.3546036.

[66] A.H. Harvey, S.G. Kaplan, J.H. Burnett, Effect of dissolved air on the density and refractive index of water, Int. J. Thermophys. 26 (2005) 1495–1514. doi:10.1007/s10765-005-8099-0.

[67] C. Wylock, S. Dehaeck, T. Cartage, P. Colinet, B. Haut, Experimental study of gas-liquid mass transfer coupled with chemical reactions by digital holographic interferometry, Chem. Eng. Sci. 66 (2011) 3400–3412. doi:10.1016/j.ces.2011.01.024.

[68] MATLAB and Image Processing Toolbox Release 2019b, The MathWorks, Inc., Natick, Massachusetts, United States., (n.d.).

[69] V. Sechenyh, J.C. Legros, A. Mialdun, J.M. Ortiz De Zárate, V. Shevtsova, Fickian Diffusion in Ternary Mixtures Composed by 1,2,3,4-Tetrahydronaphthalene, Isobutylbenzene, and n-Dodecane, J. Phys. Chem. B. 120 (2016) 535–548. doi:10.1021/acs.jpcb.5b11143.

[70] A. Mialdun, V. Yasnou, V. Shevtsova, Measurement of isothermal diffusion coefficients in ternary mixtures using counter flow diffusion cell, Comptes Rendus - Mec. 341 (2013) 462–468. doi:10.1016/j.crme.2013.02.001.

[71] T. Janzen, S. Zhang, A. Mialdun, G. Guevara-Carrion, J. Vrabec, M. He, V. Shevtsova, Mutual diffusion governed by kinetics and thermodynamics in the partially miscible mixture methanol + cyclohexane, Phys. Chem. Chem. Phys. 19 (2017) 31856–31873. doi:10.1039/c7cp06515a.

[72] M. Allen, D.F. Evans, R. Lumry, Thermodynamic properties of the ethylammonium nitrate + water system: Partial molar volumes, heat capacities, and expansivities, J. Solution Chem. 14 (1985) 549–560. doi:10.1007/BF00649520.

[73] A. Mariani, M. Campetella, C. Fasolato, M. Daniele, F. Capitani, L. Bencivenni, P. Postorino, S. Lupi, R. Caminiti, L. Gontrani, A joint experimental and

computational study on ethylammonium nitrate-ethylene glycol 1:1 mixture. Structural, kinetic, dynamic and spectroscopic properties, J. Mol. Liq. 226 (2017) 2–8. doi:10.1016/j.molliq.2016.08.043.

[74] R. Zarrougui, M. Dhahbi, D. Lemordant, Transport and thermodynamic properties of ethylammonium nitrate-water binary mixtures: Effect of temperature and composition, J. Solution Chem. 44 (2015) 686–702. doi:10.1007/s10953-014-0283-z.

[75] J.J. Parajó, M. Villanueva, L.M. Varela, J. Salgado, Ecotoxicity of EAN and Doped EAN Ionic Liquids, Proceedings. 9 (2019) 56. doi:10.3390/ecsoc-22-05793.

[76] S.A. Capelo-Avilés, amoniaco / nitrato de etilamonio y amoniaco / nitrato de propilamonio para aplicación en sistemas de refrigeración Ingeniería Termodinámica de fluidos, Universitat Rovira i Virgili, 2019.

[77] Y.J. Kim, S. Kim, Y.K. Joshi, A.G. Fedorov, P.A. Kohl, Thermodynamic analysis of an absorption refrigeration system with ionic-liquid/refrigerant mixture as a working fluid, Energy. 44 (2012) 1005–1016. doi:10.1016/j.energy.2012.04.048.

[78] G. Li, Q. Zhou, X. Zhang, L. Wang, S. Zhang, J. Li, Solubilities of ammonia in basic imidazolium ionic liquids, Fluid Phase Equilib. 297 (2010) 34–39. doi:10.1016/j.fluid.2010.06.005.

[79] C.M.S.S. Neves, K.A. Kurnia, J.A.P. Coutinho, I.M. Marrucho, J.N.C. Lopes, M.G. Freire, L.P.N. Rebelo, Systematic study of the thermophysical properties of imidazolium-based ionic liquids with cyano-functionalized anions, J. Phys. Chem. B. 117 (2013) 10271–10283. doi:10.1021/jp405913b.

[80] I. Mahmoud, K. Ishida, M. Monde, Analysis of ammonia vapor absorption into ammonia water mixtures: Mass diffusion flux, Heat Mass Transf. Waerme- Und Stoffuebertragung. 41 (2005) 875–889. doi:10.1007/s00231-004-0583-8.

[81] H. Mustafa, M. Monde, Effect of pressure on mass absorption in an ammonia-water absorption system, Heat Mass Transf. Waerme- Und Stoffuebertragung. 44 (2007) 43–50. doi:10.1007/s00231-006-0215-6.

[82] E. V Richards, Design of an apparatus to measure gas solubilities in polymers, University of Toronto, 2001.

[83] R. Tillner-Roth, D.G. Friend, A Helmholtz Free Energy Formulation of the Thermodynamic Properties of the Mixture {Water + Ammonia}, J. Phys. Chem. Ref. Data. 27 (1998) 63–96.

[84] Y.P. Zhang, C.L. Hyndman, B.B. Maini, Measurement of gas diffusivity in heavy oils, J. Pet. Sci. Eng. 25 (2000) 37–47. doi:10.1016/S0920-4105(99)00031-5.

[85] M. Jamialahmadi, M. Emadi, H. Müller-Steinhagen, Diffusion coefficients of methane in liquid hydrocarbons at high pressure and temperature, J. Pet. Sci. Eng. 53 (2006) 47–60. doi:10.1016/j.petrol.2006.01.011.

[86] E. Behzadfar, S.G. Hatzikiriakos, Diffusivity of CO2 in Bitumen: Pressure-decay measurements coupled with rheometry, Energy and Fuels. 28 (2014) 1304–1311. doi:10.1021/ef402392r.

[87] F. Du, H. Ma, Y. Gu, Three different periods of CO2 dissolution into a light crude oil, Can. J. Chem. Eng. 97 (2019) 330–343. doi:10.1002/cjce.23204.

[88] MATLAB and Statistics and Machine Learning Toolbox, Release 2018a, The MathWorks, Inc., Natick, Massachusetts, United Sates., (n.d.).

[89] J. Crank, The Mathematics of Diffusion, Second Edi, Oxford University Press, Oxford, 1975. doi:10.1115/1.3245200.

[90] S.P. Cadogan, Diffusion of CO2 in fluids relevant to carbon capture, utilisation and storage, Imperial College London Qatar, 2015.

[91] E.L. Cussler, Diffusion. Mass Transfer in Fluid Systems, Third Edit, Cambridge University Press, Cambridge, 2009. doi:10.1192/bjp.112.483.211-a.

[92] D. Bosse, Diffusion, Viscosity, and Thermodynamics in Liquid Systems, Technical University of Kaiserslautern, 2005.

[93] B.E. Poling, J.M. Prausnitz, J.P. O'Connell, The Properties of Gases and Liquids, Fifth, McGraw-Hill, New York, 2001.

[94] D.W. Green, R.H. Perry, Perry's Chemical Engineers' Handbook, 8th Editio, The McGraw-Hill Companies, Inc., New York, NY, 2008.

[95] R. Taylor, R. Krishna, Multicomponent Mass Transfer, John Wiley & Sons, Inc., New York, NY, 1993. doi:10.1016/b978-0-444-41326-0.50014-9.

[96] R.K. Ghai, H. Ertl, F.A.L. Dullien, Liquid diffusion of nonelectrolytes: Part I, AIChE J. 19 (1973) 881–900. doi:10.1002/aic.690190502.

[97] E.L. Cussler, Diffusion: Mass Transfer in Fluid Systems, 3rd ed., Cambridge University Press, 2009.

[98] R. Taylor, H.A. Koodman, Composition Derivatives of Activity Coefficient Models (For the Estimation of Thermodynamic Factors in Diffusion), Chem. Eng. Commun. 102 (1991) 87–106. doi:10.1080/00986449108910851.

[99] M.A. Siddiqi, K. Lucas, Correlations for prediction of diffusion in liquids, Can. J. Chem. Eng. 64 (1986) 839–843. doi:10.1002/cjce.5450640519.

[100] L.S. Darken, Diffusion, Mobility and Their Interrelation through Free Energy in Binary Metallic Systems, Trans. AIME. 175 (1948) 148–201.

[101] A. Vignes, Diffusion in binary solutions: Variation of Diffusion Coefficient with Composition, Ind. Eng. Chem. Fundam. 5 (1966) 189–199. doi:10.1021/i160018a007.

[102] E.L. Cussler, Cluster Diffusion in Liquids, AIChE J. 26 (1980) 43–51.

[103] Y. Hsu, Y. Chen, Correlation of the mutual diffusion coefficients of binary liquid mixtures, Fluid Phase Equilib. 152 (1998) 149–168.

[104] A. Kamgar, N. Hamedi, S. Mohsenpour, M.R. Rahimpour, Investigation of using different thermodynamic models on prediction ability of mutual diffusion coefficient model, J. Mol. Liq. 243 (2017) 781–789. doi:10.1016/j.molliq.2017.08.069.

[105] W. Chen, B. Zhang, Z. Liu, M. Zhao, Z. Miao, Investigation of the mutual diffusion coefficients of [mmim] DMP/H2O and [mmim]DMP/CH3OH at atmospheric pressure, Int. J. Heat Mass Transf. 111 (2017) 559–569. doi:10.1016/j.ijheatmasstransfer.2017.04.025.

[106] H.A. Every, A.G. Bishop, D.R. MacFarlane, G. Orädd, M. Forsyth, Transport properties in a family of dialkylimidazolium ionic liquids, Phys. Chem. Chem. Phys. 6 (2004) 1758–1765. doi:10.1039/b315813f.

[107] M. Moreno, M. Montanino, M. Carewska, G.B. Appetecchi, S. Jeremias, S. Passerini, Water-soluble, triflate-based, pyrrolidinium ionic liquids, Electrochim.

Acta. 99 (2013) 108–116. doi:10.1016/j.electacta.2013.03.046.

[108] O. Suárez-Iglesias, I. Medina, C. Pizarro, J.L. Bueno, Limiting diffusion coefficients of ethyl benzoate, benzylacetone, and eugenol in carbon dioxide at supercritical conditions, J. Chem. Eng. Data. 53 (2008) 779–784. doi:10.1021/je700646e.

[109] H. Guo, Y. Chen, W. Lu, L. Li, M. Wang, In situ Raman spectroscopic study of diffusion coefficients of methane in liquid water under high pressure and wide temperatures, Fluid Phase Equilib. 360 (2013) 274–278. doi:10.1016/j.fluid.2013.09.051.

[110] M.J. Assael, A.R.H. Goodwin, V. Vesovic, W.A. Wakeham, Experimental Thermodynamics Volume IX Advances in Transport Properties of Fluids, Royal Society of Chemistry, Cambridge, 2014.

[111] W.S. Price, Pulsed-field gradient nuclear magnetic resonance as a tool for studying translational diffusion: Part 1. Basic theory, Concepts Magn. Reson. 9 (1997) 299–336. doi:10.1002/(sici)1099-0534(1997)9:5<299::aid-cmr2>3.3.co;2-2.

[112] C.A.N. de Castro, E. Langa, A.L. Morais, M.L.M. Lopes, M.J.V. Lourenço, F.J.V. Santos, M.S.C.S. Santos, J.N.C. Lopes, H.I.M. Veiga, M. Macatrão, J.M.S.S. Esperança, C.S. Marques, L.P.N. Rebelo, C.A.M. Afonso, Studies on the density, heat capacity, surface tension and infinite dilution diffusion with the ionic liquids [C4mim][NTf2], [C4mim][dca], [C2mim][EtOSO3] and [Aliquat][dca], Fluid Phase Equilib. 294 (2010) 157–179. doi:10.1016/j.fluid.2010.03.010.

[113] I.M.J.J. Van de Ven-Lucassen, F.G. Kieviet, P.J.A.M. Kerkhof, Fast and Convenient Implementation of the Taylor Dispersion Method, J. Chem. Eng. Data. 40 (1995) 407–411. doi:10.1021/je00018a008.

[114] V. Sechenyh, J.C. Legros, V. Shevtsova, Development and validation of a new setup for measurements of diffusion coefficients in ternary mixtures using the Taylor dispersion technique, Comptes Rendus - Mec. 341 (2013) 490–496. doi:10.1016/j.crme.2013.02.004.

[115] A. Alizadeh, C.A. Nieto de Castro, W.A. Wakeham, The theory of the Taylor dispersion technique for liquid diffusivity measurements, Int. J. Thermophys. 1 (1980) 243–284. doi:10.1007/BF00517126.

[116] A. Mialdun, V. Sechenyh, J.C. Legros, J.M. Ortiz De Zárate, V. Shevtsova, Investigation of Fickian diffusion in the ternary mixture of 1,2,3,4-tetrahydronaphthalene, isobutylbenzene, and dodecane, J. Chem. Phys. 139 (2013) 104903. doi:10.1063/1.4820357.

[117] A. Leipertz, A.P. Fröba, Diffusion Measurements in Fluids by Dynamic Light Scattering, in: P. Heitjans, J. Kärger (Eds.), Diffus. Condens. Matter-Methods, Mater. Model., Springer, Berlin, 2005: pp. 581–620.

[118] T.M. Koller, A. Heller, M.H. Rausch, P. Wasserscheid, I.G. Economou, A.P. Fröba, Mutual and Self-Diffusivities in Binary Mixtures of [EMIM][B(CN)4] with Dissolved Gases by Using Dynamic Light Scattering and Molecular Dynamics Simulations, J. Phys. Chem. B. 119 (2015) 8583–8592. doi:10.1021/acs.jpcb.5b02659.

[119] M.H. Rausch, A. Heller, J. Herbst, T.M. Koller, M. Bahlmann, P.S. Schulz, P. Wasserscheid, A.P. Fröba, Mutual and thermal diffusivity of binary mixtures of the ionic liquids [BMIM][C(CN)3] and [BMIM][B(CN)4] with dissolved CO2 by dynamic light scattering, J. Phys. Chem. B. 118 (2014) 4636–4646. doi:10.1021/jp501973s.

[120] International Union of Pure and Applied Chemistry, Experimental Thermodynamics Volume IX : Advances in Transport Properties of Fluids, The Royal Society of Chemistry, Cambridge, 2014. doi:10.1039/9781782625254.

[121] M.H. Rausch, J. Lehmann, A. Leipertz, A.P. Fröba, Mutual diffusion in binary mixtures of ionic liquids and molecular liquids by dynamic light scattering (DLS), Phys. Chem. Chem. Phys. 13 (2011) 9525–9533.

[122] D.G. Miller, The History of interferometry for measuring diffusion coefficients, J. Solution Chem. 43 (2014) 6–25. doi:10.1007/s10953-014-0132-0.

[123] Y. Hou, R.E. Baltus, Experimental measurement of the solubility and diffusivity of CO2 in room-temperature ionic liquids using a transient thin-liquid-film method, Ind. Eng. Chem. Res. 46 (2007) 8166–8175. doi:10.1021/ie070501u.

[124] D. Camper, C. Becker, C. Koval, R. Noble, Diffusion and Solubility Measurements in Room Temperature Ionic Liquids, Ind. Eng. Chem. Res. 45 (2006) 445–450. doi:10.1021/ie0506668.

[125] D. Ambrosini, D. Paoletti, N. Rashidnia, Overview of diffusion measurements by optical techniques, Opt. Lasers Eng. 46 (2008) 852–864. doi:10.1016/j.optlaseng.2008.06.008.

[126] D.G. Miller, J.G. Albright, Optical methods, in: W.A. Wakeham, A. Nagashima, J. V. Sengers (Eds.), Meas. Transp. Prop. Fluids, Blackwell Scientific Publication;, Oxford, 1991: pp. 272–294.

[127] J.F. Torres, A. Komiya, E. Shoji, J. Okajima, S. Maruyama, Development of phase-shifting interferometry for measurement of isothermal diffusion coefficients in binary solutions, Opt. Lasers Eng. 50 (2012) 1287–1296. doi:10.1016/j.optlaseng.2012.03.006.

[128] G.R. Toker, Holographic Interferometry- A Mach-Zehnder Approach, CRC Press, Taylor & Francis Group, LLC, Boca Raton, FL, 2012. doi:10.1017/CBO9781107415324.004.

[129] F. Dubois, L. Joannes, O. Dupont, J.L. Dewandel, J.C. Legros, An integrated optical set-up for fluid-physics experiments under microgravity conditions, Meas. Sci. Technol. 10 (1999) 934–945. doi:10.1088/0957-0233/10/10/314.

[130] J. Colombani, J. Bert, Holographic interferometry for the study of liquids, J. Mol. Liq. 134 (2007) 8–14. doi:10.1016/j.molliq.2006.12.013.

[131] F. Mayinger, O. Feldmann, Optical Measurements: Techniques and Applications, Second, Springer-Verlag Berlin Heidelberg GmbH, Berlin, 2001. doi:10.1007/978-3-642-56443-7_3.

[132] S.S. Moganty, R.E. Baltus, Diffusivity of Carbon Dioxide in Room-Temperature Ionic Liquids, Ind. Eng. Chem. Res. 49 (2010) 9370–9376. doi:10.1021/ie101260j.

[133] M.F. Friedrich, S. Kokolakis, M. Lucas, P. Claus, Measuring Diffusion and Solubility of Slightly Soluble Gases in [CnMIM][NTf2] Ionic Liquids, J. Chem. Eng. Data. 61 (2016) 1616–1624. doi:10.1021/acs.jced.5b00990.

[134] L.F. Zubeir, T.M.J. Nijssen, T. Spyriouni, J. Meuldijk, J.R. Hill, M.C. Kroon, Carbon Dioxide Solubilities and Diffusivities in 1-Alkyl-3-methylimidazolium Tricyanomethanide Ionic Liquids: An Experimental and Modeling Study, J. Chem. Eng. Data. 61 (2016) 4281–4295. doi:10.1021/acs.jced.6b00657.

[135] A. Akgerman, J.L. Gainer, Diffusion of Gases in Liquids, Ind. Eng. Chem. Fundam.

11 (1972) 373–379. doi:10.1021/i160043a016.

[136] A. Akgerman, J.L. Gainer, Predicting Gas-Liquid Diffusivities, J. Chem. Eng. Data. 17 (1972) 372–377. doi:10.1021/je60054a008.

[137] D.S. Abrams, J.M. Prausnitz, Statistical Thermodynamics of Liquid Mixtures : A New txpression for the Excess Gibbs Energy of Partly or Completely Miscible Systems, AIChE J. 21 (1975) 116–128.

[138] Ionic Liquids Database - ILThermo (v2.0), NIST Stand. Ref. Database #147. (n.d.). https://ilthermo.boulder.nist.gov/ (accessed November 20, 2020).

[139] M.B. Shiflett, A. Yokozeki, Solubilities and diffusivities of carbon dioxide in ionic liquids: [bmim][PF6] and [bmim][BF4], Ind. Eng. Chem. Res. 44 (2005) 4453–4464. doi:10.1021/ie058003d.

[140] M.B. Shiflett, A. Yokozeki, Solubility and diffusivity of hydrofluorocarbons in room-temperature ionic liquids, AIChE J. 52 (2006) 1205–1219. doi:10.1002/aic.10685.

[141] M.B. Shiflett, M.A. Harmer, C.P. Junk, A. Yokozeki, Solubility and diffusivity of difluoromethane in room-temperature ionic liquids, J. Chem. Eng. Data. 51 (2006) 483–495. doi:10.1021/je050386z.

[142] A.H. Jalili, A. Mehdizadeh, M. Shokouhi, A.N. Ahmadi, M. Hosseini-Jenab, F. Fateminassab, Solubility and diffusion of CO2 and H2S in the ionic liquid 1-ethyl-3-methylimidazolium ethylsulfate, J. Chem. Thermodyn. 42 (2010) 1298–1303. doi:10.1016/j.jct.2010.05.008.

[143] M. Shokouhi, M. Adibi, A.H. Jalili, M. Hosseini-jenab, A. Mehdizadeh, Solubility and Diffusion of H2S and CO2 in the Ionic Liquid 1-(2-Hydroxyethyl)-3-methylimidazolium Tetrafluoroborate, J. Chem. Eng. Data. 55 (2010) 1663–1668.

[144] M. Shokouhi, A.H. Saali, M. Vahidi, A.T. Zoghi, A.H. Jalili, Diffusivity and solubility of carbonyl sulfide and sulfur dioxide in 1-ethyl-3-methylimidazolium bis (trifluoromethyl) sulfonylimide ([emim][Tf2N]): Experimental measurement and modelling, J. Chem. Thermodyn. 132 (2019) 411–422. doi:10.1016/j.jct.2019.01.019.

[145] C. Moya, J. Palomar, M. Gonzalez-Miquel, J. Bedia, F. Rodriguez, Diffusion Coefficients of CO2 in Ionic Liquids Estimated by Gravimetry, Ind. Eng. Chem. Res. 53 (2014) 13782–13789. doi:10.1021/ie501925d.

[146] T. Turnaoglu, D.L. Minnick, A.R.C. Morais, D.L. Baek, R. V. Fox, A.M. Scurto, M.B. Shiflett, High-Pressure Vapor−Liquid Equilibria of 1-Alkyl-1-Methylpyrrolidinium Bis(trifluoromethylsulfonyl)imide Ionic Liquids and CO2, J. Chem. Eng. Data. 64 (2019) 4668–4678.

[147] S. Sarraute, M.F. Costa-Gomes, A.A.H. Pádua, Diffusion Coefficients of 1-Alkyl-3-methylimidazolium Ionic Liquids in Water, Methanol, and Acetonitrile at Infinite Dilution, J. Chem. Eng. Data. 54 (2009) 2389–2394.

[148] X. He, Q. Shao, W. Kong, L. Yu, X. Zhang, Y. Deng, A simple method for estimating mutual diffusion coefficients of ionic liquids-water based on an optofluidic chip, Fluid Phase Equilib. 366 (2014) 9–15. doi:10.1016/j.fluid.2014.01.003.

[149] N.C. Merkel, C. Römich, R. Bernewitz, H. Künemund, M. Gleiß, S. Sauer, T.J.S. Schubert, G. Guthausen, K. Schaber, Thermophysical properties of the binary mixture of water + Diethylmethylammonium trifluoromethanesulfonate and the ternary mixture of water + diethylmethylammonium trifluoromethanesulfonate +

diethylmethylammonium methanesulfonate, J. Chem. Eng. Data. 59 (2014) 560–570. doi:10.1021/je400097b.

[150] M.S. Larrechi, A. Cera-Manjarres, D. Salavera, A. Coronas, Quantitative analysis of the interaction of ammonia with 1-(2-hydroxyethyl)-3-methylimidazolium tetrafluoroborate ionic liquid. Understanding the volumetric and transport properties of their mixtures, J. Mol. Liq. 301 (2020) 112440. doi:10.1016/j.molliq.2020.112440.

[151] J. Richter, A. Leuchter, N. Grober, Digital Image Holography for diffusion measurements in Molten Salts and Ionic Liquids-method and firts results, J. Mol. Liq. 103–104 (2003) 359–370. doi:10.16309/j.cnki.issn.1007-1776.2003.03.004.

[152] S.W. Peng, A.N. Soriano, R.B. Leron, M.H. Li, Ternary diffusion coefficients of DEG and LiBr in aqueous glycol-salt system (DEG+LiBr+H2O), J. Taiwan Inst. Chem. Eng. 42 (2011) 233–239. doi:10.1016/j.jtice.2010.07.015.

[153] X. Liu, P. Pan, M. He, Vapor-liquid equilibrium and diffusion coefficients of R32 + [HMIM][FEP], R152a + [HMIM][FEP] and R161 + [HMIM][FEP], J. Mol. Liq. 253 (2018) 28–35. doi:10.1016/j.molliq.2018.01.032.

[154] X. Liu, P. Pan, F. Yang, M. He, Solubilities and diffusivities of R227ea, R236fa and R245fa in 1-hexyl-3-methylimidazolium bis(trifluoromethylsulfonyl)imide, J. Chem. Thermodyn. 123 (2018) 158–164. doi:10.1016/j.jct.2018.04.004.

[155] L. Ferguson, P. Scovazzo, Solubility, Diffusivity, and Permeability of Gases in Phosphonium-Based Room Temperature Ionic Liquids: Data and Correlations, Ind. Eng. Chem. 46 (2007) 1369–1374. doi:10.1021/ie0610905.

[156] K. Kortenbruck, B. Pohrer, E. Schluecker, F. Friedel, I. Ivanovic-Burmazovic, Determination of the diffusion coefficient of CO2 in the ionic liquid EMIM NTf2 using online FTIR measurements, J. Chem. Thermodyn. 47 (2012) 76–80. doi:10.1016/j.jct.2011.09.025.

[157] N. Bochner, J. Pipman, A simple method of determining diffusion constants by holographic interferometry, J. Phys. D Appl. Phys. 9 (1976) 1825–1830.

[158] S. Zhang, M. He, Y. Zhang, S. Peng, X. He, Study of the measurement for the diffusion coefficient by digital holographic interferometry, Appl. Opt. 54 (2015) 9127–9135. doi:10.1364/ao.54.009127.

[159] A. Mialdun, V.M. Shevtsova, Development of optical digital interferometry technique for measurement of thermodiffusion coefficients, Int. J. Heat Mass Transf. 51 (2008) 3164–3178. doi:10.1016/j.ijheatmasstransfer.2007.08.020.

[160] A. Mialdun, V. Shevtsova, Digital interferometry as a powerful tool to study the thermodiffusion effect, Comptes Rendus Mec. 339 (2011) 362–368. doi:10.1016/j.crme.2011.04.001.

[161] M. Gebhardt, W. Köhler, A. Mialdun, V. Yasnou, V. Shevtsova, Diffusion, thermal diffusion, and Soret coefficients and optical contrast factors of the binary mixtures of dodecane, isobutylbenzene, and 1,2,3,4-tetrahydronaphthalene, J. Chem. Phys. 138 (2013) 114503. doi:10.1063/1.4795432.

[162] M.A. Rahman, M.Z. Saghir, Ground based measurement and theoretical calculation of Soret coefficient of binary hydrocarbon mixtures, Exp. Therm. Fluid Sci. 49 (2013) 31–39. doi:10.1016/j.expthermflusci.2013.03.008.

[163] D. Malacara, M. Servín, Z. Malacara, Interferogram Analysis For Optical Testing, 2nd Ed., CRC Press, Taylor & Francis Group, LLC, Boca Raton, FL, 2005.

doi:doi:10.1201/9781420027273.fmatt.

[164] V. Shevtsova, V. Sechenyh, A. Nepomnyashchy, J.C. Legros, Analysis of the application of optical two-wavelength techniques to measurement of the Soret coefficients in ternary mixtures, Philos. Mag. 91 (2011) 3498–3518. doi:10.1080/14786435.2011.586376.

[165] A. Mialdun, J.C. Legros, V. Yasnou, V. Sechenyh, V. Shevtsova, Contribution to the benchmark for ternary mixtures: Measurement of the Soret, diffusion and thermodiffusion coefficients in the ternary mixture THN/IBB/nC12 with 0.8/0.1/0.1 mass fractions in ground and orbital laboratories, Eur. Phys. J. E. 38 (2015). doi:10.1140/epje/i2015-15027-2.

[166] C.-L. Wong, A.N. Soriano, M. Li, Diffusion coefficients and molar conductivities in aqueous solutions of 1-ethyl-3-methylimidazolium-based ionic liquids, Fluid Phase Equilib. 271 (2008) 43–52. doi:10.1016/j.fluid.2008.07.006.

[167] W. Merzkirch, Flow Visualization, 2nd ed., Academic Press, Inc., Orlando, Florida, 1987.

[168] M. Takeda, H. Ina, S. Kobayashi, Fourier-transform method of fringe-pattern analysis for computer-based topography and interferometry, J. Opt. Soc. Am. 72 (1982) 156. doi:10.1364/JOSA.72.000156.

[169] M.B. Shiflett, A. Yokozeki, Solubilities and diffusivities of carbon dioxide in ionic liquids: [bmim][PF6] and [bmim][BF4], Ind. Eng. Chem. Res. 44 (2005) 4453–4464. doi:10.1021/ie058003d.

[170] A.K. Tharanivasan, C. Yang, Y. Gu, Comparison of three different interface mass transfer models used in the experimental measurement of solvent diffusivity in heavy oil, J. Pet. Sci. Eng. 44 (2004) 269–282. doi:10.1016/j.petrol.2004.03.003.

[171] L.F. Zubeir, G.E. Romanos, W.M.A. Weggemans, B. Iliev, T.J.S. Schubert, M.C. Kroon, Solubility and Diffusivity of CO2 in the Ionic Liquid 1-Butyl-3-methylimidazolium Tricyanomethanide within a Large Pressure Range (0.01 MPa to 10 MPa), J. Chem. Eng. Data. 60 (2015) 1544–1562.

[172] Z. Yang, S. Bryant, M. Dong, H. Hassanzadeh, An analytical method of estimating diffusion coefficients of gases in liquids from pressure decay tests, AIChE J. 65 (2019) 434–445. doi:10.1002/aic.16408.

[173] J. Palomar, M. Gonzalez-miquel, J. Bedia, F. Rodriguez, J.J. Rodriguez, Task-specific ionic liquids for efficient ammonia absorption, Sep. Purif. Technol. 82 (2011) 43–52. doi:10.1016/j.seppur.2011.08.014.

[174] M.L. Rasmussen, F. Civan, Parameters of Gas Dissolution in Liquids Obatined by Isothermal Pressure Decay, AIChE J. 55 (2009) 9–23. doi:10.1002/aic.

[175] A. Fayazi, A. Kantzas, Determining Diffusivity, Solubility, and Swelling in Gaseous Solvent-Heavy Oil Systems, Ind. Eng. Chem. Res. 58 (2019) 10031–10043. doi:10.1021/acs.iecr.9b01510.

[176] Y.A. Sanmamed, D. González-Salgado, J. Troncoso, L. Romani, A. Baylaucq, C. Boned, Experimental methodology for precise determination of density of RTILs as a function of temperature and pressure using vibrating tube densimeters, J. Chem. Thermodyn. 42 (2010) 553–563. doi:10.1016/j.jct.2009.11.014.

[177] K. Kim, S. Park, S. Choi, H. Lee, Vapor Pressures of the 1-Butyl-3-methylimidazolium Bromide + Water , 1-Butyl-3-methylimidazolium Tetrafluoroborate + Water , and 1- (2-Hydroxyethyl) -3-methylimidazolium

Tetrafluoroborate + Water Systems, J. Chem. Eng. Data. 49 (2004) 1550–1553. doi:10.1021/je034210d.

[178] N. Nie, D. Zheng, L. Dong, Y. Li, Thermodynamic Properties of the Water + 1-(2-Hydroxylethyl)-3-methylimidazolium Chloride System.pdf, J. Chem. Eng. Data. 57 (2012) 3598–3603.

[179] J. Wang, D. Zheng, L. Fan, L. Dong, Vapor Pressure Measurement for the Water + 1,3-Dimethylimidazolium Chloride System and 2,2,2-Trifluoroethanol + 1-Ethyl-3-methylimidazolium Tetrafluoroborate System, J. Chem. Eng. Data. 55 (2010) 2128–2132.

[180] F.E. Jones, G.L. Harris, ITS-90 Density of Water Formulation for Volumetric Standards Calibration, J. Res. Natl. Inst. Stand. Technol. 97 (1992) 335–340.

[181] M. Zhou, X. Yuan, Y. Yuan, K.T. Yu, Local Composition Based Maxwell−Stefan Diffusivity Model for Binary Liquid Systems, Ind. Eng. Chem. Res. 52 (2013) 10845–10852. doi:10.1021/ie4010157.

[182] E. Siimer, H. Kirss, M. Kuus, L. Kudryavtseva, Isobaric Vapor - Liquid Equilibrium for the Ternary System o -Xylene+ Nonane + Cyclohexanol, J. Chem. Eng. Data. 47 (2002) 52–55. doi:10.1021/je0101404.

[183] T. Kreis, Digital holographic interference-phase measurement using the Fourier-transform method, J. Opt. Soc. Am. A. 3 (1986) 847–855. doi:10.1364/JOSAA.3.000847.

[184] F. Croccolo, M.A. Arnaud, D. Bégué, H. Bataller, Concentration dependent refractive index of a binary mixture at high pressure, J. Chem. Phys. 135 (2011) 034901. doi:10.1063/1.3610368.

[185] Y. Clergent, C. Durou, M. Laurens, Refractive index variations for argon, nitrogen, and carbon dioxide at λ = 632.8 nm (He-Ne laser light) in the range 288.15 K ≤ T ≤ 323.15 K, 0 < p < 110 kPa, J. Chem. Eng. Data. 44 (1999) 197–199. doi:10.1021/je980133o.

[186] G. Bönsch, E. Potulski, Measurement of the refractive index of air and comparison with modified Edlén's formulae, Metrologia. 35 (1998) 133–139. doi:10.1088/0026-1394/35/2/8.

[187] K. Vedam, P. Limsuwan, Piezo- and elasto-optic properties of liquids under high pressure. I. Refractive index vs pressure and strain, J. Chem. Phys. 69 (1978) 4762–4771. doi:10.1063/1.436530.

[188] F. Li, M. Li, Q. Cui, T. Cui, Z. He, Q. Zhou, G. Zou, The velocity, refractive index, and equation of state of liquid ammonia at high temperatures and high pressures, J. Chem. Phys. 131 (2009) 134502. doi:10.1063/1.3223549.

[189] S. Shraiber, Experimental Investigation of the Thermal Dependence of the Piezo-Optical Coefficient of Water Between 5 and 90 °C, Isr. J. Chem. 13 (1975) 181–184.

[190] M.A. Rahman, M.Z. Saghir, Error scrutiny of measuring coefficients of refractive indices and Soret coefficients using Mach-Zehnder interferometer, Optik (Stuttg). 125 (2014) 4609–4613. doi:10.1016/j.ijleo.2014.05.034.

[191] X. Song, D.S. Nobes, Experimental investigation of evaporation-induced convection in water using laser based measurement techniques, Exp. Therm. Fluid Sci. 35 (2011) 910–919. doi:10.1016/j.expthermflusci.2011.01.010.

References

[192] Y.T. Kang, T. Kashiwagi, Heat transfer enhancement by Marangoni convection in the NH3-H2O absorption process, Int. J. Refrig. 25 (2002) 780–788. doi:10.1016/S0140-7007(01)00074-3.

[193] R. Khosrokhavar, G. Elsinga, R. Farajzadeh, H. Bruining, Visualization and investigation of natural convection flow of CO2 in aqueous and oleic systems, J. Pet. Sci. Eng. 122 (2014) 230–239. doi:10.1016/j.petrol.2014.07.016.

Annexes

Annex A: Calculation of the thermodynamic factor from VLE data using g^E models

The thermodynamic factor can be calculated from VLE data using different g^E models. The excess Gibbs energy is defined by the activity coefficients γ_i of all components of the mixture, which represents the deviation from ideal mixing behavior, as:

$$\frac{g^E}{RT} = \sum x_i \ln \gamma_i \qquad \text{A-1}$$

Different g^E models, such as NRTL or Wilson, rest on this relation to describe phase behavior, like VLE, with algebraic expressions for the excess Gibbs energy. These models describe activity coefficients as a function of interaction parameters that can be obtained from experimental data by regression.

At the same time, activity coefficient, γ_i, can be calculated from the phase equilibrium equation as [93]:

$$\gamma_i = \frac{y_i \phi_i P}{x_i \phi_i^s P_i^s} \qquad \text{A-2}$$

where P and P_i^s are vapor pressure of liquid mixture and pure component i at system temperature, respectively; y_i and x_i represent mole fraction of component *i* in the vapor phase and liquid phase, respectively; ϕ_i and ϕ_i^s are the fugacity coefficient of component *i* in the vapor mixture, and in its saturated state. Here, the vapor pressure of the pure component can be calculated using the Antoine equation.

For the studied mixture, i.e., H_2O(1) + [EtOHmim][BF_4](2), the vapor phase can be considered as pure water vapor $(y_i = 1)$ due to the non-volatility of the IL. Since the vapor phase composition for such binary system and for the pure solvent is same, and the pressure difference between them is relatively small, the fugacity coefficient correction can be cancelled out. Therefore, equation A-2 reduces to:

$$\gamma_i = \frac{P}{x_i P_i^s} \qquad \text{A-3}$$

The use of this expression in combination with different g^E models provides the interaction parameters needed to calculate the thermodynamic factor. This is done by minimizing the difference between the experimental value of the activity coefficient (or pressure) and the value calculated by the model.

For the binary mixture H_2O + [EtOHmim][BF_4], we found VLE data only in one source. Kim et al. [177] measured the vapor pressure of three binary mixtures containing water + ionic liquid (including H_2O + [EtOHmim][BF_4]) in the temperature range of (304.8 to 475.2) K and in the concentration range of (0.200 to 0.800) ILs mole fraction using the boiling-point method. They correlated the experimental results with an Antoine-type equation with very good fitting quality. In this work, we have correlated their experimental results using two g^E models, NRTL (Non-random, two-liquid) and Wilson, to obtain the binary interaction parameters. These g^E models are among the most popular for describing VLE in binary systems containing aqueous solutions of ionic liquids. The absolute relative deviation (ARD%) is used as criteria to evaluate the quality of the fitting:

$$ARD\% = \frac{100}{N}\sum_{i=1}^{N}\left|\frac{P_{exp}-P_{cal}}{P_{exp}}\right| \qquad \text{A-4}$$

where: *N* is the number of experimental pressure points, P_{exp} is the experimental pressure obtained from Kim et al. [177] and P_{cal} is the calculated pressure using equation A-3 in combination with a g^E model.

The procedure followed to calculate the thermodynamic factor from VLE data using NRTL and Wilson models is described below.

A.1 Calculation of the thermodynamic factor from NRTL model

NRTL model have been widely used for describing VLE in H_2O + ionic liquid binary systems [178,179]. Moreover, the NRTL equations are applicable to both vapor-liquid and liquid-liquid equilibria. Therefore, mutual solubility data can be used to determine NRTL parameters. NRTL model can also predict reliable results for partially and completely miscible systems [93]. In this model the excess Gibs energy is expressed as:

$$\frac{g^E}{RT} = x_1x_2\left(\frac{\tau_{21}G_{21}}{x_1+x_2G_{21}}+\frac{\tau_{12}G_{12}}{x_2+x_1G_{12}}\right) \qquad \text{A-5}$$

where:

$$G_{12} = \exp(-\alpha_{12}\tau_{12}) \qquad G_{21} = \exp(-\alpha_{12}\tau_{21}) \qquad \text{A-6}$$

with

$$\tau_{12} = \frac{\Delta g_{12}}{RT} \qquad \tau_{21} = \frac{\Delta g_{21}}{RT} \qquad \text{A-7}$$

Here, α_{12} is the non-randomness parameter; and τ_{12}, τ_{21} are the binary interaction parameters. These are the three adjustable parameters of the NRTL model.

The activity coefficient is the partial molar excess Gibbs energy and can therefore be obtained from partial derivatives with respect to the mole fraction. Thus, the activity coefficient of component 1 can be calculated as follows:

$$ln\gamma_1 = x_2^2\left[\tau_{21}\left(\frac{G_{21}}{x_1+x_2G_{21}}\right)^2 + \tau_{12}\left(\frac{G_{12}}{x_2+x_1G_{12}}\right)^2\right] \qquad \text{A-8}$$

The thermodynamic factor contains the derivative of $\ln\gamma_i$ with respect to lnx_1. After some algebraic treatment, it is possible to show that the thermodynamic factor can be calculated from NRTL model as [93]:

$$\Gamma = 1 + \frac{dln\gamma_1}{dlnx_1} = 1 - 2x_1x_2\left[\frac{\tau_{21}G_{21}^2}{(x_1+x_2G_{21})^3} + \frac{\tau_{12}G_{12}^2}{(x_2+x_1G_{12})^3}\right] \qquad \text{A-9}$$

To calculate the thermodynamic factor from VLE data using this model, it is necessary to determine α, τ_{12}, and τ_{21} Moreover, the temperature dependency of the binary interaction parameters can be modeled by several approaches. In this thesis, we considered a dependency in the format [178]:

$$\tau_{12} = \tau_{12}^{(0)} + \frac{\tau_{12}^{(1)}}{T} \qquad \tau_{21} = \tau_{21}^{(0)} + \frac{\tau_{21}^{(1)}}{T} \qquad \text{A-10}$$

So, when NRTL model was used to fit experimental VLE data in this thesis, there were 5 adjustable parameters, α, $\tau_{12}^{(0)}$, $\tau_{12}^{(1)}$, $\tau_{21}^{(0)}$, $\tau_{21}^{(1)}$. The regressed parameters for this model and the average relative error (ARD) from VLE data are listed in Table A-1. Figure A-1 shows the experimental vapor pressure and the calculated by the NRTL model at different mole fractions.

Table A-1. NRTL model parameters.

Parameter	α	$\tau_{12}^{(0)}$	$\tau_{12}^{(1)}$	$\tau_{21}^{(0)}$	$\tau_{21}^{(1)}$	ARD/ %
Value	0.278	-7.446E-02	-2.155	1.215E+03	-2.134e+02	3.28

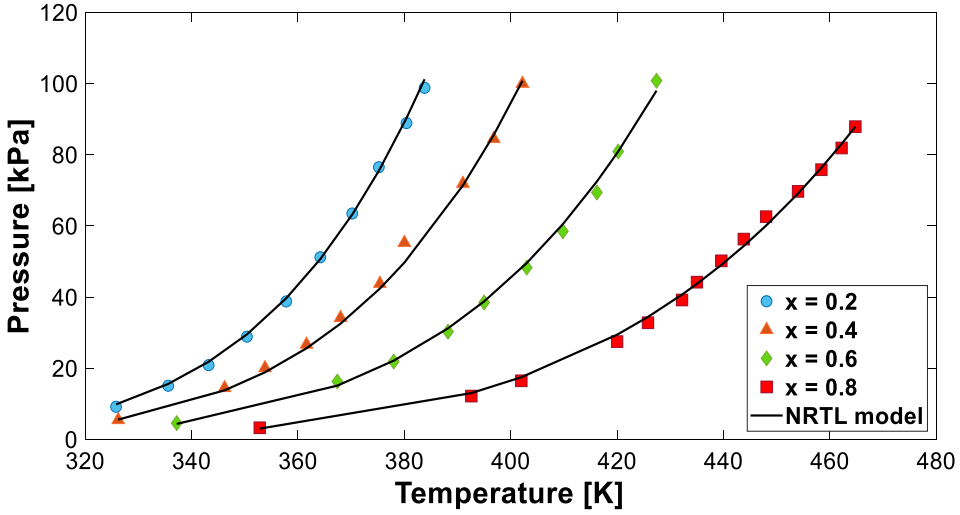

Figure A-1. Vapor pressure at different mole fractions for mixture H_2O + [EtOHmim][BF_4]. Symbols: experimental data. Lines: calculations by the NRTL model.

A.2 Calculation of the thermodynamic factor from Wilson model

Wilson model is another g^E model widely used to describe VLE. It is recommended for strongly nonideal binary mixtures, because, unlike the NRTL equation, it contains only two adjustable parameters. However, the original Wilson model is not applicable to a mixture that exhibits a miscibility gap. Although, there is a modified Wilson model capable to overcome this shortcoming [71]. In this model the excess Gibs energy is expressed as:

$$\frac{g^E}{RT} = -x_1 \ln(x_1 + \Lambda_{12} x_2) - x_2 \ln(x_2 + \Lambda_{21} x_1) \qquad \text{A-11}$$

where:

$$\Lambda_{12} = \frac{v_2}{v_1} exp\left(-\frac{\lambda_{12}-\lambda_{11}}{RT}\right) \qquad \Lambda_{21} = \frac{v_1}{v_2} exp\left(-\frac{\lambda_{21}-\lambda_{22}}{RT}\right) \qquad \text{A-12}$$

Here, v_1 and v_2 are pure component molar volumes of components 1 and 2, respectively; $\lambda_{12} - \lambda_{11}$, and $\lambda_{12} - \lambda_{11}$ are interaction energy parameters. Pure component molar volumes as a function of temperature are taken from literature [42] and [180].

In this model, activity coefficient of component 1 can be calculated as:

$$ln\gamma_1 = -ln(x_1 + \Lambda_{12}x_2) - x_2\left(\frac{\Lambda_{12}}{x_1+\Lambda_{12}x_2} - \frac{\Lambda_{21}}{\Lambda_{21}x_1+x_2}\right) \quad \text{A-13}$$

Then, the expression to calculate the thermodynamic factor is [181]:

$$\Gamma = 1 - \frac{x_1}{x_1+x_2\Lambda_{12}} + \frac{x_1\Lambda_{21}}{x_2+x_1\Lambda_{21}} - x_1x_2\left[\frac{\Lambda_{12}(1-\Lambda_{12})}{(x_1+x_2\Lambda_{12})^2} + \frac{\Lambda_{21}(1-\Lambda_{21})}{(x_2+x_1\Lambda_{21})^2}\right] \quad \text{A-14}$$

In this thesis, Λ_{12} and Λ_{21} were used as adjustable parameters. The temperature dependency of these parameters can be modeled as [182]:

$$\Lambda_{12} = \exp\left(a_{12} + \frac{b_{12}}{T}\right) \qquad \Lambda_{21} = \exp\left(a_{21} + \frac{b_{21}}{T}\right) \quad \text{A-15}$$

So, when Wilson model was used to fit experimental VLE data, there were 4 adjustable parameters, a_{12}, a_{21}, b_{12}, and b_{21}. The regressed parameters for this model and the ARD from VLE data are listed in Table A-2. Figure A-2 shows the experimental vapor pressure and the calculated by the Wilson model at different mole fractions.

Table A-1. Wilson model parameters.

Parameter	a_{12}	a_{21}	b_{12}	b_{21}	ARD/ %
Value	2.722	-2.301	-5.643E+02	9.849E+02	3.19

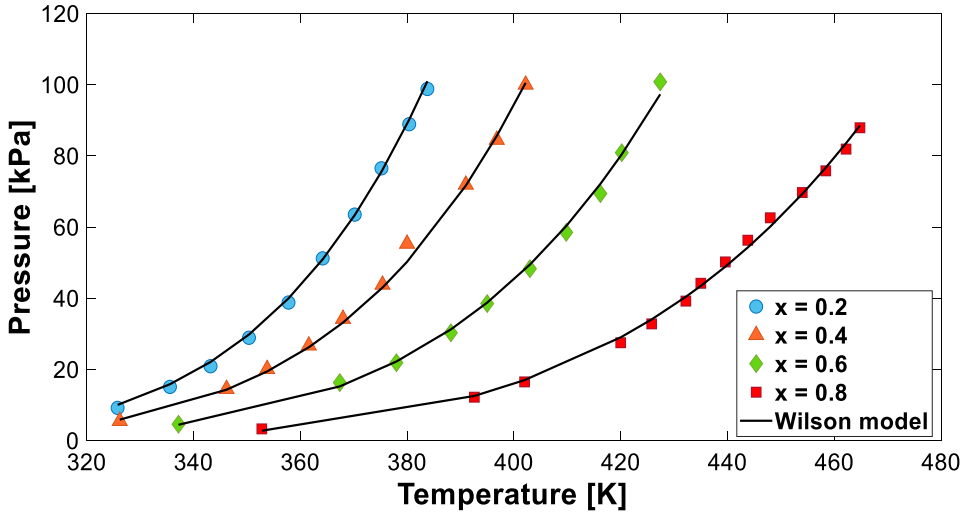

Figure A-2. Vapor pressure at different mole fractions for mixture H_2O + [EtOHmim][BF_4]. Symbols: experimental data. Lines: calculations by the Wilson model.

Annex B: Best-fit parameters of the models and correlations used to estimate the mass diffusivity in the binary mixture of H_2O + [EtOHmimBF$_4$]

Table A-3. Best-fit parameters for cluster diffusion model with binary parameters from VLE data.

Parameter	NRTL	Wilson
c	-4.943e-02	-4.798e-01
n	2.000e+00	1.999+00
β	2.345e-01	7.264e-01
r_0	8.533-09	7.862e-09
Y	-3.146+02	6.262e+01

Table A-4. Best-fit parameters for MGC model with binary parameters from VLE data.

Parameter	NRTL	Wilson
D*	1.176e-08	1.898e+02
α	3.885e-01	1.372e+01
β	-6.925e-01	-1.659e+00
a	1.130e+00	-1.262e+01
b	2.222e+00	-8.524e-01
c	1.388e+00	-2.751-01
d	-8.188e-02	-2.833e-01

Table A-5. Best-fit parameters for Vignes correlation with binary parameters regressed from diffusion data.

NRTL		Wilson	
Parameter	Value	Parameter	Value
α_{12}	1.954e+00	a_{12}	-1.573e+02
$\tau_{12}^{(0)}$	-6.327e+00	a_{21}	-2.152e-01
$\tau_{12}^{(1)}$	-2.263e+00	b_{12}	-1.813e+07
$\tau_{21}^{(0)}$	1.927e+03	b_{21}	-8.145e-05
$\tau_{21}^{(1)}$	9.835e+02		

Table A-6. Best-fit parameters for UNIDIF model.

Parameter	Value
a_{12}	6.983e-01
a_{21}	3.245e+00

Table A-7. Best-fit parameters for cluster diffusion model with binary parameters from diffusion data.

NRTL		Wilson	
Parameter	**Value**	**Parameter**	**Value**
c	7.817e-02	c	-3.367e-02
$\boldsymbol{n}$	1.992e+00	n	1.410+00
$\boldsymbol{\beta}$	1.429e+00	β	5.434e-01
$\boldsymbol{r_0}$	2.175e-11	r_0	1.311e-10
Y	-2.551e+03	Y	9.917e+00
$\boldsymbol{\alpha_{12}}$	8.921e+00	a_{12}	-5.014e+00
$\boldsymbol{\tau_{12}^{(0)}}$	2.759e-03	b_{12}	8.663e+02
$\boldsymbol{\tau_{12}^{(1)}}$	-1.065e-01	a_{21}	-7.978e+00
$\boldsymbol{\tau_{21}^{(0)}}$	6.880e+01	b_{21}	5.591e+02
$\boldsymbol{\tau_{21}^{(1)}}$	-1.375e+01		

Table A-8. Best-fit parameters for MGC model with binary parameters from diffusion data.

NRTL		Wilson	
Parameter	**Value**	**Parameter**	**Value**
D*	5.183e-11	D*	4.315e-09
$\boldsymbol{\alpha}$	4.813e-01	α	8.803e-01
$\boldsymbol{\beta}$	-3.212e+00	β	-8.353e+01
a	7.362e+00	a	-6.140e+00
b	-1.662e+00	b	7.152e+00
c	1.136e+00	c	9.252e-01
d	5.147e-01	d	-4.623e-01
$\boldsymbol{\alpha_{12}}$	1.276e-01	a_{12}	2.213e+00
$\boldsymbol{\tau_{12}^{(0)}}$	-5.732e+00	a_{21}	-2.013e+00
$\boldsymbol{\tau_{12}^{(1)}}$	4.327e+02	b_{12}	-8.202e+02
$\boldsymbol{\tau_{21}^{(0)}}$	4.356e+00	b_{21}	4.505e+02
$\boldsymbol{\tau_{21}^{(1)}}$	-2.962e+03		

Annex C: Optical phase extraction from the interferograms and unwrapping procedure

C.1 Optical phase extraction from the interferograms

The obtained interferograms are essentially digital images with the measured light intensity in each pixel. The measured intensity distribution can be expressed as:

$$i(x,z) = i_0(x,z) + m(x,z) \cdot cos\,[2\pi u_0 x + \Delta\varphi(x,z)] \qquad \text{A-16}$$

where $i_0(x,z)$ represents the background variation and $m(x,z)$ is related to the local contrast of the pattern. $2\pi u_0 x$ is the linear phase introduced by the tilted mirror, u_0 is related with the spatial frequency of the fringes and $\Delta\varphi(x,z)$ is the remaining optical phase difference between the interferometer arms. Now the fringe-pattern formula, Eq. A-17, can be written as one term around the zero frequency and two terms around the frequency u_0:

$$i(x,z) = i_0(x,z) + \exp[j2\pi u_0 x] \,.\, c(x,z) + \exp[-j2\pi u_0 x] \,.\, c^*(x,z) \qquad \text{A-17}$$

where:

$$c(x,z) = \frac{1}{2} m(x,z) \cdot \exp[j\Delta\varphi(x,z)] \qquad \text{A-18}$$

with $j = \sqrt{-1}$ and * denoting the complex conjugate. The terms of interest in Eq. A-18 are $c(x,z)$ and $c^*(x,z)$, which contain the optical phase difference term. Now, Eq. A-18 needs to be Fourier transformed, which gives:

$$I(u,v) = I_0(u,v) + C(u,v) * \delta(u - u_0) + C^*(-u,-v) * \delta(u + u_0) \qquad \text{A-18}$$

were $*$ represents the convolution operator, and the term C is the Fourier transform of $c(x,z)$. C and C* are placed symmetrically to the origin at frequencies $\pm u_0$ respectively. These terms contain equivalent information about the optical phase difference. Therefore, the next step is to filter out either one of the two spectra. Applying a Gaussian filter centered at $-u_0$, all frequencies except those that belong to C*, can be filtered out. Then, C* is shifted to the zero frequency and the inverse Fourier transform is applied, and, consequently, the term $c^*(x,z)$, defined in Eq. A-18 is obtained. Finally, the optical phase difference between the interferometer arms (without the linear phase introduced by the mirror) is calculated from $c^*(x,z)$ as:

$$\Delta\varphi(x,z) = arctan\left\{\frac{Im[c^*(x,z)]}{Re[c^*(x,z)]}\right\} \quad \text{A-19}$$

where $Im[c^*(x,z)]$ and $Re[c^*(x,z)]$ denote the real part and the imaginary part, respectively.

The optical phase map calculated from Eq. A-19 is wrapped in the range [-π, π]. A typical wrapped phase map, and the corresponding wrapped phase profile on a line located at the center of the phase map can be appreciated in Figure A-3. Two different regions can be distinguished in Figure A-3 a). A region characterized by phase lines and another where no pattern is observed. This last region corresponds to the vapor-liquid interface and the vapor phase. To determine the mutual diffusion coefficient, our main interest relies on physical phenomena taking place in the liquid bulk. Therefore, the subsequent analysis focuses on this region. In the liquid bulk, it is also possible to differentiate two areas. An area where the phase lines are closer to each other (just below the vapor-liquid interface) and another area located at the bottom of the phase map, where the phase lines are further apart. Near the vapor-liquid interface, the proximity of the phase lines implies a higher refractive index gradient than in the lower area. In this last area, the delay imposed by diffusive mass transport causes separation of the phase lines. Figure A-3 b) shows the wrapped phase profile over a line (red line in Figure A-3 a)) located at the center of the phase map. As expected, the optical phase difference shows a discontinuous profile, wrapped between -π and π. Also, it is possible to observe, the jump of the optical phase in the vapor-liquid interface. This profile shows more clearly the two areas described within the liquid bulk.

Next, we need to separate from the others, the contribution of the concentration to the variation of the refractive index of the liquid phase during the absorption process. For this, the wrapped phase of the reference interferogram is subtracted from the wrapped phase map of subsequent interferograms. Here, the reference interferogram was taken as the last image recorded just before the start of the absorption process. Then, the optical phase of subsequent interferograms includes contributions to the variation of the refractive index due to changes not only in concentration but also in temperature and pressure. To determine the mass diffusivity, we need to isolate the concentration contribution to the optical

phase shift from the other contributions. The influence of these contributions in the determination of the mass diffusivity will be considered in Appendix D.

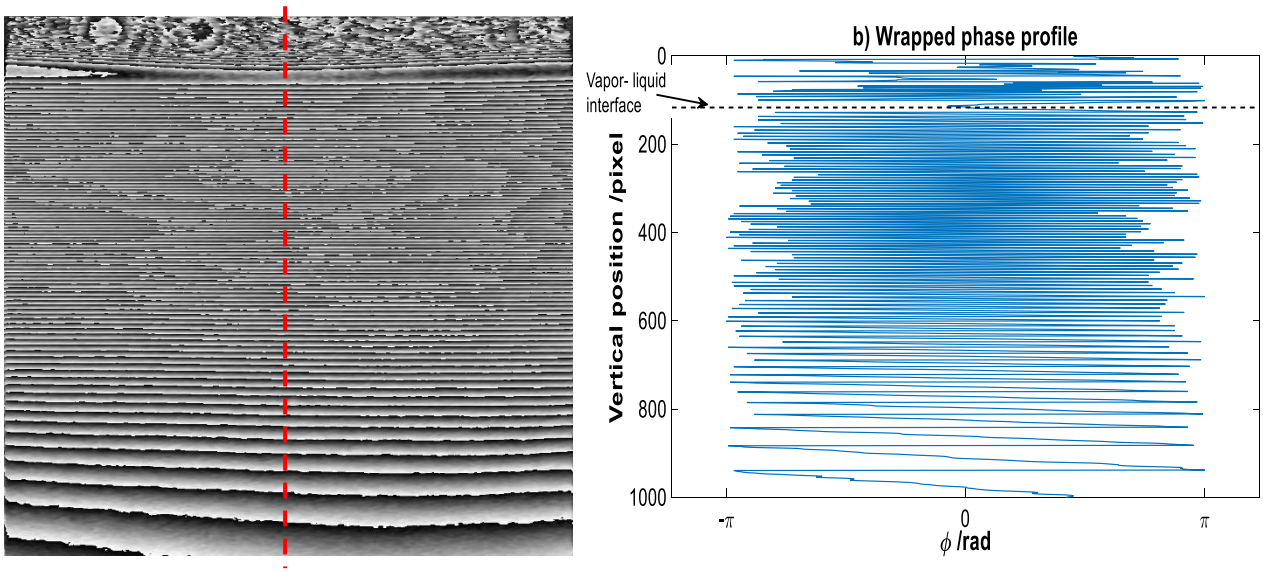

Figure A-3. Typical wrapped phase: a) Wrapped phase map; b) and the corresponding profile in the central line (red line) of the phase map.

C.2 Phase unwrapping

Two-dimensional phase unwrapping could be a demanding task, especially for noisy fringe images, for which sophisticated unwrapping techniques are required [65]. In our case, 2-D phase maps have typically good quality, thus, an approach based on the method described by Kreis [183] was adopted. The unwrapping procedure starts from the selected reference pixel. The phase of this pixel is compared with a neighboring pixel. If the magnitude of the difference between the two neighboring pixels is less than π, the optical phase remains unchanged. If the difference between two pixels is less than -π, then, 2π is added to the wrapped phase; otherwise, if the difference is more than π, 2π is subtracted from the wrapped phase at that pixel [162]. Each pixel was compared with a previously validated one in the x and z-directions, and this iterative procedure can be expressed as follows:

$$k(x_{m/2}, z_1) = 0$$

$$k(x_j, z_1) = \begin{cases} k(x_{j-1}, z_1) & if \ \left|\Delta\varphi(x_j, z_1) - \Delta\varphi(x_{j-1}, z_1)\right| < \pi \\ k(x_{j-1}, z_1) + 1 & if \ \ \Delta\varphi(x_j, z_1) - \Delta\varphi(x_{j-1}, z_1) \leq -\pi \\ k(x_{j-1}, z_1) - 1 & if \ \ \Delta\varphi(x_j, z_1) - \Delta\varphi(x_{j-1}, z_1) \geq \pi \end{cases} \quad \text{C-1}$$

where $j = \frac{m}{2}, \frac{m}{2} + 1, \dots, m \quad and \quad \frac{m}{2}, \frac{m}{2} - 1, \dots, 2$

$$k(x_j, z_i) = \begin{cases} k(x_j, z_{i-1}) & if \ \left|\Delta\varphi(x_j, z_i) - \Delta\varphi(x_j, z_{i-1})\right| < \pi \\ k(x_j, z_{i-1}) + 1 & if \ \ \Delta\varphi(x_j, z_i) - \Delta\varphi(x_j, z_{i-1}) \leq -\pi \\ k(x_j, z_{i-1}) - 1 & if \ \ \Delta\varphi(x_j, z_i) - \Delta\varphi(x_j, z_{i-1}) \geq \pi \end{cases} \quad \text{C-2}$$

where $i = 2,3, \dots l$

$$\Delta\varphi_{continuous} = \Delta\varphi(x_j, z_i) + 2\pi k(x_j, z_i) \qquad i.j = 1,2, \dots \quad \text{C-3}$$

here, i and j are coordinate index of pixels in z (vertical) and x (horizontal) directions, respectively, and m and l are number of pixels in x and z direction, respectively.

Annex D: Influence of thermal, pressure, and other effects on the refractive index variations

In this annex, the influence of thermal, pressure, and other effects in the refractive index variations is discussed. At a given wavelength, λ, the refractive index variation includes contributions from temperature, $\Delta T(z,t)$, pressure, $\Delta P(z,t)$, and concentration, $\Delta C(z,t)$, variations [184]:

$$\Delta n(z,t) = \left(\frac{\partial n}{\partial T}\right)_{P_0,C_0,\lambda} \Delta T(z,t) + \left(\frac{\partial n}{\partial P}\right)_{T_0,C_0,\lambda} \Delta P(z,t) + \left(\frac{\partial n}{\partial C}\right)_{T_0,P_0,\lambda} \Delta C(z,t) \quad \text{A-20}$$

where T_0, P_0 and C_0 are the temperature, pressure, concentration of the absorbent liquid at reference time, t_{ref}, and the derivative terms (called optical contrast factors) represent the variation of the refractive index with these variables, respectively.

Based on the above relation, the validity of the proposed methodology for the determination of the ammonia concentration profiles in the absorbent is verified.

D.1 Thermal effects on the refractive index variations

The absorption process of ammonia vapor in the studied absorbent liquids is slightly exothermic. As temperature variations can induce refractive index variations, the absorption thermal effects should be considered and analyzed.

The thermal behavior of the mixtures studied during the absorption process was discussed in Chapter II. However, for the sake of analyzing its influence in the refractive index fields, it is briefly addressed again here. For this purpose, Figure A-4 shows the temperature evolution in the absorption cell during the absorption process of ammonia vapor in the ionic liquid [emim][BF_4] at 303.15 K. After opening the valve to allow ammonia vapor and ionic liquid to come into contact, the temperature in the absorption cell increases rapidly. The temperature rise is determined by the heat of absorption, which includes the latent heat of condensation of ammonia and the heat of dissolution. In this case, the temperature increase is small compared to the temperature increase in the other absorbent liquids studied. As the absorption process progresses, the temperature rise decreases rapidly. After half an hour, the temperature remains fairly stable, with slight variations until the end of the experiment at 15 hours. These small variations (lower than 0.5 K) are due to the limited capacity of our thermal control system. Therefore, the effects of these variations on the refractive index must be

considered in the uncertainty analysis. In summary, we can conclude that the thermal effects on the refractive index fields are significant at the beginning of the absorption process and become negligible after a short time.

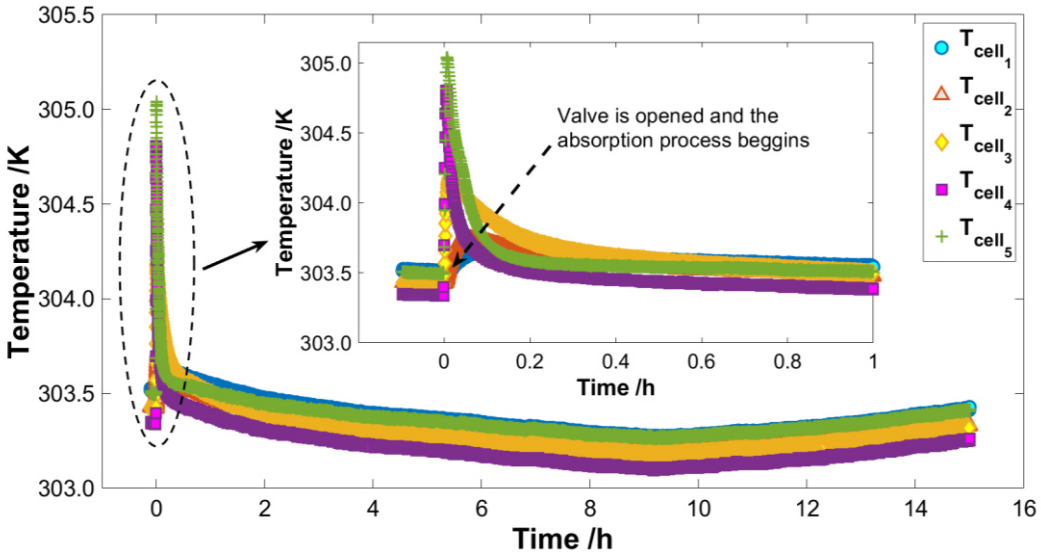

Figure A-4. Temperature behavior in the absorption cell during the absorption process of ammonia vapor in [emim][BF_4] at 303.15 K.

D.2 Pressure effects on the refractive index variations

It is well-known that pressure variations can also induce refractive index variations [184]. The pressure dependence of the refractive index has been reported for some gaseous systems [185]. Moreover, there are available correlations for the calculation of refractive index of gases that consider the contribution of pressure, such as the Edlén formula and its modifications for the refractive index of air [186]. However, there is very scarce data about the pressure dependence of the refractive in liquid mixtures [187,188]. Unfortunately, most of the data reported on this issue are at very high pressures. At high pressures, the molecular structure of liquids approaches its densest form, which differs from the structure of the liquid at normal atmospheric pressure or near it [189].

In general, the relationship between the refractive index and other thermophysical properties of a liquid system is established through density, using correlations such as Lorentz-Lorenz [184]. Therefore, if the relationship between density and pressure is well-known (for example, an appropriate equation of state for the studied mixture), the dependence of the refractive index on pressure could be

quantified. However, no universal relationship provides satisfactory results for all mixtures. Especially in strongly non-ideal liquid mixtures, such as those containing ionic liquids, estimates of the refractive index using different relationships such as that of Lorentz-Lorenz, yield results quite far from reality.

In this thesis, the system pressure during the absorption process is always less than atmospheric pressure. At or near atmospheric pressure, generally in the estimation of the density of liquids (and, therefore, on the refractive index) only temperature dependence is considered, and pressure dependence is neglected.

D.3 Influence of other effects on the refractive index variations

In addition to the influence of temperature and pressure, other unwanted effects may cause variations in the refractive index of the ammonia/absorbent liquid mixture. We have used a Mach-Zehnder interferometer, which is a very sensitive technique to any sort of errors. An exhaustive analysis, including geometrical, instrumental, and environmental errors, regarding the use of a Mach-Zehnder interferometer to determine refractive index variations, can be found in the work of Rahman and Saghir [190]. Here, it is discussed only errors peculiar to our experimental set-up and procedure.

An important source of error in experiments performed with water as absorbent liquid could be the evaporation of water. Water evaporation would lead to a temperature decrease due to the latent heat, inducing small refractive variations at the interface and an increase of the water density [67]. Water evaporation is subjected to the existing temperature and pressure conditions in the absorption cell. As discussed above, temperature and pressure of the absorption system remains virtually unchanged after a certain time from the beginning of the absorption process. In the case of experiments with water, temperature and pressure quickly attained approximately constant values. The amount of water in vapor phase after 15 hours from the beginning of the absorption process was small for all the experiments (water mass fraction in vapor phase was always less than 8%). Therefore, it is considered that the thermal effects due to water evaporation does not significantly influence the refractive index fields. Moreover, in the literature has been reported that the evaporation of water can induce surface tension gradients along the water surface that ultimately lead to a surface driven flow, known as Marangoni convection [191]. Marangoni convection in the

NH_3/H_2O absorption process with/without heat transfer additives has been studied using holographic interferometry by Kang and Kashiwagi [192]. The authors observed Marangoni convection near the vapor-liquid interface only in the cases with heat transfer additive. In perfect compliance with the above, here, no convection was visualized in any of the experiments performed with water as absorbent.

In vapor-liquid absorption experiments, a critical issue in diffusion measurements is to avoid the appearance of convection currents in the liquid phase. If the ammonia/absorbent liquid mixture is denser than the absorbent liquid itself, the system is unstable, and density-driven natural convection will be set up after a short time of contact. The onset of natural convection flows in the absorption process of CO_2 in aqueous and oleic systems have been visualized using a schlieren technique by Khosrokhavar et al. [193]. However, the absorption process of NH_3 in the absorbent liquids studied always leads to a decrease in the density of the liquid phase. Therefore, density-driven natural convection does not occur in any of the absorption experiments performed. It is important to notice that this is not the general case and the possible appearance of convective currents should be investigated for each particular fluid pairs.

Other source of error in the absorption experiments could be the temperature drop caused by the expansion of the ammonia vapor (Joule-Thompson effects). To investigate if these effects can significantly disturb the refractive index fields a preliminary test experiment was performed. The pressure drop due to ammonia vapor expansion was recorded after the valve was opened using an initially dry evacuated absorption cell. The temperature and pressure drops were found to be less than 0.5 K and 10% of the initial pressure in the cylindrical tank, respectively. Moreover, Joule-Thompson effects have the greatest influence for time intervals that immediately follow the opening of the inlet valve of the absorption cell to start the measurements. Therefore, these effects are negligible for the time interval used in determining the diffusion coefficient.

UNIVERSITAT ROVIRA I VIRGILI
THEORETICAL AND EXPERIMENTAL STUDY OF THE ABSORPTION PROCESS OF AMMONIA IN IONIC LIQUIDS FOR ABSORPTION REFRIGERATION SYSTEMS
Ronny Rives Sanz

UNIVERSITAT
ROVIRA i VIRGILI